



Bennett, Mark (2018) *Dependence of cellular behaviour on viscosity defined ligand mobility in supported lipid bilayers*. PhD thesis.

<https://theses.gla.ac.uk/30587/>

Copyright and moral rights for this work are retained by the author

A copy can be downloaded for personal non-commercial research or study, without prior permission or charge

This work cannot be reproduced or quoted extensively from without first obtaining permission in writing from the author

The content must not be changed in any way or sold commercially in any format or medium without the formal permission of the author

When referring to this work, full bibliographic details including the author, title, awarding institution and date of the thesis must be given

Enlighten: Theses

<https://theses.gla.ac.uk/>
research-enlighten@glasgow.ac.uk

DEPENDENCE OF CELLULAR BEHAVIOUR ON VISCOSITY-DEFINED LIGAND MOBILITY IN SUPPORTED LIPID BILAYERS



Mark Bennett

BSc. Hons (International), MSc, MRes

Submitted in fulfilment of the requirements of the Degree of Doctor of
Philosophy in Biomedical Engineering

The School of Engineering, College of Science and Engineering

University of Glasgow

ABSTRACT

This thesis has explored the nature of cellular behaviour in response to the mobility of ligands presented on supported lipid bilayers of varying viscosity (diffusive characteristics). This was inspired by the various characteristics of the *in vivo* microenvironment, controlling the cell response. For example, the viscoelastic, topographical, or chemical nature of the extracellular matrix can control cellular behaviours, such as adhesion, proliferation, migration and differentiation. Numerous biomaterials have alternately sought to understand the nature of the cell response and also to take advantage of it; the current work predominantly falls into the former of these categories. Whereas elastic stiffness is one side of the coin of viscoelasticity, viscosity is the other. Further, while much work has sought to understand the nature of both the elastic and viscoelastic nature of the cell response, as of yet few have sought to understand the role of viscosity in isolation. This is despite some work seeking to take advantage of this viscosity, by observing cellular behaviour on surfaces with known viscous components. This work has noted that cellular adhesion and spreading, focal adhesions, and differentiation are all affected by the viscous component of the surface without addressing why. Supported lipid bilayers (SLBs) present an excellent opportunity to understand these mechanisms. Commonly used as biosensing platforms, non-fouling coatings and model systems, they have also found use in both cell culture systems and in understanding mechanobiology. Individual lipids may exhibit a phase transition, T_m , at a temperature defined by the chemistry of the SLB component lipids; as such, they can exhibit significantly different, viscosity-defining, diffusive characteristics. This work describes the use of SLBs of differing T_m that exhibit fluid-like or gel-like properties in cell culture conditions. These non-fouling SLBs were functionalised with the cell adhesive ligand RGD, derived from the matrix protein fibronectin, with the response of the cell on both the cell-wide and molecular scale determined. The cell response was then understood via pathways related to the mechanical sensing of the environment. Further, initial forays into the nature of the response of human mesenchymal stem cells (hMSCs) was determined, to test the applicability of the system to the overall field of biomedical engineering.

The first area of study was the production and characterisation of supported lipid bilayers of differing diffusive characteristics; at cell culture temperature one SLB is in the fluid phase (DOPC) and the other in the gel phase (DPPC). Initial steps included the confirmation of the

effectiveness of the vesicle fusion method in this instance, via zeta-sizing and atomic force microscopy (AFM). The former determined that mechanical extrusion was sufficient in forming small unilamellar vesicles of sufficient diameter so as to maximise the chances of rupture on glass surfaces, upon incubation. Further, AFM imaging was used to determine the contiguous nature of the bilayer, confirming that minimal defects were present in either of the DOPC or DPPC-based SLBs. Force spectroscopy, using the same system, also confirmed the presence of a single bilayer of thickness in the single nanometre range. Fluorescence correlation spectroscopy (FCS) determined the diffusive characteristics of both SLBs, with diffusion coefficients shown to differ by an order of magnitude. Applied to the Saffman-Delbruck equation, this was able to estimate the values for viscosity of the SLBs, which allowed for the understanding of ligand mobility in the context of SLB viscosity. The degree of functionalisation of the SLBs was quantified via quantitative fluorescence microscopy (QFM) and it was established that the amount of neutravidin present on the surface was within the range estimated from the cross-sectional lipid area. Further, the stability of the SLBs was determined to be adequate for the purposes of this study, with degradation occurring after 8 days. This chapter has confirmed that the methods employed in this study are appropriate to form continuous and defect-free SLBs, of varying diffusive characteristics, on glass surfaces. Furthermore, the SLBs were shown to have distinct diffusion coefficients and viscosities, each varying by at least an order of magnitude.

The second area of study was to ascertain how the cells responded to the differing ligand mobility, brought on by the differences in viscosity through the lipid bilayers. Despite being naturally non-fouling, SLBs, functionalised with various molecules related to cell-adhesion, have been shown to promote cell binding. Furthermore, the mobility of other surfaces has been shown to have a significant effect on cellular behaviour, with changes in the degree of adhesion and cell spreading noted as the ligand mobility changes. Relating this to the diffusive characteristics of the surfaces, it has also been seen that the size and number of the focal adhesions (FAs), the key binding points of the cell to the surface, decrease inversely with diffusion rate. It was shown that both the SLBs were non-fouling, in initial cellular adhesion studies, and that the inclusion of the RGD cell adhesion peptide rescued cell binding. The overall response was determined to be significantly different between the fluid DOPC and the gel DPPC, with the cell area decreased and circularity increased on DOPC relative to DPPC.

Further, FAs were noted to decrease in size and activity with an increased diffusion rate, in agreement with previously reported findings on related systems. The role of integrins in the cell response was also confirmed with inhibition of RGD-binding integrins. Overall, these findings were related to the diffusive properties, and thus the viscosity, of the SLBs, through the exertion of force on these SLBs; the fluid phase SLB was associated with lower cellular forces, relative to the gel phase DPPC, which was hypothesised to permit higher cellular forces due to the lower rate of diffusion in the SLB.

The third area of study sought to understand how this cell response to these SLBs could be understood on the molecular level, using the SLB viscosity (determinant of the ligand mobility) as the defining property. It has been demonstrated in number of recent studies that the ‘molecular clutch’ model is capable of predicting, with high accuracy, the nature of the cell response to surfaces of different stiffness and topography. Here it was extended further, relating the response of viscosity of the SLBs to the mechanical response of the cell on a molecular level. Initially, the model predicted a response on surfaces that were of significantly higher viscosity (lower diffusion rates) than that estimated by the SD equation. The hallmark indication of the ‘engagement’ of the clutch, retrograde (rearward) actin flow reduced on the higher viscosity DPPC surface, relative to the lower viscosity DOPC, indicating viscosity in the former case was high enough to engage the clutch. Further, these differences were eradicated upon the inhibition of cytoskeletal contractility, with blebbistatin (inhibition of myosin II), or inhibition of FA-actin association, through the vinculin head-only mutant, VD1. Furthermore, clutch predictions relating to the change in adhesion size with ligand density was also confirmed, with DOPC showing no change and adhesion size increasing on DPPC. The discrepancy between the SD predicted values was alleviated with an alternate equation relating the diffusion to the viscosity. The hypothesis was that the binding of cells to the SLBs leads a significant decrease in the viscosity within the cell area, due to integrin bound RGD-lipids acting as ‘roadblocks’ to the diffusion of molecules within the cell area. Beyond the initial adhesion the downstream consequences of the changes in the membrane viscosity was also observed. The mechanosensitive transcription factor, YAP, was seen to localise to the nucleus more in line with viscosity and differentiation was also upregulated on the higher viscosity DPPC.

The final area of study sought to apply the SLBs to a medically relevant context, in the culturing of human mesenchymal stem cells (hMSCs). While SLBs have been used as a model system in determining the mechanobiology of cells, as well as cell culture platforms, their applicability in stem cell culture has few examples. The only previous example of hMSCs on SLBs of varying viscosity found cell behaviour to not fully agree with that expected by the literature and by the current study. Initial analysis of hMSC behaviour on SLBs showed that cell area significantly reduced between 3 and 24 hrs of adhesion. The greatest difference was noted on DPPC, where cells initially spread well, but then lost both cellular and FA area within 24 hrs. Furthermore, cell growth was noted to be minimal on both SLBs. Larger molecules, the full fibronectin protein and the fibronectin III₇₋₁₀ cell binding domain, were biotinylated in an effort to alleviate this. While biotinylation showed no effect on the cell response to these molecules the hMSC behaviour was not changed by their inclusion. The endocytosis of functional molecules was hypothesised to be the likely cause of this change, with lower ligand density on a non-fouling surface preventing any further deposition of cell binding molecules. However, by including a positively charged lipid at varying concentrations in the liposome formulations it was shown that cell adhesion could be promoted in DPPC, despite no change in adhesion on DOPC. This was attributed to an interplay between the electrostatic attraction of the positively charged surface for the negatively charged cell membrane, and the diffusion of the SLBs. It is possible that the higher diffusion of the DOPC reduced the binding strength of the cells, negating the electrostatic attraction. However, the slower diffusion in DPPC allowed for successful electrostatic-based adhesion of cells. This type of adhesion is supported by the observation that no significant difference in FAs were seen between any of the surfaces, indicating that the association is not integrin mediated. Importantly, the cells also show no loss in cell area after 24 hrs, demonstrating a potential of this system adjustment in future work.

CONTENTS

Abstract	2
Author's Declaration	10
Acknowledgements	11
Publications and Conference Proceedings.....	13
Publications.....	13
Conference Proceedings	13
List of Tables	14
List of Figures.....	15
List of Abbreviations	27
1. Introduction	28
1.1. The Role of Biomaterials	30
1.1.1. An Overview of Biomaterials.....	30
1.1.2. The Effect of Surface Mobility on the Cell Response	34
1.2. Molecules and Processes Dictating the Cellular Response.....	38
1.2.1. The Extracellular Matrix	39
1.2.2. Integrins and the Focal Adhesion Complex.....	41
1.2.3. The Molecular Clutch.....	46
1.2.4. Downstream Cellular Signalling and Cellular Behaviour	48
1.3. Lipid Systems: Their Properties and Applications	49
1.3.1. The Phase Transition.....	51
1.3.2. Production of Surface Supported Lipid Systems.....	53
1.3.3. Understanding the Diffusive Characteristics of Supported Lipid Bilayers	58
1.3.4. Supported Lipid Bilayers in Cell Studies.....	61
1.4. The Current Work	65
1.4.1. Thesis Aims	65
1.4.2. Thesis Outline	65
2. Methods & Materials	67
2.1. Lipid Preparation and Vesicle Production	67
2.1.1. Preparation of Lipid Solutions.....	67
2.1.2. Rehydration and Production of Small Unilamellar Lipid Vesicles	68
2.2. Preparation of Glass Surfaces	69
2.2.1. Glass Preparation for Fixed Cell Experiments.....	70
2.2.2. Glass Preparation for Live Cell Experiments.....	70
2.3. Production of PDMS Wells	70

2.4. Production of Supported Lipid Bilayers and Glass Control	71
2.4.1. Production of Supported Lipid Bilayers	71
2.4.2. Production of RGD-Glass Control.....	72
2.5. Functionalisation of Surfaces	73
2.5.1. Functionalisation Calculations and Protocols	73
2.5.2. Biotinylation of Extracelluar Matrix Proteins	74
2.5.3. Quantification of Biotinylation	75
2.5.4. Determining Properties of Biotinylated Proteins	76
2.6. Atomic Force Microscopy	77
2.6.1. Setup and Calibration	77
2.6.2. Imaging Mode	78
2.6.3. Force Mapping Mode.....	78
2.7. Quantitative Fluorescence Microscopy	79
2.7.1. Standard Solutions	79
2.7.2. Bulk Calibrations	79
2.7.3. Bilayer Calibration and Determination of Molecular Density	80
2.8. Fluorescence Correlation Spectroscopy	80
2.9. Cell Culture & Staining	82
2.9.1. Cell Culture	82
2.9.2. Antibodies	83
2.9.3. Adhesion of C2C12 Mouse Myoblasts	83
2.9.4. Differentiation of C2C12 Mouse Myoblasts	85
2.9.5. C2C12 Cell Transfection.....	85
2.9.6. Live Cell Imaging of Actin Flow.....	86
2.9.7. Modelling the Cell Response	87
2.10. Data Analysis.....	87
2.10.2. Focal Adhesion Quantification	88
2.10.3. Statistical Analysis	89
3. Production and Characterisation of Differentially Mobile Surfaces	90
3.1. Introduction.....	90
3.2. Production of Differentially Mobile Supported Lipid Bilayers	92
3.3. Diffusion of Supported Lipid Bilayers	98
3.4. Functionalisation of Surfaces	101
3.4.1. Functionalisation of a Glass Control	101
3.4.2. Quantification of Surface Ligand Density	103
3.5. Stability of Supported Lipid Bilayers.....	106
3.6. Conclusions	109

4. Determining Cellular Behaviour in Response to Changes in Ligand Mobility	110
4.1. Introduction	110
4.2. Cellular Behaviour on Supported Lipid Bilayers	112
4.2.1. Early Cell Adhesion	112
4.2.2. Cell Spreading and Morphology	114
4.3. Ligand Mobility Dependent Changes in Focal Adhesions	117
4.4. Conclusions	123
5. Understanding the Nature of the Response to Viscosity and Ligand Mobility	124
5.1. Introduction	124
5.2. Applying the Molecular Clutch to Ligand Mobility/Surface Viscosity	126
5.2.1. Modelling the Molecular Clutch for Ligand Mobility/Surface Viscosity	126
5.2.2. Viscosity Dependent Changes in Actin Flow	131
5.2.3. Confirming Model Predictions in Response to Ligand Density	138
5.3. Downstream Effects of Ligand Mobility/Surface Viscosity	143
5.3.1. Viscosity Dependent YAP Localisation	144
5.3.2. Controlling Differentiation Through Viscosity	146
5.4. Conclusions	149
6. Supported Lipid Bilayers for Mesenchymal Stem Cell Culture	151
6.1. Introduction	151
6.2. Adhesion and Growth of Mesenchymal Stem Cells on RGD Functionalised Supported Lipid Bilayers	153
6.2.1. Adhesion of Mesenchymal Stem Cells	153
6.2.2. Growth of Mesenchymal Stem Cells	157
6.3. System Development	161
6.3.1. Presenting Proteins and Protein Fragments	161
6.3.2. Positively Charged Supported Lipid Bilayers	166
6.4. Conclusions	174
7. Conclusions and Future Perspectives	176
7.1. Conclusions	176
7.1.1. Production and Characterisation of Supported Lipid Bilayers with Defined Diffusive Properties	176
7.1.2. Determining and Understanding the Nature of the Cell Response	177
7.1.3. Applying Supported Lipid Bilayers to Biomedical Applications	180
7.2. Future Perspectives	182
7.2.1. Bilayer Modifications	182
7.2.2. Understanding Cell-Surface and Cell-Cell Interactions	184
7.2.3. Applications in Cell Differentiation	185

8. Appendix A – Description of the Molecular Clutch Model.....	186
9. References.....	188

AUTHOR'S DECLARATION

“I declare that, except where explicit reference is made to the contribution of others, this thesis is the result of my own work and has not been submitted for any other degree at the University of Glasgow or any other institution”

Mark Bennett

ACKNOWLEDGEMENTS

I have met and worked with so many amazing people during my time as a PhD student, so I apologise to anyone I have missed; know that I am forever grateful.

I would first like to acknowledge and thank both of my supervisors: Manuel Salmerón-Sánchez and Julien Reboud. Initially, with giving me the opportunity to undertake my PhD under their supervision, but also for their continued guidance and support through the course of it. I could not have asked for better, more dedicated people to oversee my work. My special thanks also goes to Dr Marco Cantini, who was instrumental in his help throughout the course of this work. His humour and optimism were key in dragging me through the more difficult parts of the project.

I would also like to thank all the members the Microenvironments for Medicine group for their help and support through the years. While we started off rather small, there are now far too many names, but I would like them to know that I have not before encountered a friendlier, more welcoming and positive lab environment. I think that without them and the overall attitude of the lab I would not have made it through to the end of my work, and for that I am eternally grateful. I would also like to mention my thanks and gratitude for the members of Professors Pere Roca-Cusachs and Xavier Trepat's lab at IBEC in Barcelona for making me feel so welcome and helping me in my brief time there. My special thanks go to Prof. Pere Roca-Cusachs, for his passionate and positive support with my work, and to Victor González-Tarragó, my guide to all things Catalanian.

I would be remiss by not thanking all the members of the Student Learning Service team, now the Learning Enhancement and Academic Development Service, here at Glasgow University. While I am hugely grateful they employed me as a teaching assistant during my PhD, I am more grateful for how working with such a gifted and dedicated group changed my outlook and approach to work for the better. To Dr. Scott Ramsay and Dr. Carol Collins, better managers

could not be hoped for. It is without a doubt because of the wonderful people in this team that I would not have had such rewarding and fantastic opportunities during my time at Glasgow.

To my friends and family I also thank you all. To my parents, who have always told me exactly what I needed to hear; your help and support has been and always will be a welcome part of my life, even when you remind me I haven't paid any tax in 29 years. To my 'little' brother and littler sister, the trips home would not have been the same without the inundation of YouTube videos the minute I arrived. To all my friends outside the PhD, thank you; it's very easy to become obsessed with research and having you has kept me grounded. To Ricky and Jake, my semi-illegal flatmates, I still think the IPL and the darts are dull, but the PhD would not have been anywhere near as fun without both of your shenanigans.

Finally, but by no means least, my partner Katy, I could not have achieved any of this without you. The man I am today is down to you; your constant drive and dedication gave me an example to strive towards. You helped me enjoy the good times and got me through the bad, of which there were more than a few. The last four years with you have been amazing and here's to countless more.

PUBLICATIONS

1. Bennett M, Cantini M, Reboud J, Cooper JM, Roca-Cusachs P, Salmeron-Sanchez M. Molecular clutch drives cell response to surface viscosity. *Proceedings of the National Academy of Sciences*. 2018 Jan 22;201710653.
2. Zhao M, Altankov G, Grabiec U, Bennett M, Salmeron-Sanchez M, Dehghani F, Groth T. Molecular composition of GAG-collagen I multilayers affects remodeling of terminal layers and osteogenic differentiation of adipose-derived stem cells. *Acta biomaterialia*. 2016 Sep 1;41:86-99.
3. Bathawab F, Bennett M, Cantini M, Reboud J, Dalby MJ, Salmerón-Sánchez M. Lateral chain length in polyalkyl acrylates determines the mobility of fibronectin at the cell/material interface. *Langmuir*. 2016 Jan 7;32(3):800-9.

CONFERENCE PROCEEDINGS

1. Bennett M, Cantini M, Reboud J, Cooper JM, Roca-Cusachs P, Salmeron-Sanchez M. “*The Molecular Clutch Drives Cell Response to Surface Viscosity.*” FEBS Workshop: Biointerfaces, Sant Feliu, Spain, June 2017
2. Bennett M, Cantini M, Reboud J, Salmeron-Sanchez M. “*Mobility Dependent Cellular Behaviour on Supported Lipid Bilayers.*” Bionterfaces International, ETH Zurich, Zurich, August 2016
3. Bennett M, Bathawab F, Cantini M, Reboud J, Dalby MJ, Salmerón-Sánchez M. “*Lateral chain length in polyalkyl acrylates determines the mobility of fibronectin at the cell/material interface.*” TCES Conference, Southampton, UK, July 2015.

LIST OF TABLES

Table 1.1. Lipids commonly used to produce lipid bilayers, with their phase transition temperature, T_m , demonstrating the importance of the structure to the point at when the lipids change from fluid to gel phase. (All images taken from Avanti Polar Lipids website).	52
Table 2.1. A list of antibodies used to stain for proteins of interest.	83
Table 2.2. The conditions required to transfect C2C12 cells with plasmids of interest. The stars indicated deviation from the provided protocol, which required 5×10^6 cells/ml in a 10 μ l tip. However, the cell density was increased by approximately 10x to account for the larger, 100 μ l tips used.	86
Table 3.1. A summary of the attained values of the DOPC and DPPC diffusion coefficients as determined by FCS, and the resulting, viscosity values, calculated by the SD equation.	101
Table 3.2. Predicted density of neutravidin adsorbed to the surface, based upon the amount of binding events on one neutravidin molecule.	105
Table 5.1. Statistical values comparing the cell and FA area on each ligand density when comparing DOPC to DPPC. P values indicating significance, ns > 0.05, ** \leq 0.01, **** \leq 0.0001.	142
Table 5.2. Statistical comparison between of the cell and FA area ligand density changes on each of the SLBs. P values indicating significance, ns > 0.05, ** \leq 0.01, **** \leq 0.0001.	142

LIST OF FIGURES

- Figure 1.1. The Effects of Biomaterials.** A summary of the effects of biomaterials on the cell behaviour, such as spreading, shape, adhesion and differentiation are affected by factors, such as: (A) stiffness, which allows for greater cell spreading on surfaces of higher stiffness (34); (B) topography, which can change a cell's ability to spread and survive (13); (C) chemistry, which can promote specific differentiation to specific lineages of capable cells (49); (D) mobility, which can control cellular adhesion, spreading and differentiation (52). Together these examples, show the multitude of cell responses that can be tuned by controlling the nature of the biomaterial that is used. Figure reproduced with permission. **33**
- Figure 1.2. The Extracellular Matrix and Fibronectin.** (A) The cells reside in a heterogeneous environment of varying physical and chemical properties, with different proteins, at different densities, presenting different ligands, as well as other soluble molecules used for cell signalling. (B) A schematic representation of FN, the repeats shown in blue (type I), brown, (type II) and green (type III). The binding domains for different molecules are indicated above the associated areas. Binding sites for the specific integrins are shown below the associated areas. Alternatively spliced extra-domains are also shown (B, A, a variable region; V) (93). (C) Shows the RGD tripeptide, present in the III₁₀ repeat of the fibronectin and responsible for the binding of the cell to the protein (taken from Sigma-Aldrich website). **40**
- Figure 1.3. Integrins.** Summary of the different integrin subunit combinations and their specificity for cell adhesive molecules. Highlighted here are the integrins specific for RGD, as this is the molecule used to bind cells in this project. (Adapted from Barczyk et al 2010 (17)) **43**
- Figure 1.4. Focal Adhesions and the Actin Cytoskeleton.** While integrins bind to the cell surfaces step 1 is the myosin-II generated forces, which can affect the multitude of adaptor proteins. These can include actin-linking modules (such as talin), signalling molecules (such as FAK) and actin-polymerising module (such as zyxin). In step 2 the overall response of these modules to the mechanical properties of the network, in conjunction with the actin cytoskeleton, defines the mechanical response. This leads to step 3, whereby the signalling module, activates downstream G-proteins, such as Rho. **45**

These have a significant effect actin-polymerisation and contractility (step 4), thus modulating the activity of the force-generating apparatus of the cell (step 5). (Adapted from Geiger et al (18)).

Figure 1.5. The Molecular Clutch. (A) A schematic representation of the model that ties the response of the cell to the nature of the surface. Applied to stiffness the model dictates that the actin cytoskeleton must be linked to the surface via an ECM-integrin-talin clutch, which can engage upon the exceeding of a force threshold. (B) Shows average lifetime of FN- $\alpha_v\beta_3$ as a function of force (red points) and the average unfolding lifetime of talin (a proposed clutch molecule (blue line)). This demonstrates that at lower forces ECM-integrin bonds unbind faster than talin can unfold; however, higher than the threshold force (grey dashed line) the talin unfolds faster (adapted from Eloegui-Artola et al., 2016 (47)). (C) Shows the resulting change in the localisation of the nuclear transcription factor, YAP, to the nucleus to a greater extent on surfaces of greater stiffness (21). 47

Figure 1.6. Lipids and the Phase Transition. (A) The amphipathic structure of a lipid, showing the hydrophilic head group and hydrophobic tail. Together these lead to the spontaneous self-assembly into structures such as unilamellar or multilamellar vesicles, or bilayers, based on their intrinsic properties. (B) Shows an example structure of the phospholipid, DOPC, a commonly used lipid, and one of particular importance in this study. The hydrophobic and hydrophilic regions are noted, with double bond present in each of the tail groups. (C) Shows the nature of the phase transition and the change in structure that occurs upon the exceeding of the temperature, T_m , characteristic of each specific lipid. This leads to a melting of the carbon chains and reduction in the order of the lipid packing, increasing the fluidity. 50

Figure 1.7. Supported Lipid Systems. A schematic summary of the different types of lipid systems that can be deposited on a solid support for various applications. (A) Shows a free-standing bilayer; (B) a supported lipid bilayer, as used in this study; (C) shows a polymer cushioned lipid bilayer, with (D) showing a similar construct of a polymer tethered bilayer; (E) shows a vesicle presenting bilayer, which has applications in drug delivery systems and (F) shows a supported vesicular layer. While not all of these are widely used, they exemplify the types of systems at a researcher's disposal. (Adapted from (64)). 54

Figure 1.8. Formation of Supported Lipid Bilayers. The process of vesicle deposition, leading to the formation of SLBs. Initially, vesicles adsorb to the surface e.g. glass, mica, gold etc. In (A) the vesicle solution is added to the surface. The buffer is important, due to the electrostatic interactions, as well as the osmotic pressure caused. These vesicles may contain a number of modifications, including fluorescence or functional groups; however, these may change the vesicle-vesicle and surface-vesicle interactions. In the (B) the vesicles adsorb to the surface and, depending on the nature of the interaction, either remain as intact vesicles or, as in (C), spontaneously rupture and form a single bilayer. This latter event depends on variables, such as the vesicle concentration, the vesicle-surface interactions, the vesicle-vesicle interactions and the vesicle buffer interactions. The proximal and distal leaflets can have different physical properties, such as diffusion coefficients, due to the proximity of the proximal leaflet to the surface and the interstitial water layer (blue). 57

Figure 1.9. Measuring Diffusion in Supported Lipid Bilayers. (A) FRAP: A high intensity laser excites the fluorophores in a given area to the point of bleaching. The rate at which the fluorescence returns is dependent on the diffusion of the bilayer and the area bleached. (B) FCS: Fluorophores in the bilayer are illuminated as they pass through an illumination volume. The photon residence time and thus the decay in the autocorrelation function (relating the probability of two events being a single photon), thus the decay is dependent on the diffusion. (C) FLIM: The lifetime of the fluorophore in the excited state is dependent on the rotation within its environment. This can be related to the viscosity using standard of known values. The viscosity can then be related to the diffusion, through the Saffman-Delbruck equation. 59

Figure 2.1. Extrusion. The Avanti mini-extruder system, showing the means of assembly for the system. (Image taken from the website of Avanti Polar Lipids (178)) 69

Figure 2.2. Experimental Setup. The dimensions of the PDMS wells used to produce SLBs. All measurements are to scale. 71

Figure 2.3. Protein Biotinylation. The process used by the EZ-link biotinylation kit, through the NHS ester-based linking of biotin molecules to primary amines on the protein of interest (image taken from product datasheet provided by Thermo (183)). 75

Figure 2.4. Analysis of Focal Adhesions Flow Chart. A small area of the cell is expanded for detail. Steps (1) and (2) were performed with the settings shown in Table 88

2.2. Steps (4) and (5) were set in light of the experimental conditions and maintained at a constant setting throughout the analysis of the experimental data set. To this end, exposure times during imaging was also kept constant. In step (6) only particles above $0.75 \mu\text{m}^2$ were counted as focal adhesions.

Figure 3.1. Lipid Vesicle Extrusion. Measuring the size of vesicles of (A) DOPC and (B) DPPC both before and after extrusion through membranes of differing pore sizes, using dynamic light scattering (DLS). (C) Shows the resulting average diameter of lipid vesicles, including the mean hydrodynamic vesicle diameter above each column for clarity. 92

Figure 3.2. Glass and SLB Surfaces. The images show the cleaned glass surfaces both before and after incubation with either DOPC or DPPC as measured using AFM contact mode imaging. This lack of contrast demonstrates the contiguous nature of the SLBs, with a minimal presence of defects (Scale Bar = $2 \mu\text{m}$). 94

Figure 3.3. Schematic Representation of Force Spectroscopy of SLBs. (A) The tip approaches the surface during the cantilever approach. (B) As the tip approaches and interacts with the SLB the vertical deflection increases until (C) the tip eventually breaks through the packed lipid and (D) contacts with the glass surface. (E) Shows a representative force map and the curves generated; in this $8 \times 8, 10 \mu\text{m}^2$ map the cantilever pushes on the surface in each square generating the force curves shown in (A) – (E). As the curves are indicative of interaction with the SLB, the thickness can be determined between the points shown. (All forces curves shown here are taken from those attained in the measurement SLBs and are representative of that which was obtained) 95

Figure 3.4. Supported Lipid Bilayer Thickness. Force mapping, as shown in Figure 3.3E produced a series of multiple force curves for each SLB, which was categorised into bins of 1 nm thickness. The relative percentage frequency of these values for DOPC and DPPC is shown here, with a gaussian fit to determine the average thickness. 98

Figure 3.5. Schematic Representation of Fluorescence Correlation Spectroscopy. (A) Shows the illumination of the fluorophores within the confocal volume, which is then detected by the avalanche photodiode (APD). The photon count signal over time (B) is then correlated to one another showing a decay in the correlation over time (C). 99

This can be used to calculate the diffusion coefficient if the beam radius is known from previous calibrations. (Adapted from 212)

Figure 3.6. Diffusion in SLBs. (A) & (B) Show the correlation curves produced by the diffusion of fluorophores through the FCS confocal volume in DOPC and DPPC respectively. (C) Shows the resulting diffusion coefficients of DOPC and DPPC SLBs, calculated using the equations shown in section 2.8, (Inset – FITC bead calibration used to determine beam width, required to calculate the diffusion coefficient). **100**

Figure 3.7. Functionalisation of Glass with RGDStatic Water Contact Angle (WCA). (A) Shows a schematic of the progressive functionalisation of glass leading to RGD being presented on the surface. (B) Shows the WCA after RCA cleaning and (C) shows the WCA after silanisation with APTMS, demonstrating the change in surface hydrophobicity upon incubation with this silane. (D) and (E) show the fluorescence histogram before and after functionalisation with neutravidin, respectively (insets show representative images; scale bar = 25 μm). **102**

Figure 3.8. Quantitative Fluorescence Imaging (QFI) Calibration. Determination of the amount of protein per μm^2 on a bilayer sample by first determining a scaling factor (F) between the linear gradients of bulk solutions of (A) protein (in this case neutravidin) and (B) lipid vesicles (DOPC). This scaling factor is then applied to the linear gradient of fluorescent lipids in a bilayer (C), which can then be used to determine fluorescence as an amount of protein molecules per μm^2 (D). **104**

Figure 3.9. QFI of DOPC and DPPC SLBs. (A) and (B) show the DOPC and DPPC SLB intensity histograms upon increasing surface density of functionalised lipid (0.4, 2 and 10 mol% of biotin-lipid); the corresponding representative images are colour-coded to the relevant concentration (scale bar = 25 μm^2). (C) Shows the calculated amount of neutravidin molecules per μm^2 and (D) shows the extrapolated surface density of the neutravidin molecules. **106**

Figure 3.10. Bilayer Stability over Time. An image series of the bilayer over a period of 15 days, showing the overall coverage and stability of SLBs in cell culture conditions. The red box highlights ROI 1, an indicator of the bleaching of the DPPC surface after 15 days, indicating that the SLB is still present, with defects. **108**

Figure 4.1. Initial Cellular Adhesion. The interaction of cells with the lipid surfaces was seen to be minimal without RGD being present at 3 hours. Upon functionalisation **112**

with RGD, at 2 mol% functionalised lipid, cell adhesion was seen to be comparable to that of the RGD-Glass control. P values indicating significance, * \leq 0.05, **** \leq 0.0001.

Figure 4.2. Morphology Dependence on Ligand Mobility. (A) Shows the average cell area on DOPC (high ligand mobility, low viscosity) and DPPC (low ligand mobility, high viscosity), with (B) showing their characteristic circularity. (C) – (E) are representative images of the cells on DOPC, DPPC and RGD-Glass respectively. (Scale Bar = 25 μ m). P values indicating significance, ** \leq 0.01, **** \leq 0.0001. 114

Figure 4.3. Inhibition of $\alpha_5\beta_1$ and $\alpha_v\beta_3$ Integrins. (A) Shows an array of the representative images of cells incubated with one or both inhibitors for $\alpha_5\beta_1$ and $\alpha_v\beta_3$ integrins on surfaces of all ligand mobility values. (B) Shows the consequent quantification of these images in terms of the change in cell area upon inhibition on each of the surfaces P values indicating significance, * \leq 0.05, ** \leq 0.01, **** \leq 0.0001. 116

Figure 4.4. Focal Adhesion Changes in Response to Ligand Mobility. (A) – (C) Show representative images of the cells on DOPC, DPPC and RGD-Glass respectively with actin stained in green, and vinculin stained in red. (D) Shows the average size of the focal adhesions on the each of the surfaces with (E) showing the number of focal adhesions per cell. (Scale Bar = 25 μ m). P values indicating significance, ** \leq 0.01, **** \leq 0.0001. 118

Figure 4.5. Focal Adhesion Distribution. The distribution of FAs is shown here on the each of the surfaces. In the analysis the minimal size of the FAs was set to 0.75 μ m; as such, the initial bin was set to 1 μ m, with a bin width of 0.5 μ m. 119

Figure 4.6. Phosphorylation of FAK in Response to Ligand Mobility. (A) – (C) Show representative images of pFAK present in the cells seeded on DOPC, DPPC and RGD-Glass respectively. (D) Shows the integrated density of the pFAK within the cell area. (Scale Bar = 25 μ m). P values indicating significance, * \leq 0.05, **** \leq 0.0001. 121

Figure 4.7. Protein Activation in Response to Ligand Mobility. The schematic shows a proposed effect of the viscosity-defined ligand mobility on the FA proteins present in the complex; as viscosity increases and ligand mobility decreases, the assumed amount of force increases. (A) Shows how mechanical force is capable of exposing phosphorylation sites present in FAK, leading its conversion to pFAK and its consequential activation. (B) Shows that mechanical pulling of adaptor proteins linking integrins, and thus the surface, to the actin cytoskeleton leads to the exposure of 122

vinculin binding sites on proteins such as talin. Vinculin can then subsequently bind to F-actin as well as other signalling molecules.

Figure 5.1. Cell Response to Viscosity through the Molecular Clutch. The speed of actin retrograde flow is controlled by the myosin motors. If the ECM-integrin bond lifetime is of sufficient length then the force exerted on the talin by the actin flow allows for the unfolding of talin at a specific rate. This unfolding leads to force enhancement through stabilisation of the talin-actin linkage through molecules, such as vinculin (adapted from Elsogui-Artola et al. (2016) (47)).

Figure 5.2 Model Predictions of the Effect of Viscosity. The left y-axis (blue) shows the predicted effect of the viscosity on the actin flow with a reduction in flow seen at approximately 10^{-4} N.s/m. The right y-axis (red) shows the adhesion growth upon and increase in the viscosity of the surface, being seen to increase from a lower viscosity than that of the actin flow. Model data provided by Prof. Pere Roca-Cusachs of IBEC, Barcelona.

Figure 5.3. Changes in Characteristic Length Affect Viscosity. This graph demonstrates how the alternative equation presented by Gambin et al., (13) predicts changes in viscosity on the degree to which the membrane is perturbed by the diffusing molecule. This was predicted for both DOPC (blue) and DPPC (red). The two data points show a characteristic length of the same scale as the average cell radii on each of the SLBs, estimated from Figure 4.2. These gives values in the ranges of 10^{-5} and 10^{-4} Pa.s.m for DOPC and DPPC respectively, with the latter in the range of detectable viscosity as predicted by the molecular clutch model.

Figure 5.4. Viscosity Dependent Actin Flow. Due to the importance of the actin flow in the molecular clutch model the viscosity dependent actin flow was determined on the surfaces. (A) Shows an example kymograph taken from an image stack (1Hz for 2 min). By selecting a region of interest, the image in the region can be re-stacked to show how the fluorescence changes position with time. By taking the $\tan \theta$ of the angle this displacement the speed of the actin flow can be determined. This is shown in (B) where the actin flow on each of the surfaces is shown. This shows that the actin flow is lower on surfaces that exhibit lower or no viscosity. (C) Shows representative images of the cells on each of the surfaces, with the insets showing the relevant

kymograph of each selected region. (Scale Bar = 25 μm). P values indicating significance, **** ≤ 0.0001 .

Figure 5.5. Actin Flow upon Myosin II Inhibition (A) Shows the mode of action of 134
the myosin II inhibitor, blebbistatin, which blocks the activity of myosin II rather than
its binding to F-actin. (B) Shows the consequent effect of the blocking of myosin II on
surfaces of differing viscosity, where the actin flow rate was the not statistically
significant between any surface. (C) Shows the representative images of cells and their
corresponding kymographs used to determine the actin flow. (Scale Bar = 25 μm). P
values indicating significance, **** ≤ 0.0001 .

Figure 5.6. Actin Flow upon Vinculin Inhibition. (A) Shows, schematically, the 135
mode of action of VD1, which blocks force enhancement upon substrate binding by
preventing the binding of native vinculin. Subsequently, it does not have tail domain
through which to bind to F-actin and thus stabilise the talin-mediated link between
integrins the cytoskeleton. (B) Shows the consequential effect of transfection of
C2C12 cells with VD1, whereby there are no observed differences between the actin
flow on any of the surfaces. (C) Shows representative images of cells and kymographs
used to determine the difference in actin flow rate in cells on the each of the surfaces.
(Scale Bar = 25 μm). P values indicating significance, ns > 0.05 .

Figure 5.7. Focal Adhesion Properties upon VD1 Transfection. (A) Shows the 137
quantified average FA area in cells (after 3 hrs, as in Chapter 4) on each of the surfaces
in native, wild-type cells and those transfected with the VD1 plasmid; statistical
analysis through two-way ANOVA showed that there was no difference in FA
properties between native and VD1 cells on each surface. (B) Shows the representative
images used to determine the FA properties, with native cells (VD1 –ve) being stained
with anti-vinculin monoclonal antibodies. The vinculin head domain encoded by the
VD1 plasmid (VD1 +ve) is fluorescent and was not stained for vinculin. (Scale Bar =
25 μm). P values indicating significance, ns > 0.05 .

Figure 5.8. Schematic of Cell Behaviour in Response to Surface Viscosity. In 138
DOPC, on the left, the pulling of actin on the RGD ligand through a talin-integrin
linkage, displaces the ligand to a large extent, DH, meaning that the force loading rate
is low on molecules such as talin. Therefore, in the case of talin, this prevents, unfolding
and so the binding of vinculin and formation of FAs. In DPPC, on the right, the higher
viscosity means that ligand displacement is smaller, DL, when actin pulls on the

surface. This, in turn, means that the force loading rate on the talin is higher, allowing unfolding within the integrin-RGD bond lifetime. Vinculin can then bind to exposed sites, thus leading to greater forces exerted on the surface and FA formation.

Figure 5.9. Model Prediction of Adhesion Size as Ligand Number Increases. By taking the model at viscosity values where the clutch is and is not ‘engaged’ the change in adhesion size can be predicted. At high viscosity (after engagement, 10^{-2} N.s/m) the number of ligands was seen to increase up to a specific ligand density (~50) and then decreases above this. At low viscosity (before engagement, 10^{-5} N.s/m) the adhesion size shows no change regardless of the number of ligands. Model data provided by Prof. Pere Roca-Cusachs of IBEC, Barcelona. **139**

Figure 5.10. The Change in Cell and Focal Adhesion Size with Ligand Density. (A) Shows the representative images of the actin and vinculin stains on DOPC at 0.02, 0.2, 2 and 10 mol% of functionalised lipid. The distribution of FA area on these surfaces is shown to the right of these images, demonstrating that this is similar on all surfaces. (B) Shows this on the DPPC, with the consequent change in the FA distribution as the ligand density changes. (C) Shows the change in average cell area on each SLB as the ligand density changes, and (D) shows the change in FA area under the same conditions. (Scale Bar = $25\mu\text{m}$). **141**

Figure 5.11. YAP Localisation in Response to Viscosity. (A) – (C) Show the representative images of the YAP staining, demonstrating the extent of its localisation to the nucleus on DOPC, DPPC and RGD-Glass respectively. For clarity, on DOPC (A) the location of the nuclei in each cell is indicated by the red-dashed circles. (D) Shows the attained fluorescent intensity in nucleus compared to the cytoplasm immediately surrounding it in all surfaces. (Scale Bar = $50\mu\text{m}$). P values indicating significance, $**** \leq 0.0001$. **145**

Figure 5.12. Viscosity Dependent Differentiation. (A) Shows the early stages of differentiation of C2C12s, after 2 days, on each of the surfaces through determining the percentage of nuclei staining positive for the transcription factor, myogenin. (B) Shows the terminal differentiation of C2C12s, after 4 days, by the percentage of nuclei within the sarcomeric positive cells. (C) Shows the representative images of stained cells at both of these time points. (Scale Bar = $150\mu\text{m}$). P values indicating significance, $*** \leq 0.001$, $**** \leq 0.0001$. **148**

Figure 6.1. hMSC Adhesion of 3 and 24 Hours. (A) Shows the representative images 153
the area of hMSCs on all surfaces, after 3 hrs and 24 hrs of cell culture (Scale Bar =
150 μm). (B) Shows the quantification, demonstrating that there is a reduction in cell
area at 24 hrs compared to 3 hrs on all surfaces to differing degrees. (C) Shows the
percentage reduction in cell area between 3 and 24 hrs, demonstrating that cells lose a
large percentage of area on both DOPC and DPPC, with a smaller reduction on the
RGD-Glass control. P values indicating significance, * ≤ 0.05 , **** ≤ 0.0001 .

Figure 6.2. Focal Adhesion Area at 3 & 24 hrs on hMSCs. (A) Shows the 155
representative images of FAs, as stained for by vinculin on hMSCs seeded on DOPC,
DPPC and RGD-Glass surfaces after 3 and 24 hrs of adhesion, demonstrating both the
lack of change in the FAs on DOPC and RGD-Glass, and the significant difference on
DPPC (Scale Bar = 25 μm). (B) Quantifies the area of the FAs over all surfaces and
time points, showing that only DPPC has a significant difference in FA area between 3
and 24 hrs. P values indicating significance, ns > 0.05 , ** ≤ 0.01 .

Figure 6.3. Proliferation of hMSCs on SLBs. (A) – (C) Show representative images 157
of cells grown for 1 day on DOPC, DPPC and RGD-Glass respectively, with the nuclei
shown in cyan and the BrdU shown in red. The nuclei where there was BrdU present
were considered new cells (Scale Bar = 100 μm). (D) Shows the resulting quantification
of % of nuclei staining positively for BrdU, indicating that they are cells that have
grown after seeding on the surface rather than in culture. P values indicating
significance, ns > 0.05 , **** ≤ 0.0001 .

Figure 6.4. Cell Morphology after 5 Days. (A) – (C) Show hMSCs on DOPC, DPPC 159
and RGD-Glass respectively after 5 days of culture in growth media. The dashed line
represents the estimated seeding density. It is noted that the cells on DOPC exhibited a
more spread morphology than previously seen, whereas cells on DPPC appeared
rounded as noted after 24 hrs of culture. (Green = actin, cyan = nuclei, scale bar = 50
 μm). (D) Shows the cell number after 5 days, confirming results shown in Figure 6.3
that shows minimal cell growth on bilayers.

Figure 6.6. Biotinylation of Proteins. (A) Shows a schematic representation of the 162
full fibronectin protein. The * under each module indicates how many lysine residue
there are in each, giving an indication as to how many available binding sites there are
for the NHS-biotin across the entire molecule, as well as the within the FNIII₇₋₁₀
fragment (indicated in brackets). The RGD containing III₁₀ module is indicated by a

red outline. The number of biotins per molecule was calculated to be approximately 1 for the FNIII₇₋₁₀ fragment and ~6 for full fibronectin. (B) & (C) Show the effect of biotinylation of protein on C2C12 cells by determining the cell area and focal adhesion area respectively. In all cases cells were more spread and had larger focal adhesions on the proteins (coated on glass surfaces) compared to plain glass. In the case of FAs there was no difference between the areas on all proteins. (D) Shows the representative images of cells on each surface. P values indicating significance, ns > 0.05, ** ≤ 0.01, **** ≤ 0.0001.

Figure 6.7. Protein on SLBs. An ELISA showing the relative amount of biotinylated protein adsorbed onto the DOPC (blue) and DPPC (red) surfaces. In all cases there was no significant differences in adsorption regardless of the SLB or the protein used. **164**

Figure 6.8. Protein Functionalised SLBs. (A) Shows the quantification of the cell area on DOPC, DPPC and glass, with the presentation of RGD peptide, FNIII₇₋₁₀ protein fragment, and FN full protein after 24 hrs. (B) Shows the representative images of cells on each of the surfaces (green = actin, nuclei = blue, Scale Bar = 150 µm). On DOPC functionalised with FNIII₇₋₁₀ no cells were noted to bind on any sample. P values indicating significance, ns > 0.05, * ≤ 0.05. **165**

Figure 6.9. Non-specific Binding of C2C12s to SLBs. Using DOPC, this graph shows that the cells bind to avidin regardless of functionality. However, removing the deglycosylated form, neutravidin, used throughout this thesis shows no binding without RGD present. P values indicating significance, ns > 0.05, **** ≤ 0.0001. **167**

Figure 6.10. Adhesion to SLBs Containing Positively Charged Lipid. (A) Shows the structure of the DOTAP (1,2-dioleoyl-3-trimethylammonium-propane) molecule. (B) Shows the number of hMSCs adhered per mm² as the mol% of the positively charged DOTAP is changed in both DOPC and DPPC (mol% of DOTAP is indicated by the number after the surface identifier). It also shows the cells adhered when fibronectin (FN) is allowed to adsorb on the surface prior to cell seeding (at 20 µg/ml). P values indicating significance, ns > 0.05. **168**

Figure 6.11. Cell Area on DPPC:DOTAP SLBs. (A) Shows the cell area of hMSCs after 3 hours on DPPC, with increasing mol% of DOTAP, with (B) showing the representative images of the surfaces. The effect of FN is also determined with incubation of 20 µg/ml of FN protein prior to cell seeding. (C) Shows the cell area after cells were allowed to adhere and spread for 24 hrs, again with and without prior **170**

adsorption of FN. (D) Shows the representative cell images after 24 hours. In both cases FBS free media was used, to allow for direct comparison of cell behaviour over time, with and without matrix protein. P values indicating significance, ns > 0.05, ** ≤ 0.01, **** ≤ 0.0001.

Figure 6.12. Area Change Between 3 and 24 Hours. This shows the percentage of change in the cell area on the DPPC:DOTAP surfaces between 3 and 24 hrs, when the hMSCs were seeded the SLBs with and without FN. **171**

Figure 6.13. Focal Adhesions on DPPC:DOTAP SLBs. (A) Shows the average area of detected focal adhesions present on the DPPC SLBs, when differing mol% of DOTAP is used. This shows that the concentration of DOTAP has no significant effect on the FA behaviour and any detected FAs are smaller than those seen on glass surfaces, incubated with and without FN. (B) and (C) show representative images of these cells at 3 and 24 hrs respectively. This demonstrates that the presence of a larger, diffuse vinculin background present in the cells on the DPPC:DOTAP SLBs may induce a false positive of FA area. This is contrasted with glass, with shows well-defined FAs. (Scale Bar = 50 µm). P values indicating significance, ns > 0.05, **** ≤ 0.0001. **173**

LIST OF ABBREVIATIONS

hMSC	Human Mesenchymal Stem Cells
ECM	Extracellular Matrix
FN	Fibronectin
FA	Focal Adhesion
MLV	Multilamellar Vesicles
LUV	Large Unilamellar Vesicles
SUV	Small Unilamellar Vesicles
SLB	Supported Lipid Bilayer
SDS	Sodium Dodecyl Sulphate
DOPC	1,2-dioleoyl-sn-glycero-3-phosphocholine
DPPC	1,2-dipalmitoyl-sn-glycero-3-phosphocholine
DOTAP	1,2-dioleoyl-3-trimethylammonium-propane
BODIPY	boron-dipyrromethene
PE	Phosphoethanolamine
DPBS	Dulbecco's Phosphate Buffered Saline
FCS	Fluorescence Correlation Spectroscopy
FRAP	Fluorescence Recovery After Photobleaching
AFM	Atomic Force Microscopy
RGD	Arginine-Glycine-Aspartate
YAP	Yes-Associated Protein
FLIM	Fluorescence Lifetime Imaging
SD	Saffman-Delbruck
NHS	N-Hydroxysuccinimide ester
PDMS	Polydimethylsiloxane
APTMS	(3-Aminopropyl)trimethoxysilane
DMF	Dimethylformamide
BSA	Bovine Serum Albumin
FAK	Focal Adhesion Kinase
WCA	Water Contact Angle
QFM	Quantitative Fluorescence Microscopy

1. INTRODUCTION

Cells, *in vivo*, are surrounded by a vastly complex extracellular environment, with components demonstrating various physical and chemical properties over many scales, from the meso- to nanoscale (1). Healthy human cells, being anchorage dependent, rely on an encompassing protein network, the extracellular matrix (ECM), upon which to proliferate, migrate and differentiate (2). The properties of this network, made up of proteins such as collagen, fibronectin and laminin, is of paramount importance to the cellular behaviour. Depending on the tissue (3), the ECM varies in properties such as relative protein abundance, viscoelasticity and topography (4). In turn, even nanoscale changes in these, as well as other, properties can lead to massive changes in the cellular behaviour; for example, the induction of differentiation (5). Further to these physical properties, the ECM also serves as a reservoir for further molecules responsible for controlling cellular characteristics, such as promoting the proliferation of specific cell types (6). It is from this dizzying array of components and properties that researchers have sought to find inspiration as a means to recapitulate cellular behaviours of interest. Commonly applied to regenerative medicine, a thorough and complete understanding of the cellular microenvironment may, in the future, allow for the replacement of select tissues and even whole organs (7).

Biomaterials, first defined by the National Institute of Health in 1983 (8), are the principal means of recapitulating this structure and function of the cellular microenvironment *in vitro*. These materials may be anything that, “*treats, augments, or replaces any tissue, organ, or function of the body.* (8)” While accurate nearly 35 years ago, this has since expanded to include almost any material that is used in a biological context. To this end, researchers have used naturally derived materials, such as nacre (9), as well as synthetically derived systems (10) applied to wide variety of cell-based systems. In the case of the latter the approaches vary widely, but they can commonly be partitioned into the manipulation of discrete properties, such as viscoelasticity (either as separate components, or as an overall variable), topography and chemistry, as well as a combination of these components. By controlling these properties researchers have been able to use biomaterials to control behaviours such as migration (11), shape (12, 13), forces (14), proliferation (15) and differentiation (16).

Further to this, researchers have taken the opportunity presented by these material-driven changes in behaviour to understand how and why these properties change the cellular behaviour. This stems from the changes induced in cellular processes, by the interfacing of the cell with a specific biomaterial. To sense their environment cells employ integral membrane proteins, integrins, to bind to various moieties presented on the surface; the type of integrin recruited to the site of adhesion is dependent on the nature of the surface (17). This, in turn, recruits further adaptor proteins, which connect the integrin to the actin cytoskeleton (18). Known as focal adhesions (FAs), these large protein constructs are a key means through which cells detect their surrounding environment, the key role being the coupling of the surface to the actin cytoskeleton. These focal adhesions can be made of various components, termed the 'integrin adhesome' (19), and it is this that controls downstream properties of the cells, such as signalling pathways (e.g. ROCK pathway) (20), as well as regulating transcription factors, capable of upregulating or downregulating genes responsible for key cell behaviours (21). It is therefore clear that the physical properties of biomaterials can completely alter the cell response and is therefore of key importance to understand how and why.

To this field of biomaterial-manipulated cell behaviour, enter lipid-based systems. Lipids are a widespread and incredibly varied group of molecules; one of their principal functions in biology is to enclose and separate the cellular components from the extracellular environment (22). Phospholipids account for the majority of the components of the cell membrane, and many of these amphipathic molecules may orient themselves into a single bilayer, enclosing their hydrophobic domains from the surrounding aqueous environment; this envelope contains an array of proteins and carbohydrates responsible for a huge number of cell number processes; for example, adhesion, signalling and exo and endocytosis. Taking advantage of the intrinsic properties of lipid molecules, researchers have successfully used them to produce a number of constructs (23). Prime examples include unilamellar vesicles, which have been used as therapeutic delivery vehicles (24), or bilayers, which are able to serve as non-fouling coatings, membrane mimics or as platforms for biological studies (25, 26). It is the latter's use in cellular studies that is of particular importance here; with their well-defined and easily tuneable properties lipid bilayers are able to present a hugely varied series of molecules and functionalities, which can be used as a means to elucidate hitherto poorly understood cellular processes.

The current work seeks to characterise and develop a deeper understanding of supported lipid bilayers as potential biomaterials. By predominantly using neutral lipid bilayers, this allows for the production of surfaces of varying viscosity, which, in turn, directly controls the lateral mobility of presented ligands and minimising the effect of non-specific binding. How manipulating this core property of lipid bilayers affects the cellular response, can allow for new modality through which cellular behaviour can be controlled. Further to this, the work has also sought to understand this behaviour at a more molecular level. This system has not yet been used to study how viscosity affects the cellular response; beyond this the system can be further manipulated (e.g. inclusion of charge) to further control the cell response. Here the state of the field, as it pertains to biomaterials, is reviewed, addressing the cellular response to their environment, properties of lipids and the previous applications of these systems in this field.

1.1. THE ROLE OF BIOMATERIALS

1.1.1. AN OVERVIEW OF BIOMATERIALS

Understanding how the cell response is dictated by the cellular environment be used to tune cell response more effectively; it is this purpose that the field of biomaterials can fulfil. With respect to the previously mentioned definition, these can be considered as materials that, in some way, mimic the properties of an extracellular environment, through which to mediate the desired cellular response. To that end, any property that reflects this environment may be used as a template. Commonly, researchers have isolated one specific property, such as varying stiffness, mobility, topography and chemistry, in order to ascertain how any one of these properties affect the cell response.

The stiffness of the cellular microenvironment has commonly been considered a source of inspiration in deriving biomaterials of varying stiffness. Here the stiffness is considered the elastic stiffness; the elastic (i.e. non-permanent) deformation of a material as force is applied in the linear regime. This is measured here by the Young's modulus (E): the ratio between the stress and the strain. Tissues present Young's moduli (E) over a huge range of magnitudes, from 10^2 Pa in neural tissues (27), to 10^4 Pa in non-mineralised bone (~40 kPa) (10), and

extending to 10^9 Pa in cortical bone (28). To recapitulate this poly(acrylamide) (PAAm) hydrogels are commonly used, which are easily manipulated by manipulating the concentration of the crosslinker present. However, they do not directly interact with the cell and require functionalisation with cell-binding molecules. Additionally, alginate fibres (29) have also been used as well as PEG-based hydrogels (30). These latter materials are able to crosslink specific biological molecules, such as ECM-based peptides; for example, GFOGER, the cell-binding peptide of collagen (31). Varying the stiffness has a marked effect on the cell response; on stiffer substrates cells are more spread, have more defined actin fibres (32), larger focal adhesions (14), and exhibit greater activation of focal adhesion-associated proteins, such as focal adhesion kinase (FAK) (33) and RhoA (32). This has further consequences for cellular behaviour, with activation or inhibition of downstream processes depending on the stiffness of the material. For example, Engler et al. (2006) (34), show that cells spread more on higher stiffness materials (Figure 1.1A), defined by the Young's Modulus, E . Beyond this, surfaces representative of the relevant microenvironment commit cell lineage to that path. More specifically, a biomaterial with stiffness similar to that of pre-collagenous bone will direct specific differentiation capable cells (mesenchymal stem cells) down the osteoblastic lineage; conversely, surfaces with stiffness similar to that of the neuronal environment will promote these same cells down the neuronal lineages (Figure 1.1A). Other work has also shown that this holds true for other cell lines, such as myoblasts (skeletal muscle) (35) and neural cells (27), as well as other types of environment, such as 3D cultures (36). Biomaterials with altered stiffness therefore show that they can be used to determine how the cell responds to the elastic nature of its environment in various modalities.

Topography of the microenvironment, with its various structures on the meso-, micro- and nanoscale, has also served to be of particular interest in producing biomaterials. Initially, properties such the roughness of a surface were observed to change the cellular response (37, 38); however, variability of the surfaces, despite similar roughness values, proved this an unreliable system. More recently, biomaterials with defined nanotopographies, have allowed for remarkable insight into the cell's ability to spatially detect their environment. Commonly, lithographic and electrospinning, as well as injection moulding techniques, have been used to generate, pillars (39) (injection moulding); grooves (40) and pits (16) (nano-lithography); or fibres (41) (electrospinning). Further to this, microcontact printing can also be used to present

cell-adhesive molecules of defined spacing (13, 42), or change nature of the topography presented, for example different shapes (12, 43, 44) or the degree of order (16, 45). Seminal work in this field has shown that various, vital cellular behaviours are controlled by the nature of the topography; for example, the differential spatial distribution of the cell-adhesive peptide, RGD, derived from the ECM protein fibronectin (and recognition tripeptide for integrins, the proteins cell use to adhere to the ECM), demonstrated a marked effect on the nature of the cellular adhesion machinery. Specifically, cells are sensitive to the magnitude of ligand spacing and are only capable of forming mature focal adhesions provided the ligand spacing is no more than ~60 nm (42). On a more cell-wide level the production of nanogrooves, or even larger scale grooves, has driven anisotropic cell spreading down the axis of the grooves (40, 46). Further, different shapes also can have an effect, with a specific example showing an increase in cytoskeletal tension in a ‘holly-leaf’ patterning of fibronectin compared to circularly patterned (12). This topographically defined control of cell behaviour has even greater implications on cellular processes. Work has shown that differentiation of mesenchymal stem cells can be promoted, *in vitro*, by introduction of a specific degree of disorder in a nanopit array; conversely, a highly ordered array allowed for population expansion (16). Other work has also used topography to promote differentiation (39). Beyond this, topographical cues have also shown a distinct role of geometry in the life and death of cells (Figure 1.1B); Cells that were constricted on small adhesive islands entered apoptotic pathways compared with those on larger islands, which were more able to survive and spread (13). These examples serve to demonstrate that biomaterials of varying topographical features have been used widely to both determine the cell response to the environment and impact on cellular behaviour.

Biomaterials displaying simple chemistries have also been used to determine the nature of the cell response. Comparative to the cell response to stiffness and topography the response to varying surface chemistries is less understood. Whereas in the case of stiffness and topography the biomaterial surface is known to adjust the cell response through adhesion-associated mechanisms (47, 48), the response mechanisms to surface chemistries are more elusive (10). Due to this much of the work related to this has focused more on the applicability of this biomaterial property, rather than the underlying mechanisms. For example, small chemical groups, such as phosphate groups and t-butyl methacrylate groups were capable of promoting osteogenic (Figure 1.1C) or adipogenic differentiation respectively (49), with yet others

promoting stem cell renewal (50). There is some evidence that the interactions with these materials is also mediated by focal adhesions and sequestering of growth factors, but again the mechanisms remain unclear (51). Thus, while a potentially useful biomaterial, the lack of understanding of how these modifications reflect the ECM and change the cell response make them less relevant to the current study.

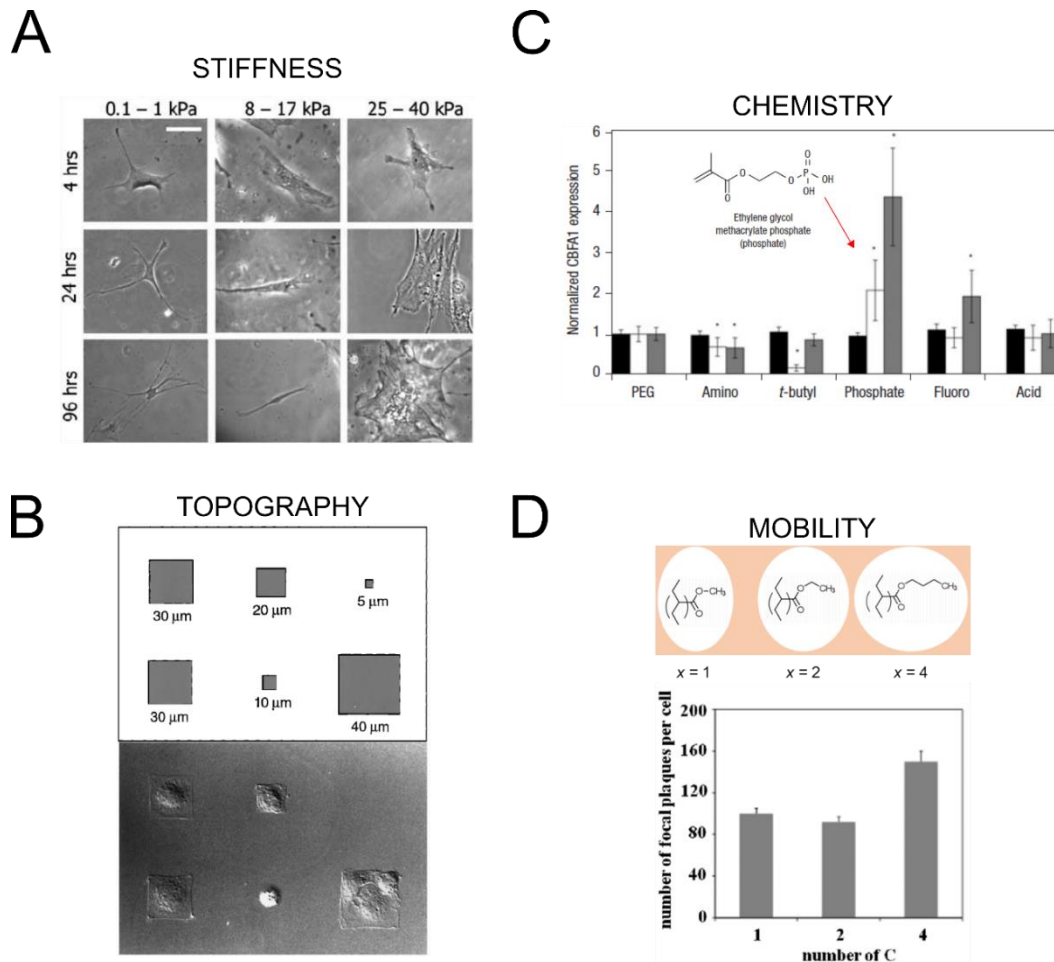


Figure 1.1. The Effects of Biomaterials. A summary of the effects of biomaterials on the cell behaviour, such as spreading, shape, adhesion and differentiation are affected by factors, such as: (A) stiffness, which allows for greater cell spreading on surfaces of higher stiffness (34); (B) topography, which can change a cell's ability to spread and survive (13); (C) chemistry, which can promote specific differentiation to specific lineages of capable cells (49); (D) mobility, which can control cellular adhesion, spreading and differentiation (52). Together these examples, show the multitude of cell responses that can be tuned by controlling the nature of the biomaterial that is used. Figure reproduced with permission.

1.1.2. THE EFFECT OF SURFACE MOBILITY ON THE CELL RESPONSE

As mentioned above, a further means by which the cellular response can be controlled is by altering the molecular mobility of the surface, i.e. the degree to which the substrate, upon which the cells reside, is free to move. While this property remains less well-studied than the archetypal stiffness and topography alterations, there is increasing evidence that mobility can alter the cellular behaviour (53-55). In instances of changing the surface mobility of laterally mobile ligands (and in related systems), mobility may be considered a simulation of the viscous component of the ECM, and thus the other side of the coin to stiffness when drawing inspiration from its viscoelastic properties; further, it is the viscosity that defines the ligand mobility, a crucial link throughout this current study. Viscosity defines the resistance of a fluid to flow and to what degree said fluid resists motion of objects through them. A viscoelastic material exhibits both viscosity and elasticity in response to applied force. However, it is this viscosity component of the ECM that is of particular importance to this study; as the lipid bilayers used in this system are 2D fluids, with particular diffusive characteristics, they also have differing degrees of viscosity, which can change the lateral mobility of cell adhesive ligands present on the bilayer.

In producing materials that present distinct mobility, polymer surfaces (53, 56, 57) and lipid bilayer surfaces (58-61) are commonly used, with some examples of hydrogels also being used (62). The latter presents an added complexity due to the simultaneous elastic component of hydrogels. In the case of polymers various techniques have been used, with spin coating (56), polymer brushes (63), and block copolymers (55) all finding applications in studying the cell response to mobility. Lipid bilayers, however, present a narrower range of production methods, predominantly being either Langmuir-Blodgett deposition, or vesicle deposition (64). It is the latter than is more commonly used in this context, due to their ease of use. While the vesicle deposition technique itself is very simple, these can be deposited on to either solid supports, such as glass (65), mica (66), or gold (67), or on polymer based supports, which can act as tethering or cushioning molecules (68). Together these surface preparation techniques produce surfaces of differing ligand mobility/surface viscosity, which has varying impacts on the cell response, dependent upon the system.

Early, direct observations of the effect of molecular mobility on the cell response were reported in the 1970s, with the finding that the mobility of cell receptors, in this case lectins, were likely a contributing factor in cell-to-cell attachments and thus had a role in controlling cellular processes (69). This work, in turn, arose from the deduction that cell receptors clustered in response to ligand binding, which must be related to the lateral mobility of the receptors themselves (70, 71). While receptor mobility is distinct from the ligands considered in this work, parallels can be drawn through a similar freedom of motion; it is from these early studies that study of the effect of the mobility of molecules expanded into various fields, such as biomaterials. This conclusion that the receptor mobility influenced cellular processes was therefore further studied by a number of groups in the following years, predominantly via the production of surfaces using polymers (72-74), or on lipids (75, 76). A key characteristic of both these surfaces, as it pertains to molecular mobility, is that they have a transition temperature at which the nature of the surfaces change from a less mobile to a more mobile structure; in polymers this is referred to as the glass transition, T_g , and in lipids it is referred to as the phase transition, T_m . The latter of these will be discussed in further detail later, but in both cases the surfaces are considered far less mobile until the temperature is raised above this defined transition temperature, which is accompanied by significant increases in the overall mobility of molecules present on the surface.

Since the early observations of ligand-mobility dependent cell behaviour, work has sought to observe what manner of changes this surface can produce. In the first instance, this ligand mobility has been seen to have the potential to control both the initial adhesion and/or the morphology of the cells. The results are varied, with one study reporting a reduction in cell attachment *in vivo* with surfaces presenting a higher mobility (74) and another reporting this leading to a greater degree of cell attachment (57). Other work has determined there is no difference in initial adhesion upon alteration of ligand mobility, instead showing that this mobility affects the morphology of the adherent cells (54). However, direct comparisons may not be drawn due to the distinct differences in the methodologies applied in these systems. What is perhaps more illuminating, in regards to the current work, is the fact that on a high ligand mobility (low surface viscosity), peptide-presenting lipid bilayer, cells were seen to require a larger effective ligand density to achieve the same adhesion characteristics as those on a surface presenting immobile ligands (76).

In a more general sense, upon adhesion of cells to the surface, spreading has been often noted to tie closely with the ligand mobility (53, 55, 58, 59, 77). While again key differences in results may be attributed to the difference between systems, there does appear to be some disagreement over the role of viscosity-defined ligand mobility. Despite either being based on polymer or lipid mobility, these systems all utilise surfaces with freely diffusive surfaces (without ligand in (53)). However, there does appear to be some disagreement between these, as to the effect of mobility on cellular morphology. Alternatively, this previous work has demonstrated that there is less spreading (53, 58, 77), more spreading (59) or a biphasic response (78) as the mobility of the surface increases. Furthermore, when considering this viscous component in conjunction with stiffness, as part of a viscoelastic system it also appears that there is an increase in the cell spreading upon decreasing the mobility (62); however, in this case stress relaxation (reduction of stress within the material over time) is considered the viscous component, so direct comparison is limited.

The adhesion machinery, i.e. the focal adhesions, regulating the cell-surface interactions are highly dependent on the mobility of surface ligands, as demonstrated in Figure 1.1D. Initial insights show that block copolymers of varying diffusion coefficients, functionalised with RGD, also vary the size of focal adhesions (55); slower diffusion (thus higher viscosity) was associated with a lower ligand mobility in the polymer. While the authors noted biphasic behaviour in the cell spreading, leading to a proposal of adhesion-dependent and independent spreading, the key implication of this work is that cells were able to detect the ligand mobility of the surface on the single protein level. More recent work, using fluid lipid bilayers, patterned with barriers of varying thickness demonstrated that this lateral ligand mobility is important to the spreading of cells and the formation of adhesions (58, 77, 79). Cells were seen to bind to the RGD ligands and pull them towards the cell centre. Due to the fluid nature of the lipid bilayer used, the cells retracted to the point of maximum force, clustering ligands within the cell area. However, if barriers to the diffusion were introduced ($\sim 1 \mu\text{m}$) they prevented further rearward motion of the ligand and caused recruitment of the focal adhesion associated protein paxillin (79); further, both ligands and integrins were seen to cluster around the barriers. This work demonstrates that cells cannot form traction forces on fluid-phase bilayers; indeed, instead of forming defined focal adhesions, the cell line used in this study produced podosome-

like structures, commonly associated with invasive cell lines such as macrophages (62) or cancerous cells (80).

This lack of forces on lower viscosity systems, exhibiting higher ligand mobility, is also implied by studies in more complex systems that have sought to understand viscosity in conjunction with stiffness, as the effect of viscoelasticity. For example, using a stacked bilayer system (adding further bilayers on top of the original), an increase in the amount of stacked bilayers was demonstrated to increase the ligand mobility and decrease traction forces exerted through both cell-cell (cadherin) (81) and cell-surface (integrin) adhesions (82). By stacking bilayers, this work also added the element of stiffness to the viscosity thus determining the viscoelastic contributions, rather than the viscosity in isolation that, amongst others (62), shows how biomaterials exhibiting both elastic stiffness and viscosity-defined ligand surface mobility can be used to determine the cell response to its environment. As alluded to above, a further example as to the role of stiffness within viscoelasticity is the work of Chaudhuri et al., (62), which changed the stress-relaxation (viscous component) in hydrogels of the same stiffness. This is distinct from the stacked bilayer system in that the ligands did not have the two-dimensional surface diffusion; however, this work noted that elastically soft hydrogels that exhibited stress-relaxation elicited similar responses to that of stiff hydrogels. Together, this work on these systems implies that cells detect ligand mobility on varying viscosity surfaces in a similar way to that of stiffness, utilising similar mechanisms. As the ligand mobility increases, the cell spreading is hindered, as is the formation of well-defined focal adhesion complexes. This is linked with lower forces exerted at the cell-material interface, with the faster high mobility ligands detected in a similar manner to a 'softer' substrate, with the opposite true in the case of less mobile ligands. The question remains, however, as to how the cell response to these two distinct physical properties can be merged.

With the cell's mechanical response being affected by surface viscosity, work has also looked at how these biomaterials change other cell responses. However, the direct role of diffusive surface ligands, whose mobility is defined by the viscosity of the surface, has not been widely studied. As such, parallels must be implied from other, related, work that has sought to understand the contribution of the viscous component. For example, hydrogels exhibiting stress relaxation showed higher localisation of the mechanosensitive YAP (Yes-associated protein)

transcription factor to the nucleus (62). Furthermore, adsorbed ligand mobility on spin-coated polymers has shown increased differentiation in both model and stem cell lines in response to decreased mobility of the polymer surface (52, 56). In the latter case hMSCs, cells capable of differentiation into cells such as osteoblasts (related to bone production) showed increased levels of osteogenic markers, a lineage commitment consistent with higher forces (10). This increased differentiation was seen as a consequence of the mobility of surface-adsorbed fibronectin induced by larger side-chains in the spin-coated polymer used (Figure 1.1D). Differentiation that is dependent on ligand mobility, and thus by implication viscosity, has also been supported by another group who have showed that cells respond to the anchoring density of collagen on polyacrylamide gels of similar stiffness (83). They saw that lower degrees of crosslinking between the collagen and the gel led to cell behaviour typical of softer gels, with a concomitant increase in differentiation. This work implied that the increased mobility of the collagen (due to less anchoring points) reduced the amount of force the cell could apply on the surface; this, in turn, led to changes in mechanically activated differentiation pathways.

As can be concluded here, the effect of manipulating the mobility of ligands, through the viscosity of the surface in which they are presented, is not settled. It can also be seen here that the role of ligand mobility is not limited to the manipulation of the diffusive characteristics of the surface. However, it is also clear that despite inroads into understanding how the diffusive characteristics of surface ligands can affect cellular behaviour, there is yet more that than can be understood in terms of the molecular behaviour and the effect on downstream pathways. Despite this, these applications, attest to the potential effect of manipulating surface viscosity and thus the lateral diffusion, therefore making understanding how the cell responds to these viscous surfaces of great interest.

1.2. MOLECULES AND PROCESSES DICTATING THE CELLULAR RESPONSE

While the cell response to biomaterials of various physical properties has been detailed above, it is necessary to understand how the surfaces simulate the extracellular environment. Further, it is also necessary to understand how and why cells respond in a defined way to their surroundings, be it *in vivo*, or *in vitro*. As has been mentioned and alluded to above, this

response is highly varied and dictated by a series of complex processes and molecules that lead to the eventual change in the gene expression and consequently the protein profile of the cell. While there is a great deal of interplay and overlap between these, for simplicity these can be grouped into contributions from the ECM proteins, the cellular binding machinery and complexes, and the signalling molecules and processes; together these dictate in what manner cells respond to their physical environment.

1.2.1. THE EXTRACELLULAR MATRIX

The initial point of contact between the cell and their environment are the ECM proteins; in the case of synthetic materials, cells do not bind directly to the surface, but instead interact indirectly through a layer of these proteins. In vivo these mediating molecules form a mesh surrounding the cells and include proteins such as collagen, fibronectin (FN), and laminin (shown schematically in Figure 1.2A), with key roles being to provide structural support to the cells, partition tissues and the providing various cues and stimuli to the cell. Secreted and organised by the resident cells, the properties of the ECM, such as the relative protein abundance, physical properties, such as mechanical and topographical properties, and signalling molecules, is therefore defined by the cell type (4). Taking the physical properties as an example, various tissues are well noted to have distinct viscoelastic properties. Specifically, the elastic moduli of various ECMs/tissues, that is their stiffness, is shown to have a huge variance throughout the body. As mentioned above, in Pascals this can extend over a range of at least six orders of magnitude from 10^2 Pa in neural tissues (27) and extending to 10^9 Pa in cortical bone (28). Analysis of the viscous nature of the ECM is more limited; however, cells are able to manipulate the ECM viscosity on the order of 10s of Pa.s (84). With cells so responsive to external stimuli, this property, as well as the others mentioned, is capable of directing the behaviour relevant to their environment (34, 85).

In order to support cells within the matrix all ECM scaffold proteins contain cell binding regions. Of key importance to this study is the cell binding region of fibronectin (Figure 1.2B): the RGD tripeptide (arginine-glycine-aspartate, Figure 1.2C), found twice in the fibronectin dimer, in the III₁₀ repeat domain of each monomer (86). This, as shown in Figure 1.3 is capable of binding to various types of integrins; proteins responsible for cell adhesion (detailed in the

next section). In addition there are also the IKVAV and GFOGER sequences found in laminin (87) and collagen (88) respectively. The latter of these has also been found to be of special interest in the biomedical field, with its ability to accelerate bone healing times in mouse models (89). The binding of cells to these different binding sites is capable of changing the nature of these adhesions and thus the response of the cells. For example, mesenchymal stem cells may upregulate myogenic or osteogenic differentiation if they are bound to fibronectin or collagen respectively (90). Furthermore, recruitment of specific integrins can be indications of specific processes, such as mechanotransduction (91), or cancer and development (92).

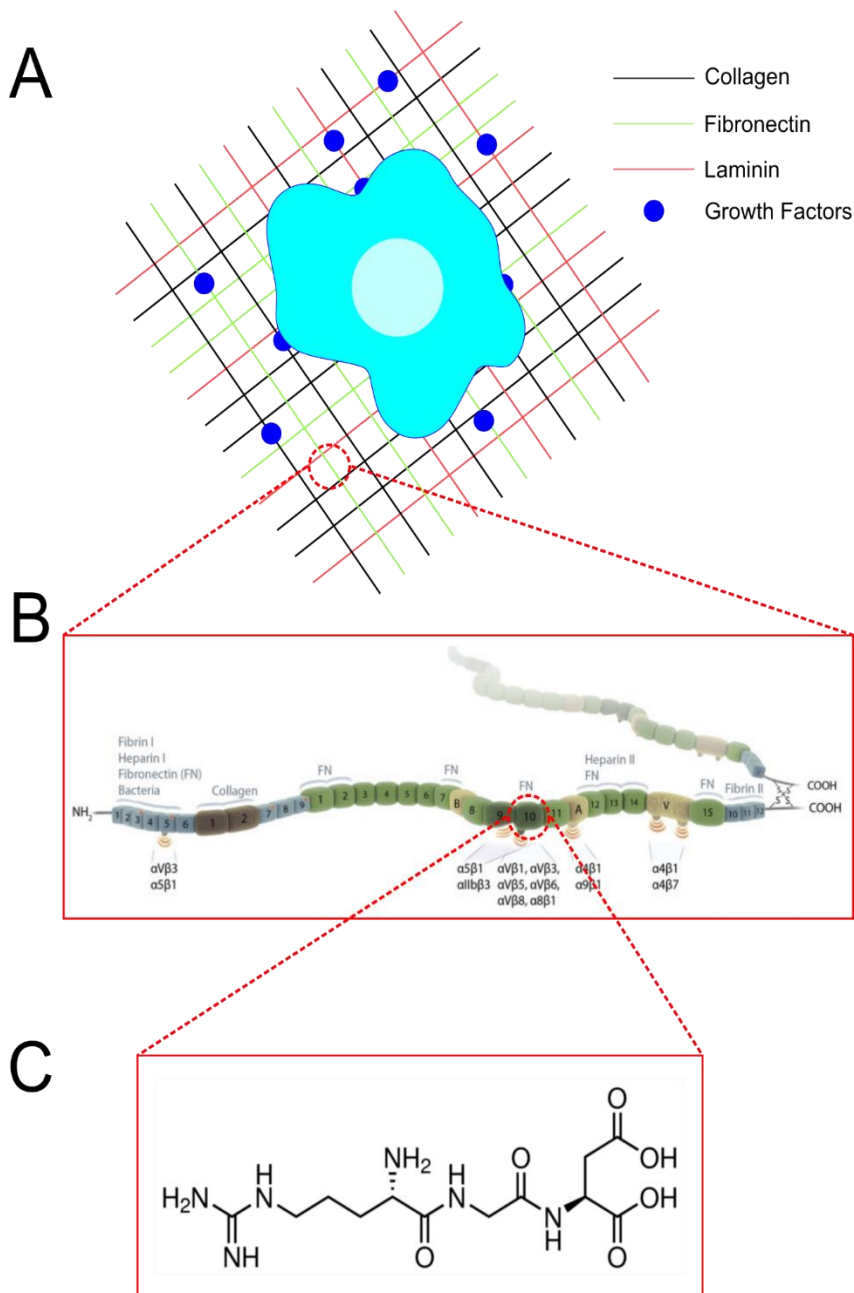


Figure 1.2. The Extracellular Matrix and Fibronectin. (A) The cells reside in a heterogeneous environment of varying physical and chemical properties, with different proteins, at different densities, presenting different ligands, as well as other soluble molecules used for cell signalling. (B) A schematic representation of FN, the repeats shown in blue (type I), brown, (type II) and green (type III). The binding domains for different molecules are indicated above the associated areas. Binding sites for the specific integrins are shown below the associated areas. Alternatively spliced extra-domains are also shown (B, A, a variable region; V) (93). (C) Shows the RGD tripeptide, present in the III₁₀ repeat of the fibronectin and responsible for the binding of the cell to the protein (taken from Sigma-Aldrich website).

In addition to forming a mesh-like structure, enclosing and adhering the cells, the ECM proteins are capable of acting as a reservoir of further signalling molecules, capable of controlling cell behaviour (6). Prime examples of these are growth factors, proteins that can affect various cellular functions, including proliferation, migration and differentiation (94). Of this, molecules such as BMP (bone morphogenic proteins), VEGF (vascular endothelial growth factor) and FGF (fibroblast growth factor) have found particular use in biomaterials. Not only are they involved in the processes of tissues regeneration, but they are also known to bind to various ECM proteins. For example, BMP-2 can bind to the III₁₂₋₁₄ repeat of fibronectin and is capable of inducing osteogenic differentiation in mesenchymal stem cells (95). Furthermore, fibronectin is also shown to be highly capable of binding both FGF-2 and VEGF on the same repeats (96). Through interactions with the ECM and their relevant cellular receptor, these growth factors are presented in a defined spatial distribution, thus determining the nature of cell response (97).

1.2.2. INTEGRINS AND THE FOCAL ADHESION COMPLEX

As alluded to above, when discussing the adhesion of cell to the ECM cells dynamically detect and interact with their environment through a family transmembrane receptor molecules called integrins (17). Heterodimeric proteins with extracellular, membrane-spanning and cytoplasmic domains, these proteins are pivotal in the translation of physical cues to intracellular signals. There are 24 different integrin types within this family, produced from a combination of one α and one β subunit (17). These are shown in Figure 1.3, with emphasis on those integrins capable

of binding the RGD peptide. Integrin recruitment to the site cellular adhesion is dependent on the ECM protein present, with different integrins having varying affinities for specific peptide sequences. For example, the RGD tripeptide is well known to bind integrins, which include $\alpha_5\beta_1$, associated with adhesion and mechanotransduction (91), $\alpha_v\beta_3$, previously related to processes such as angiogenesis (98) and $\alpha_v\beta_6$, which is associated with cancer invasiveness (99).

Integrins are first in a series of proteins whose role is to transduce and then translate external cues into a distinct cell response. Key to this is linking the actin cytoskeleton to the external environment. As the integrins do not have an actin binding domain they require the recruitment of adaptor proteins, through which to mediate this interaction. These proteins may be responsible for actin-linking, signalling or actin polymerisation, as indicated in Figure 1.4. It is these protein complexes, resulting from this recruitment of the adaptor proteins to the nascent adhesion of the integrins to the ECM, which are termed 'focal adhesions' (Figure 1.4). The proteins that are recruited are collectively termed the 'integrin adhesome', which consists of over 230 components (18), with key roles being the structural, linking the integrin to the cytoskeleton (100), signalling (19), and the polymerisation of actin (101).

The focal adhesions therefore allow for the cell to detect and respond to chemical and mechanical signals; for example, there is synergistic enhancement of extracellular signalling in response to cells binding to FN and VEGF simultaneously (102). However, it is the latter, the mechanosensitive nature of these adhesions, that is of key relevance to the current work. A number of proteins that make up the integrin adhesome serve as important mechanosensitive receptors, capable of transducing physical cues, related to the physical properties of the ECM to the cell. For example, talin, existing in two redundant isoforms (talin 1 and 2) has been observed to be vital for the formation and maintenance of stable focal adhesions (100). Capable of linking integrins to the actin cytoskeleton (Figure 1.4, steps 1 & 2), talin is known to have a role in mechanotransduction, unfolding under force (103), exposing binding sites for further protein binding (104), which stabilises the overall focal adhesions. Specifically, the binding sites exposed are for that of the protein vinculin, a 116 kDa cytoplasmic protein (105). Existing in an autoinhibited state, due to interactions of the head and tail group (106), the exposure of its binding sites by the stretching of talin, through actin pulling, leads to activation of the this

protein (107). The head group binds to talin and the tail to actin, with the neck capable of binding further signalling molecules, thus stabilising (108) the interaction of talin with the actin cytoskeleton. This enhanced lifetime allows for the formation and maturation stable focal adhesions. These are by no means the only two mechanosensitive proteins; indeed, vinculin recruitment only accounts for 30% of the adhesion strength within a focal adhesion (109), with models also suggesting that talin only experiences approximately 7% of total force (47). Other proteins, such as focal adhesion kinase (FAK), are also known to exhibit mechanosensitivity, with the exposure of phosphorylation sites upon force-induced unfolding (110). The focal adhesions, with their ability to sense a wide variety of environmental cues, therefore serve as an important link between the cell and its environment.

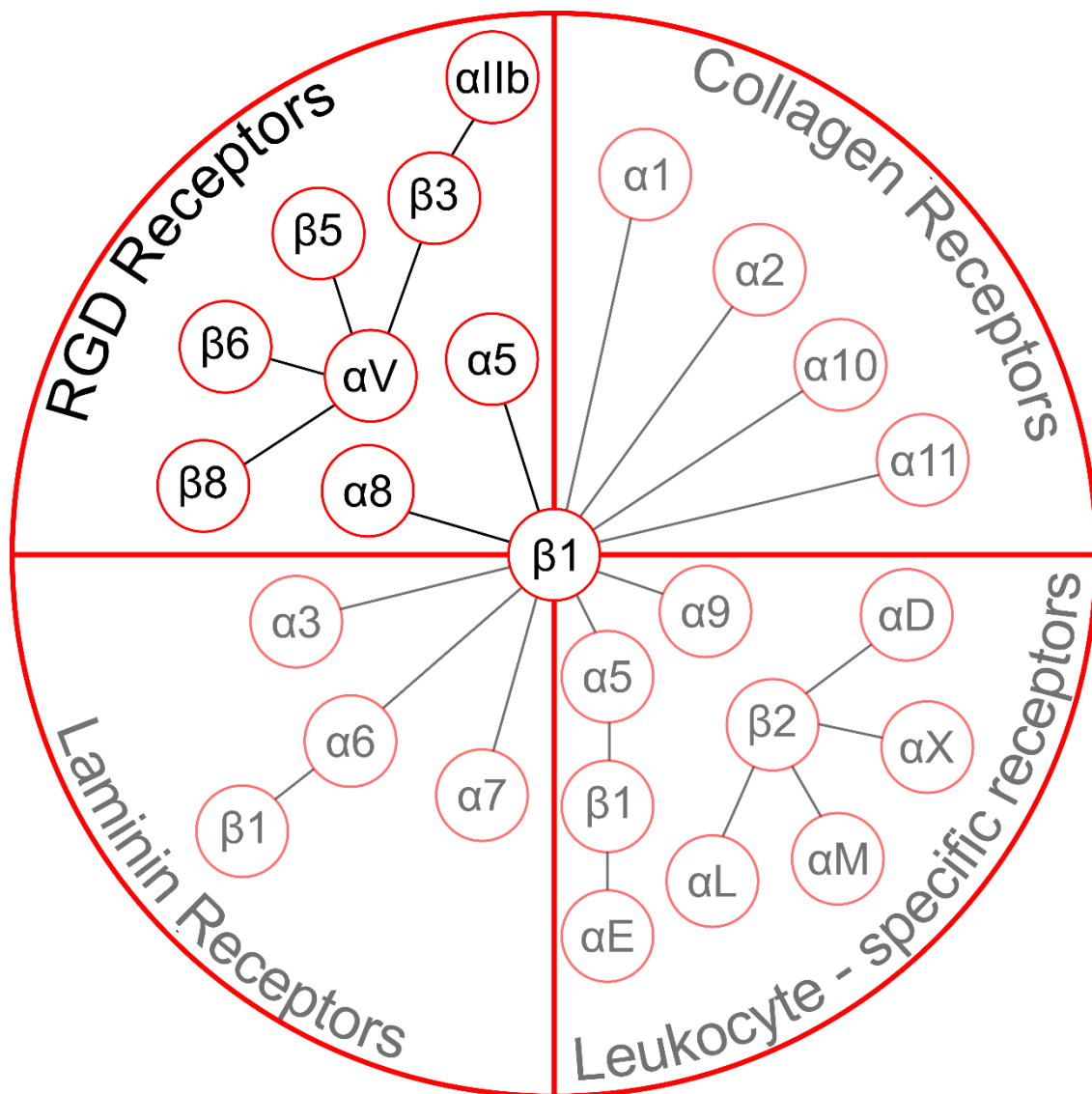


Figure 1.3. Integrins. Summary of the different integrin subunit combinations and their specificity for cell adhesive molecules. Highlighted here are the integrins specific for RGD, as this is the molecule used to bind cells in this project. (Adapted from Barczyk et al 2010 (17))

After the binding of integrins to the ECM and the recruitment of adaptor proteins (Figure 1.4), the next stage of environmental sensing is the recruitment of the actin cytoskeleton, this idea of discrete ‘stages’ is somewhat of a misnomer. While it is helpful to imagine the process in this way, the sensing of the environment, through the linking of the cytoskeleton to the ECM (or indeed an *in vitro* environment), is more of a tightly regulated feedback cycle, as shown in Figure 1.4. The actin that makes up the cytoskeleton exists in a globular form (G-actin) before recruitment, and a filamentous (F-actin) form, upon recruitment at the leading edge of the actin filaments (i.e. the region immediately adjacent to the cell membrane) (111). The actin cytoskeleton provides structure to the cell, acts as a means of intracellular transport, and is its key means of propulsion (112). Indeed, cell motility is variably ascribed to the continuing polymerisation at the cell to edge and the action of myosin II. This protein works to pull rearwards on the actin filaments, in an ATP-dependent process. This rearward motion, provided it is linked to the ECM through the focal adhesions, drives a counter force propelling the cell in the opposite direction, in a ‘treadmill-like’ effect. The forces actin is capable of exerting on the surface therefore lead to larger focal adhesion complexes (14). Conversely, focal adhesions are capable of leading to increased actin polymerisation; for example, zyxin, recruited in response to mechanical force (113), is responsible for force-dependent actin polymerisation (101). Together, this process develops mature FAs from the initial binding of integrin to the ECM, recruitment of adaptor molecules and eventually ECM-actin linking FAs. This linking of actin to the ECM, and its related feedback cycle, is the basis of the ‘molecular clutch’ model, which has sought to explain how the cells convert this rearward actin flow into forward

movement. In conjunction with this, it has modelled how the mechanical nature of the environment affects the cell response (114).

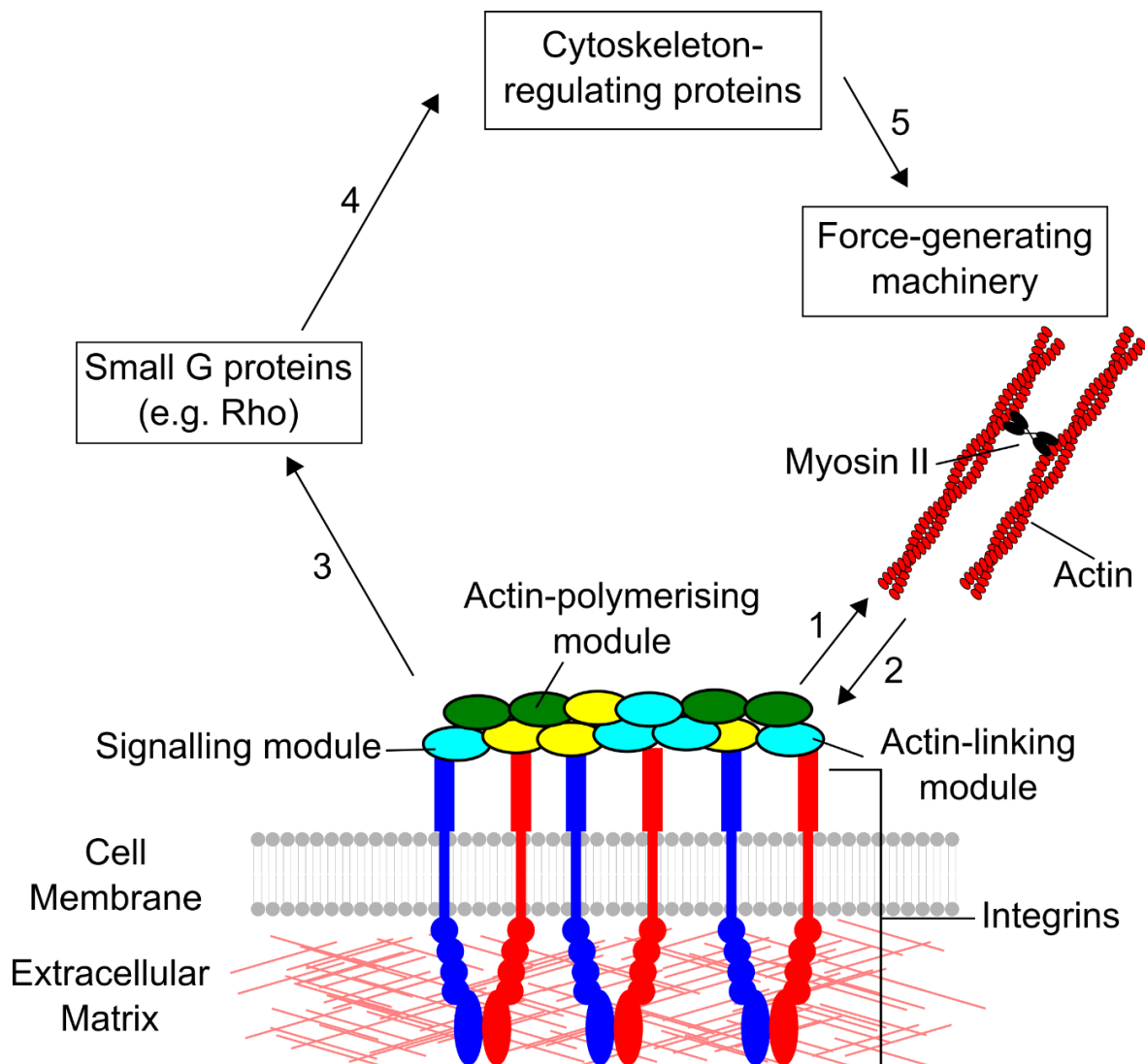


Figure 1.4. Focal Adhesions and the Actin Cytoskeleton. While integrins bind to the cell surfaces step 1 is the myosin-II generated forces, which can affect the multitude of adaptor proteins. These can include actin-linking modules (such as talin), signalling molecules (such as FAK) and actin-polymerising module (such as zyxin). In step 2 the overall response of these modules to the mechanical properties of the network, in conjunction with the actin cytoskeleton, defines the mechanical response. This leads to step 3, whereby the signalling module, activates downstream G-proteins, such as Rho. These have a significant effect actin-polymerisation and contractility (step 4), thus modulating the activity of the force-generating apparatus of the cell (step 5). (Adapted from Geiger et al (18)).

1.2.3. THE MOLECULAR CLUTCH

As may be assumed from above, the processes defining the cell response to their environment is multi-faceted, but can be summarised by one over-arching factor: the linking of cytoskeleton to the surface. By doing this the cells can thereby “feel” the surface, exerting forces, with responses to these stimuli fed back through the pathways detailed above. In recent years it has been proposed that the cell response may be understood in simple terms. To this end, recent work has confirmed the role of a ‘molecular clutch’ in the cell sensing of a surface (47). An elegantly simple modelling of the cell, on a single molecule level, as a series of Hookean springs (115) has unveiled a key means through which the cells can couple their cytoskeleton to the surface.

The ‘molecular clutch’, a term originally coined by Mitchison and Kirschner in 1988 (116), was first modelled by Chan and Odde (117). Their stochastic model, represented in Figure 1.5, was determined to rely on a series of factors, such as the stiffness of the substrate, the rearward velocity of the actin, as driven by myosin II, the binding rate and the unfolding rate of the ‘clutch’ molecules. In essence, the actin is physically linked to the surface through an actin-clutch-integrin-ECM chain. The role of myosin II in the cells is to pull on the actin, generating force; this myosin contractility powers a continuous flow of actin towards the cell centre, termed retrograde (rearward) flow (114). When disconnected from the surface the rate of this retrograde flow is allowed to continue unabated. However, upon the coupling of the actin flow to the ECM, via the focal adhesions and integrins bound to the ECM, this myosin contractility is countered by the resistance of the environment. The degree to which the environment resists the forces exerted by the cell is key to the response, as this defines the rate at which force builds within the adhesion site: the force loading rate. This is linked to the k_{on}/k_{off} and the k_{fold}/k_{unfold} (118); that is the integrin-ECM binding rate and the folding/unfolding rate of the clutch molecule respectively. In order for the clutch to be ‘engaged’ the force loading rate must be high enough to unfold the clutch molecule within the lifetime of the integrin-ECM bond. Taking an as example stiffness, a low compliance (elastically stiff) substrate will have less ‘give’. This will mean that as the cell pulls on the ligand the force loading rate will be higher. This will allow for the force sensitive clutch proteins to unfold before the integrin-ECM connection breaks, as shown in the inset of Figure 1.5B. At a low elastic stiffness the opposite is true; a slower force loading means that the integrin-ECM bond will break before allowing

unfolding of the force sensitive clutch molecules. This unfolding is key; for example, as mentioned previously talin unfolding, successfully proven to be a force-sensitive clutch molecule (47), exposes binding sites for vinculin (104, 107), which can further stabilise the adhesion and lead to reinforcement of the forces exerted on the surface. Were this not to unfold within the bond lifetime, the vinculin could not bind.

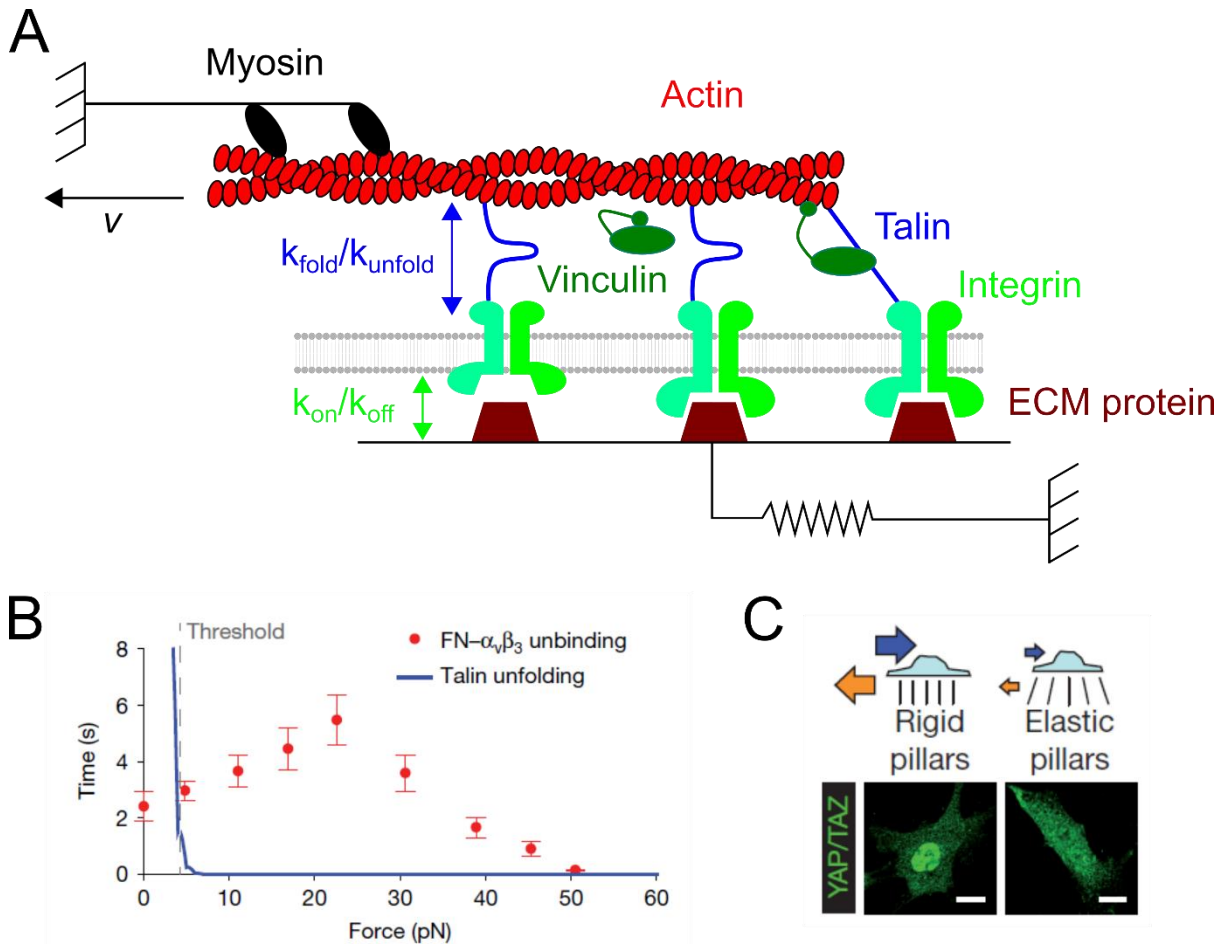


Figure 1.5. The Molecular Clutch. (A) A schematic representation of the model that ties the response of the cell to the nature of the surface. Applied to stiffness the model dictates that the actin cytoskeleton must be linked to the surface via an ECM-integrin-talin clutch, which can engage upon the exceeding of a force threshold. (B) Shows average lifetime of FN- $\alpha_v\beta_3$ as a function of force (red points) and the average unfolding lifetime of talin (a proposed clutch molecule (blue line)). This demonstrates that at lower forces ECM-integrin bonds unbind faster than talin can unfold; however, higher than the threshold force (grey dashed line) the talin unfolds faster (adapted from Elosegui-Artola et al., 2016 (47)). (C) Shows the resulting change in the localisation of the nuclear transcription factor, YAP, to the nucleus to a greater extent on surfaces of greater stiffness (21).

Originally used to model the cell response to elastic stiffness (117), the model is capable of predicting various parameters relating to the adhesion strength and forces exerted by the cell. For example, the clutch can predict properties such as traction forces, adhesion size and actin flow, which can be supported by quantitative measurements. Furthermore, it has been used in conjunction with inhibition of molecules of interest to identify key proteins, such as talin, and their role in the regulation of the cell response to the environment. Beyond this the clutch model has been expanded to predict how cells respond to the viscoelasticity, rather than just the elasticity, of their environment (62). Furthermore, recent work has shown that the clutch model can predict the cell's response to the topography of their environment (48). Importantly, this demonstrates that the molecular clutch hypothesis is capable of tying together the disparate properties affecting the cell response, from the properties of the ECM to the nature of the focal adhesions, to the response of the cytoskeleton.

1.2.4. DOWNSTREAM CELLULAR SIGNALLING AND CELLULAR BEHAVIOUR

The cellular response to a surface, irrespective of its nature, depends on how these signals are transduced through the ECM proteins and detected by the focal adhesion machinery. Figure 1.4 the focal adhesions lead to a recruitment of signalling molecules, such as FAK, which lead to the promotion of pathways downstream from adhesions (119). As shown in Figure 1.4 shows the interplay between the actin and the focal adhesions leads to the downstream activation of signalling molecules, with several processes being key to this. The phosphorylation or dephosphorylation of proteins is an important example, with Src-mediated phosphorylation of FAK, upon exposure of target sites, being key to regulating the focal adhesion behaviour (120). Beyond this the Rho GTPases, for example Rho and Rac, are vital to the function of the actin cytoskeleton (121). For example, RhoA is activated by several molecules associated with focal adhesions in response to ECM interaction (122); RhoA then activates ROCK (Rho-associated kinase), which upregulates actin stress fibre assembly (123). These behaviours are associated with the physical properties of the microenvironment, with higher activity of RhoA being associated with more force and greater cell spreading (32).

Beyond the molecules and pathways immediately upregulated by the formation of adhesions, there is also an impact on the genes within the cell. An important, but by no means solitary, example is that of the transcription factor YAP (Yes-associated protein). Biochemically controlled by its phosphorylation in the Hippo-pathway (124) and mechanically controlled by the cellular environment (47, 125, 126), YAP localises to the nucleus in response to higher forces (Figure 1.5C) and plays a major role in development (127), as well as cancer (128). With the mechanical response controlled by the integrity of the actin cytoskeleton, the transcription of genes key for *in vivo* properties, such as organ size (129), it is clear that the environmentally defined adhesion is key to further, downstream cellular behaviour.

This is of particular importance in differentiation capable cell lines, specifically stem cells. Stem cells are progenitor cells, capable of differentiating into a number of lineages, of which there are various types, and may include haemopoietic stem cells or mesenchymal stem cells. While the applications of both are highly studied, it is the latter that is of particular importance to the current work. Human mesenchymal stem cells (hMSCs) are multipotent, commonly found in the bone marrow (but also exist in other tissues such as adipose tissue) and are capable of differentiating into cell types such as osteoblasts (bone cells), adipocytes (fat cells) and chondrocytes (cartilage cells) (130). The differentiation of hMSCs is highly sensitive to the physical nature of the local environment. For example, by manipulating the stiffness of the local environment to reflect a specific tissue hMSCs demonstrated upregulation of markers for neural, muscle or bone cell lineages (34). Furthermore, other cells, such as C2C12 mouse myoblastic cells (muscle progenitor cell line) also show this like-begets-like behaviour, with optimal differentiation seen when the environment is of the same stiffness as muscle tissue (85).

1.3. LIPID SYSTEMS: THEIR PROPERTIES AND APPLICATIONS

As mentioned previously, the nature of the cell's response to the viscosity-defined ligand mobility is the key property of interest to the current work. This work seeks to understand how the changing the viscosity, thus also the ligand mobility of the surface can change the cell response. To this end supported lipid bilayers (SLBs) present an ideal avenue to pursue this research. Lipid bilayers predominantly enclose and surround the cell, presenting different

molecules, such as proteins and carbohydrates, vital for signalling or recognition. Supported lipid bilayers (SLBs) present a simplified, model version of this structure, in which the physical properties can be manipulated. As the name suggests these bilayers are made up lipid molecules, whose intrinsic properties define the overall properties of the bilayer. One important characteristic is that of the phase transition, T_m , where the lipid system moves from a gel-like state to a fluid state. It is this characteristic property of the bilayer that is important to the current work.

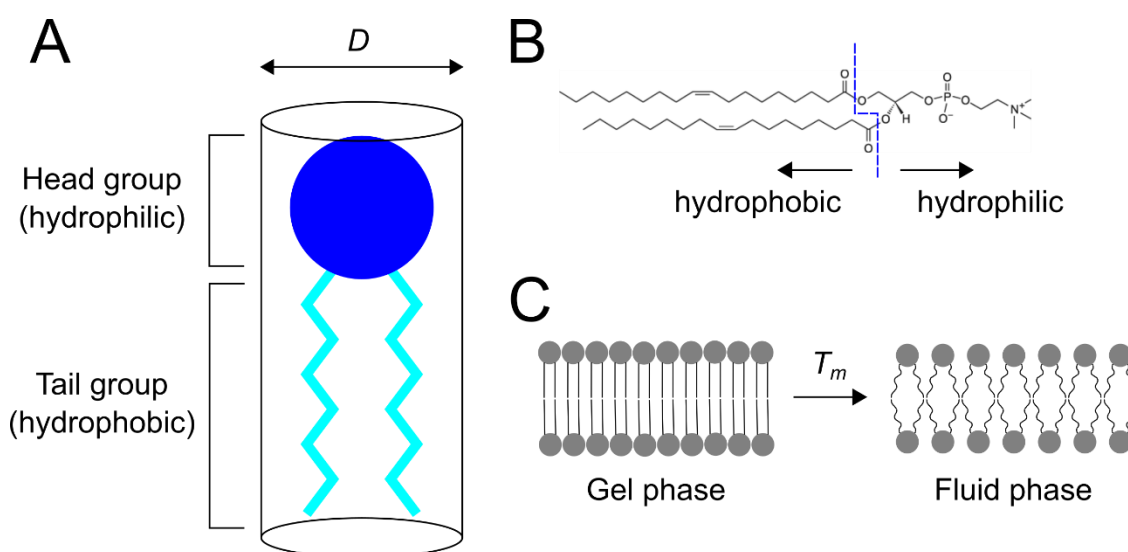


Figure 1.6. Lipids and the Phase Transition. (A) The amphipathic structure of a lipid, showing the hydrophilic head group and hydrophobic tail. Together these lead to the spontaneous self-assembly into structures such as unilamellar or multilamellar vesicles, or bilayers, based on their intrinsic properties. (B) Shows an example structure of the phospholipid, DOPC, a commonly used lipid, and one of particular importance in this study. The hydrophobic and hydrophilic regions are noted, with double bond present in each of the tail groups. (C) Shows the nature of the phase transition and the change in structure that occurs upon the exceeding of the temperature, T_m , characteristic of each specific lipid. This leads to a melting of the carbon chains and reduction in the order of the lipid packing, increasing the fluidity.

Lipids are wide ranging groups of molecules encompassing molecules such as phospholipids, sphingolipids or cholesterol amongst others. An example of a phospholipid structure is shown in Figure 1.6A (for simplicity, unless otherwise stated the term lipid will refer to phospholipids). These are amphiphilic molecules, containing a hydrophilic head and a

hydrophobic tail (Figure 1.6B) that make up the majority of the plasma membrane, enclosing the cell and its organelles and protecting it from the environment. Due to this amphiphilic nature, these molecules orient themselves in an aqueous solution so as to maximise positive interactions. The larger scale structures formed are highly dependent on the lipid structure (131). For example, while a cylindrical shape is shown in Figure 1.6A is representative of the molecular structure of DOPC (Figure 1.6B), this can be more conical, with either the head or tail having a wider hydrodynamic radius than the other. This in turn can change larger-order structures formed. In the case of the cell membrane they form a planar bilayer, composed of an inner and outer leaflet. First imagined as a ‘fluid mosaic’ by Singer and Nicholson (132), it is a highly dynamic and varied system, capable of adapting to the environment, as well as containing a multitude of proteins vital to function of cells. For example, lipid rafts are domains of the plasma membrane containing high concentrations of cholesterol and sphingolipids, which sequester important membrane proteins and are involved in signalling (133). Expanding this role further, the composition of the membrane of the cell can illuminate its behaviour, with higher composition of certain lipids (e.g. phosphatidylserine) present in the outer leaflet of the membrane signalling apoptosis (134). More importantly, in this context, the lipid capability of spontaneous production of a bilayer upon exposure to a hydrophilic environment has led to a wide array of applications; these lipid based constructs can be used as model systems, through which to study phenomena such as membrane dynamics (25, 60, 135), or, importantly in this case, cell behaviour (78).

1.3.1. THE PHASE TRANSITION

One key property of individual lipid molecules that is of specific importance to the current work, as mentioned above, is the phase transition: T_m . This is highly dependent on the intrinsic properties of the lipid, and is affected by intrinsic properties, such as head group (136), tail group length (137) and degree of bond saturation (138). The lipid phase transition, shown schematically in Figure 1.6C, may be considered similar to the glass transition found in polymers, in that at a specific temperature a lipid structure will transform from an ordered, highly packed state, known commonly as either the gel phase to a more disordered, loosely packed state, known as the fluid phase (139). Table 1.1 shows the structures and phase transition temperatures of lipids commonly used to form bilayers.

Lipid	T _m (°C)	Structure
DOPC (1,2-dioleoyl- <i>sn</i> -glycero-3-phosphocholine)	-17	
POPC (1-palmitoyl-2-oleoyl- <i>sn</i> -glycero-3-phosphocholine)	-2	
DMPC (1,2-dimyristoyl- <i>sn</i> -glycero-3-phosphocholine)	24	
 DPPC (1,2-dipalmitoyl- <i>sn</i> -glycero-3-phosphocholine)	41	

Table 1.1. Lipids commonly used to produce lipid bilayers, with their phase transition temperature, T_m , demonstrating the importance of the structure to the point at when the lipids change from fluid to gel phase. (All images taken from Avanti Polar Lipids website).

This table serves to demonstrate how the phase transition is affected by the structure. The factors that affect this transition are related to the nature of the Van der Waals (VdW) interactions between the lipid molecules. In the gel phase the hydrocarbon tail is in a fully extended conformation, which leads to tighter packing on the component lipids. In this state the system has a high viscosity and thus the membrane components have a low mobility. As the T_m is reached the chains ‘melt’ and the hydrocarbon chains are oriented randomly, disrupting the packing of the lipid structure and leading to the fluid phase, with a concomitant decrease in the viscosity. As it may be assumed, an increased length of this chain would increase the VdW interactions, thus requiring greater energy to disrupt this packing. Further, the unsaturated bonds induce an inflexible ‘kink’ in the chain, which increases the effective

area of the lipid, reducing the VdW interactions between each molecule. DOPC shown here has two such bonds and thus has the lowest T_m , with the saturated DMPC and DPPC having much T_m due to their saturated chains. DPPC has a longer chain than DMPC and therefore has a higher T_m . This shows that the nature of the phase transition, as well as the accompanying changes in the system's viscosity, is highly dependent on a series of easily controllable factors. It is this property that makes lipid-based systems attractive as a means of cellular study. By using different lipid compositions or combinations thereof it is possible to define, in a specific manner, the diffusion coefficient. Were all other factors kept constant it is therefore possible to associate the cellular behaviour, in a quantifiable way, with the viscosity of the lipid surface.

1.3.2. PRODUCTION OF SURFACE SUPPORTED LIPID SYSTEMS

Surface supported lipid systems have long been seen as a useful model through which to observe biological interactions. They have applications in microfluidics and lab-on-a-chip fields, as well as biosensing (140). There is also an emerging focus on the use of these as surfaces within the field of cell biology, studying their response (78). These systems have advantages, such as biological similarity and ease of functionalisation, with the current research falling within this latter area. However, the types of lipid-based systems that can be used are as varied as the fields in which they are applied, with a summary of possible constructs shown in Figure 1.7. Free-standing bilayers (Figure 1.7A) have had applications in the production of pores or membranes, to study membrane proteins (141, 142). Supported lipid bilayers, as well as those that are cushion or tethered via polymer coatings (Figures 1.7B, C and D), also have wide biophysical applications. Supported vesicular layers (Figures 1.7E and F), are often an intermediate step in the formation of a complete bilayer on the surface; however, they have found applications in the monitoring of molecular interactions (143, 144). As supported lipid bilayers (SLBs) are used in this study it necessary to understand the factors behind how these surfaces are formed.

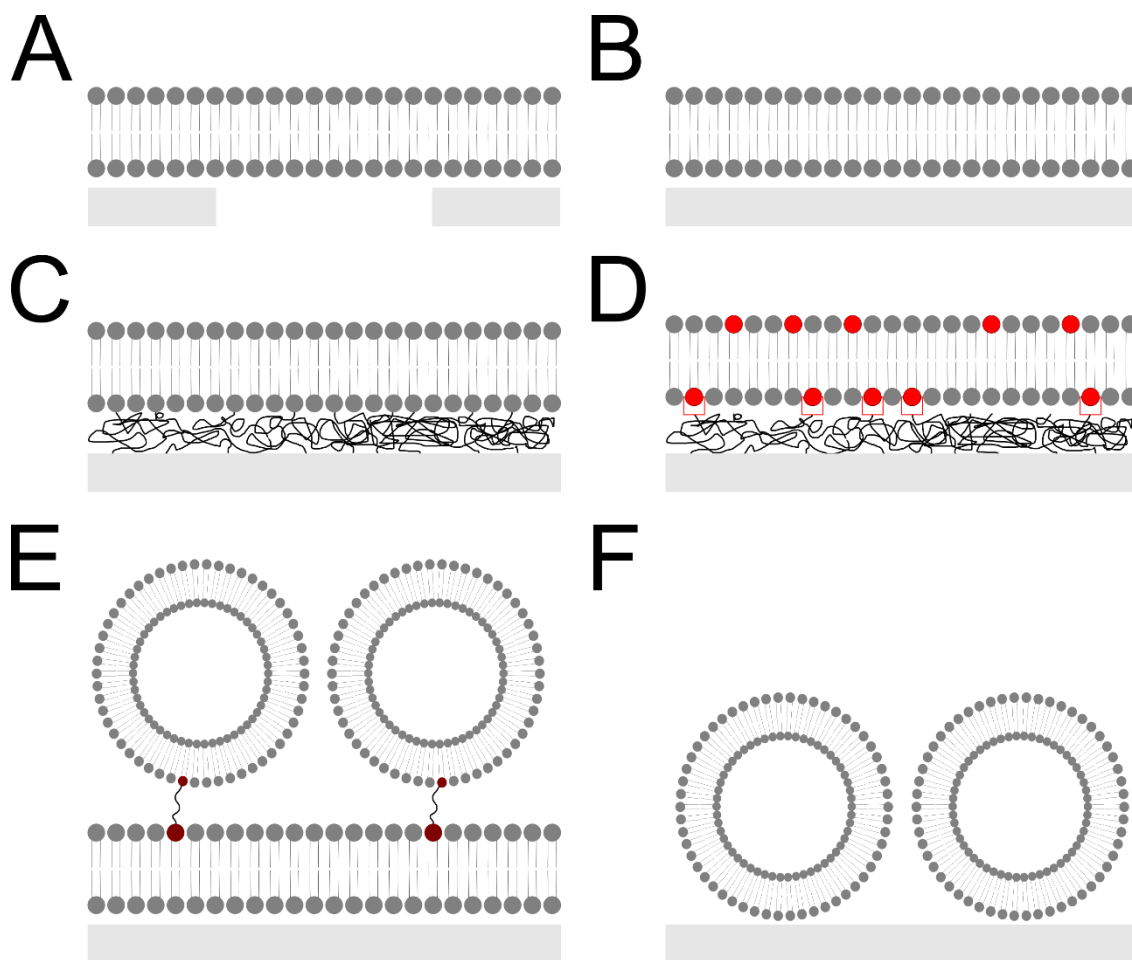


Figure 1.7. Supported Lipid Systems. A schematic summary of the different types of lipid systems that can be deposited on a solid support for various applications. (A) Shows a free-standing bilayer; (B) a supported lipid bilayer, as used in this study; (C) shows a polymer cushioned lipid bilayer, with (D) showing a similar construct of a polymer tethered bilayer; (E) shows a vesicle presenting bilayer, which has applications in drug delivery systems and (F) shows a supported vesicular layer. While not all of these are widely used, they exemplify the types of systems at a researcher's disposal. (Adapted from (64)).

There are two key methods in the production of SLBs: vesicle deposition and Langmuir-Blodgett troughs. Both have advantages and disadvantages; however, the former will be discussed here as, due to the ease of production, this system was used throughout this project. Terminology of the field uses the terms 'vesicles' and 'liposomes' sometimes interchangeably and sometimes using the term 'vesicle' as a more general term for all vesicular lipid structures, with liposome specifically referring to unilamellar vesicles. However, throughout this work,

the term 'vesicle' has been used with specific regards to unilamellar vesicles, with different structures noted. This is to prevent any confusion between terminology used here and the commonly used naming conventions e.g. vesicle-vesicle interactions or vesicle deposition.

The process whereby vesicle deposition produces SLBs is shown schematically in Figure 1.8. Key to forming a SLB on a surface is a variety of factors, one such being the role of electrostatic interactions. These govern both the interaction of the vesicles with one another and with the surface. For example, in Figure 1.8A were the ionic strength of surrounding buffer changed, or indeed its pH (145), then SLB-formation would be significantly affected. Further divalent cations, such as Ca^{2+} or Mg^{2+} can promote the formation of SLBs, likely due to electrostatic screening, even in mM concentrations (146). The ionic strength in general can not only change the electrostatics, but also the stability of the vesicles themselves, by changing the osmotic pressure. It has previously been noted that SLB formation progresses more quickly with a higher osmolarity in the surrounding buffer, compared to within the vesicle (147). Further, the same work showed that the size of the vesicles themselves governs SLB formation, with larger vesicles less capable of forming bilayers.

Beyond simply addressing the nature of the vesicles, the contribution of the solid support cannot be underestimated. Figure 1.8B shows the intact vesicles adsorbed to a solid support. This concentration of vesicles is important, with a critical coverage required for the formation of bilayers. Indeed, single vesicles were seen to be stable over a significant time if adsorbed individually. However, if adsorbed in larger concentrations the vesicle rupture was seen, leading to continuous bilayer formation (148). This bilayer formation was only observed on specific substrates, such as glass and mica, whereas on surface such as TiO_2 , there was minimal SLB formation (without additional strategies), regardless of the vesicle coverage (147). The charge of the surface can also have an effect on the formation of SLBs as shown previously (149). Interestingly, if the surface charge, provided by NH_3^+ groups, was screened using a $-\text{COOH}$ containing buffer, then vesicles, rather than an SLB were seen on the surface. This contribution of charge is also related to the vital role of the hydrophilicity of a surface. It has been noted that in order to maximise favourable interactions between the vesicles and the surface the surface must be highly hydrophilic, with a water contact angle $<10^\circ$ required to induce vesicle rupture (150). However, vesicles may still only partially fuse or adsorb on top

of the bilayer even after maximising the vesicle-vesicle and vesicle-surface interactions. Thus, with the vesicle deposition technique it is often the case that thorough optimisation of these factors to the experimental setup is required.

The nature of surface continues to have a significant effect on the nature of the bilayer beyond its initial formation. As shown in Figure 1.8C, there is a 1-2 nm thick water layer formed between the solid support and the bilayer. This water layer and the interaction with the solid support significantly effects the mobility of the lipids in the bilayer, with the diffusion coefficient reduced by ~ 2-fold on SLBs compared to that in vesicles (151). This induces a separation in the properties of the two leaflets making up the SLB. For example, due to interactions the water layer, the diffusion of the proximal leaflet is slower than that of the distal leaflet (152, 153). Similarly, the phase transitions of the leaflets are dissimilar, with the melting of the lipid chains occurring at a higher than normal temperatures in the proximal leaflet, attributed to a stabilising effect of the solid support itself. The roughness can also have a significant effect, inducing large changes in the lateral mobility of the SLB components, with rougher surfaces leading to higher diffusion coefficients (61). This proximity of the SLB to the surface has a knock-on effect on their applicability. For example, membrane-spanning proteins cannot be successfully incorporated into these constructs due to the limited space between the SLB and the surface (140). This has been alleviated by the production of the polymer cushioned and tethered SLBs (Figure 1.7C and D respectively), which allow for the inclusion of these proteins (154).

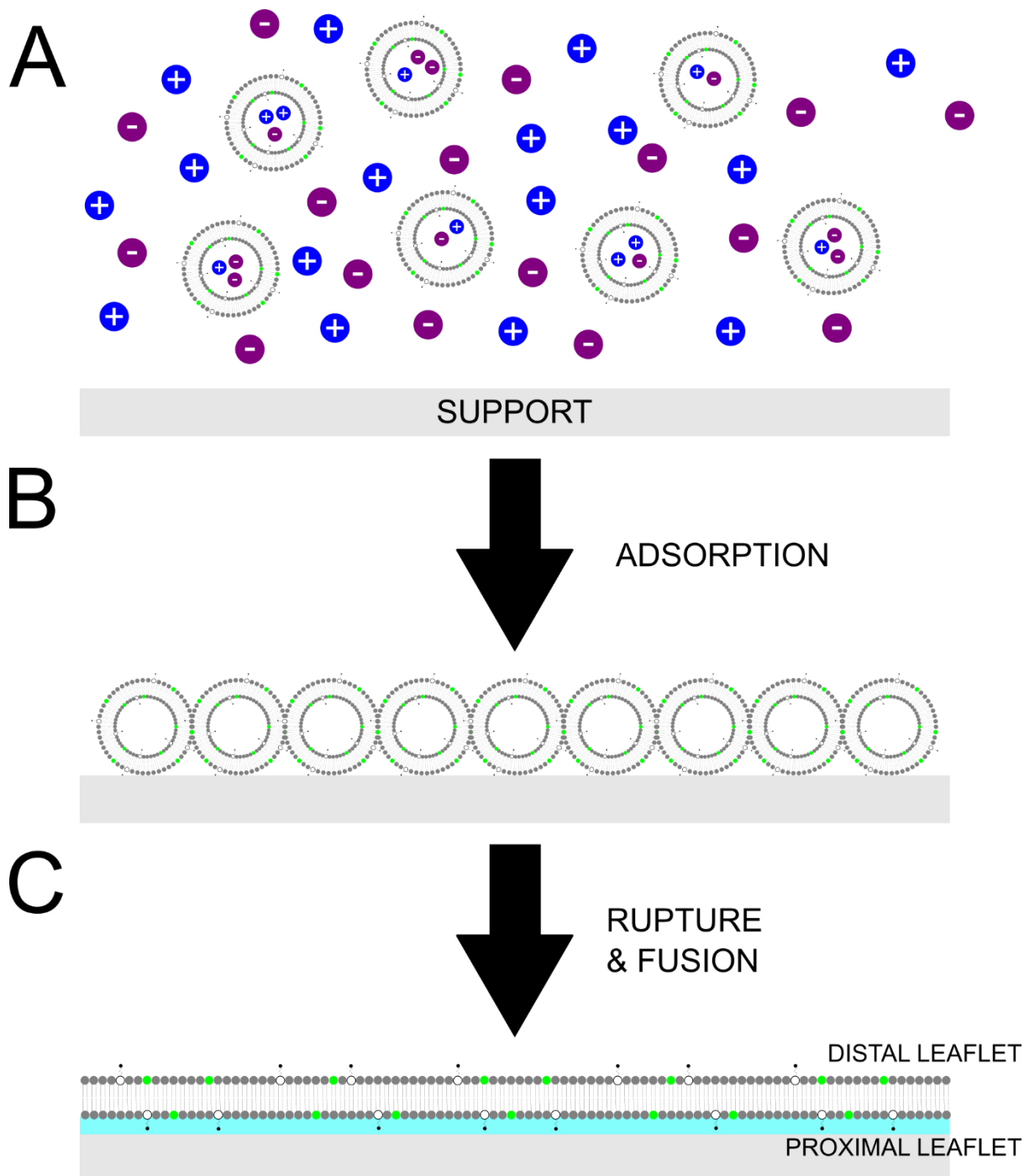


Figure 1.8. Formation of Supported Lipid Bilayers. The process of vesicle deposition, leading to the formation of SLBs. Initially, vesicles adsorb to the surface e.g. glass, mica, gold etc. In (A) the vesicle solution is added to the surface. The buffer is important, due to the electrostatic interactions, as well as the osmotic pressure caused. These vesicles may contain a number of modifications, including fluorescence or functional groups; however, these may change the vesicle-vesicle and surface-vesicle interactions. In the (B) the vesicles adsorb to the surface and, depending on the nature of the interaction, either remain as intact vesicles or, as in (C),

spontaneously rupture and form a single bilayer. This latter event depends on variables, such as the vesicle concentration, the vesicle-surface interactions, the vesicle-vesicle interactions and the vesicle buffer interactions. The proximal and distal leaflets can have different physical properties, such as diffusion coefficients, due to the proximity of the proximal leaflet to the surface and the interstitial water layer (blue).

1.3.3. UNDERSTANDING THE DIFFUSIVE CHARACTERISTICS OF SUPPORTED LIPID BILAYERS

Together, the previous two sections demonstrate how the phase transition can change the physical properties of the bilayer and how these can be formed on solid surfaces. However, it has also alluded to how the diffusive characteristics may also be affected. Therefore, it is also important to understand how these factors combine to produce supported lipid bilayers of defined diffusive characteristics.

The diffusion of bilayers can be measured by several fluorescence based techniques, including FRAP (fluorescence recovery after photobleaching), FCS (fluorescence correlation spectroscopy) and FLIM (fluorescence lifetime imaging). Each of these provide distinct advantages and disadvantages, but, either directly or indirectly, allow for the calculation of the diffusion coefficient, D , of a lipid bilayer. The nature of these techniques is summarised in Figure 1.9. In Figure 1.9A, FRAP bleaches a spot of defined area, and the return of the fluorescence is then measured over time. FCS (Figure 1.9B), relates photon counts over time to a decay in the probability of the two counts being the same event. The decay in this probability is related to the diffusion time (details on this in section 2.8). FLIM (Figure 1.9C), is a more indirect measure of the diffusion, and measures the rotation of a fluorophore in the membrane. Fluorophores that are sensitive to the viscosity of their environment will have different fluorescence lifetimes, which is related to the diffusion. Together, or separately, these approaches can give key insights into the environment of a molecule in a bilayer.

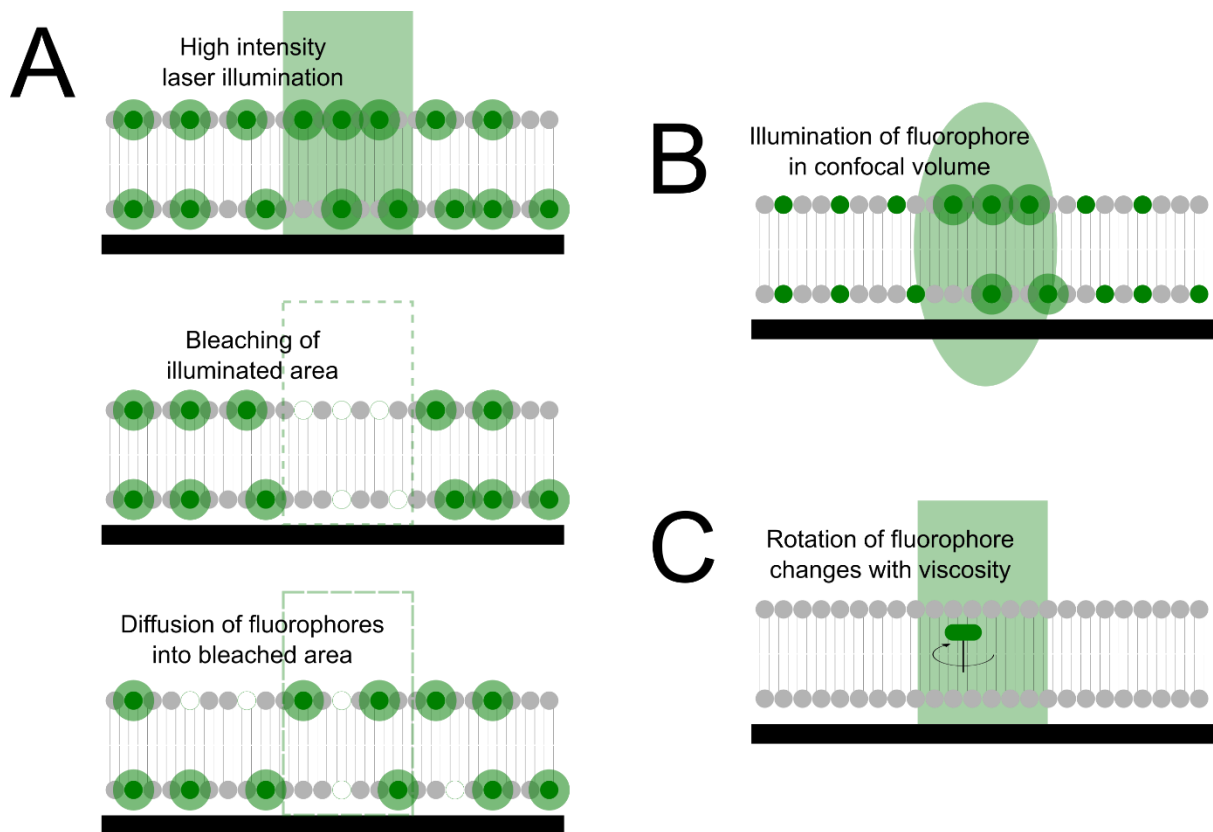


Figure 1.9. Measuring Diffusion in Supported Lipid Bilayers. (A) FRAP: A high intensity laser excites the fluorophores in a given area to the point of bleaching. The rate at which the fluorescence returns is dependent on the diffusion of the bilayer and the area bleached. (B) FCS: Fluorophores in the bilayer are illuminated as they pass through an illumination volume. The photon residence time and thus the decay in the autocorrelation function (relating the probability of two events being a single photon), thus the decay is dependent on the diffusion. (C) FLIM: The lifetime of the fluorophore in the excited state is dependent on the rotation within its environment. This can be related to the viscosity using standard of known values. The viscosity can then be related to the diffusion, through the Saffman-Delbruck equation.

The diffusion coefficient, as measured in $(\mu\text{m}^2/\text{s})$, is a good indicator of the mobility of the ligand, but is also connected to and controlled by further properties, such as, importantly, the viscosity, as well as the radius of the diffusing molecule and the thickness of the bilayer. These connections were first determined by Saffman and Delbruck in 1978 (155). Inventively named the Saffman-Delbruck (SD) equation (shown in equation 1.1), it demonstrates a relationship between these contributing factors:

$$D = \frac{k_B T}{4\pi\eta_m h} \left[\ln\left(\frac{2L_{SD}}{R}\right) - \gamma \right] \quad (1.1)$$

Where D is the diffusion coefficient, k_B is the Boltzmann constant, T the absolute temperature, η_m the membrane viscosity, L_{SD} , the Saffman-Delbruck length, R the radius of the diffusing molecule and γ the Euler-Mascheroni constant (0.577). The SD length is:

$$L_{SD} = \frac{h \eta_m}{2 \eta_f} \quad (1.2)$$

Where h is the thickness of the bilayer and η_f is the viscosity of the surrounding fluid.

Over the years, this has been further developed by other groups (156, 157), with different degrees of applicability. For example, the HPW model, can only be solved computationally, but its relevant development allows for a more accessible solution (157). Together these have sought to expand the validity of the SD equation, as, in its original form it remains valid only as long as the inclusion radius is significantly smaller than the SD length. In larger diffusions, such as micron-scale lipid domains, the original equation fails, which is not the case in these developments. The modified predictions were, however, valid at all length scales. However, beyond these developments, another group has also produced an alternative means of calculating the diffusive characteristics of molecules within the bilayer as shown in equation 1.3 (135):

$$D = \frac{(k_B T) \lambda}{4\pi\eta_m h R} \quad (1.3)$$

Where λ is the characteristic length.

This equation has sought to compensate for the valid range of the original SD equation, with the key differences between these equations being the relationship of the radius of the diffusing

molecule to its diffusion coefficient. While the SD equation stipulates that there is a weak logarithmic dependence of the diffusion on the diffusing radius, this alternative equation demonstrates a $1/R$ relationship. Further, they have proven that this equation holds true for protein diffusions determined elsewhere. They also define a characteristic length (λ), introduced for dimensional reasons and a measure of the membrane perturbation caused by the diffusing object. As the radii of these membrane inclusions radii can range from 0.5 nm, in a single lipid, to hundreds of nm in protein complexes, this length can give huge ranges of diffusion values, depending on how the inclusion is predicted to interact with the bilayer. Gambin et al. (2006), which proposed this equation, validated this proposal by producing bilayers of tuneable thickness (h) to determine if the equation would predict the diffusion values when adjusting this variable. Furthermore, by incorporating proteins of variable size into the bilayer of giant unilamellar vesicles they also tested if the equation was valid at different inclusion radii (R). In both cases the $1/R$ relationship predictions agreed well with attained values for the diffusion. In addition to this, diffusion values obtained from the literature also showed good agreement with these predictions. Therefore, according to results previously observed in the literature, both of these equations appear valid, but it is not clear to what extent, nor which is more accurate.

Beyond these issues, a key point to note is that the determination of the diffusion coefficient is related to the viscosity of the bilayer. This therefore means that bilayers of known diffusion can define the viscous properties of the bilayer. This has applications in the study of mechanobiology as the cells response to the surface can be linked to the bilayer's viscous properties. It is this relationship that is of interest, when seeking to understand the molecular basis of the cell response to supported lipid bilayers of differing diffusive characteristics.

1.3.4. SUPPORTED LIPID BILAYERS IN CELL STUDIES

Due to their biomimetic nature, lipid bilayers have a great deal of potential in cell-based studies; further, the ease with which they can be altered with different moieties also serves to enhance their appeal. To this end they have been used in a wide array of different cellular based studies. Examples include bilayers used as a means to adhere and culture cells, using different adhesion promoting moieties (158-160), as well as using these systems to study the nature of the cell-

cell (81, 161) or the cell-interface (77, 79, 82) interactions. As a subset of these cellular studies, the fluid nature of the bilayer has led to these systems being of particular interest in studying the field of mechanobiology (78). The diffusive characteristics, detailed above demonstrate how they can allow for relatively simple means of understanding how the cell responds to the mechanical properties of the environment.

Naturally non-fouling as a consequence of either the mobility of the lipids (162) or their neutral charge at physiological pH (163), SLBs must first be functionalised to be used as a cellular platform. However, this in itself presents a myriad of opportunities, as this can be used to present a wide variety of molecules on the surface. Crosslinking strategies such as avidin-based proteins with biotinylated lipids, as done in this work, present simple and effective means of stable conjugation of biological molecules to the SLBs (164). Functionalisation can also be performed through the use of carbodiimide links (165), amongst other covalent methods. To introduce functionality these moieties can be bound to a variety of functional molecules, such as cadherin (81), collagen (165), EGF (166), RGD (159) and DNA (167). The wide variety of simple strategies, as well as a bank of biological molecules upon which to draw from, means that SLBs have a wide potential for their use as platforms to study a wide array of biological processes.

Upon functionalisation, SLBs can be used to probe a wide number of biophysical and biological processes. For example, they have been used to produce an idealised model synapse system, understanding the role of the component lipids and strength of interaction (167). Further they have been used to probe the interaction of T-cells with antigen presenting cells (168). In more cell-based studies they can be functionalised with cadherin molecules in order to probe cell-cell adhesion (169). Cadherins play a major role in cell-cell adhesion, akin to the role of integrins in cell-surface interactions (170); thus, using lipid bilayers to study how their physical environment changes how cells respond is vitally important. Further, cadherin-functionalised SLBs were used in conjunction with PDMS microwells to produce a 3D single-cell environment in order to study the effect of dimensionality and ligand mobility on the cell (161).

This is not the only example looking at how the nature of a SLB controls the cell adhesion, with other using it as a general adhesion platform for cell culture (171), as well as others looking at the nature of the cell-surface interactions using QCM-D (quartz crystal microbalance-dissipation) (172). Yet others have used SLBs, tethered to doxorubicin-loaded (anti-cancer) liposomes, as a model cancer therapy (173). In addition to these applications, SLBs also present an opportunity to change the nature of the cell i.e. control lineage commitment in relevant cell lines. As already noted, the response to the lateral mobility (as controlled by viscosity) is akin to that of stiffness, with it being possible therefore to control cell behaviour in this manner. The viscosity of lipid bilayers defines their lateral mobility, which can control cell spreading and cytoskeleton organisation (161); thus it is possible, and indeed implied, in recent work that differentiation is also controlled through the ligand mobility (59). However, unlike the biomaterials detailed in section 1, SLBs have not found widespread use in longer-term cell cultures, relevant to differentiation studies.

In addition to the usage of SLBs as a simple biological platform it has also found applications in the field of mechanobiology (78). This is despite the lack of applicability of well-characterised force-sensing techniques, such as traction force microscopy, in determining the force exerted with regards to the fluid component of SLBs. Typically, in traction force microscopy the displacement of fluorescent beads, embedded within a surface (e.g. hydrogel), gives values pertaining to the forces exerted on surface by the cell. However, as SLBs are laterally mobile, displacement of any molecule present on or within the surface will also be acted upon by forces related to this. Despite this limitation, inroads have been made in determining biological forces exerted on SLBs. For example, tension sensors have been used in conjunction with SLBs to measure the forces present within the cell-surface interactions (174). By using a DNA ‘spring’ pN forces can pull apart the fluorophore and its intramolecular quencher, which can be related to the mechanical force present on the surface. Known as MTFM (molecular tension fluorescence microscopy), it has been successfully applied in to determine the forces in T-cell receptors, but currently not for the cell adhesive integrins. Other work has used stacked SLBs, as means to attempt to apply traction force microscopy to these fluid surfaces. By embedding fluorescent beads within a hydrogel and stacking SLBs (up to four) on top (crosslinked together) this work was able to ascertain an idea as to the traction forces present. However, the presence of crosslinked laminin networks on the surface meant

that the elastic contribution of the laminin on the surface was observed rather than the contribution of the underlying fluid SLB. These examples, despite demonstrating possible difficulties, also allude to the potential of using these surfaces in understanding the role of viscosity in the production of force at the surface.

Addressing mechanobiology in cell adhesion specifically, this has been covered superficially in section 1.1.2. While not a SLB based study Garcia et al. nonetheless used supported lipid monolayers of DOPC and DPPC to show that increasing the lateral mobility of the surface increases cell spreading. In contrast, Kocer et al. saw the opposite was true in SLBs of the same components, citing increased clustering in the DOPC as the principal cause. Stacked lipid bilayers have also contributed to this field (81, 82); as noted previously the interaction of the SLB with the solid support leads to a decrease in the diffusion coefficient. Using a number of separate bilayer stacked on one another and attached via PEG-based linkers, this work showed that as the number of bilayer stacks increased so too did the diffusion, with a concomitant decrease in cell spreading. It must be noted, however, that this does not account strictly for bilayer mobility, with the increasing number of stacks also decreasing the detected stiffness; nonetheless is an interesting approach to adjusting the diffusion of a bilayer.

On a more molecular level SLBs have also been used to determine the nature of the adhesion machinery at the cell-surface. Interestingly, this has led to the discovery that initial adhesion is independent of force, with integrin clustering similar on both fluid SLBs and the glass control (175). Further, proteins such as paxillin, FAK and talin, all implicated in force generation, are recruited independently of lateral forces (79). This is not true of vinculin, however, which required contractile forces for recruitment. This change in the nature of the forces has wider implications on the adhesion structures themselves. For example, the removal of traction forces, by culturing cells on DOPC SLBs led to the formation of podosome-like adhesions rather than focal adhesions (58). This has implications in cancer metastasis as these ring-like podosomes are related to more invasive cell lines, such as cancer cells (80). Further, endocytic machinery is also upregulated in upon the removal of traction forces, as cells were noted to have increased levels of internalised ligand on fluid DOPC SLBs (77). Due to talin and the endocytic adaptor protein, Dab2, being mutually exclusive at integrin clusters, it is interesting to note that force generation may act as a switch between mechanical and biochemical means

of signal transduction in the cell. These studies therefore illuminate the potential of SLBs for the studying of various processes and consequences relating to the mechanical sensing of the surface.

1.4. THE CURRENT WORK

1.4.1. THESIS AIMS

The core objective of this thesis was to understand, in greater depth, how the cell response is controlled by the viscosity-defined ligand mobility, with a mind as to how this can be applied to a cell system relevant to regenerative medicine. To this end the aims of this thesis were:

1. The production and characterisation of supported lipid bilayer of varying viscosity.
2. Determining how the changes in the viscosity-defined ligand mobility affect the cellular response, specifically in terms of the nature of the adhesion and morphology.
3. Elucidation of the underlying molecular principles related to how the cells detect the viscosity-defined ligand mobility, and the consequential downstream effects on the cell.
4. Application of supported lipid bilayers as a platform, upon which to grow and manipulate human mesenchymal stem cells.

1.4.2. THESIS OUTLINE

Chapter 2 outlines the methodology of how the supported lipid bilayers were produced and characterised, as well as the relevant control. It also details the nature of the cell assays and the different methods to determine the nature of the cell response.

Chapter 3 shows the production and characterisation of the supported lipid bilayers through atomic force microscopy and fluorescence correlation spectroscopy, as well as using fluorescence to ascertain the stability of the system. The functionalisation of the SLBs was then quantified using quantitative fluorescence microscopy.

Chapter 4 details the cell response in terms of the initial adhesion and morphology behaviour of the cell. To this end the chapter quantifies the response of the cells in terms of the nature of their morphology and their focal adhesion properties.

Chapter 5 has sought to develop from chapter 4, by attributing the cell response to the ligand mobility to the viscosity of the lipid bilayer. To this end the molecular clutch developed by Prof. Pere Roca-Cusachs et. al., previously applied to stiffness, was used to attempt to understand the cells response to surface. The actin flow was determined with and without the presence of inhibitors. Further to this, the consequential downstream effects of the cell response, i.e. transcription factors localisation and differentiation, was also determined.

Chapter 6 has applied the SLBs as a cell culture platform for mesenchymal stem cells (MSCs). This chapter details the initial adhesion and morphology of MSCs over 24 and applies further strategies to optimise and promote more effective long-term adhesion.

2. METHODS & MATERIALS

2.1. LIPID PREPARATION AND VESICLE PRODUCTION

2.1.1. PREPARATION OF LIPID SOLUTIONS

The two bilayer forming lipids were used in this project were DOPC (1,2-dioleoyl-sn-glycero-3-phosphocholine, Avanti Polar Lipids, AL, USA), and DPPC (1,2-dipalmitoyl-sn-glycero-3-phosphocholine, Avanti Polar Lipids, AL, USA). The former has a transition temperature of -17°C , and is in the fluid-phase at the cell culture temperature of 37°C . The latter has a transition temperature of 41°C , and is in the gel-phase at cell culture temperature. Both of these were provided already suspended in chloroform and were used at the delivered stock concentrations.

In order to functionalise the SLBs b-cap-PE (1,2-dioleoyl-sn-glycero-3-phosphoethanolamine-N-(cap biotiny), Avanti Polar Lipids, AL, USA) was added in various amounts. Initially, the number of moles of DOPC or DPPC used was calculated and necessary percentage of moles (mol%) of the functionalised lipid was added in a range from 0.02 – 10 mol%. This lipid was provided in powder and dissolved in a solution of 65:35:8 v/v chloroform:methanol:water to a stock concentration of 5.5 mg/ml. For regular usage a more dilute solution was used at a concentration of 0.5 mg/ml, in 1.9 ml of chloroform and lipid solution, adding 100 μl of methanol (to ensure solubility), to a final volume of 2 ml. Functionalisation was also achieved through the addition of positively charged lipid to the lipid mixture. This was only included in mesenchymal stem cell (MSC) cultures, as detailed later. To produce positively charge bilayers DOTAP (1,2-dioleoyl-3-trimethylammonium-propane (chloride salt), Avanti Polar Lipids, USA) was included at 0 – 30 mol%.

When needed, fluorescent lipids were also added to the lipid mixture; for example, when determining diffusion. For the study of diffusive characteristics and initial visualisation BODIPY-conjugated lipid molecule TopFluor-PE (23-(dipyrrrometheneboron difluoride)-24-norcholesterol and 1-palmitoyl-2-(dipyrrrometheneboron difluoride)undecanoyl-sn-glycero-3-phosphoethanolamine, Avanti Polar Lipids, AL, USA), with an excitation/emission wavelength of 495/503 nm, was used in a concentration of 0.01 – 0.5 mol%. For fluorescence

correlation spectroscopy measurements a lower concentration was used, for reasons described in the relevant section. For imaging, higher concentrations were used so as to compensate for any bleaching caused by excitation. Texas Red DHPE (Texas Red™ 1,2-Dihexadecanoyl-sn-Glycero-3-Phosphoethanolamine, Triethylammonium Salt, Molecular Probes, USA) was also added to the bilayer when performing quantitative fluorescence imaging, as detailed in the relevant section.

Lipid mixtures were produced by adding 2 mg of DOPC or DPPC to a glass vial. Other lipids, detailed above were added as required, as a mol% of DOPC or DPPC. These mixtures were then dried thorough under a steady stream of N₂ gas, which evaporated the chloroform, leaving a dry lipid film in the vial. Any excess chloroform was subsequently removed by further drying under vacuum for ≥ 1 hr.

2.1.2. REHYDRATION AND PRODUCTION OF SMALL UNILAMELLAR LIPID VESICLES

For the suspension of the lipids in aqueous solution, samples were rehydrated in R (rehydration) buffer. This buffer was made with 150 mM NaCl and 10 mM Tris and to a pH of 7.4. For DOPC room temperature (RT) buffer was added to a final concentration of 3 mg/ml of lipid and allowed to swell for 1 hour, with occasional vortex mixing to remove any remaining lipid film from the vial. In the case of DPPC, the preparation was the same, but the R buffer was pre-warmed to above the transition temperature and maintained throughout the rehydration process.

The rehydration of the lipid film in aqueous solution produced a large multilamellar vesicle (LMV) solution; that is, a solution of vesicles that are of various different structures and sizes. However, to produce contiguous, supported lipid bilayers (SLBs), vesicles ideally should be below 90 nm in diameter, so as to maximise the membrane tension and promote fusion to the surface (176). To this end LMV solutions were extruded through polycarbonate membranes (Whatman® Nucleopore Track-etched membrane, Avanti Polar Lipids, AL, USA) of 50 nm and 100 nm pore size, using the mini-extruder system (Avanti Polar Lipids, AL, USA). The system is set up as shown in Figure 2.1. The filter supports and the polycarbonate membranes

were wet with R buffer prior to assembly and the system was constructed as directed. Prior to extrusion of the lipids the whole assembly, including the syringes, was washed through with R buffer several times. Concerning the polycarbonate membrane, the DOPC LMV solution was extruded through a membrane with a pore size of 50 nm at RT, producing small unilamellar vesicles (SUVs) of DOPC. However, DPPC required an adjusted method; prior to extrusion, the whole apparatus, and the DPPC, was heated to 70°C. This is under the recommendation of previous work that has noted typical temperatures of bilayer formation was much higher than the 41°C transition temperature (177). To produce DPPC SUVs, the heated solution was first extruded through a 100 nm membrane. This membrane was then replaced and the solution extruded again through a 50 nm membrane. In each extrusion, in both the case of DPPC and DOPC, solutions were extruded a minimum of 11 times to produce the final SUV solution. In the case of all vesicles the effect of the extrusion was determined through dynamic light scattering (DLS) measurements, confirming the size and polydispersity of the solutions (Zetasizer Nano Z, Malvern, UK).

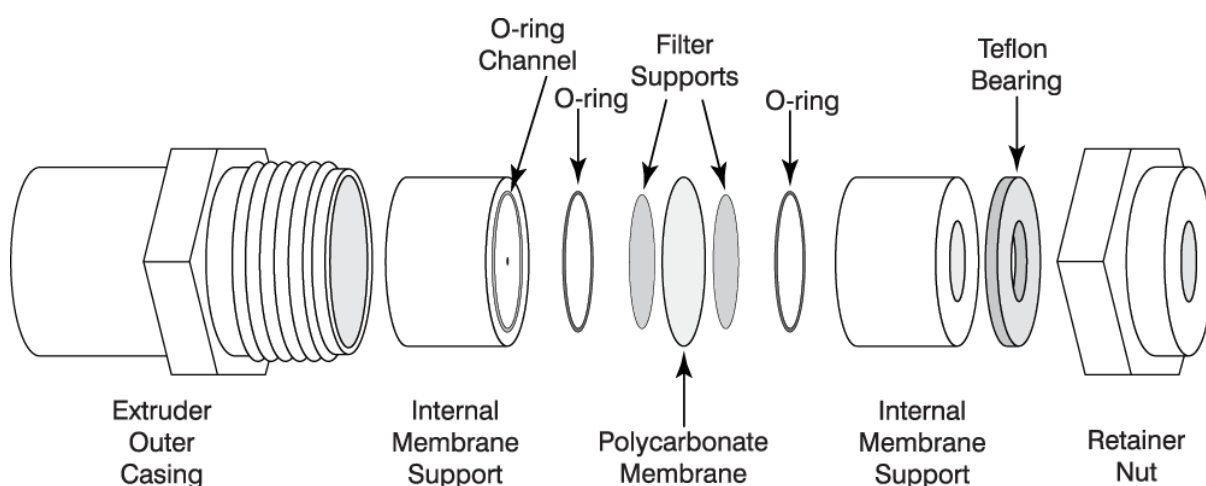


Figure 2.1. Extrusion. The Avanti mini-extruder system, showing the means of assembly for the system. (Image taken the website of Avanti Polar Lipids (178))

2.2. PREPARATION OF GLASS SURFACES

In order for SLBs to form on the glass surfaces were required to be both very clean and hydrophilic; ideally, the contact angle must be below 10° on glass surfaces, in order to maximise vesicle-substrate interactions (150). In order to prepare the surfaces for SLB formation two preparation methods were used; one method was used to prepare glass for fixed

cell experiments (for antibody staining), and the other for live cell experiments (dynamic process observations) in glass bottomed multi-well plates.

2.2.1. GLASS PREPARATION FOR FIXED CELL EXPERIMENTS

For fixed cell experiments glass coverslips of thickness 0.08 – 0.13 mm (thickness no. 0) with a diameter of 32 mm were used. Coverslips were sonicated first by ultrapure water and then with ethanol for 15 mins each, and washed in between each step with ultrapure water. The cleaning solution used was an RCA solution and was produced by mixing ultrapure water, ammonium hydroxide and hydrogen peroxide in a ratio of 5:1:1. This solution was then heated to 60 – 70°C; upon the reaching the desired temperature, the coverslips were immersed in the solution for 20 mins. Subsequently, samples were washed extensively in ultrapure water and dried using a stream of N₂ gas. After drying samples were stored in a sealed container until use.

2.2.2. GLASS PREPARATION FOR LIVE CELL EXPERIMENTS

For live cell experiments, glass-bottom multi-well plates (Mattek, USA) were used and so a highly aggressive clean of organic contaminants could not be performed in this case. As such the plates, with no. 0 thickness, as before, and a 20 mm glass well diameter, were cleaned by sonicating the surface with ethanol for 1 hr and washed with ultrapure water. Surfaces were then dried with a stream of N₂ gas. Plates were then cleaned with an oxygen plasma for 20 min at the highest power setting (Expanded Plasma Cleaner, PDC-002, Harrick Scientific, USA), and sealed until use.

2.3. PRODUCTION OF PDMS WELLS

Due to the necessity of keeping the SLBs hydrated at all times, wells were produced on the glass coverslips for fixed cell experiments, so as to make washing and culturing of cells easier. Polydimethylsiloxane (PDMS) was used due to its biocompatibility and simple means of production. Initially, the PDMS elastomer (Sylgard 184, Farnell, UK) was mixed in a 9:1 ratio with its crosslinker and mixed thoroughly. The mixture was then poured into a flat, plastic dish, taking care to ensure the mixture was as evenly distributed as possible. The mixture was then

degassed, under vacuum for 30 mins and cured for 2 hrs at 65°C. After curing, the wells were made, from the now solid PDMS, first by cutting a larger samples of 26 mm using a metal stamp. Smaller wells, to hold the SLBs, were cut from these, using a stamp with a diameter of 9 mm. The well dimensions are shown to scale in Figure 2.2. These cut surfaces were then cleaned by sonicating in methanol for 10 mins and rinsing with further methanol; they were then covered and dried at 65°C. The cleaned and cut PDMS was then bonded to the glass coverslips using a handheld plasma corona (BD-20V, Electro-Technic Products). Both the glass and the PDMS was activated by exposing to plasma for 20 s each and bonded by applying the activated surfaces to each other under pressure immediately. For use in cell culture the resulting glass-bottomed wells were then sterilised with UV light for 30 mins and stored in a sealed, sterile container until use.

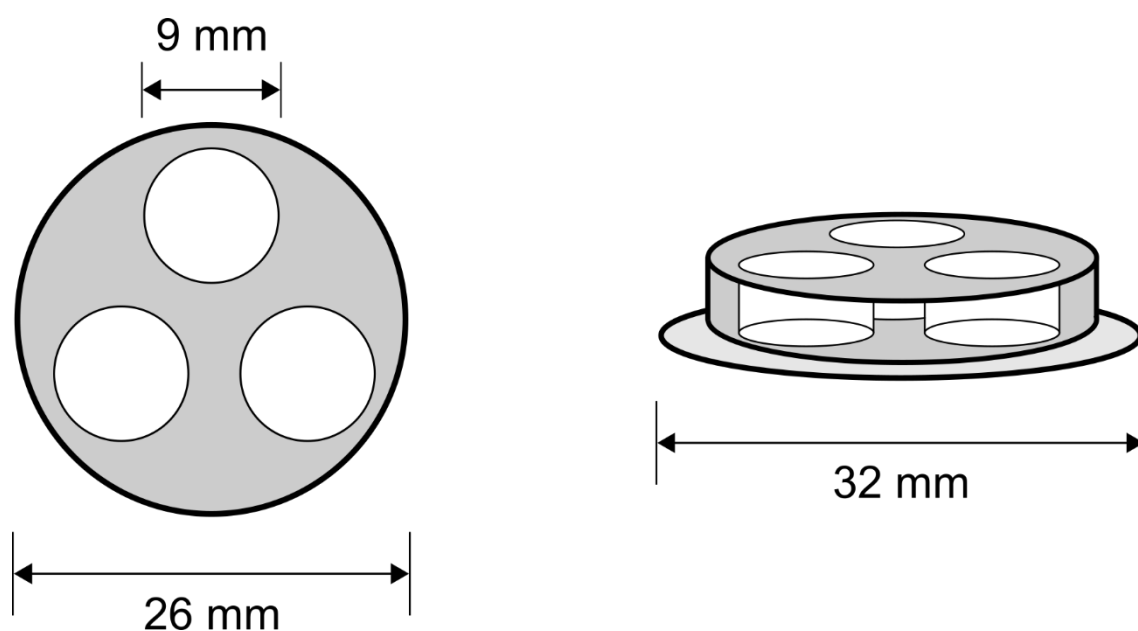


Figure 2.2. Experimental Setup. The dimensions of the PDMS wells used to produce SLBs. All measurements are to scale.

2.4. PRODUCTION OF SUPPORTED LIPID BILAYERS AND GLASS CONTROL

2.4.1. PRODUCTION OF SUPPORTED LIPID BILAYERS

To produce and wash both DOPC and DPPC based SLBs F (fusion) buffer was used. This is of a higher NaCl concentration to increase the osmotic pressure on the vesicles, made with 300 mM NaCl, 10 mM Tris and 10 mM MgCl₂. The higher osmotic pressure on the outside the vesicles compared to the inside and the presence of a divalent cation improves the efficiency of bilayer formation (179). The SUV solutions were diluted in F buffer immediately before use; the final concentrations of DOPC and DPPC were 0.1 mg/ml and 0.2 mg/ml respectively and either kept at RT (DOPC) or at 70°C (DPPC). To ensure sterility these solutions were then filtered through a 200 nm membrane (Sartorius) prior to incubation on the glass surfaces. Immediately prior to incubation with the final SUV solutions the glass surfaces were activated by oxygen plasma for 10 mins in fixed cell experiments (Diener Electronics, 150W) and 20 mins for live cell experiments (Harrick Scientific, high power). Samples were then sterilised using UV light for 5 mins and the SUV solutions were incubated for 20 mins. In DPPC, this was performed at 70°C. After incubation samples were then washed extensively with F buffer and, subsequently, ultrapure water at RT (DOPC) or 70°C (DPPC). At all times care was taken to ensure the lipid coated area was kept hydrated to prevent bilayer destruction.

2.4.2. PRODUCTION OF RGD-GLASS CONTROL

To contrast the effect of a mobile and immobile ligand a representative glass control was produced. Initial steps in the preparation of these surfaces was the same as with bilayers in both fixed and live cell experiments. However, once cleaned the methodologies diverge. To produce the immobile control, the cleaned glass surfaces, either the PDMS wells, or the glass-bottomed dishes, were incubated for 1 hr with 1% v/v APTMS (3-amino(propyl)trimethoxysilane, Sigma-Aldrich, USA) solution in propanol-2-ol (Sigma-Aldrich, USA). Surfaces were then washed with propan-2-ol and dried with N₂ gas. Samples were then allowed to cure at 65°C overnight, and were subsequently sterilised with UV light for 20 minutes. Samples were stored in a sealed container before use. The presence of silanes on the surface was confirmed with static water contact angle measurements (Attension Theta, Biolin Scientific, USA).

To biotinylate the surface a heterobifunctional crosslinker was used: biotinamidocaproate N-hydroxysuccinimide ester (Sigma-Aldrich, MO, USA), with the NHS-ester group binding to the amino group on the silane. A stock solution was made up in dimethylformamide (DMF)

and used within 1 month. Immediately before use, this was diluted to 1 mg/ml in ultrapure water and incubated on the silanised glass surfaces for 1 hr. Surfaces were then washed extensively with ultrapure water. It is here that the methodologies once again converge, so as to functionalise all surfaces with the RGD tripeptide.

2.5. FUNCTIONALISATION OF SURFACES

Functionalisation of all samples was done using the biotin-avidin interaction. A biotinylated cyclic-RGD peptide was used to adhere cells to the SLB surface (Peptides International, KY, USA). This was mediated by either neutravidin (Fisher Scientific, USA) or Texas Red neutravidin (TR-neutravidin, Fisher Scientific, USA). All were provided in powder form; neutravidin was dissolved to a stock concentration of 5 mg/ml in water and stored at 4°C. Both biotinylated cyclic-RGD and TR-neutravidin were dissolved to a stock concentration of 1 mg/ml, with the former in water and the latter in DPBS (Gibco), and were stored at -20°C in aliquots. All steps were done in sterile conditions.

2.5.1. FUNCTIONALISATION CALCULATIONS AND PROTOCOLS

The desired concentration of both neutravidin and RGD was determined from an estimation of the moles of functionalised lipid present on the surface. For this the radius of all lipids were taken as the previously determined area of a single DOPC molecule of 0.73 nm² (180, 181). Taking as an example the 9 mm diameter PDMS wells, described above, the area here would be 63.6 mm². Therefore, the assumed number of lipids within this area would be 8.8×10^{13} , with 2% of this being 1.8×10^{12} . From Avogadro's number (6.02×10^{23} /mol), the number of moles of biotinylated lipid was calculated to be 2.9×10^{-12} moles. For a 10x mole excess 10^{-11} moles of neutravidin and cyclic-RGD were added in this case. The required number of moles was calculated for different surface areas and concentrations were adjusted accordingly. Samples were incubated for 30 mins in both the case of neutravidin and RGD incubation. Between each incubation samples were washed extensively with ultrapure water. In all cases care was taken to ensure samples remained sterile and hydrated.

2.5.2. BIOTINYLATION OF EXTRACELLULAR MATRIX PROTEINS

Further to the SLB functionalisation detailed above, other functionalisation strategies were used to determine any effect on the cell response. To this end both fibronectin and a fragment of the full protein was biotinylated for use in conjunction with this system (reaction shown schematically in Figure 2.3). The full fibronectin protein was acquired from R&D Systems. The fragment used was the Type III domain, repeats 7-10 (FNIII₇₋₁₀). This is a 44.1 kDa fragment, containing both the cell binding, RGD, peptide and the synergy site (PHSRN), which is cited as also playing a role in cell binding (182). This fragment was kindly produced and gifted by Alex Rodrigo-Navarro, of the Microenvironments for Medicine lab, University of Glasgow, UK. Both were biotinylated with the EZ-Link Micro-Sulfo-NHS-LC-Biotinylation Kit (Thermo), using the protocol provided. 200 µg of either fibronectin or FNIII₇₋₁₀ was diluted to a total volume of 500 µl. Immediately prior to use 1 mg of sulfo-NHS-LC-biotin (NHS-biotin) was dissolved in 200 µl water to concentration of 9 mM. As NHS-esters are readily hydrolysed in aqueous solutions, the NHS-biotin was not stored. The amount required was calculated, first by calculating the required mmol of NHS-biotin (Equation 2.1), assuming a 50-fold excess and then by using this to determine the required reaction volume to add to the protein sample using Equation 2.2.

$$\text{mmol Biotin} = \text{ml protein} \times \frac{\text{mg protein}}{\text{ml protein}} \times \frac{\text{mmol protein}}{\text{mg protein}} \times \frac{50 \text{ mmol Biotin}}{\text{mmol protein}} \quad (2.1)$$

$$\mu\text{l biotin solution} = \text{mmol Biotin} \times \frac{557 \text{ mg}}{\text{mmol biotin}} \times \frac{200 \mu\text{l}}{1 \text{ mg}} \quad (2.2)$$

Where 50 mmol (1) accounts the 50-fold molar excess, 557 g/mol is the molecular weight of NHS-biotin and 200 is the µl of water used to dissolve the 1 mg of NHS-biotin, making the 9 mM solution. Upon adding the NHS-biotin solution to the protein solution the samples were incubated for 60 mins at RT.

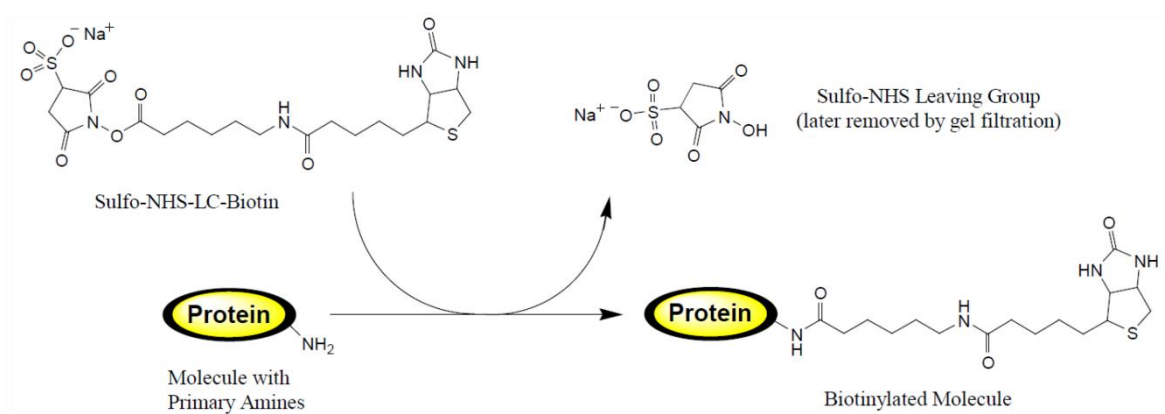


Figure 2.3. Protein Biotinylation. The process used by the EZ-link biotinylation kit, through the NHS ester-based linking of biotin molecules to primary amines on the protein of interest (image taken from product datasheet provided by Thermo (183)).

After the necessary incubation time the samples were then de-salted to remove any un-reacted NHS-biotin reagent. The provided spin desalting columns were first separated from the storage buffer by centrifugation at 1000 g for 2 mins. Liquid from the columns was collected in each step by placing the column in a 15 ml centrifuge tube. To equilibrate 1 ml of PBS was added to column and spun at 1000 g for 2 mins; this was repeated a further 2 times. The spin column was placed in a fresh 15 ml and the 500 μ l reaction solution was added and allowed to absorb into the column resin. The sample was collected by centrifuging at 1000 g for 2 mins. The purified solutions were then aliquoted and stored at -20°C until use.

2.5.3. QUANTIFICATION OF BIOTINYLATION

The degree of biotinylation of each of the proteins was determined using the HABA/Avidin (4-Hydroxyazobenzene-2-carboxylic acid, Sigma) reagent. The powdered reagent was reconstituted in 10 ml of ultrapure water and stored at 4°C . This protocol is based on the displacement of HABA from the avidin upon the inclusion of biotin and results in a change of absorbance at 500 nm (A_{500}). In a cuvette the A_{500} of 900 μ l of HABA/Avidin solution was first recorded using a spectrophotometer (6715 UV/Vis Spectrophotometer, Jenway). Subsequently 100 μ l of the biotinylated protein solution was added and incubated for 2 mins to allow the signal to stabilise. The A_{500} of the samples was then determined. This change in

absorbance was then calculated by subtracting the A_{500} of the HABA/Avidin/Protein(biotin) from 0.9x the A_{500} of the HABA/Avidin solution. This 0.9 is a correction value for the difference in total volumes. The concentration (in mg/ml) of the protein was then determined by measuring the absorbance at 280 nm (A_{280}) using a Nanodrop spectrophotometer (Nanodrop 1000, Thermo). Knowing the molecular weight (M_w) of both fibronectin and FNIII₇₋₁₀, this was used to calculate the moles of protein. Rearranging the Beer Lambert Law (shown in Equation 2.3) allows for the determination of the moles of biotin.

$$mmol\ biotin = \left(\frac{(0.9 \times A_{500\ HABA/Avidin}) - A_{500\ HABA/Avidin/Protein}}{34,000 \times 1} \right) \times 10 \quad (2.3)$$

Where 34,000 is the extinction coefficient of HABA and 1 is the path length in cm, and the x10 multiplication compensates for the dilution in the reaction volumes. Dividing this by the mmol of the protein determined via the Nanodrop, gives an estimation of the number of biotin molecules per fibronectin or FNIII₇₋₁₀ molecule.

2.5.4. DETERMINING PROPERTIES OF BIOTINYLATED PROTEINS

The function of the biotinylated proteins was determined via cellular experiments, comparing the biotinylated proteins to the native proteins. Firstly, glass coverslips were washed by sonicating in ethanol and dried at 70°C and then sterilised using UV light. All proteins were adsorbed to glass coverslips by incubating 100 µl of a 20 µg/ml solution of each protein for 1 hr and washed with PBS. Cells were prepared and used as described later (in section 2.9.1 and 2.9.3. respectively), and their properties analysed to ensure the biotinylation process had no detrimental effects on the protein function.

The presence of the biotinylated proteins on the SLB surface was performed using a qualitative enzyme-linked immunosorbent assay (ELISA). Firstly, the SLBs were created as described in section 2.4.1 and functionalised with neutravidin as described in section 2.5.1. The necessary calculations for the required concentrations were also made (section 2.5.1). Incubation with fibronectin and FNIII₇₋₁₀ was done by diluting the samples to the necessary concentrations in

ultrapure water and incubating on the SLBs for 30 mins. After incubation the samples were also washed with ultrapure water as previously described. Control samples, with no functionalisation were used as a blank control.

After washing the surfaces were blocked for 30 mins with 1% BSA in PBS. Samples were then incubated with HFN7.1 (DSHB, USA) primary antibody for the RGD tripeptide at a 0.1 $\mu\text{g/ml}$ (in 1% BSA solution) for 1 hr. Samples were washed extensively, by several cycles of agitation in PBS and blocked a second time with 1% BSA for 30 min. The anti-mouse HRP (horseradish peroxidase) secondary antibody (ThermoFisher) was incubated for 1 hr in 1% BSA, at a 1:1000 dilution, and washed as with the primary antibody. Solutions A and B and the Stop solution (R&D Systems) were allowed to equilibrate to RT and solutions A and B were mixed in a 1:1 ratio to the required volume. These were then added to each well and incubated for 20 mins, protected from light. The reaction could be followed by the presence of a blue colour, with the intensity proportional to the amount of protein in the sample. The reaction was stopped with the Stop solution, which turned the protein positive samples from blue to yellow. These solutions, including the relevant controls, were then aliquoted into a 96-well plate and read using a microplate reader at 450 nm and 540 nm (Synergy 2, BioTek), with the latter acting as a correction wavelength, to ensure no erroneous readings from the system. The background from the controls was subtracted from the samples and compared between SLB surfaces to compare the relative amount of protein on the surface.

2.6. ATOMIC FORCE MICROSCOPY

2.6.1. SETUP AND CALIBRATION

Atomic Force Microscopy was performed using a Nanowizard[®] 3 Bioscience AFM (JPK, CA, USA), set up on a Zeiss Observer Z1 microscope. This was used with the software provided by the manufacturer. Cantilevers, with an estimated spring constant and resonant frequency of 0.32 N/m and 67 kHz respectively (PNP-TR-Au, Nanoworld, Switzerland), were used to determine the properties of the lipid bilayers. All measurements were performed under ultrapure water. Before use the true spring constant and resonant frequency of each cantilever was confirmed by calibration through force spectroscopy. To calibrate a glass surface, prepared in the same way as the substrates for the lipid samples (except for plasma cleaning to prevent

attractive interactions between the sample and the tip), was used. The calibration procedure was performed as detailed in the user manual; briefly, the tip was landed on the surface and was then used to produce a force-distance curve. Using the linear, repulsive area of the curve (when the cantilever is in contact with the surface) the cantilever sensitivity was determined. This is defined as nm/V, as the deflection of the cantilever is given in volts, depending on where reflected laser impacts the photodiode. From this, the spring constant was determined by measuring the oscillation of the cantilever freely in solution, selecting one of the peaks at one of the cantilever harmonic frequencies and fitting it to a Lorentz curve. Depending on the peak selected a correction value, provided by the software was used to calculate the spring constant.

2.6.2. IMAGING MODE

Both contact and AC imaging modes were used to image the surfaces of the SLBs. In AC mode the cantilever was tuned to ensure the frequency and phase of oscillations matched using the AC Feedback Mode Wizard, provided in the software. In the case of both AC and contact mode imaging areas were selected from 2 – 10 μm^2 and a line rate of ≤ 0.5 Hz was used to reduce the potential of imaging artefacts caused by the SLBs. The set-point i.e. the force exerted on the sample, was adjusted as required to maintain contact and kept as low as possible to prevent damage to both the tip and the SLB surface. After use tips were cleaned of possible lipid contaminants using 2% SDS and rinsed thoroughly with ultrapure water.

2.6.3. FORCE MAPPING MODE

To measure the physical properties of the bilayers force mapping was used. The relative set point was set at 20 nN and the approach velocity of 1 $\mu\text{m/s}$, with 64 measurements taken on each surface within a 5 μm^2 , 8x8 square grid. After use tips were cleaned of possible lipid contaminants using 2% SDS and rinsed thoroughly with ultrapure water. All images and data were analysed using the offline processing software (version 5.0.84) provided, as detailed in section 2.10.1.

2.7. QUANTITATIVE FLUORESCENCE MICROSCOPY

2.7.1. STANDARD SOLUTIONS

Quantitative fluorescence imaging was used to quantify the number of fluorescent neutravidin molecules present on the surfaces and was carried out as described in Nair et al. 2011 (184). Vesicles were produced in the same manner as described in section 2.1. Three vesicle solutions were prepared; the first was used to produce a calibration curve of bulk lipid concentration (referred to from herein as solution 1) and contained 99.9 mol% DOPC and 0.1 mol% Texas Red DHPE (TR-DHPE), rehydrated and used in R buffer only. The second and third were used to produce a bilayer standard used for fluorescence calibration and contained 99.5 mol% DOPC and 0.5 mol% TR-DHPE (solution 2) or 100 mol% DOPC only (solution 3). To determine the fluorescence as it pertained to bulk protein fluorescence TR-neutravidin was prepared in R buffer at a concentration of 0.304 μM .

2.7.2. BULK CALIBRATIONS

To determine the calibration curve of the bulk lipid fluorescence serial dilutions of solution 1 were made, producing 5 solutions in a concentration range of 0 – 0.74 μM . Using a 20x objective and focusing the beam within the solution, images were taken of the fluorescence intensity. To calibrate the bulk fluorescence signal of the protein solution, serial dilutions of the TR-neutravidin was made in a concentration range from 0 – 0.304 μM . In all cases the exposure time and exposure time was kept constant to prevent any erroneous changes in fluorescence signal. The change in fluorescence as a consequence of the concentration was plotted and a linear fit, through the origin, provided the intensity/ μM of the bulk solutions. These were designated I_{protein} and I_{lipid} for the protein and lipid respectively. As the same fluorophore was used in the same buffer, this allowed for determination of a scaling factor (F) between the fluorescence in the bulk lipid and protein solutions, as shown in equation (2.4):

$$F = I_{\text{protein}} / I_{\text{lipid}} \quad (2.4)$$

2.7.3. BILAYER CALIBRATION AND DETERMINATION OF MOLECULAR DENSITY

Solutions 2 and 3 were used to produce a series of bilayer calibration standards. The bilayers were prepared as previously described in section 2.4.1. The ratios in which they were mixed produced bilayers containing concentrations of TR-DHPE ranging from 0 – 0.5 mol%. Using a high magnification objective (63x), the fluorescent intensity was determined at a consistent exposure time and plotted against the estimated number of TR-DHPE molecules. By using the size of a DOPC molecule, 0.73 nm^2 , as a determinate of lipid area the number of fluorescence lipid molecules could be estimated in the same way as detailed in section 2.5. Once again, a linear fit, through the origin, was used to determine the value of the gradient, giving the fluorescence of the bilayer as a consequence of the number of fluorescent molecules; this was designated $I_{\text{bilayer}(\text{lipid})}$. This was multiplied by the scaling factor to determine the amount of protein (Equation 2.5):

$$I_{\text{bilayer}(\text{proten})} = F \times I_{\text{bilayer}(\text{lipid})} \quad (2.5)$$

Here $I_{\text{bilayer}(\text{protein})}$ denotes the fluorescent intensity of the protein on a lipid bilayer. This is described as the fluorescence as a consequence of the number of protein molecules per μm^2 and produces a calibration curve, which was used to determine the number of molecules per μm^2 of an unknown sample. In this case, SLBs of either DOPC or DPPC were incubated with the TR-neutravidin and the fluorescence value applied to the equation of the gradient of fluorescence vs. protein per μm^2 to determine the number of neutravidin molecules on the surface. Comparing this to the theoretically expected value, based on the 4 available binding sites of neutravidin for biotin, the amount of RGD on the surface was also calculated.

2.8. FLUORESCENCE CORRELATION SPECTROSCOPY

Fluorescence correlation spectroscopy (FCS) was performed using a DCS-120 confocal scanning system, provided by Becker and Hickl. The laser was set to pulsed mode at a frequency of 50 MHz and an excitation filter of 448 nm, and an emission filter of 535 nm was used to select for the required fluorescence. The detection of emitted fluorescence was done

through a hybrid photo-multiplier tube, HPM-100-40 detection unit. An 40x water immersion objective, C-Aprochromat, was used, with an numerical aperture of 1.2.

The system was calibrated to determine the width of the laser beam using a standard solution of 100 μm FITC-tagged fluorescent microspheres (0.1% v/v in water, Sigma). The diffusion of the microspheres can be determined mathematically by the Stokes-Einstein equation, as shown below in Equation 2.6:

$$D = \frac{k_B T}{6 \pi \eta R} \quad (2.6)$$

Where D is the diffusion coefficient, k_B is the Boltzmann constant ($1.38064852 \times 10^{-23} \text{ m}^2 \text{ kg s}^{-2} \text{ K}^{-1}$), T the absolute temperature (310 K), η the solution viscosity ($0.692 \text{ kg (m.s)}^{-1}$ at 37 °C), and R the beam radius.

To measure the diffusion coefficient of lipid bilayers BODIPY-based fluorophores TopFluor-PE (phosphoethanolamine) (Avanti Polar Lipids, AL, USA) were used in concentrations varying from 0.01% - 0.5% of total lipid. Initially, the decay of the correlation factor with (log) time was plotted and fitted with Equation 2.8 in order to determine the decay time.

$$G_\tau = \frac{1}{N} \frac{1}{(1 + \tau/\tau_D)} + 1 \quad (2.7)$$

Where $G(\tau)$ is the correlation factor, N the average number of diffusing molecules, τ the correlation time, τ_D the diffusion time. The equation was added to the database in OriginPro V8 and the curves were fitted using this software, providing the diffusion time values.

In the case of beam calibration Equation 2.6 provides the diffusion coefficient of the microspheres in water at RT; Equation 2.7 provides the diffusion time, which when combined with (1) gives the beam width. From this the diffusion time attained from the bilayer samples

can then be applied to Equation 2.8 to determine the diffusion coefficient of the bilayer of interest.

$$\tau_D = \frac{\omega^2}{4D} \quad (2.8)$$

Where ω is the beam radius and D is the diffusion coefficient.

2.9. CELL CULTURE & STAINING

2.9.1. CELL CULTURE

C2C12 mouse myoblasts were cultured in a growth media of DMEM (1x) Dulbecco's Modified Eagle Medium (+ 4.5 g/L D-Glucose, + L-Glutamine) (Gibco), containing 1% antibiotic mix of penicillin and streptomycin, 1% Fungizone (Gibco) and 20% FBS. Cells were seeded in T75 flasks and used after reaching near confluence ($\leq 70\%$ surface coverage).

Human mesenchymal stem cells (hMSCs) were derived from adipose tissue and were used as a further study to understand the effect of SLB viscosity on the cell behaviour. Prior to experiments the cell population was expanded using T75 flasks, growth medium 2 (Promocell, Germany) and supplemented with a growth supplement. 24 hours before usage the media was replaced with DMEM (1x) Dulbecco's Modified Eagle Medium (+ 4.5 g/L D-Glucose, + L-Glutamine), supplemented with 100 μ M pyruvate (Gibco), 1% NEAA (non-essential amino acids), 10 % FBS, 1 % P/S (Gibco), and 1% Fungizone (Gibco).

When cells of either cell line reached the required density they were prepared first by gently washing the cells with DPBS. Cells were then removed from the flask surface by adding 2 ml of trypsin and incubating at 37°C for 5 min, or until all cells were removed from the surface. The reaction was then quenched using the relevant growth media and centrifuged for 5 min at 1,000 rpm, with the resulting cell pellet being re-suspended in the appropriate media, as detailed in each relevant section. The number of cells was counted using a Countessa II

automated cell counter (Thermo), by mixing cells and Trypan Blue (Invitrogen), in a 1:1 ratio, pipetting onto the counter insert.

2.9.2. ANTIBODIES

In order to stain the necessary proteins, using the methods detailed below a variety of separate antibodies were used, and are summarised in Table 2.1.

Protein Specificity	Species	Company	Dilution	Fluorescence
Vinculin	Mouse	Sigma	1:400	N/A
FAK	Rabbit	Millipore	1:200	N/A
pFAK	Mouse	Millipore	1:200	N/A
YAP	Mouse	Santa-Cruz	1:100	N/A
Myogenin	Mouse	Santa-Cruz	1:100	N/A
Sarcomeric myosin	Mouse	DSHB	1:125	N/A
Fibronectin (RGD)	Mouse	DSHB	1:330	N/A
Mouse	Rabbit	Jackson Immunoresearch	1:200	Cy3
Rabbit	Chicken	Molecular Probes	1:200	AlexaFluor 488

Table 2.1. A list of antibodies used to stain for proteins of interest.

2.9.3. ADHESION OF C2C12 MOUSE MYOBLASTS

To analyse the cellular adhesion of either C2C12 or MSCs re-suspended cells were diluted to a seeding density of 5,000 cells/cm², for C2C12s, or 2,000 cell/cm² for MSCs in depleted DMEM (no FBS). The differences in cell density are due to the relative sizes of the cells. A

sparse cell distribution was needed in this scenario, so as to understand the individual adhesion characteristics; therefore, minimal cell-to-cell contact is required. The final cell sample volume added to each well was 50 μ l. Therefore, prior to adding cells the samples, all samples were washed first with sterile PBS and then with the corresponding media. This was equilibrate the samples to that of cell culture conditions, preventing any dilution of the media or osmotic differences caused by the ultrapure water that was used to wash the samples.

Cells were then added to the sample wells, containing either lipid bilayers or the immobile control, and allowed to adhere for 3 hrs for C2C12s, and for either 3 hrs or 24 hrs with MSCs. Samples were then washed with PBS and fixed with 4% formaldehyde for 15 min at RT. After washing, cells were permeabilised with 0.1% Triton X-100 (Sigma) for 5 min. The concentration was not higher so as to prevent damage to the SLBs caused by the Triton X-100 detergent. Samples were then washed with PBS again, before blocking for 30 minutes with 1% BSA solution. The primary antibody was diluted to the concentration shown in Table 2.1. in a blocking buffer of 1% BSA solution and incubated on the samples for 1 hr. Samples were washed extensively with PBS, with agitation and blocked for a further 30 min with 1% BSA solution. The secondary antibody was diluted to the concentration shown in Table 2.1 in blocking buffer (1% BSA). Phalloidin, specific for actin was also added at a 1:100 dilution; the fluorescence of phalloidin was dependent on the combination of antibodies used and was either BODIPY, rhodamine or Cy5 labelled. The antibody/phalloidin solution was incubated on the sample for 1 hr. Samples were again extensively washed with PBS, mounted with DAPI containing medium and imaged. Samples were imaged using a Zeiss Observer.Z1 fluorescence microscope at 10x, 20x and 63x, using MicroManager software (185). Images were then processed using Fiji software (186). Morphological characteristics such as area and circularity were measured (the latter was defined as $4\pi \times (\text{area}/\text{perimeter}^2)$). Further information on image processing, specifically in the quantification of focal adhesions, is detailed in section 2.10.2.

To observe YAP localisation to the nucleus, the pixel intensity of the YAP stain within the nucleus was divided by the pixel intensity in the cytoplasm, producing a nucleus:cytoplasm ratio. The nucleus was the area defined through staining of the nucleus by DAPI and the cytoplasm was defined by the phalloidin actin stain (where the nucleus had not also stained positively).

2.9.4. DIFFERENTIATION OF C2C12 MOUSE MYOBLASTS

After culture, re-suspended cells were diluted to a concentration associated with a seeding density of 40,000 cells/cm² in media containing 1% FBS and 1% ITS (insulin transferrin selenium, GIBCO, USA) for either 2 or 4 days. Samples were then washed with PBS and fixed with 4% formaldehyde for 15 min at RT. After washing, cells were permeabilised with 0.1% Triton X-100 for 5 min and washed with PBS again before blocking for 30 minutes with 1% BSA solution. Samples at 2 days were then incubated with an anti-myogenin primary antibody and those at 4 days were incubated MF-20 primary antibody against sarcomeric myosin. Both were diluted in blocking buffer and incubated on the samples for 1 hr. Samples were then washed extensively with PBS, with agitation and blocked for a further 30 min with 1% BSA solution and incubated with the secondary antibody (rabbit anti-mouse) diluted to 1:200 in 1% BSA for 1 hr. Samples were again extensively washed in PBS, with agitation. Mounting medium with DAPI was added to stain the nuclei. This allowed for the counting of the nuclei staining positively for the transcription factor myogenin at 2 days and for sarcomeric myosin at 4 days. Images were taken with a 20x objective using a Zeiss Observer Z1 and MicroManager software. Myogenin images were processed using Fiji software. Sarcomeric myosin images were processed and analysed using the CellC counter standalone extension for Matlab (187).

2.9.5. C2C12 CELL TRANSFECTION

Cells were transfected using the Neon transfection system (Thermo Fisher Scientific, USA), and the procedure was adapted from the described protocol. Cells were cultured using T150 flasks, to maximise the number of cells available for transfection. Upon reaching approximately 70% confluency cells were washed, trypsinised and centrifuged at 500 rpm for 5 min. Excess media was carefully removed from the pellet and the pellet washed by centrifuging in PBS for 5 min at 500 rpm. The pellet was then suspended in 120 µl of the resuspension buffer (pre-warmed to 37°C prior to use, Thermo) provided. This yielded a final cell density of ~ 10⁷ cells/ml. This is to compensate for the differences between the 100 µl tip used and the 10µl detailed in the protocol. This solution was then mixed with required plasmid, with a final, total mass of plasmid of 5 µg added to the cell suspension in each instance. Plasmids used to transfect the C2C12 cells were LifeAct-RFP and LifeAct-GFP for actin, and

VD1 (Addgene plasmid no. 46271, described as pEGFPC1/GgVcl 1-258 A50I) (106), which were provided by the Cellular and Molecular Mechanobiology group (Pere Roca-Cusachs, IBEC, Barcelona, Spain). These were used both individually and combination to ascertain viscosity based changes in cell behaviour.

The cell/plasmid solution was then then taken into the Neon tip, taking care to prevent the production of air bubbles within the tip, as this would allow for arcing of the electric charge, killing the cells. The cell/plasmid containing tip was then placed in a reaction cuvette, containing 3 ml of pre-warmed (37°C) E2, electrolytic buffer (Thermo). The transfection parameters, shown in Table 2.2, were taken from the data sheet for C2C12 transfection with the Neon transfection system, with cells/ml changed to account for the larger tip volume. Immediately after transfection the cells were added to a T75 flask containing pre-warmed (37°C) DMEM media, with 20% FBS. They were then allowed to adhere and spread for 24 hrs prior to use in live cell experiments.

Pulse Voltage (v)	Pulse width (ms)	Pulse number	Cell Density (cells/ml)	Transfection Efficiency	Viability	Tip type
1,650	10	3	*~10 ⁷	95%	96%	*100 µl

Table 2.2. The conditions required to transfect C2C12 cells with plasmids of interest. The stars indicated deviation from the provided protocol, which required 5×10^6 cells/ml in a 10 µl tip. However, the cell density was increased by approximately 10x to account for the larger, 100 µl tips used.

2.9.6. LIVE CELL IMAGING OF ACTIN FLOW

Imaging of live cells on supported lipid bilayers was performed on transfected cells. Samples were imaged using purchased glass bottom dishes, with a no. 0 thickness and a sample diameter of 20 mm (Mattek, USA). Before use the dishes were first cleaned as described in section 2.2.2 with surfaces being produced as described in section 2.4. The cell solutions were also produced as detailed in section 2.9.3. However, in this case cells were seeded at a density of 10,000

cells/cm²; this was to compensate for any issues in the transfection efficiency of the protocol in section 2.9.5. Cells were seeded in depleted DMEM media and allowed to adhere for 1 hr. In order to perturb the actin flow, blebbistatin was included in the media at a concentration of 50 μ M where required. This ensured almost complete inhibition of the myosin II action on the actin cytoskeleton, as shown previously by the lack of traction forces (47).

Time lapse imaging was performed using a Nikon Eclipse Ti spinning disk confocal microscope. Samples were kept at 37°C and supplemented with 5% CO₂ using a heated, sealed chamber, surrounding the microscope stage. Samples were imaged using a 60x oil objective, with a numerical aperture of 1.4. The LifeAct plasmid was used to fluorescently label actin and the actin flow was determined by imaging the samples at 1 Hz for 2 mins, using Andor Q3 Software. Image stacks were then analysed using Fiji software; areas of interest were resliced, producing kymographs that plotted displacement of fluorescence over time (representative images shown in Chapter 5).

2.9.7. MODELLING THE CELL RESPONSE

The nature of the cell response to viscosity was modelled computationally by Prof. Pere Roca-Cusachs of the Institute for Bioengineering of Catalonia. This provided information of the predicted actin flow and adhesion size based on the viscosity of the surface. The details of this model, including the variables used, can be found in Appendix A.

2.10. DATA ANALYSIS

2.10.1. AFM ANALYSIS

All attained AFM data and images were processed using the analysis software provided by JPK (JPKSPM Data Processing Software, JPK, USA). Height images were processed by subtracting a polynomial fit from each scan line. From this a cross-section of a region of interest could be attained. For force mapping measurements, the software was used to process the resulting individual force curves in the map. Firstly, a baseline was set, using the non-contact region of the extend curve, correcting for both offset and tilt. Secondly, the change in the detected height of the cantilever was corrected for using the sensitivity and spring constant determine through

the calibration performed in section 2.6.1. After processing the data was analysed using OriginPro v8 software to determine the thickness of the bilayers.

2.10.2. FOCAL ADHESION QUANTIFICATION

The quantification of the focal adhesions (FAs) is adapted from methods previously described in the literature (188). This was performed using the Fiji software and using a number of plugins provided. The analytical process is shown as a flow chart, with an example image in Figure 2.4. Steps 1 – 3 were performed using the macro in Table 2.3. However, due to the variable nature of the images attained steps were 4 and 5 were adjusted between experiments. As such no comparisons were made between samples of different experimental data sets. Briefly, the image was cropped so that only the FAs of one cell were analysed. The background of the image was then subtracted, and the contrast enhanced through the CLAHE plugin (settings shown in Table 2.3). An exponential fit was then run on the surface to further minimise the background. By adjusting the brightness and the contrast of the image the FAs could be sharply separated from the minimised background. From this a threshold was applied and the particle analysis function of Fiji was used to analyse the FAs. By selecting different measurements, information on properties such as the area, length and number of FAs could be attained.

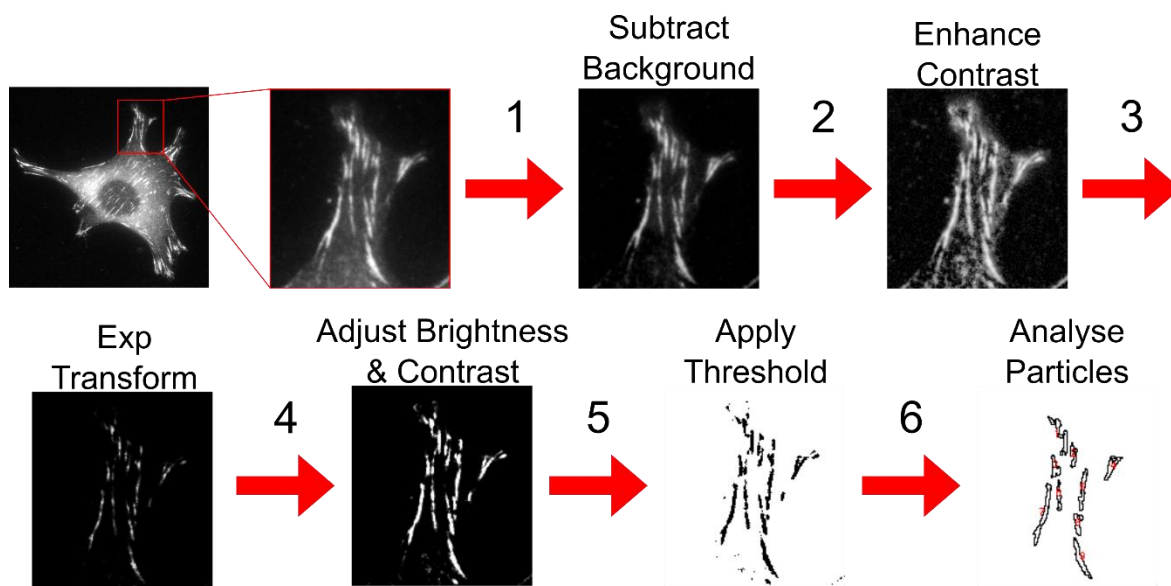


Figure 2.4. Analysis of Focal Adhesions Flow Chart. A small area of the cell is expanded for detail. Steps (1) and (2) were performed with the settings shown in Table 2.2. Steps (4) and (5)

were set in light of the experimental conditions and maintained at a constant setting throughout the analysis of the experimental data set. To this end, exposure times during imaging was also kept constant. In step (6) only particles above $0.75 \mu\text{m}^2$ were counted as focal adhesions.

```
run("Subtract Background...", "rolling=30");  
run("Enhance Local Contrast (CLAHE)", "blocksize=15 histogram=256 maximum=6  
mask=*None*");  
run("Exp");
```

Table 2.3. The macro code used to process images of cells before analysing the focal adhesion properties.

2.10.3. STATISTICAL ANALYSIS

Analysis of statistical differences between conditions in all experiments was performed using GraphPad Prism 6 software, with one-way or two-way ANOVA (analysis of variance) as appropriate. One-way ANOVA was used where there was one independent variable and two-way ANOVA was used where there were two independent variables. Prior to this, the data distribution was determined to be either normal or non-normal using a D'Agostino-Pearson normality test. Statistical significance was determined by multiple comparison tests within the ANOVA; were the data distribution normal, a Tukey test was performed to determine the significance and if non-normal a Bonferroni test carried out to determine significance. Statistical differences were defined by P values and confidence intervals were indicated with a *. As a guide: ns > 0.05, * ≤ 0.05, ** ≤ 0.01, *** ≤ 0.001, **** ≤ 0.0001. Other statistical analyses were performed as required, using the methods provided by the software; if required, outliers were removed using the ROUT test. To ensure robust statistical analysis all experiments were performed using at least 3 separate samples per condition and at least 10 images were taken of each sample. In all cases the error bars shown represent standard deviation (SD).

3. PRODUCTION AND CHARACTERISATION OF DIFFERENTIALLY MOBILE SURFACES

3.1. INTRODUCTION

The literature available on supported lipid bilayers is widespread and varied, with the implication that, through the years, they have been well characterised both in terms of methodology and properties. However, when any project is undertaken there is a need to characterise the system to ensure that what is observed is due to the system of interest. As such, the main aim of this chapter is to detail the production and subsequent characterisation of both lipid bilayers, of varying diffusive characteristics, and the immobile control, through which to compare them. Fortunately, the nature of SLBs, in that they can be produced on solid supports, means that their properties can be measured and quantified through a wide array of techniques.

Atomic force microscopy (AFM), since its inception in 1986 (189), has been utilised in a vast array of high resolution applications from writing on the nanoscale (190) to imaging at the molecular scale (191). Of more relevant interest here is the ability of the AFM to measure the surface properties of a system. By using a cantilever that has a micron-scale tip on the sample facing side and a reflective coating on the other, the deflection of the tip as it moves across the surface is determined by measuring the deflection of a laser reflecting from the top of the cantilever. This can not only produce a three-dimensional projection of the probed surface, but also, by knowing the physical properties of the tip, give an insight into the material properties of the surface. The AFM can, therefore, be used in various modes; such as contact mode, where the tip is “dragged” across the surface; tapping mode, where the tip is oscillated at its resonant frequency; or force spectroscopy, where the tip is pressed against the surface, as well as variations of these also. These are of particular interest to the study of SLBs as they can, and have, elucidated the characteristics of the bilayer at the nanoscale, such as the thickness (192), phase partitions (152, 193), rupture forces (194) and elastic moduli (195).

Fluorescence correlation spectroscopy (FCS) was developed in the 1970s (196), but did not receive much interest until a single molecule detection capability was developed (197). Since then it has been widely applied in the study of biological systems (198, 199), with an ability to

measure biologically important changes such as diffusion of molecules (200) or receptor-ligand interactions (201). It has also found a place in the measurement of SLB lipid bilayers as a manner of competing technique to that of FRAP (fluorescence return after photobleaching). By using a confocal microscope, molecules within a very small volume (\leq fL) can be illuminated and detected, allowing for the use of very small amounts of fluorophore. The fluorescence is detected as a stream of photons with an avalanche photodiode (APD), rather than a camera (as in FRAP) and the raw data is processed to correlate the probability of one event being the same as the previously detected event. The decay in this probability, related to an appropriate calibration standard, allows for the calculation of the diffusion coefficient of a sample, in this case a SLB.

In contrast to AFM and FCS, quantitative fluorescence imaging requires no special equipment to perform, with only a fluorescent microscope being required. As a methodology it was first demonstrated in 2008 by Galush and colleagues (180); it fortuitously used fluorescent lipid bilayers as standards to determine the amount of protein present on a surface. Since this it has been widely used to determine protein functionalisation of surfaces in a number of systems from cancer studies to mechanotransduction (58, 77, 202-204).

The techniques detailed here are not an exhaustive list of the means through which to measure various SLB properties. Indeed, many surface characterisation techniques lend themselves well to the study of these systems. These can include, but are not limited to: the aforementioned FRAP to measure diffusion (205); quartz crystal microbalance with dissipation monitoring (QCM-D), to measure the dynamics of bilayer formation (148, 150), or functionalisation; surface plasmon resonance (SPR), for ligand-receptor binding (206); or ellipsometry, for formation kinetics (207). However, the techniques used in this study are both well-characterised and widely used, allowing for the characterisation of all the necessary steps, from bilayer production to functionalisation.

3.2. PRODUCTION OF DIFFERENTIALLY MOBILE SUPPORTED LIPID BILAYERS

The first step in the production of a SLB via the vesicle deposition method is to produce vesicles of an ideal, defined size. While this can be done either through extrusion or sonication, as stated previously extrusion was chosen as it produced a monodisperse solutions of vesicles in a cost-effective way, without the need for further, post-production processing (e.g. centrifugal removal of sonicator tip particles) of the vesicle solution.

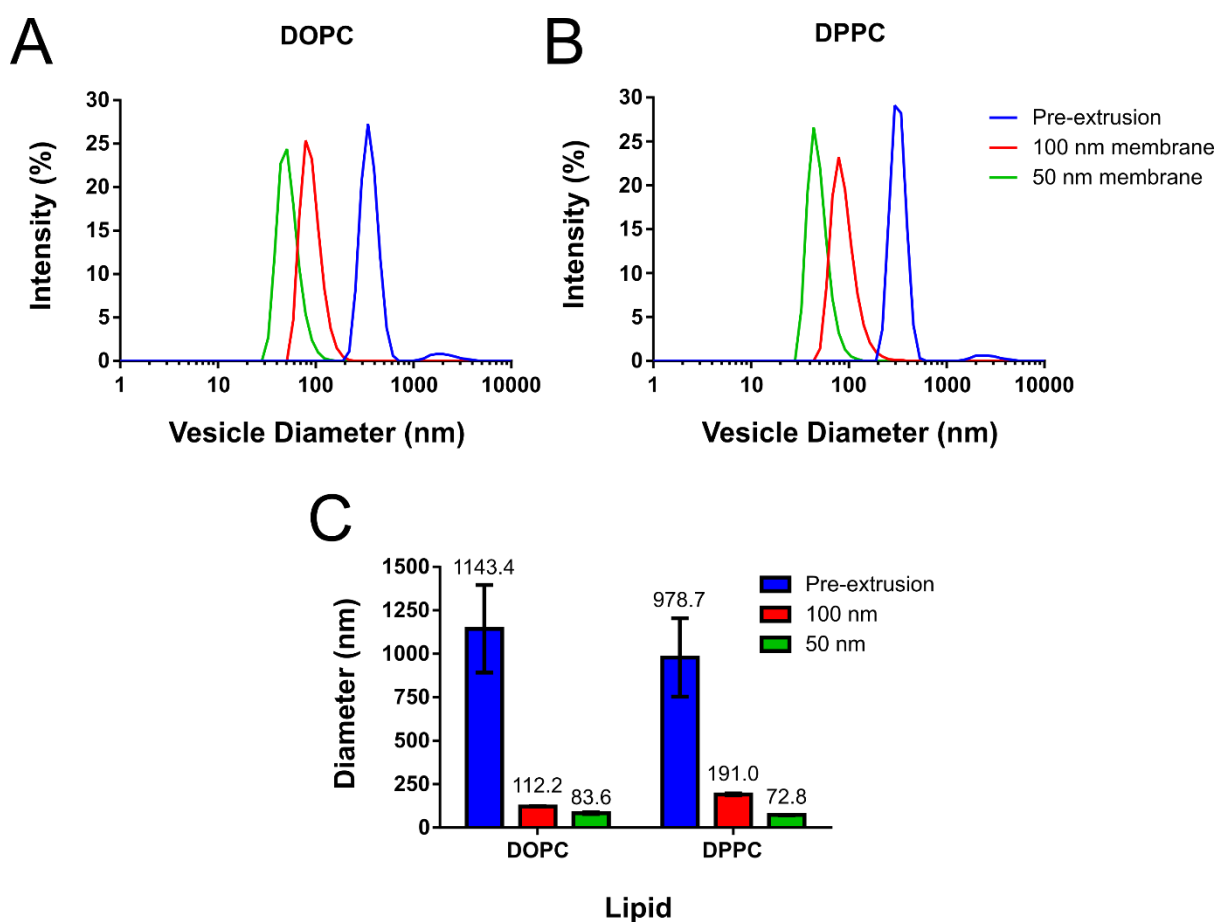


Figure 3.1. Lipid Vesicle Extrusion. Measuring the size of vesicles of (A) DOPC and (B) DPPC both before and after extrusion through membranes of differing pore sizes, using dynamic light scattering (DLS). (C) Shows the resulting average diameter of lipid vesicles, including the mean hydrodynamic vesicle diameter above each column for clarity.

Detailed in the introduction the predominant factors controlling successful formation of vesicle bilayers are i) membrane tension, ii) vesicle-substrate interaction and iii) vesicle-vesicle interaction. When optimising the first of these factors the ideal size of vesicles for SLB

formation is below 90 nm in diameter (150). To that end, Figures 3.1A & B show the DOPC and DPPC vesicles before and after extrusion through both a 100 nm and 50 nm polycarbonate membrane. The extrusion of both samples produced significantly reduced average sizes, with little variance from the average as shown by the standard deviation in Figure 3.1C. In the case of the 50 nm membrane the average size of the small unilamellar vesicles (SUVs) was seen to be below the maximum size to allow SLB formation. However, in both membranes the vesicles were seen to be, on average, larger than the membrane pore size. It has been observed previously (208) that in membranes with larger pores the vesicles are predominantly smaller than the pore size (≥ 200 nm), whereas in smaller membranes pores the vesicles are larger (< 200 nm). This may be attributed to the overall pressure of the extrusion system used. Indeed, extrusion has been shown to work by inducing a pressure over the tension necessary to lyse a lipid vesicle (209). This causes the multilamellar vesicles to rupture and subsequently reform as a unilamellar, monodisperse populations of pore-size defined vesicles.

The size of the DOPC and DPPC liposomes produced is of the right scale in which to produce SLBs (~ 90 nm) (150). Indeed, the measurement technique, dynamic light scattering (DLS), used here is likely to overestimate the size of the liposomes. DLS relies on the scattering of light not only from the lipid bilayer of the liposomes, but also of the aqueous ions surrounding it. The charge of the lipid head groups will attract a layer of ions to the surface, which will then scatter the light photons. As such, the size measured here is likely larger than the actual size of the liposomes; thus they will be smaller than the limit required and capable of forming SLBs when incubated on an appropriate surface.

In terms of the aforementioned factors controlling the formation of SLBs the production of vesicles of this size. Firstly, it has been previously noted that the reduction in the size of the lipid vesicles increases the tension of membrane (150). This, in conjunction with buffer induced osmotic pressure on the membrane, makes the SUVs more unstable and more likely to rupture when present of the surface. Further to this, the size of the SUVs will control the interaction between vesicles by allowing a greater number of vesicles to adsorb to the surface. As SLB formation is partially dependent on a critical coverage of vesicles (147), this size would allow for more lipid to be present on the surface; this would more effectively allow for the critical vesicle coverage to be exceeded and a SLB to form. What this process does not allow for is the

optimisation of the vesicle-substrate interaction. This was instead achieved by plasma treating the glass surface; this surface treatment makes the glass surface highly charged and strengthens the electrostatic interaction between vesicle and the surface, likely causing deformation and consequent rupture (64), forming a SLB.

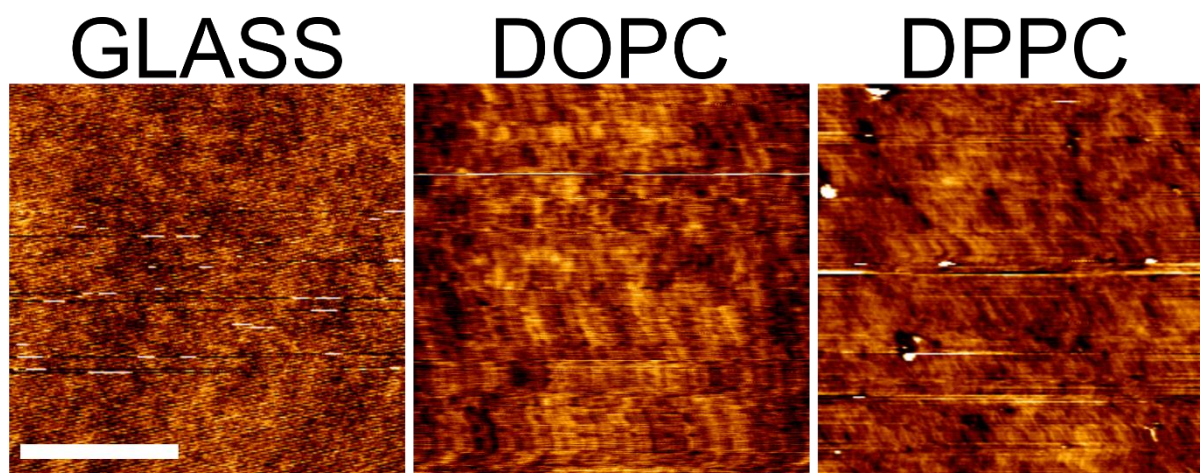


Figure 3.2. Glass and SLB Surfaces. The images show the cleaned glass surfaces both before and after incubation with either DOPC or DPPC as measured using AFM contact mode imaging. This lack of contrast demonstrates the contiguous nature of the SLBs, with a minimal presence of defects (Scale Bar = 2 μm).

As AFM is widely used in the characterising of lipid bilayers (152, 192-195) it was used here to determine both the presence of the SLBs and their physical properties. Figure 3.2 shows the surface of glass slides before and after incubation with DOPC and DPPC. The glass surface can be seen to be flat with an RMS value of 514 pm, indicating a highly cleaned surface, with few defects, comparable to the 356 pm and 549 pm RMS values seen on the DOPC and DPPC surfaces respectively. This cleanliness was confirmed with static water contact angles (WCA) of $<10^\circ$ (data not shown); the previously noted required hydrophilicity for successful and continuous SLB formation (64, 150). It can be clearly seen here that the lack of contrast on the surface prevents the accurate assessment of the presence of a bilayer; however, small peaks on the surface of the DPPC SLB can be attributed to the partial fusing of vesicles that were not removed in the washing steps.

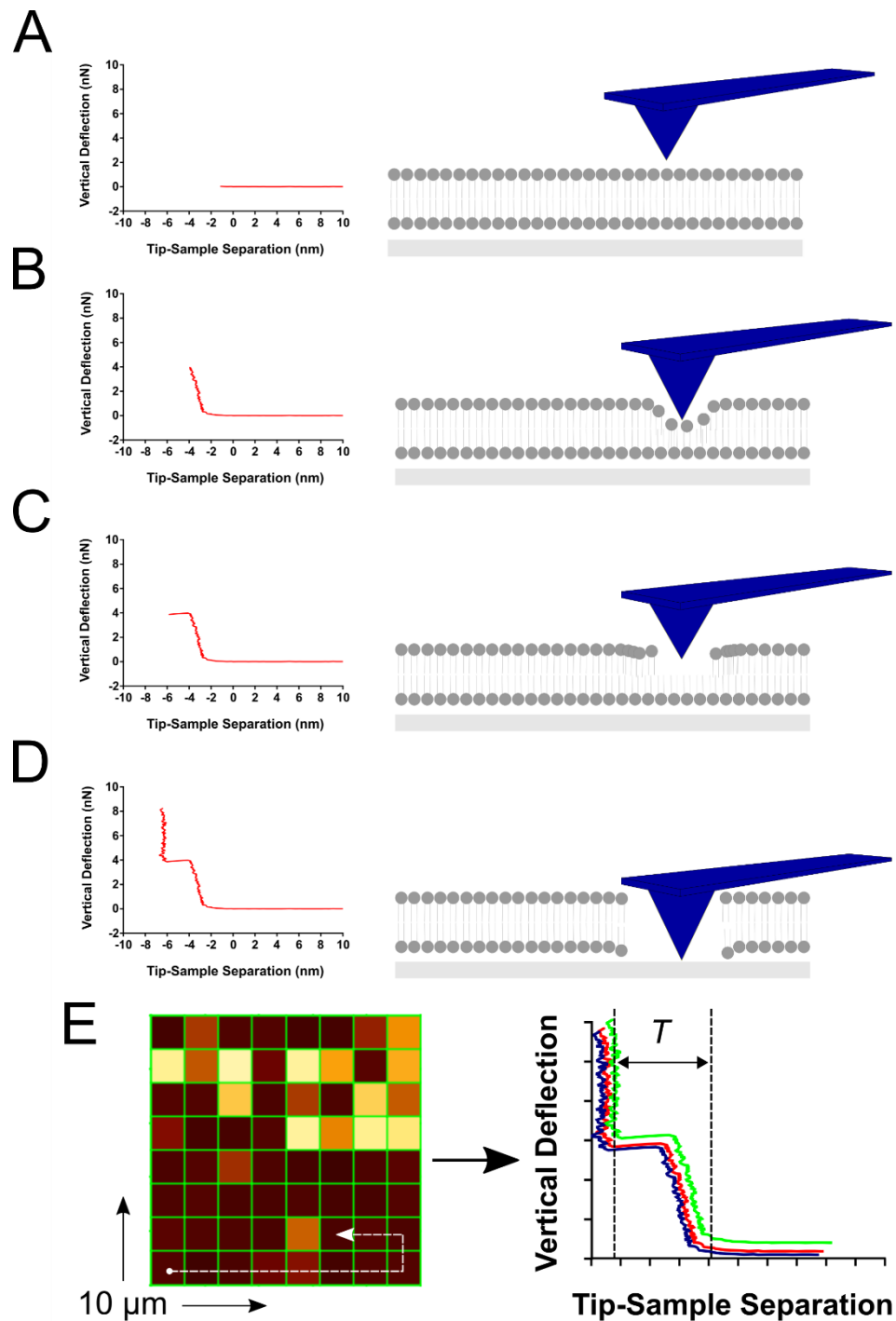


Figure 3.3. Schematic Representation of Force Spectroscopy of SLBs. (A) The tip approaches the surface during the cantilever approach. (B) As the tip approaches and interacts with the SLB the vertical deflection increases until (C) the tip eventually breaks through the packed lipid and (D) contacts with the glass surface. (E) Shows a representative force map and the curves generated; in this 8×8 , $10 \mu\text{m}^2$ map the cantilever pushes on the surface in each square generating the force curves shown in (A) – (E). As the curves are indicative of interaction with the SLB, the thickness can

be determined between the points shown. (All forces curves shown here are taken from those attained in the measurement SLBs and are representative of that which was obtained)

Using force spectroscopy it is possible not only to confirm the presence of a SLB, but also to probe the physical properties of the SLBs. The schematic shown in Figure 3.3 demonstrates the proposed interaction between the tip and the lipids in a SLB, with different parts of the curve indicating different properties, as noted by previous work (177, 195, 210). The tip moves towards the surface (Figure 3.3A) until, upon initial interaction with the surface (3.3B), there is a large increase in detected force, when compared to the small reduction in tip sample separation. This is related to the interaction of the tip with lipid headgroups, which, as they are identical in DOPC and DPPC, can be assumed to be similar. This interaction is also likely affected by the ions present in the solution also interacting with the bilayer, as previously noted (177). The tip then presses on the bilayer until, at a specific magnitude of force, the “rupture force”, the tip then breaks through the surface of the SLB (3.3C). This shows a characteristic “jump” in both the force and the tip-sample separation when compared to the plain glass surface. In short order, due to the minimal interaction of the tip with hydrophobic core of the SLB contacts the underlying glass surface (3.3D). This is demonstrated by no change in tip-sample separation despite an increase in cantilever deflection indicating increased force.

This force curve, indicative of single bilayer present on the surface, can be used to determine various physical properties of the lipid bilayer. For example, the change in tip-sample separation (Figure 3.3E) gives an indicator of the thickness of the bilayer from the proximal head group to the glass surface. One drawback can be that electrostatic interactions and the basal water layer between the bilayer and the surface can lead to an overestimation in the thickness (177). Further data of interest is the force required to break through the bilayer (rupture force), the force at which the tip breaks through the SLB (maximal y-axis, 3.3B), and the inferred Young’s modulus of the bilayer (Hertz model), from the slope shown in Figure 3.3B. Though the latter has been mentioned in previous work (195), the estimated stiffness is indicated as being in the MPa range. On the surface this appears to be counter-intuitive; SLBs are fluids, confined into two-dimensions through energetic interactions and thus it could be argued that they would not exhibit an elastic stiffness. It is therefore possible that the underlying

glass stiffness partially contributes to this detected value. However, were SLBs to indeed exhibit an elastic stiffness, this MPa value would preclude detection by the cells. As cells, on average, exhibit 1–5 nN/ μm^2 (2) it is unlikely the cells would be able to deform the SLBs elastically. As this is vital to cells sensing their environment (52), it can therefore be assumed that in this work cells do not sense the SLBs through their elastic properties.

Of the physical characteristics that can be determined, the most useful in this context is that of bilayer thickness. This was calculated for each curve in the force map and the thickness distribution for each curve was fitted to a Gaussian distribution as shown in Figure 3.4. This shows that average thicknesses of the DOPC and DPPC SLBs are 5.88 ± 0.42 nm and 6.32 ± 0.64 nm respectively. Both of these values are indicative of a single lipid bilayer structure present on the glass surfaces (177). However, it was not expected that the SLBs would be, statistically, of similar thickness. It would be expected that DPPC would be thicker due to the measurements being performed below the T_m for DPPC (and above that of DOPC); in light of this, and as detailed in Section 1.3.1, the tail group of DPPC would be more extended, providing a greater effective length (211). It may be that electrostatic interactions and the basal water has led to added interaction between the tip and the SLB in both cases (177), thus leading to a change in the measured thickness. While this theory cannot be confirmed, it is apparent that in both cases a single bilayer has been formed. Results from Figures 3.2 and 3.4 work in tandem to confirm that not only is the bilayer present on the glass surfaces, but that there is continuous lipid coverage over the sample.

In this series of experiments AFM has served as an ideal means through which to qualitatively and quantitatively probe the physical characteristics of differently mobile SLBs. From this, the presence of continuous SLBs has been confirmed via contact mode imaging and force spectroscopy measurements in both the DOPC and DPPC surfaces. Furthermore, force mapping of defined areas of the bilayer has served to successfully produce thickness measurements indicating single bilayers present on the surface. From this initial characterisation, it is then possible to move on to quantifying the viscosity of these two systems through fluorescent correlation spectroscopy (FCS).

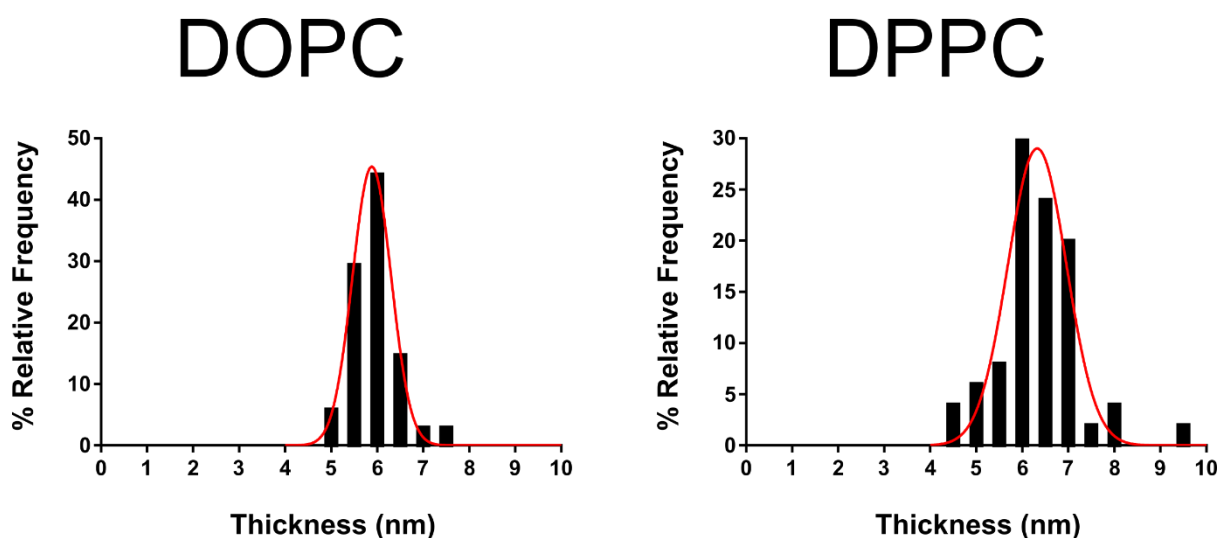


Figure 3.4. Supported Lipid Bilayer Thickness. Force mapping, as shown in Figure 3.3E produced a series of multiple force curves for each SLB, which was categorised into bins of 1 nm thickness. The relative percentage frequency of these values for DOPC and DPPC is shown here, with a gaussian fit to determine the average thickness.

3.3. DIFFUSION OF SUPPORTED LIPID BILAYERS

As the main focus of this work is determining how the viscosity of a surface, specifically the SLB viscosity, can manipulate cellular behaviour, an important step was to quantify the diffusion characteristics of the surfaces; as mentioned previously this can be linked through the Saffman-Delbruck (SD) equation to the viscosity. Further, in the case of SLB viscosity, the lateral ligand mobility can also be understood through the diffusion coefficients of lipid-fluorophore conjugates present in the bilayer. Measurements were performed on both SLBs at 37°C. This is summarised schematically in Figure 3.5. Using the confocal volume, defined by the objective numerical aperture (Figure 3.5A), time-dependent changes in detected fluorescent intensity over time (Figure 3B) can be detected using very small numbers of fluorophores; the decay in the autocorrelation $G(\tau)$ (Figure 3.5C) is proportional to the diffusion of the fluorophore and related in the equations detailed in the methods section.

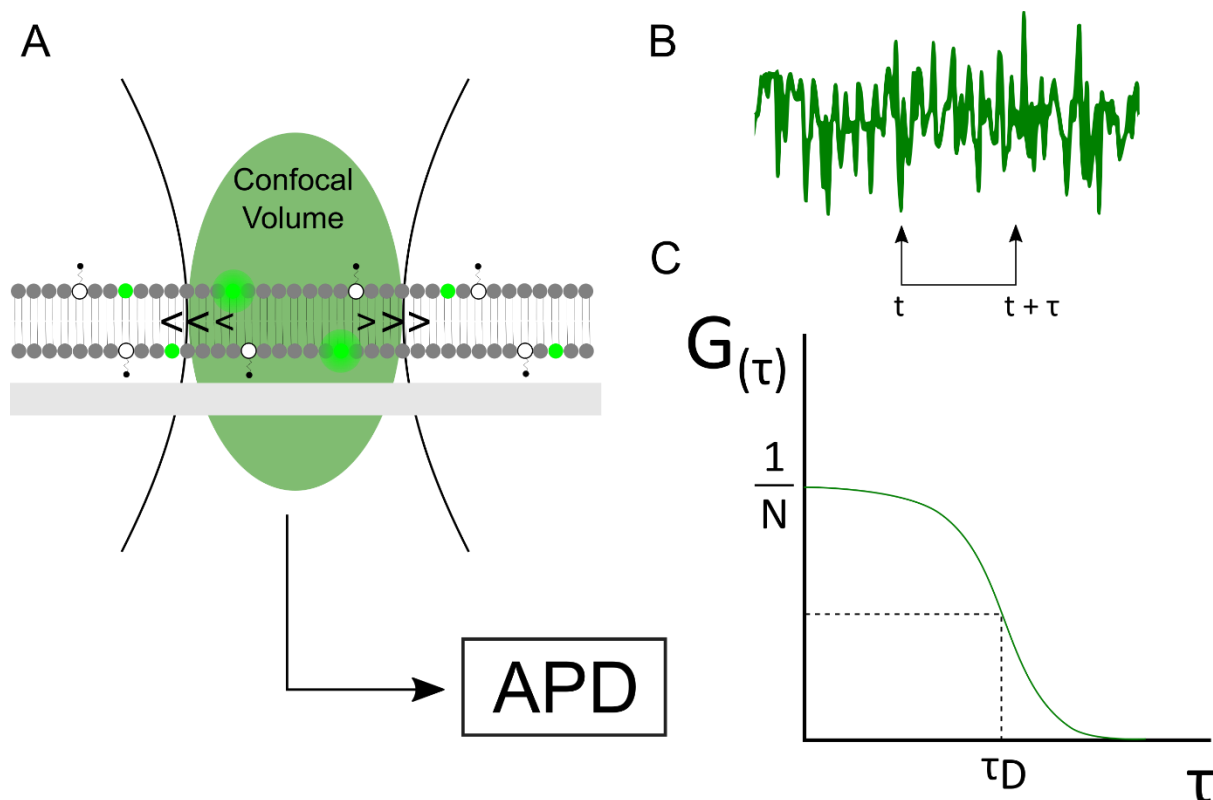


Figure 3.5. Schematic Representation of Fluorescence Correlation Spectroscopy. (A) Shows the illumination of the fluorophores within the confocal volume, which is then detected by the avalanche photodiode (APD). The photon count signal over time (B) is then correlated to one another showing a decay in the correlation over time (C). This can be used to calculate the diffusion coefficient if the beam radius is known from previous calibrations. (Adapted from (212))

Figure 3.6 shows the initial measurements taken from the SLBs, plotting the correlation factor, G , against time. Before measurements were taken the device was calibrated using 100 nm fluorescent beads and the beam radius was determined to be $0.26 \mu\text{m}$, via Equation 2.6 (Chapter 2.8) (3.6C Inset). By fitting the data to Equations 2.7 and 2.8 a measurement of the diffusion coefficient of the SLBs was determined (Figure 3.6C, summarised in Table 3.1) was $3.63 \pm 0.99 \mu\text{m}^2/\text{s}$ for DOPC and $0.13 \pm 0.06 \mu\text{m}^2/\text{s}$ for DPPC, giving an order of magnitude difference in the diffusion of fluorescent molecules within the SLBs. This can be attributed to the difference in the packing of the lipids in SLBs, which is, in turn, controlled by the phase, with DOPC being in the gel phase and DPPC being in the gel phase.

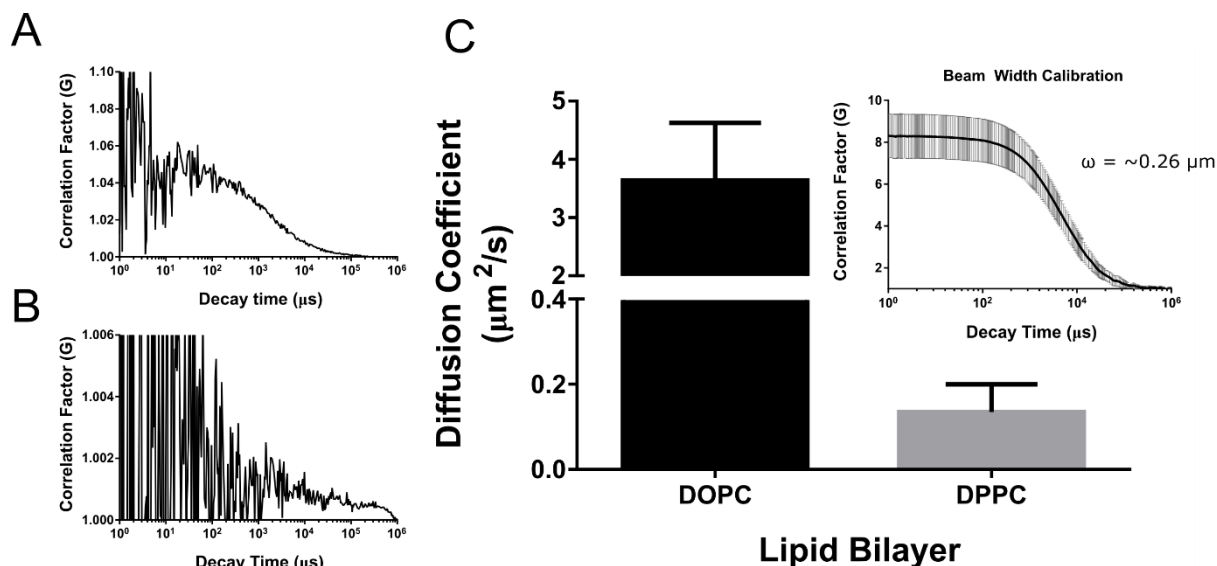


Figure 3.6. Diffusion in SLBs. (A) & (B) Show the correlation curves produced by the diffusion of fluorophores through the FCS confocal volume in DOPC and DPPC respectively. (C) Shows the resulting diffusion coefficients of DOPC and DPPC SLBs, calculated using the equations shown in section 2.8, (Inset – FITC bead calibration used to determine beam width, required to calculate the diffusion coefficient).

The acquired diffusion coefficients are within the right order of magnitude for supported lipid bilayers, with previous work proposing that DOPC SLBs have a diffusion range between 1 – 10 $\mu\text{m}^2/\text{s}$. Interestingly, this is lower than that measured in free standing bilayers or in those bilayers that form vesicles. This may be ascribed to the influence of the solid support and a coupling between it and the proximal leaflet of the SLB (153, 213). In contrast, due to the gel-like nature of the DPPC at 37°C it is not apparent what the diffusion coefficient should be. Indeed, the difficulty in these experiments was the optimisation of the fluorophore (0.5 mol%) concentration and laser strength to produce a decay curve. It must be stated here that despite this and the averaging of large data sets, the data itself still has a large degree of noise present. From this, it must therefore be concluded that the average value of $D = 0.13 \pm 0.06 \mu\text{m}^2/\text{s}$ may well be an indication as to the order of magnitude of the overall diffusion of the bilayer, rather than a definitive determination. Importantly, the diffusion coefficient of the fluorescence dyes within the molecules are a good indicator of the viscosity of the surrounding membranes, as the diffusion coefficient (D) and the viscosity (η) are related by the SD equation (155, 214). This is restated here for clarity:

$$D = \frac{k_B T}{4\pi\eta_m h} \left[\ln \left(\frac{2LSD}{R} \right) - \gamma \right] \quad (1.1)$$

Where D is the diffusion coefficient, k_B is the Boltzmann constant, T the absolute temperature, η_m the membrane diffusion, η_f the viscosity of the fluid (given as water at 37°C – 0.691 x 10⁻³ Pa.s), r the radius of the inclusion in this case a lipid molecule) and γ the Euler-Mascheroni constant (0.577).

SLB	Diffusion coefficient ($\mu\text{m}^2/\text{s}$)	Calculated viscosity (Pa.s.m)
DOPC	3.6 ± 0.99	7.98 x 10 ⁻¹⁰
DPPC	0.13 ± 0.06	3.95 x 10 ⁻⁸

Table 3.1. A summary of the attained values of the DOPC and DPPC diffusion coefficients as determined by FCS, and the resulting, viscosity values, calculated by the SD equation.

By applying this here viscosity values of 7.18 x 10⁻¹⁰ Pa.s.m and 3.95 x 10⁻⁸ Pa.s.m were estimated for DOPC and DPPC respectively (Table 3.1). The latter of these values shows agreement with lipids measured in a vesicle system, which may provide a template for these values (215); however, extrapolations of DPPC viscosity from diffusion was not found. The closest value stated is using a three component system of DPPC:cholesterol:DiPhyPC, which reported a value in order of 10⁻⁹ Pa.s.m. However, as cholesterol can disrupt the ordering of DPPC molecules in a gel-phase bilayer (216), it is not clear whether this may be a good indicator of viscosity in a purely DPPC SLB. This associated of the diffusion with the viscosity is of key importance when considering cellular behaviour in the later chapters; however, here it confirms the validity of the diffusion measurements for both DOPC and DPPC.

3.4. FUNCTIONALISATION OF SURFACES

3.4.1. FUNCTIONALISATION OF A GLASS CONTROL

An RGD-functionalised glass control used to represent an immobile surface, represented schematically in Figure 3.7A, was also produced and characterised so as to make a more effective comparison between mobile and immobile surfaces.

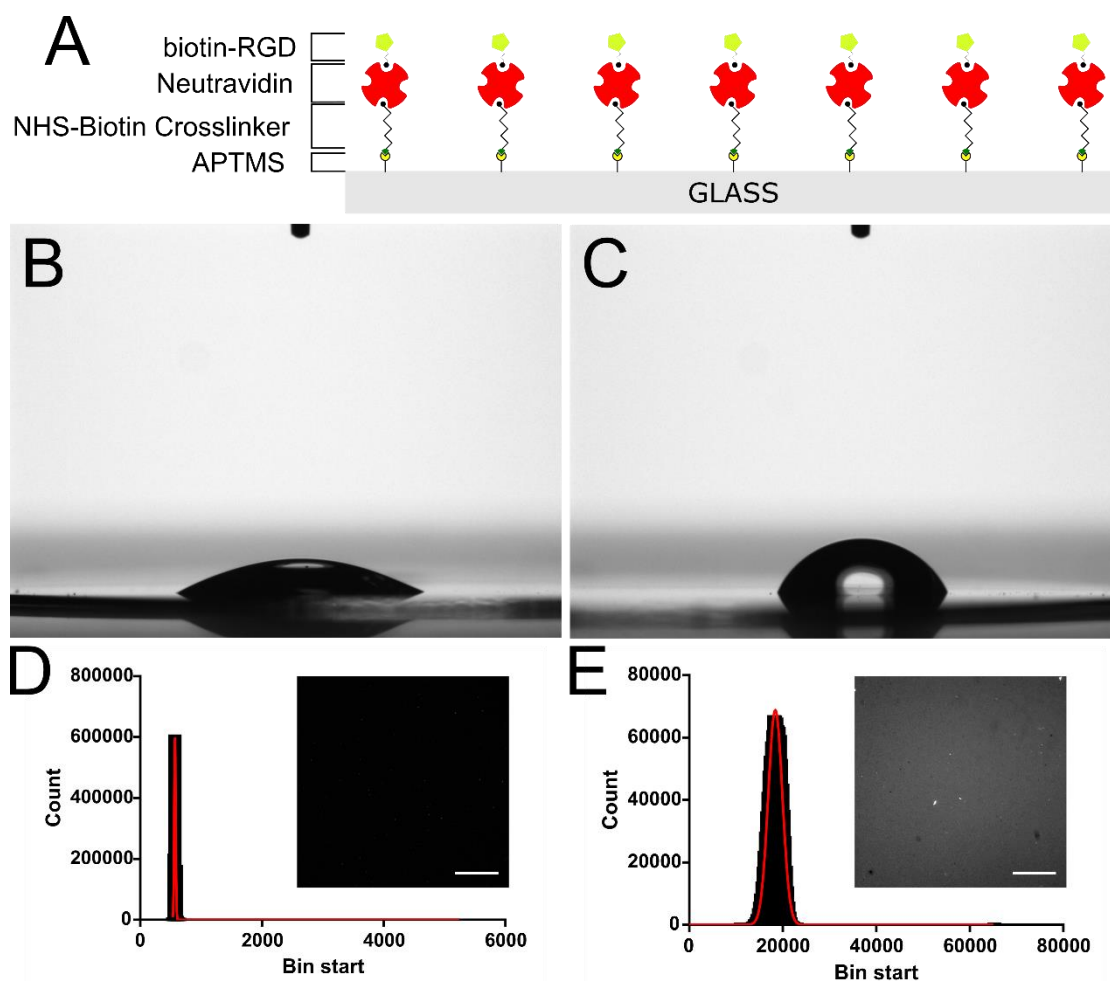


Figure 3.7. Functionalisation of Glass with RGDStatic Water Contact Angle (WCA). (A) Shows a schematic of the progressive functionalisation of glass leading to RGD being presented on the surface. (B) Shows the WCA after RCA cleaning and (C) shows the WCA after silanisation with APTMS, demonstrating the change in surface hydrophobicity upon incubation with this silane. (D) and (E) show the fluorescence histogram before and after functionalisation with neutravidin, respectively (insets show representative images; scale bar = 25 μm).

The control was designed to mimic the SLB as closely as possible and thus RGD was conjugated to a glass surface a similarly as possible to that of the SLBs. Initially, the control was silanised via (3-aminopropyl)trimethoxysilane (ATPMS) and the binding was confirmed with contact angle measurements, as shown in Figure 3.7B and C, with a large increase in the

static contact angle from $26.7 \pm 2.9^\circ$ before silane addition (and after RCA cleaning) to $65.4 \pm 2.2^\circ$ after silane addition. This is more hydrophobic than a previously determined value on a similar system ($\sim 40\text{-}50^\circ$ on APTES) (217), which may be related to the differences between using a purely silicon surface, rather than glass or the methoxy and ethoxy groups in the silane. Upon incubation with the crosslinker and fluorescent neutravidin it was seen that there was a difference in fluorescence between a plain glass surface (Figure 3.7D) and a silane-treated surface (Figure 3.7E), indicating the presence of protein on the sample.

3.4.2. QUANTIFICATION OF SURFACE LIGAND DENSITY

The functionalisation of DOPC and DPPC SLBs was quantified, to ensure a consistent ligand presentation, regardless of viscosity-defined ligand mobility. Quantitative fluorescence microscopy (QFM) (184), as described previously in the literature allowed for the approximate number of protein molecules on each surface to be calculated. Initially, the system was calibrated using standards of neutravidin and lipid vesicle solutions (Figure 3.8A & B respectively); as detailed in the methods the scaling factor (F) was given by $I_{\text{protein}} / I_{\text{lipid}}$, where I is the gradient, giving a value of 0.51. Using a SLB, with a known quantity of TR-DHPE per μm^2 , the fluorescent intensity based on the number molecules present on a bilayer was also determined, from the gradient (I_{bilayer}) (Figure 3.8C). By combining the scaling factor and I_{bilayer} , fluorescence related to the fluorescent protein per μm^2 was calculated (Figure 3.8D). These values were applied to the fluorescence images shown in Figure 3.10A, which allowed for the amount of neutravidin per μm^2 to be calculated (Figure 3.9C) and thus the surface density (Figure 3.9D). In all cases the protein density was seen to be in a similar range for both DOPC and DPPC SLBs, indicating that the main difference between the two surfaces was mobility of the ligands, as defined by the viscosity.

From the values attained in Figure 3.9, combined with the assumed cross-sectional area of a lipid as 0.725 nm^2 (218), it can be concluded that the attained values are within the maximum expected values of the neutravidin density for each of the lipid surfaces. This degree of fluorescence indicates that on each surface the number of biotinylated lipid per neutravidin is approximately 2:1, thus allowing two binding sites for biotinylated RGD groups. Further to this, previous work has shown a comparable surface density of neutravidin on these lipid

surfaces within the ranges expected for the surface concentration. For example, at 0.4 mol% biotinylated lipid 1,750 molecules per μm^2 were seen (79), indicating between 1 – 2 biotinylated lipid to neutravidin each molecule.

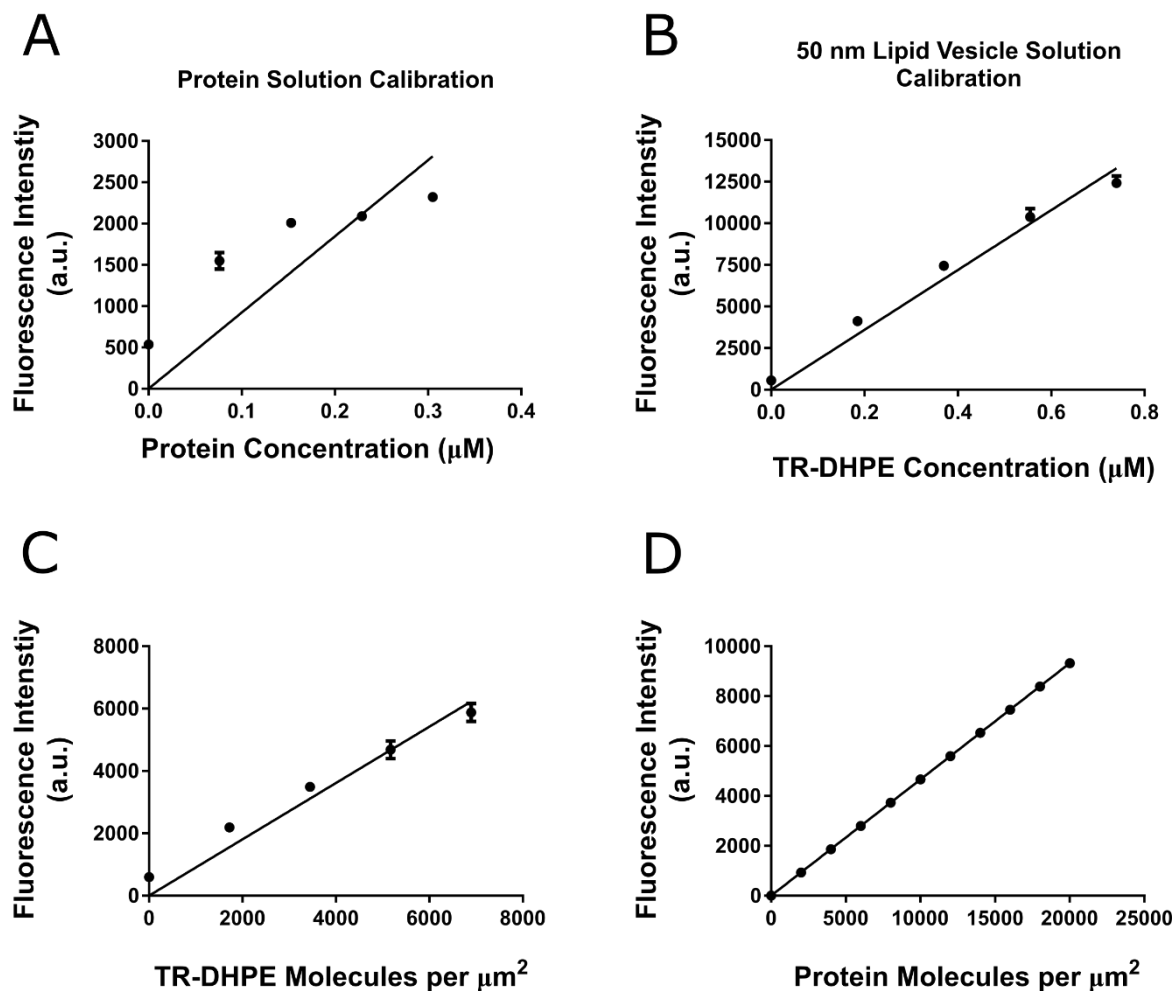


Figure 3.8. Quantitative Fluorescence Imaging (QFI) Calibration. Determination of the amount of protein per μm^2 on a bilayer sample by first determining a scaling factor (F) between the linear gradients of bulk solutions of (A) protein (in this case neutravidin) and (B) lipid vesicles (DOPC). This scaling factor is then applied to the linear gradient of fluorescent lipids in a bilayer (C), which can then be used to determine fluorescence as an amount of protein molecules per μm^2 (D).

%mol of Biotin-cap-PE	Lipid:Neutravidin Ratio			
	1:1	2:1	3:1	4:1
0.4	2,312	1,156	771	578
2	11,560	5,780	3,853	2,890
10	57,803	28,902	19,268	14,451

Table 3.2. Predicted density of neutravidin per μm^2 adsorbed to the surface, based upon the amount of binding events on one neutravidin molecule.

Table 3.2 shows the expected neutravidin density on the SLBs, which is also dependent on the stoichiometry of binding, with neutravidin having 4 possible binding sites for biotin. From this the stoichiometry for each surface shows that there is at least one binding site available for a biotinylated RGD. While it is possible, and indeed likely, that more RGD is present than protein, it is likely that a cell would be incapable of detecting them. Approximate values of the spacing between biotin binding sites, taken from the crystal structure neutravidin indicate that the spacing between the biotin binding sites on the neutravidin being approximately < 3 nm (219). However, the size of the extracellular domain of an integrin molecule is on the order of 10s of nm (220). Therefore, at this separation between RGD molecules, integrin molecules would not be able to cluster to a sufficient degree through which to take advantage of any additional RGD molecules present on a single neutravidin protein, effectively presenting a single RGD molecule. As a further point to note on the cell response, it has previously been noted that ligand spacing controls the size and dynamics of focal adhesions (18, 42). In SLBs, either in the fluid or gel phase, the absolute intermolecular distance cannot be determined due to a degree of viscous flow in the membrane; however, an average spacing based on the ascertained number of molecules determines and approximate distance of 12.9 nm in both cases (2 mol% functionalisation). This therefore, disregards this as a defining factor between the lipid surfaces, ensuring that any changes in observed cell adhesion would be more likely related to the nature of the surface, rather than the distribution of the ligands.

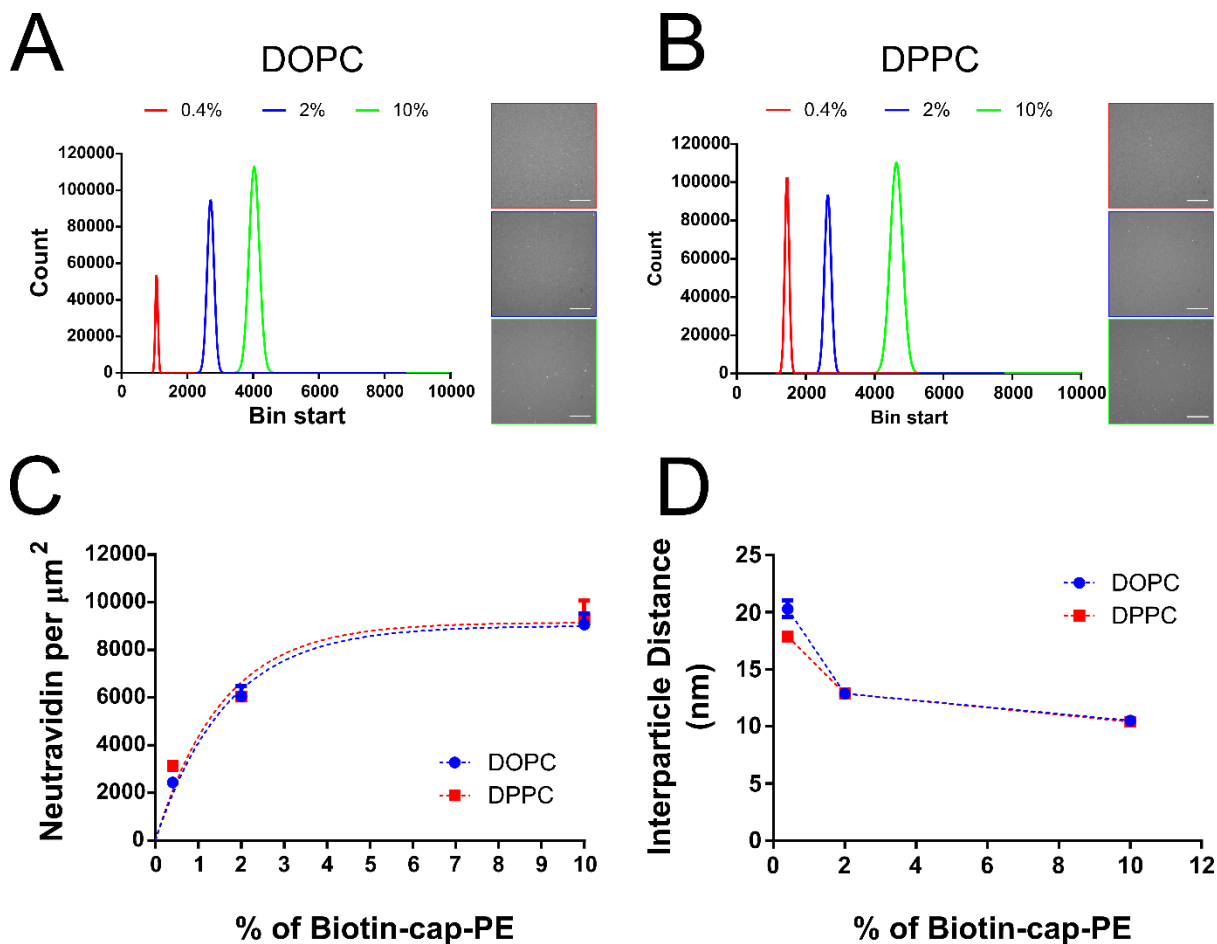


Figure 3.9. QFI of DOPC and DPPC SLBs. (A) and (B) show the DOPC and DPPC SLB intensity histograms upon increasing surface density of functionalised lipid (0.4, 2 and 10 mol% of biotin-lipid); the corresponding representative images are colour-coded to the relevant concentration (scale bar = $25 \mu\text{m}^2$). (C) Shows the calculated amount of neutravidin molecules per μm^2 and (D) shows the extrapolated surface density of the neutravidin molecules.

3.5 STABILITY OF SUPPORTED LIPID BILAYERS

Finally, the stability of the SLBs over time was assessed. This assessed the longer-term applicability of the lipid systems in a cell culture environment (in media at 37°C). The resulting lipid coverage was measured using the FCS system over 15 days (Figure 3.10). The nature of the SLBs changed between 8–15 days; in the fluid, DOPC SLB the bilayer was seen to breakdown, with large defects present and a reduction in overall coverage seen. In the gel DPPC SLB there appeared to be large globular defects present on the surface. However, by

bleaching a small area of the surface (ROI 1) it was confirmed that the SLB was still present and that there was no overall reduction in the surface coverage.

The difference in the SLBs after 15 days may be due to the difference in their phases. In a more general sense, the literature has previously reported SLBs being stable for at least 7 days under constant buffer exchange (221), which agrees well with the current results. However, there does not appear to be work on the longer-term stability e.g. up to 28 days, for use cell culture. While 15 days is short of this time scale, it does allow for the assessment of biomarkers in cell lines such as the model C2C12 mouse fibroblasts or even early markers of differentiation in mesenchymal stem cells (hMSCs). While this shows good potential for stability this can only be used as an indicator of the stability prior to the addition of cells. With the presence of the RGD ligands on the bilayer cells will interact with the normally non-fouling SLB. It would therefore be reasonable to assume that the nature of the bilayer, for example deterioration of surface coverage over time, would change. However, this initial assessment serves as a proof-of-concept as to the potential applicability of this system in the long term.

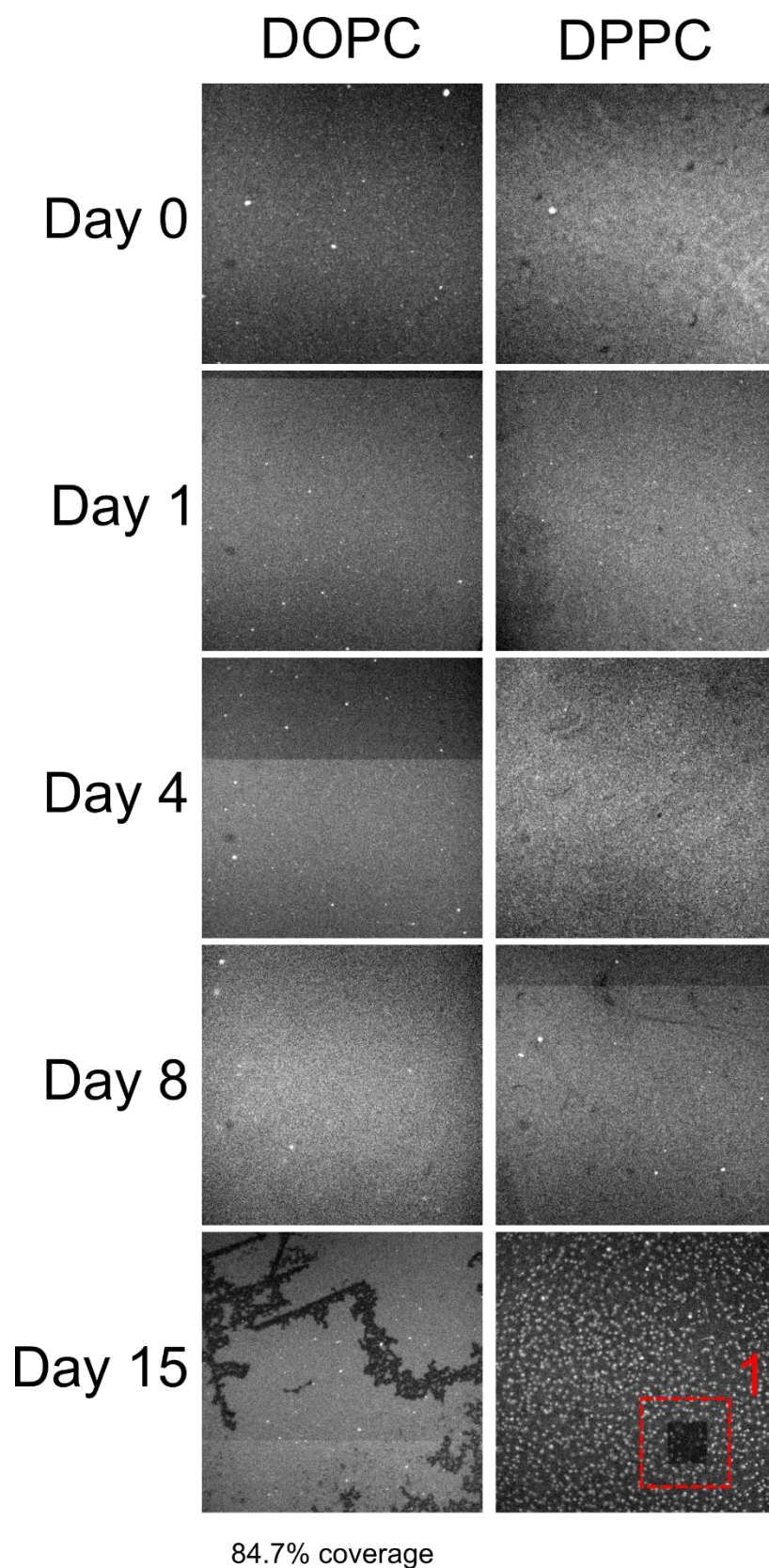


Figure 3.10. Bilayer Stability over Time. An image series of the bilayer over a period of 15 days, showing the overall coverage and stability of SLBs in cell culture conditions. The red box

highlights ROI 1, an indicator of the bleaching of the DPPC surface after 15 days, indicating that the SLB is still present, with defects.

3.6. CONCLUSIONS

This chapter has shown that the techniques employed are capable of successfully producing lipid bilayers that can then be functionalised, in order to produce a system capable of being applied to cell studies. AFM imaging showed that both fluid and gel phase lipid could be used to produce contiguous SLBs on glass substrates. Further to this, probing of the physical properties supported the argument that a single bilayer was formed upon deposition of the relevant vesicles upon the glass surfaces. Upon this production, confocal based FCS measurements of the relevant SLBs showed that they displayed diffusion speeds that varied by an order of magnitude, in agreement with the literature. Further, these values were able to be applied to the SD equation in order to calculate the viscosity of each SLB. This, in turn, can be assumed to have a significant effect on the mobility of any ligands attached to the membrane. Finally, functionalisation of the bilayers, as well as a glass control, were quantified using fluorescence-based determination of the amount protein adsorbed on the surface via fluorescent intensity. By determining the amount of protein present the amount of RGD-ligand presented to the cells and the average intermolecular distance has been calculated. In light of this successful production and characterisation of these SLBs, the work detailed in the next chapter has used these systems to understand how and why the mobility of the ligand, defined by the viscosity, can change the cellular response.

4. DETERMINING CELLULAR BEHAVIOUR IN RESPONSE TO CHANGES IN LIGAND MOBILITY

4.1. INTRODUCTION

With the system characterised in the previous chapter, the next step was to determine the cell behaviour. Bilayer systems have been used previously (58, 77, 79) to understand the nature of the interaction of the cells with an interface. However, the effect of bilayer viscosity, and the mechanisms by which it acts, have not been well characterised in the literature. This chapter has therefore studied the nature of the cell response to different surfaces, as well as seeking to understand the basis for this behaviour.

Cellular adhesion *in vivo* is vital for survival, proliferation and differentiation in various cell types, with the nature of this adhesion controlled by the interaction of the cell with the extracellular matrix (ECM). The physical and chemical properties of this network are of vital importance when considering how a specific cell population will behave. For example, the ECM may be composed of specific proteins, with notable examples including, but not limited to, collagen, fibronectin and laminin (222). These proteins have varying cellular adhesion peptide sequences, which can bind and activate ECM-binding integrins present on the cell surface (223). There may also be further proteins present within the ECM, such as growth factors, which can bind to further cell surface receptors (1, 224). Further to the molecular properties, physical properties, such as topography or viscoelasticity also have significant effects (10). *In vivo* all these factors act in unison to direct the behaviour of specific cellular populations within specific environments, be it adhesion, spreading, migration or differentiation.

Understanding the influence of these stimuli in isolation allows researchers to elucidate the nature of the processes dictating the cell response to specific stimuli. This knowledge can therefore be utilised in an effort to dictate a desired cellular response, both *in vitro* and *in vivo*. Concerning the molecular makeup of the ECM: the types of integrin recruited vary depending on matrix protein present (17). Topography has also been shown to have a significant effect on the cellular response. For example, ligand spacing (10) and disorder (16) can change cellular

behaviour, as well as other topographical characteristics affecting spreading, adhesion dynamics (42) and differentiation (16). The viscoelasticity of the ECM is, in itself, two separate factors: the viscosity and the elasticity. The latter of these has been well studied, with various work reporting that the elasticity, otherwise termed stiffness, has a major effect on cellular properties such as migration (225), spreading (226) and differentiation (34). Interestingly, in the case of stiffness like begets like; *in vitro* stem cells can be directed down specific lineages, such as neural, muscle, or bone lineage, by producing a matrix that simulates the stiffness of the *in vivo* environments of the differentiated cells (34, 85). The impact of overall viscoelasticity on cells has also been determined (62, 227). However, topography and stiffness remain the most widely studied properties in terms of understanding the cellular response.

Despite less studies being undertaken on the nature of the cell response to viscosity, there is still work that considers this effect. Much of this work uses polymers, with viscosity defined as the mobility of the polymer, and has found varying degrees of cell response in different studies. Similarly to the properties detailed above, this property of mobility has been seen to have an effect on cell adhesion (54) and spreading (53), as well as having a significant impact on the nature of the cellular adhesive machinery (55). At a molecular level, this mobility can also change the conformation of ECM proteins such as fibronectin (228, 229) as well as the presentation of associated growth factors (230, 231). Further to this, and in line with other ECM properties studied, surfaces with lateral mobility have been shown to control the adhesion, spreading and differentiation of different cell lines (52, 56, 229). This collection of work indicates the mobility of the ligand may well be a source of further means through which modulate cell behaviour.

While there is a large degree of evidence to say that the surface viscosity or mobility of a ligand control the cellular response, there is currently minimal literature that has sought to understand the mechanism in an isolated environment. This chapter utilises the entirely viscous nature of the supported lipid bilayer (SLB) as a means through which to understand how the viscosity-defined ligand mobility of the RGD-lipid ligand affects the cellular response.

4.2. CELLULAR BEHAVIOUR ON SUPPORTED LIPID BILAYERS

4.2.1. EARLY CELL ADHESION

The previous chapter established that SLBs of different viscosity can be formed using the current methods. It also showed that these bilayers have characteristics that are similar to those of systems previously reported. From this starting point, initial cell studies focused on the nature of the cell binding, including the adhesion of the cells, spreading and the properties of the focal adhesions. These properties begin to elucidate the nature of the response to the viscosity-defined ligand mobility in the SLBs.

The first stage of cellular interaction with any interface is that of adhesion. As such Figure 4.1 shows the attachment of cells to the SLBs with and without RGD present. Without RGD the adhesion of cells to the SLBs was almost negligible. However, upon functionalisation the cell density was seen to be comparable to that of the RGD-Glass control. Furthermore, there does appear to be a small, but significant difference in the number of cells adhered on the less mobile DPPC surfaces than on the DOPC upon functionalisation (DPPC vs. RGD-Glass = ns).

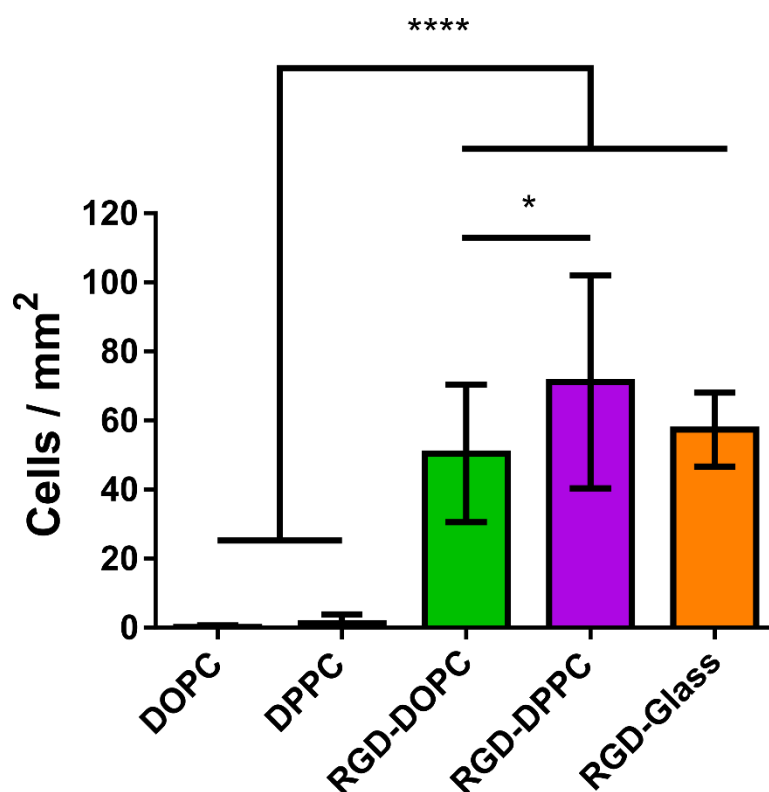


Figure 4.1. Initial Cellular Adhesion. *The interaction of cells with the lipid surfaces was seen to be minimal without RGD being present at 3 hours. Upon functionalisation with RGD, at 2 mol% functionalised lipid, cell adhesion was seen to be comparable to that of the RGD-Glass control. P values indicating significance, * ≤ 0.05 , **** ≤ 0.0001 .*

A lack of cell binding to both the DOPC and DPPC can be attributed to the non-fouling nature of zwitterionic lipid bilayers. The dominant theories as to why bilayers prevent cell binding are i) they are charge neutral and/or ii) the mobility of the component lipids prevents cell adhesion (232, 233). The former of these has been more studied with the inclusion of charge in a SLB promoting cellular adhesion (158). It is possible, however, based on these and previous findings, that both of these are contributing factors. Without functionalisation the difference in cell binding was not significant, implying that the viscosity of the bilayer, and thus the ligand may not affect binding; however, upon functionalisation the small, but statistically significant difference in cell binding may imply a role of this ligand mobility in adhesion in lipid systems. While no parallels can be drawn to previous SLBs, the mobility of polymer surfaces has been shown to affect cellular adhesion (54), with changes to the hydrated mobility of the polymers showing different cellular adhesion characteristics. In spite of these small differences the main contribution to cellular adhesion must be considered to be the presence of RGD. Present in the repeat III₁₀ domain of fibronectin (86) RGD can bind several types of integrin receptor present on the cell surface (17), leading to the initial stages of cell adhesion.

While not studied in-depth in this work, the role of surface charge can also be considered. Both DOPC and DPPC are neutrally charged, which may contribute to the non-fouling nature; previously, it has been shown that introducing positive charge into a lipid bilayer can promote cell binding (158), likely due to interaction with the negative charge present on the membrane of cells. Electrostatic charge is an important consideration in various studies. Taking a relevant example avidin, has been noted to cause significant background binding due to the positive charge it possesses at neutral pH; however, neutravidin does not, thus significantly reducing the extent of background binding.

4.2.2. CELL SPREADING AND MORPHOLOGY

After the initial adhesion cells then further interact with the surface causing changes in cellular morphology, which, as stated above, are dependent on the characteristics of the environment in which the cell resides. After functionalisation (2 mol% unless otherwise stated), the change in viscosity dependent change in cellular morphology upon surfaces of different ligand mobility is shown in Figure 4.2. Between DOPC and DPPC it was observed that the cell area was larger on the latter, gel-phase SLB, with a further increase in area seen on the immobile control (Figure 4.2A). Furthermore, Figure 4.2B demonstrates that the shape of the cell is also affected, with cells showing more circular characteristics on DOPC, the most mobile of the surfaces; DPPC and the glass control, however, demonstrate a lower circularity, which is statistically comparable between these two surfaces. Qualitatively, on each of the surfaces, it can also be seen that the cell cytoskeleton is well-defined on both the DPPC and RGD-glass, with defined stress fibres being apparent throughout the cell. However, on DOPC the actin cytoskeleton cannot be clearly seen, with a far more diffuse fluorescence seen throughout the cell.

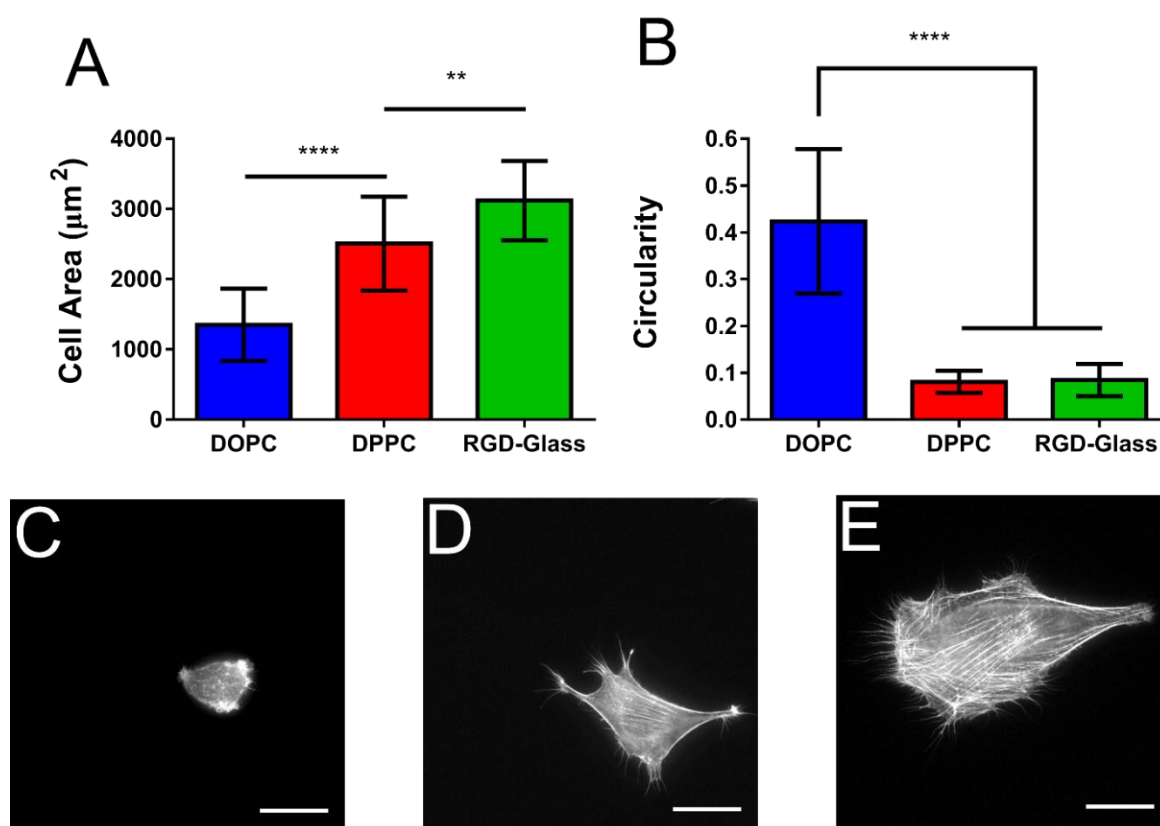


Figure 4.2. Morphology Dependence on Ligand Mobility. (A) Shows the average cell area on DOPC (high ligand mobility, low viscosity) and DPPC (low ligand mobility, high viscosity),

with (B) showing their characteristic circularity. (C) – (E) are representative images of the cells on DOPC, DPPC and RGD-Glass respectively. (Scale Bar = 25 μ m). *P* values indicating significance, ** ≤ 0.01 , **** ≤ 0.0001 .

In order to confirm that this observed cell spreading was indeed due to the influence of the RGD present on the surface, integrins were selectively blocked. Figure 4.3A shows the resulting representative images of cells incubated with inhibitors for $\alpha_5\beta_1$ and $\alpha_v\beta_3$. The former was blocked with an anti- $\alpha_5\beta_1$ antibody and the latter with a soluble cyclic-RGD (the concentration of which blocked $\alpha_v\beta_3$, but not $\alpha_5\beta_1$ (91, 234)). As both of these integrins are key for cell binding to RGD it would be assumed that one or both would have an effect on cell morphology. Indeed, this is what is seen in Figure 4.3A and quantified in Figure 4.3B. Upon incubation with one or both of these inhibitors a reduction in cell area is seen on all surfaces, with the exception of cells on DOPC incubated with only the $\alpha_5\beta_1$ inhibitor.

Cell morphology is highly dependent on the nature of the environment in which the cell resides, with higher stiffness, ideal ligand spacing, and the presentation of specific chemical groups all enhancing this spreading. Specifically to ligand mobility, cells are seen to change their morphology in response to even small changes. In the literature, mobility of the ligand has a varying effect on the morphology of cells, with some observing a greater cell spreading (235) upon increased ligand mobility, while others observe less spreading (53); still others noticed other behaviours such as biphasic (55) or no changes (56). As many of these use different polymer surfaces it may be that there are other factors at play between these surfaces, such as different chemistries. However, when using lipid bilayers cells have predominantly been noted to adopt a more rounded and, less spread morphology on fluid-phase bilayers (58, 77, 79), with gel phase bilayers not previously being studied in-depth. These previous studies have noted the lateral, unrestricted mobility of the ligand to be an important factor in the cell shape; indeed, upon introducing barriers through which to restrict bilayer movement an increase in overall cell size was seen (79). Interestingly, the size was also dependent on the barrier spacing, implying the degree of motion is a factor in the cell size. This concurs with current findings, where it is noted that there is a decreasing degree of lateral motion of RGD in DOPC > DPPC > Glass; this reduced spreading is reminiscent of the cell response to changes in the stiffness, where cells are smaller and more rounded on softer surfaces (226). This is also supported by

the properties of the actin cytoskeleton of the cells. The formation of a well-defined actin cytoskeleton is tightly controlled by the cell-surface interactions (18), with exertion of force on the surface playing a key role in the polymerisation of actin. Indeed, FAs, the means by which cells exert force on the surface are key nucleation sites of actin polymerisation (236). This is also noted on fluid phase bilayers (79), with less defined actin formation in response to lower forces being exerted by the cell.

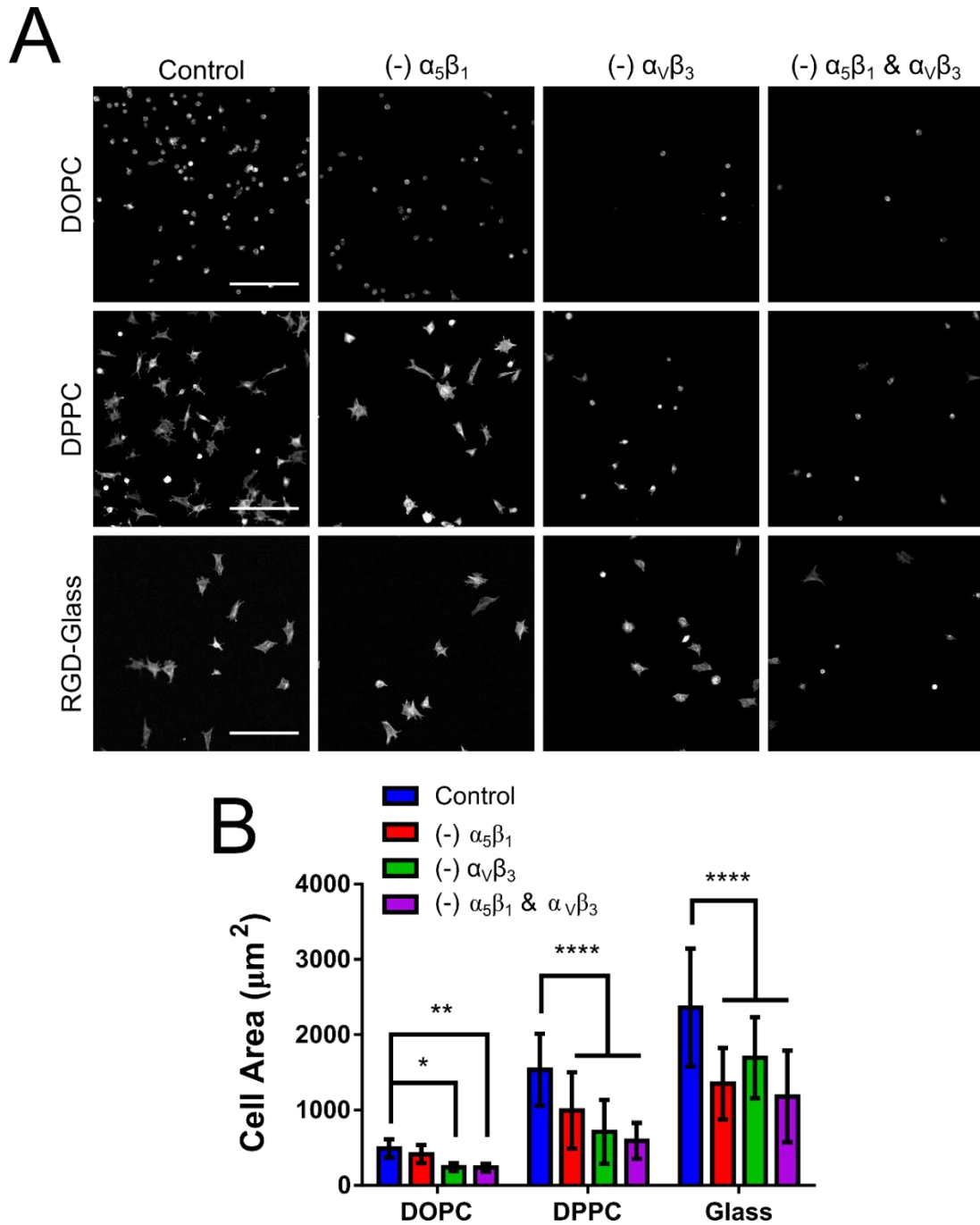


Figure 4.3. Inhibition of $\alpha_5\beta_1$ and $\alpha_V\beta_3$ Integrins. (A) Shows an array of the representative images of cells incubated with one or both inhibitors for $\alpha_5\beta_1$ and $\alpha_V\beta_3$ integrins on surfaces of

*all ligand mobility values. (B) Shows the consequent quantification of these images in terms of the change in cell area upon inhibition on each of the surfaces P values indicating significance, * ≤ 0.05 , ** ≤ 0.01 , **** ≤ 0.0001 .*

It has also been confirmed here that integrins binding to RGD mediate the response of the cells to the surface. The interaction of the integrins with molecules on the lipid surface is an important first step to the linking of the surface to the cellular processes. Indeed, integrins not only serve as an initial link for the cell to the surface, but also as key signalling molecules in both directions across the plasma membrane (237). Specifically, $\alpha_5\beta_1$ and $\alpha_v\beta_3$ integrins have a significant role in the determination of adhesion strength and mechanotransduction (91). Previously, it has been noted that the former determines the adhesion strength, with a greater ability to sustain higher forces; however, the latter, through a less stable bond, enables mechanotransduction, the process through which cells convert mechanical stimuli into biochemical signals. Together, the effects of the ligand mobility and integrin inhibition on the morphological characteristics of the cell may imply a mechanosensitive-based response to the surface. Other factors, such as chemistry and ligand distribution, can be disregarded due to both being of a comparable nature on both of the lipid surfaces.

4.3. LIGAND MOBILITY DEPENDENT CHANGES IN FOCAL ADHESIONS

To gain further insight into the nature of the cell response to the surfaces, key mediators of this response, focal adhesions (FAs), were analysed. As micron-scale complexes, filled with hundreds of different proteins, FAs serve a vital link between the actin cytoskeleton and the surface. As such, the physical properties of these protein complexes is highly dependent upon the nature of the surface, and thus is capable of elucidating, in greater detail, the nature of the cell response to the viscosity-defined ligand mobility.

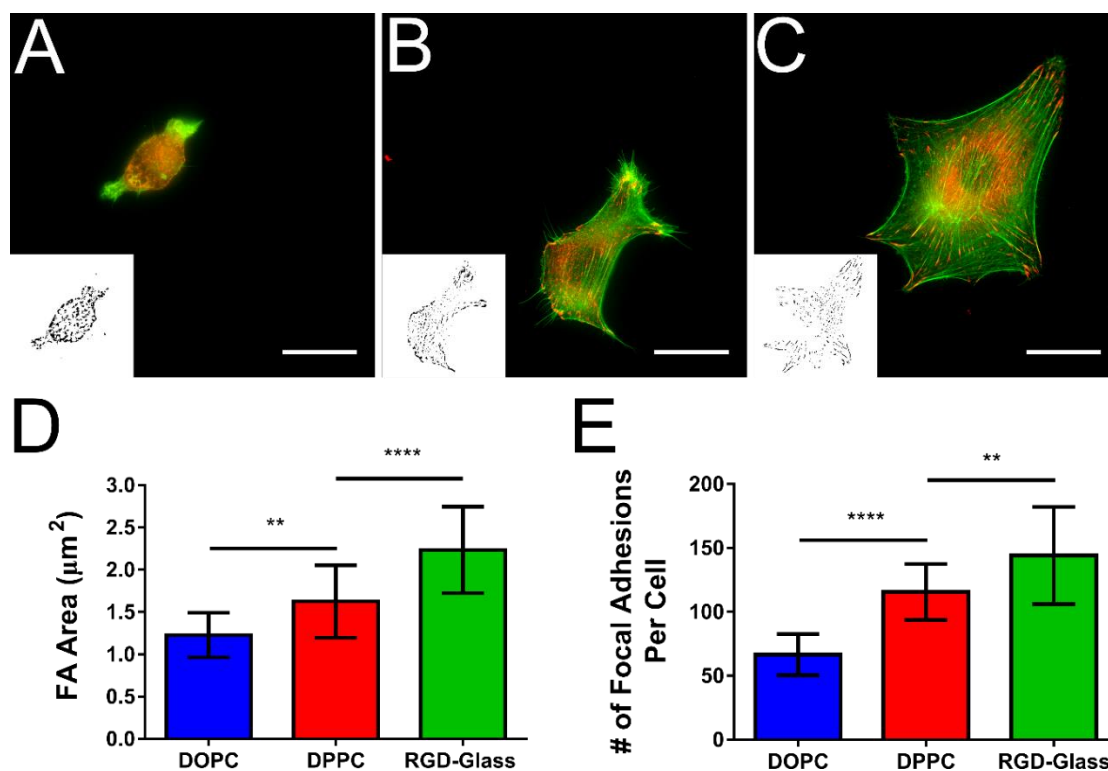


Figure 4.4. Focal Adhesion Changes in Response to Ligand Mobility. (A) – (C) Show representative images of the cells on DOPC, DPPC and RGD-Glass respectively with actin stained in green, and vinculin stained in red. (D) Shows the average size of the focal adhesions on the each of the surfaces with (E) showing the number of focal adhesions per cell. (Scale Bar = 25 µm). P values indicating significance, ** ≤ 0.01, **** ≤ 0.0001.

To this end the FA protein vinculin was used to stain for FAs present in the cell on each surface. Figure 4.4A – C shows the representative images of vinculin (red) and the cytoskeleton (green) on DOPC, DPPC and RGD-Glass respectively. Here the FAs were seen to be more well-defined on DPPC and RGD-Glass than on DOPC. Furthermore, vinculin stained positively at the ends of the actin stress fibres (Figure 4.4A – C), as would be expected (238), on these surfaces. However, on DOPC a more diffuse vinculin stain, with aggregates present and not associated with any stress fibres, was seen. Figure 4.4D and 4.4E seek to quantify these FA properties, by determining the average size (area) of the FAs and their number respectively. In line with the qualitative observations seen in Figures 4.4A – C, FA size was noted to increase as ligand mobility decreased (i.e. as the viscosity increase), with the largest seen on the RGD-glass surface. Furthermore, 4.4E shows that there is also an increase in the average number of

FAs per cell as the viscosity increased. Analysing this further, the distribution of the FA area is shown Figure 4.5; with a bin width of $0.5 \mu\text{m}$, the DOPC surfaces showed a large prevalence of much small adhesions, with nearly 80% being smaller than $1.25 \mu\text{m}$ and all being smaller than $2.25 \mu\text{m}$ (as represented by the largest FA size allowed in these bin groupings). In contrast, a greater proportion of adhesions were seen to be larger on both DPPC and RGD-Glass, with maximum adhesion size bin centred at being $2.5 \mu\text{m}$ and $3.0 \mu\text{m}$ respectively, and more adhesions at these higher distributions.

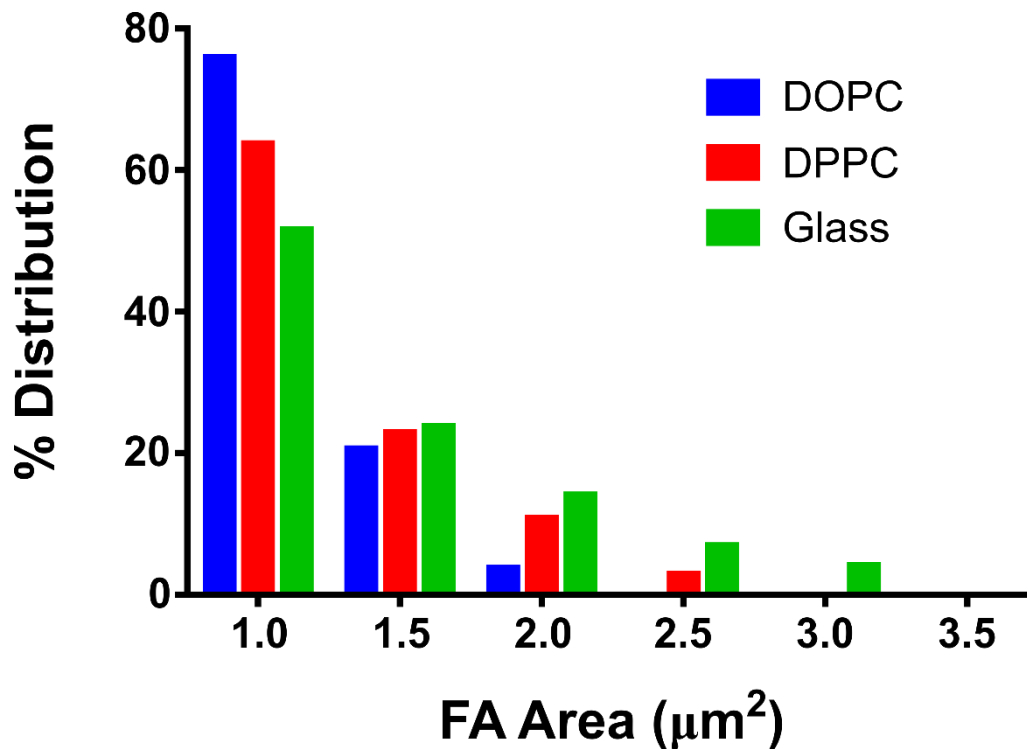


Figure 4.5. Focal Adhesion Distribution. The distribution of FAs is shown here on the each of the surfaces. In the analysis the minimal size of the FAs was set to $0.75 \mu\text{m}^2$; as such, the initial bin was set to $1 \mu\text{m}$, with a bin width of $0.5 \mu\text{m}$.

Focal adhesions (FAs) are well understood to be the one of the main mediators between the surface properties and the nature of the cell response (18). The formation of FAs has also been noted to be highly responsive to physical cues, with size (14, 239) and number (240, 241) being key initial indicators. Specifically, both a greater number of FAs and an increased area have been observed when cells are able to exert more force on the surface (240). For example, stiffer surfaces are more able to promote the formation of traction forces, producing more numerous and larger FAs (14). As noted above, it is implied, from cell spreading and cytoskeleton organisation, that cells may be exerting a greater force on DPPC, where a less mobile ligand is

presented. As other factors have been disregarded this result provides further support for this hypothesis. However, one weakness in the focal adhesions analysis may be that due to their larger area, larger cells are more likely to have more focal adhesions. While this cannot be discounted as a factor here, qualitatively the focal adhesions are observed to be more well-defined on the higher viscosity DPPC and the glass control. The shape and localisation of the FAs at the ends of actin stress fibres are also more in line with what has previously been noted in other studies (18). Further, FA size is less linked to the size of the cells, thus better representing the force on the surface (14).

As integrins cannot bind directly to the actin cytoskeleton, FAs are made up of potentially hundreds of adaptor proteins (18); therefore not only the size and number can change, but so too can the type of proteins as well as their properties. For example, FA proteins such as talin or α -actinin are present as linkers between integrin and actin and vital for FA maturation and stabilisation (242). The properties of these proteins change with the extent of force generated at the adhesion site; for example, force on talin exposes binding sites for vinculin and yet other proteins have their phosphorylation sites exposed under force, inducing further signalling pathways. Conversely, proteins such as p120^{cas} (243) or Arp2/3 (244) are recruited specifically in response to force. The protein stained for in Figure 4.4 is vinculin, whose properties within FAs are highly dependent on the mechanical properties of the surface. It has previously been noted that vinculin is recruited to site of adhesion in response to force (245-247), where the N-terminal head group can bind to actin-integrin linker proteins talin and α -actinin and the C-terminal tail group binds to F-actin (248). Further to this, vinculin in its unbound conformation is auto-inhibited by the head-tail interactions and is activated upon binding, likely to a number of ligands (249). Vinculin therefore acts as a means to regulate the amount of force exerted on a surface, with not only the head and tail sites contributing, but also the neck region binding further signalling proteins, such as VASP (250). This, in turn, leads to cell FA stabilisation, thus regulating cell mechanics and spreading (251). In the representative images in Figure 4.3A – C vinculin can be qualitatively seen to localise to focal adhesions more in cells on DPPC and the RGD-Glass control than it does on DOPC, where a more diffuse background is seen. This would imply that the focal adhesions formed in the presence of less mobile ligands are capable of exerting more force on the surface.

This assertion was further tested by assessing the presence of pFAK in the cells (Figure 4.6). The phosphorylated form of focal adhesion kinase (FAK), pFAK is also an indicator of the amount of force exerted by the cell on a surface; this is due to the exertion of force exposing tyrosine sites capable of phosphorylation (33). Figure 4.6A – C shows that pFAK is more prevalent as the ligand mobility decreases, with high fluorescence and similar morphology to that seen on vinculin stains in Figure 4.4. Furthermore, the integrated density of the pFAK present within the cell increases as the ligand mobility decreases (Figure 4.4D). With FAK previously shown to phosphorylate under force, it can therefore be assumed here that the increased pFAK present is likely an indicator of increased phosphorylation due to forces exerted on the surface. This, in turn, can be linked to the mobility of the ligand, with higher phosphorylation noted on more viscous surfaces, with lower ligand mobility. One possible consequence of this is that there may be increased downstream signalling through the Ras signalling pathway (33) and through proteins such as RhoA and Rac (252).

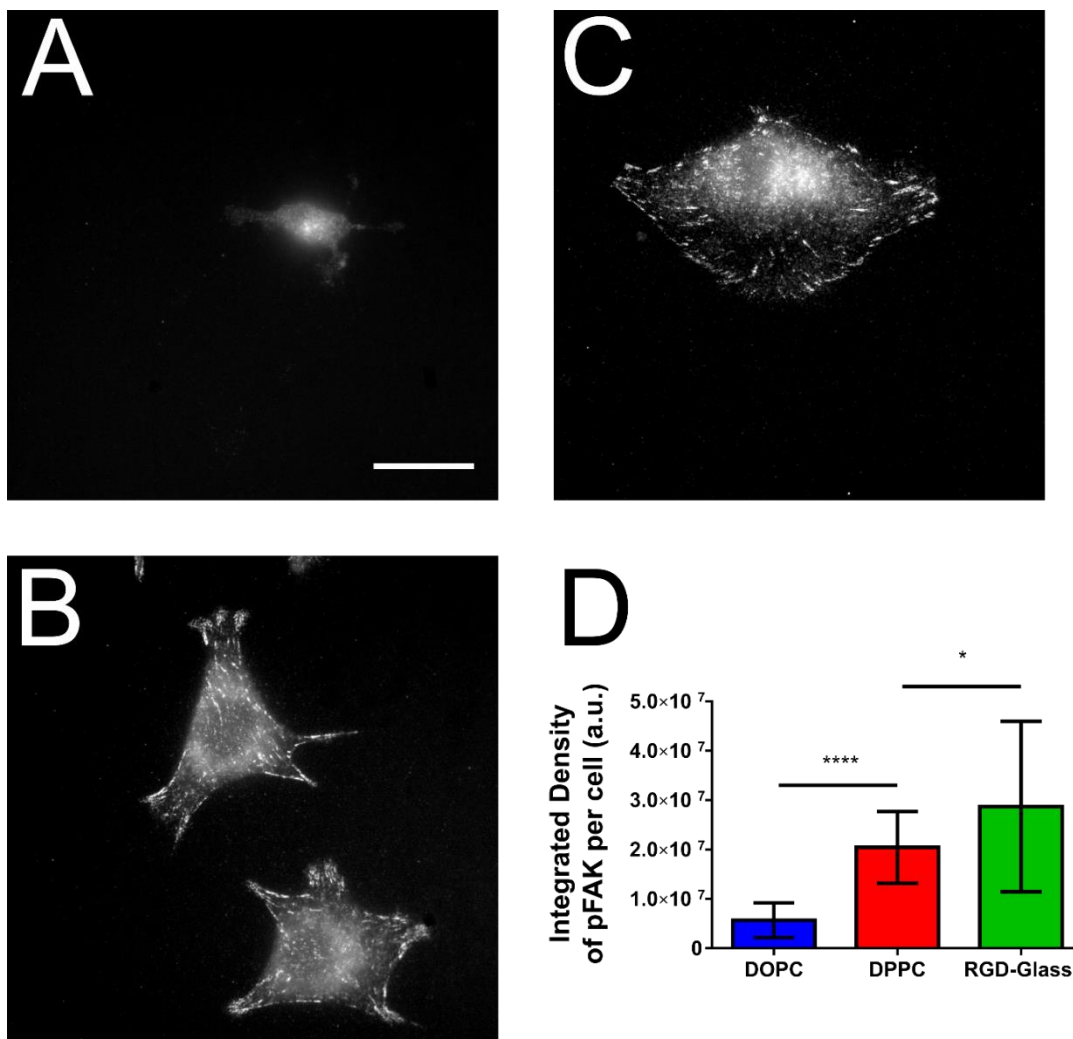


Figure 4.6. Phosphorylation of FAK in Response to Ligand Mobility. (A) – (C) Show representative images of pFAK present in the cells seeded on DOPC, DPPC and RGD-Glass respectively. (D) Shows the integrated density of the pFAK within the cell area. (Scale Bar = 25 μm). P values indicating significance, * ≤ 0.05 , **** ≤ 0.0001 .

In light of the findings above, Figure 4.7 summarises the proposed mechanism of the sensing of viscosity-defined ligand mobility that was implied by the findings above, combined with the previous literature. Here, it was hypothesised that a decrease in ligand mobility, through increased viscosity, leads to an increased force exerted on the surface; it was hypothesised that this was due to the greater resistance to ligand motion in the less mobile (more viscous) DPPC. In response to this increased force, mechanosensitive proteins are activated through the physical process of exposing sites of activation, in the case of FAK or binding, in the case of adaptor proteins such as talin (indicated from the presence of vinculin). In the former case this leads to phosphorylation and activation of downstream pathways. In the latter this leads to vinculin binding to exposed sites on adaptor proteins, providing a further link to F-actin and increasing further signalling pathways.

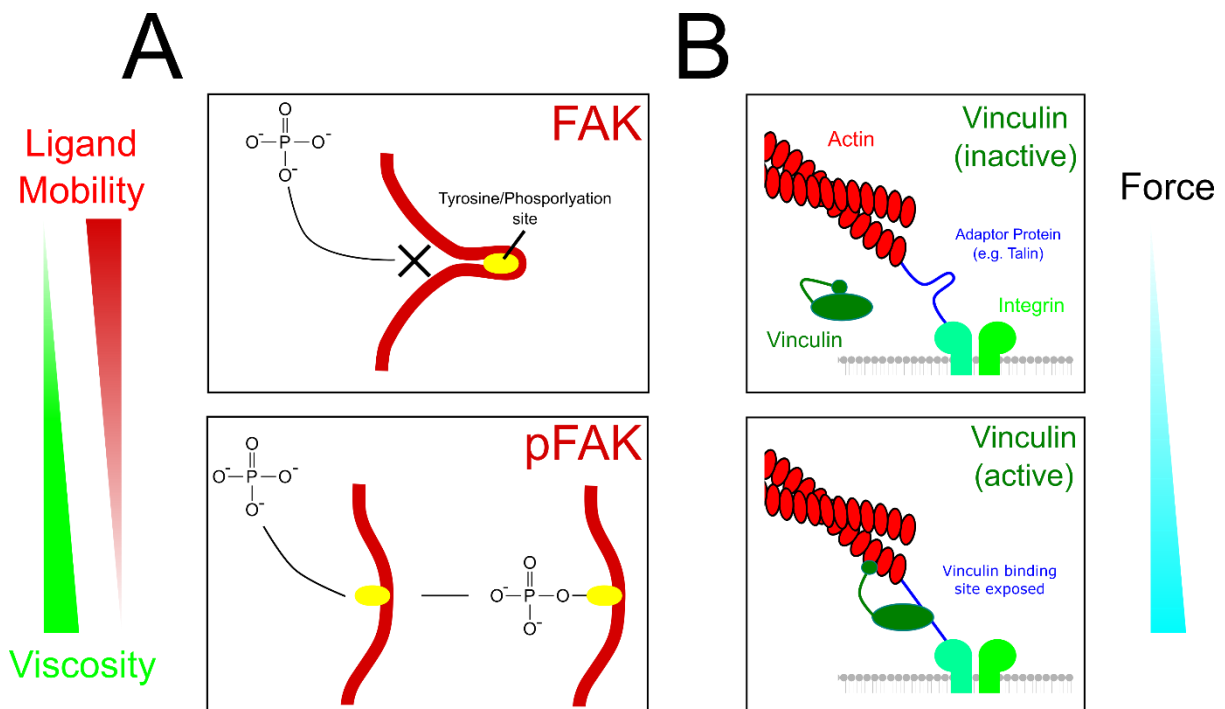


Figure 4.7. Protein Activation in Response to Ligand Mobility. The schematic shows a proposed effect of the viscosity-defined ligand mobility on the FA proteins present in the complex; as viscosity increases and ligand mobility decreases, the assumed amount of force

increases. (A) Shows how mechanical force is capable of exposing phosphorylation sites present in FAK, leading its conversion to pFAK and its consequential activation. (B) Shows that mechanical pulling of adaptor proteins linking integrins, and thus the surface, to the actin cytoskeleton leads to the exposure of vinculin binding sites on proteins such as talin. Vinculin can then subsequently bind to F-actin as well as other signalling molecules.

4.4. CONCLUSIONS

This chapter has begun to understand the nature of the cell response to ligand mobility. After successfully producing and characterising SLBs of varying viscosity in the previous chapter, it was shown here that this viscosity-defined ligand mobility can control cellular behaviour, with cells spreading to a greater extent on the more viscous DPPC, which present lower mobility ligands. This is supported by the above noted observations with cell spreading, cytoskeletal organisation, focal adhesion size, number and activity all seen to be inversely proportional to the ligand mobility. With other factors (chemistry and ligand distribution) previously accounted for, these observations lead to the hypothesis that the mechanisms that control the cell response to the viscosity and the accompanying ligand mobility are mechanosensitive in nature. Indeed, the nature of the cell response to this viscosity is reminiscent of that of the response to stiffness, with cells on less viscous surfaces being smaller, more rounded and having less well-defined FAs than those on more viscous surfaces. However, while these results imply that this is the case, they do not prove this outright. With respect to this, the next chapter will focus on understanding the mechanisms that dictate this, in an effort to more deeply understand the molecular nature of cellular response.

5. UNDERSTANDING THE NATURE OF THE RESPONSE TO VISCOSITY AND LIGAND MOBILITY

5.1. INTRODUCTION

The previous chapter has noted that the ligand mobility, directly controlled by the viscosity of the SLB, has a significant effect on cellular behaviour and morphology. As this behaviour was reminiscent of the response of cells to stiffness it was hypothesised that the pathways used by the cell to detect the surface viscosity would be similar. This chapter has therefore sought to test this hypothesis in order to better understand of the mechanisms and pathways involved.

The cell response to stiffness is a multifaceted process relying on the linking of the cytoskeleton to the surface via the FAs and associated proteins. The consequent signalling of this process can lead to further downstream processes, such as transcription factor localisation, regulation of gene expression, or changes in cellular motility. However, the initial detection of the cell surface is through the transmembrane integrin proteins, of which there are 24 heterodimers present in humans (17). Containing one α and one β subunit, specific integrins can have different affinities for different peptide sequences (17), as well as different binding profiles and strengths (118). This provides a degree of versatility to the system, with some integrins capable of binding strongly to the surface and others, with weaker binding affinities, acting as mechanosensors, capable of triggering downstream events.

Upon binding to the integrin the extracellular matrix (ECM) becomes coupled to the cytoskeleton and it is this coupling that defines the cellular response to the surface. The predominant model of the process whereby cells respond to stiffness is that of an actin-talin-integrin-matrix clutch; this has widely become known as “the molecular clutch” and is described in detail in Section 1.2.3. This model was first proposed by Mitchison and Kirschner in 1988 (116), who aimed to describe the molecular nature of actin dynamics in axonal nerve growth cones. This was proposed, initially, because actin retrograde flow (i.e. the flow of actin inwards from the cell edge) was known to be continuous, whereas forward motion was variable. This implied that the coupling between the actin and the adaptor proteins allowed for “variable slippage,” which they defined as a molecular clutch; as with a mechanical clutch, this molecule

would prevent or allow for force to be transmitted dependent on whether it was “engaged” or not. The next key development of this model came 20 years later, when Chan & Odde developed a stochastic model to predict the nature of this clutch (115), whereby the system was considered as a series of springs, attached to the F-actin filament moving at a constant velocity. It was eventually shown that the adaptor protein, talin, acts as the clutch in this system, with the mechanical linking of the ECM and the substrate occurring only if talin unfolded within the integrin-ligand bond lifetime (47).

In order to have an effect on the cell response, the nature of the surface must be transmitted further downstream than the cytoskeleton, with numerous studies indeed finding this to be the case. External, mechanical cues are translated into biochemical signals (e.g. transcription factors), that are capable of affecting gene expression. Key examples of downstream proteins include RhoA and Yes-associated protein (YAP). The former, a GTPase, has been associated with higher spreading and subsequent commitment of capable cells into more contractile lineages, such as osteoblasts (32). The latter has also been noted to be a key mechanosensitive protein, which localises to the nucleus to a greater extent upon stiffer substrates, as well as requiring cytoskeleton tension for its activity (21). Furthermore, YAP has also been shown to be necessary for stiffness-induced differentiation of mesenchymal stem cells (21).

To probe the mechanisms that the cells use to define their response to the surface viscosity, actin dynamics and the consequent effect on downstream effector molecules are vital to understand. Furthermore, as these can have effects on differentiation capable cells, overall impact of the viscosity can be studied further by determining the consequences of this change in actin dynamics and downstream signalling.

5.2. APPLYING THE MOLECULAR CLUTCH TO LIGAND MOBILITY/SURFACE VISCOSITY

The molecular clutch model, at its heart, seeks to explain how the cell converts the retrograde (rearward) actin flow (herein referred to as “actin flow”), resulting from F-actin polymerisation at the leading edge of the cell and the action of myosin, into forward movement. In previous, seminal, work it has been applied successfully to predict the response of the cell to substrates of varying rigidity (47, 118). It showed that modelling cytoskeletal machinery as an elegant series of discrete variables was accurately able to predict the nature of the cell response, such as the integrin density (118), magnitude of traction forces and actin flow (47). However, this work has modelled the system solely with regards to elastic stiffness, with substrates considered to have minimal contribution from the viscous element. With the ECM being a viscoelastic system, it is vital moving forwards that the contribution of the viscous element be considered. Some research has sought to determine this, with Chaudhri et. al., (2015) (62) demonstrating that stress relaxation (considered the viscous element), that is the reduction in stress over time when a material is under constant strain, can also define the cell response; cell spreading on soft substrates, exhibiting stress relaxation, was similar to that of cells on stiff substrates. However, there is currently no work determining whether or not this model can be applied to wholly viscous materials. SLBs provide a unique opportunity for this, as they are two-dimensional confined fluids with a minimal elastic element. Therefore, they are the ideal tool through which to study the applicability of the molecular clutch to viscosity, i.e. the mobility of the ligand.

5.2.1. MODELLING THE MOLECULAR CLUTCH FOR LIGAND MOBILITY/SURFACE VISCOSITY

As the nature of the clutch has been thoroughly modelled in relation to stiffness, the model was adjusted to apply to the lipid surfaces. This was done through considering the lipid surfaces as an entirely viscous system. This is shown schematically in Figure 5.1, where the substrate is modelled with a viscous dashpot, rather than an elastic spring (as in Figure 1.5). It was therefore possible to determine the role of the molecular clutch in the cell sensing of viscosity.

Initially the diffusion coefficient, originally measured in Figure 3.6, was used to estimate the viscosity of the surface by applying the Saffman-Delbruck (SD) equation, first noted in section 1.3.3. and recounted for convenience here (155, 214):

$$D = \frac{k_B T}{4\pi\eta_m h} \left[\ln \left(\frac{2L_{SD}}{R} \right) - \gamma \right] \quad (1.1)$$

Where D is the diffusion coefficient, k_B is the Boltzmann constant, and T the absolute temperature. The L_{SD} is the SD length and comprised of, η_m the membrane diffusion, η_f the viscosity of the fluid (given as water at 37°C – 0.691 x 10⁻³ Pa.s). Further, R is the radius of the inclusion (in this case a lipid molecule) and γ the Euler-Mascheroni constant (0.577).

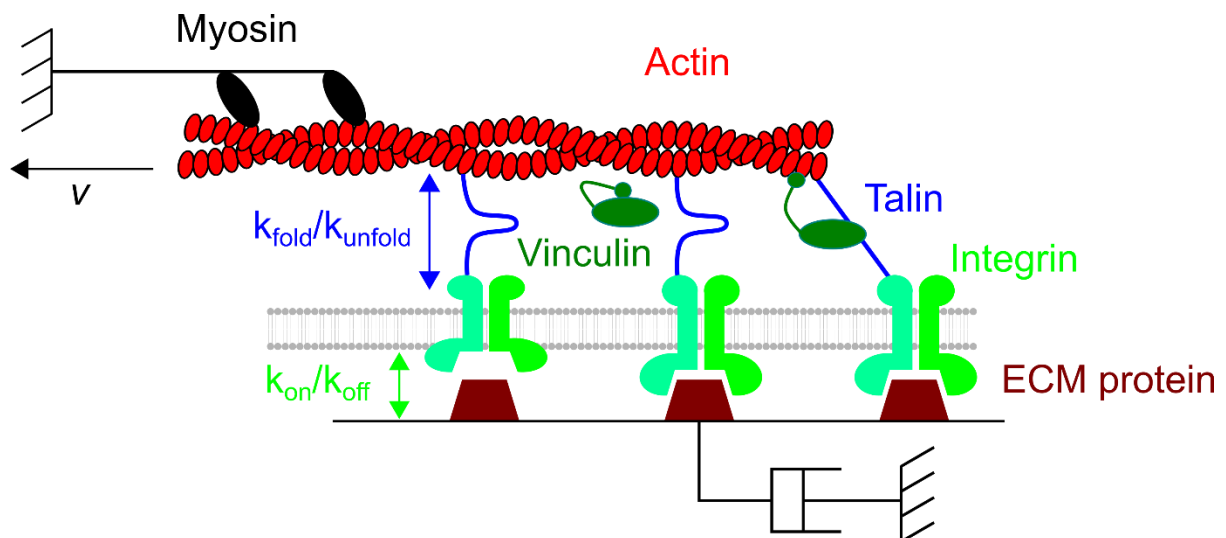


Figure 5.1. Cell Response to Viscosity through the Molecular Clutch. The speed of actin retrograde flow is controlled by the myosin motors. If the ECM-integrin bond lifetime is of sufficient length then the force exerted on the talin by the actin flow allows for the unfolding of talin at a specific rate. This unfolding leads to force enhancement through stabilisation of the talin-actin linkage through molecules, such as vinculin (adapted from Elsogui-Artola et al. (2016) (47)).

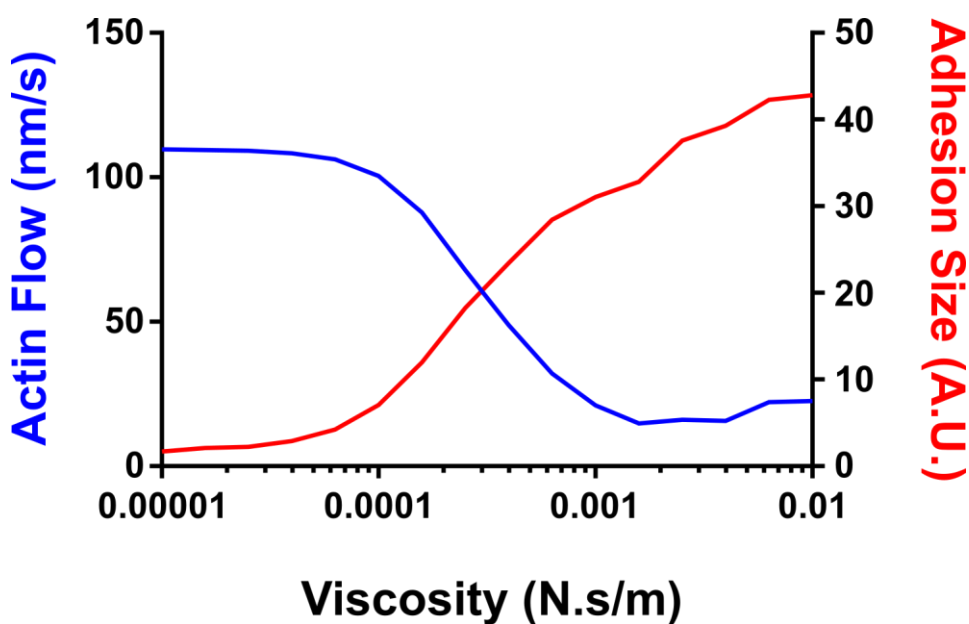


Figure 5.2 Model Predictions of the Effect of Viscosity. The left y-axis (blue) shows the predicted effect of the viscosity on the actin flow with a reduction in flow seen at approximately 10^{-4} N.s/m. The right y-axis (red) shows the adhesion growth upon and increase in the viscosity of the surface, being seen to increase from a lower viscosity than that of the actin flow. Model data provided by Prof. Pere Roca-Cusachs of IBEC, Barcelona.

As previously noted, applying this equation to the diffusion values previous attained in Chapter 3 gives viscosity values of 7.18×10^{-10} Pa.s.m and 3.95×10^{-8} Pa.s.m for DOPC and DPPC respectively; in the case of DOPC this was similar to values from previous observations in giant unilamellar vesicles (215) and DPPC was believed to be a reasonable estimate, based on comparable values (216). Subsequent to the calculation of viscosity, the molecular clutch model was adjusted to account for viscosity rather than stiffness. As the units of viscosity here, Pa.s.m, are a comparable unit to that of N.s/m – the units used in the original clutch – the application of viscosity to the molecular clutch model was directly applicable with small alterations; the resulting computational predictions are shown in Figure 5.2. This computational prediction demonstrates that as the viscosity increases the actin flow will reduce and the adhesion size will increase. However, the key point of note here is that these changes in both flow rate and adhesion size only begin to show significant changes at viscosity values of approximately 10^{-4} N.s/m. This is in contrast to previously measured values on the order of 10^{-8} and 10^{-10} N.s/m for DPPC and DOPC respectively. Taking this model in isolation it would therefore be assumed that the change in actin flow and adhesion size would be the same

between DOPC and DPPC. However, in the case of the latter, this has been shown in the previous chapter (Figure 4.4) to not be the case. This, therefore, raises the question as to how there is any response from the cells.

A likely scenario is that the SD equation is no longer valid. A key variable of this equation is the SD length: L_{SD} , which only holds true a certain length scales. Specifically, L_{SD} is valid only when the radius of the diffusing particle is considerably smaller than this length ($R \ll L_{SD}$) (157). However, when the diffusing particle becomes larger the SD equation fails completely. While further developments of the equation compensate for this (156, 157), other work has sought to rethink the SD equation entirely. This equation, from Gambin et al., (2006) (135) states that the diffusion has a $1/R$ relationship to the size of the diffusing molecule; this contrasts with the SD equation, which predicts a logarithmic relationship. This equation was first noted as an alternative in Section 1.3.3. and is restated here for convenience:

$$D = \frac{(k_B T) \lambda}{4\pi\eta_m h R} \quad (1.3)$$

Where D is the diffusion coefficient, k_B is the Boltzmann constant, T the absolute temperature, η_m the membrane viscosity, R the radius, h is the bilayer thickness and λ is the characteristic length.

Applying the originally measured diffusion values to this equation slightly lower estimates for the viscosity values are attained: 8.4×10^{-11} Pa.s.m for DOPC and 2.33×10^{-9} for DPPC. In DOPC, previous estimates were attained from giant unilamellar vesicles, which may account for this discrepancy. As viscosity of DPPC SLBs was not found it is unclear whether this or the previous ascertained value from the SD equation are more accurate. However, a key difference between this and the SD equation is the presence of the characteristic length (λ). This was included for dimensional reasons and is noted by the authors to be a measure of the perturbation of the membrane by the diffusion molecule. In the case of a single lipid this may be small, with values of 1 – 10 angstroms appropriate, reflecting the size of the lipid molecule. When determining the diffusion of proteins this may significantly increase into the 10s of nm

range. In this work the equation was also shown to be valid across not only the measurements they made, but also of others they had analysed, where the SD equation was not valid.

Changes in λ may account for the discrepancy seen between the originally estimated viscosity values and those predicted to induce a change in actin flow and adhesion size in the model. As already stated λ is a measure of the degree of membrane perturbation caused by the diffusing object; in the case of cells binding to an SLB this may be incredibly large. Specifically, Chapter 3 noted that there was approximately 6,000 neutravidin molecules per μm^2 . It has been shown previously that even the inclusion of small fractions of immobile molecules within a bilayer can reduce the diffusion coefficient (253). With the reduction in the diffusion coefficient comes a concomitant increase in the viscosity. Further, it would also be reasonable to assume that this number of binding interactions between the SLB and the cell, would significantly perturb the SLB.

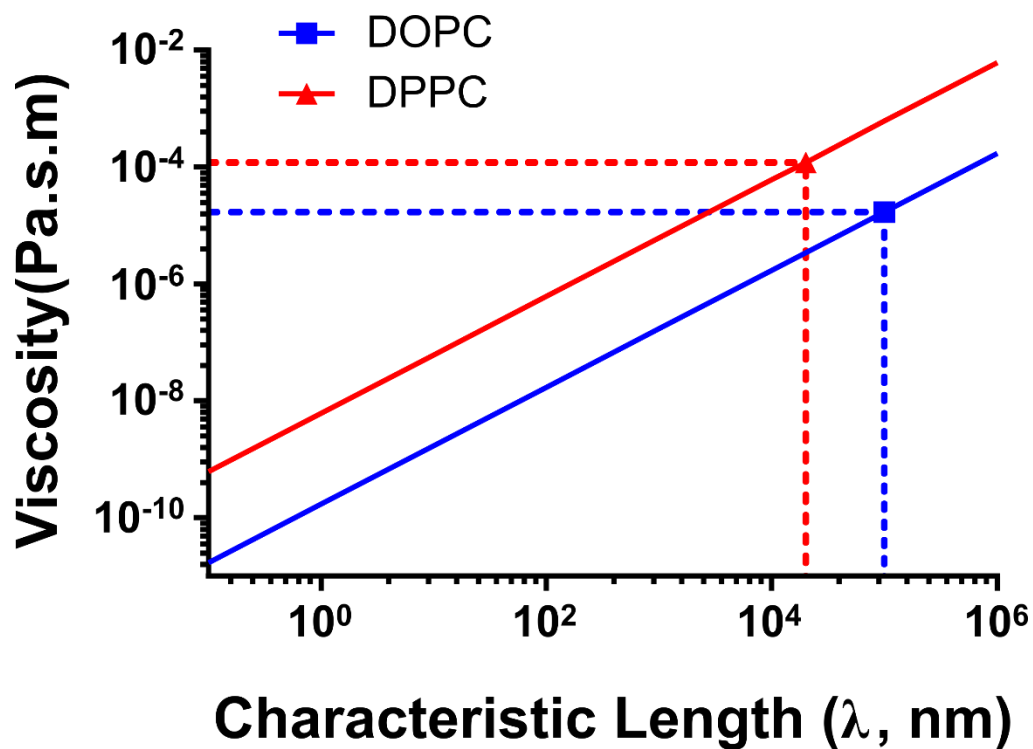


Figure 5.3. Changes in Characteristic Length Affect Viscosity. This graph demonstrates how the alternative equation presented by Gambin et al., (135) predicts changes in viscosity on the degree to which the membrane is perturbed by the diffusing molecule. This was predicted for both DOPC (blue) and DPPC (red). The two data points show a characteristic length of the same scale as the average

cell radii on each of the SLBs, estimated from Figure 4.2. These gives values in the ranges of 10^{-5} and 10^{-4} Pa.s.m for DOPC and DPPC respectively, with the latter in the range of detectable viscosity as predicted by the molecular clutch model.

As this equation provides a possible solution to the mismatch between the measured viscosity and the predicted magnitude at which the cells respond Figure 5.3 shows the predicted changes in viscosity based on the changes in the characteristic length. Despite the diffusion coefficient being kept constant it is clear from this graph that the viscosity will change based on the extent of the interaction between the SLB and the cell. At this point a key assumption was made: the cell was considered a single entity, with many binding sites; as such, the characteristic length should reflect the extent to which the whole cell perturbs the membrane, not just each individual integrin-RGD-lipid interaction. As such a characteristic length scale was estimated from the average radii (assuming a perfect circle) from Figure 4.2. These values were 10 μm and 20 μm for DOPC and DPPC respectively and give viscosity estimates of 1.6×10^{-6} Pa.s.m and 1.2×10^{-4} Pa.s.m respectively; the data points are shown on Figure 5.3. This led to good agreement of the viscosity values with those predicted to induce a cell response. Specifically, the viscosity of DPPC was high enough to activate the clutch, whereas DOPC was not. This also aligns with the hypothesis of the previous chapter that cells can therefore exert forces on the DPPC SLB and not on DOPC. From this, it may therefore be concluded that there is a significant increase in viscosity within the area of the cell, induced by the extensive binding of cellular integrins to the RGD presented by each of the SLBs. In the case of DPPC reduction is enough to activate the molecular clutch. The further sections sought to confirm the predictions through the measurement of the actin flow.

5.2.2. VISCOSITY DEPENDENT CHANGES IN ACTIN FLOW

Actin retrograde flow is a vital component of the molecular clutch model, as well as a key indicator of its role in the cell response. The actin flow on the varying viscosity surfaces was measured to determine what the differences were in the cellular response. As stated previously the clutch model has been applied to, and successfully proven, on elastic substrates. However, its role has not been determined in how cells respond the viscosity of the substrate, here defined by the mobility of the ligands. As the adhesion size was not quantitatively seen to directly

match the model it was also therefore hypothesised that there would also be a difference in the actin flow in cells on each of the surfaces. Transfected cells were imaged at a frequency of 1 Hz over the course of 2 mins. By splitting the image stack to display time vs. position, giving a kymograph, the overall flow of actin could be observed by taking $\tan \theta$ (Figure 5.4A), which gives pixels/sec, then converted into nm/sec. These kymographs were then used to determine the resulting action flow values for the cells on each surface, as shown in Figure 5.4B. The array in Figure 5.4C shows the representative sample of cells, with the red line showing the part of the image that was measured and the inset showing the resulting kymograph of displacement over time. It was seen that retrograde flow is highest on the surface presenting the most mobile ligands; DOPC. In turn, this flow was seen to decrease in line with increasing viscosity (decreasing ligand mobility), with cells on the glass seen to have the slowest actin flow.

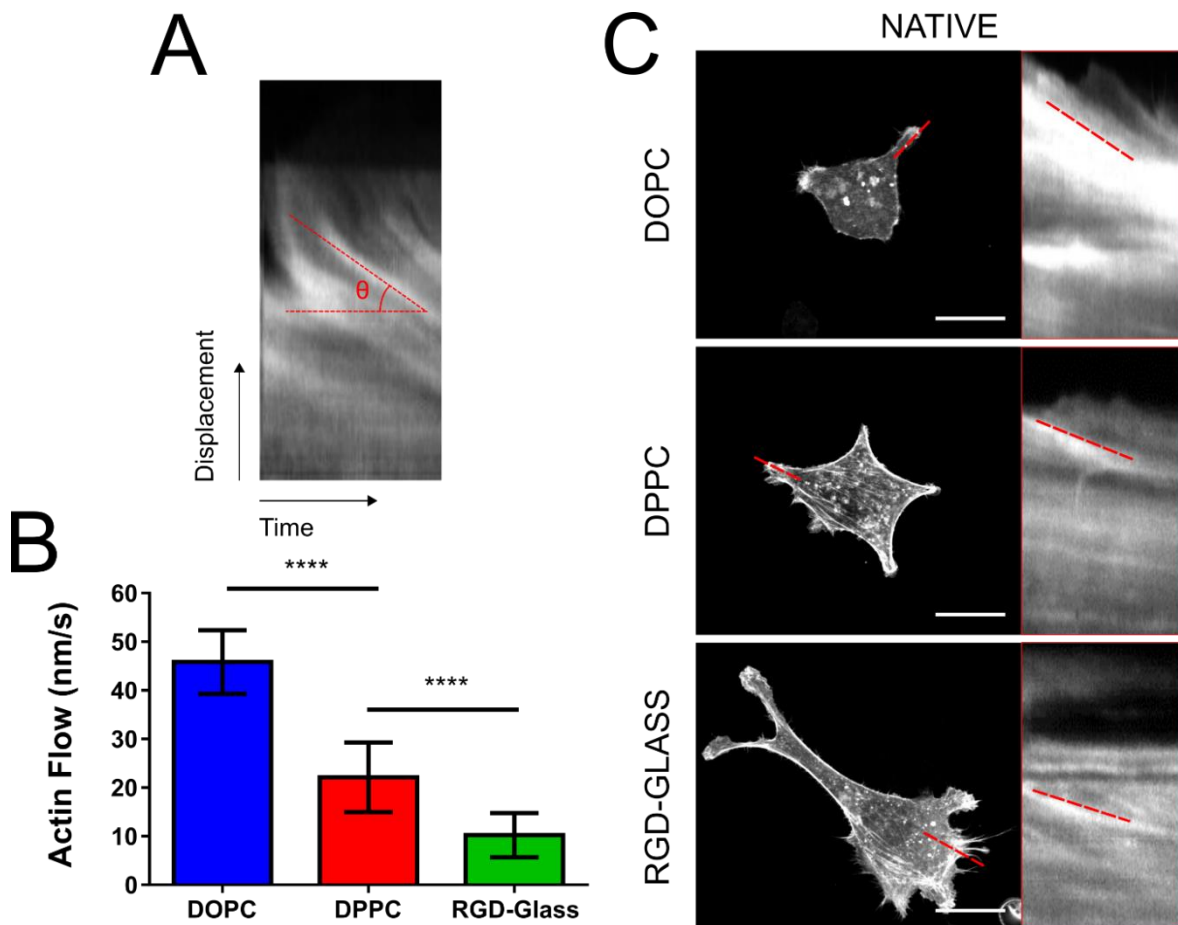


Figure 5.4. Viscosity Dependent Actin Flow. Due to the importance of the actin flow in the molecular clutch model the viscosity dependent actin flow was determined on the surfaces. (A) Shows an example kymograph taken from an image stack (1Hz for 2 min). By selecting a region of interest, the image in the region can be re-stacked to show how the fluorescence

*changes position with time. By taking the $\tan \theta$ of the angle this displacement the speed of the actin flow can be determined. This is shown in (B) where the actin flow on each of the surfaces is shown. This shows that the actin flow is lower on surfaces that exhibit lower or no viscosity. (C) Shows representative images of the cells on each of the surfaces, with the insets showing the relevant kymograph of each selected region. (Scale Bar = 25 μm). P values indicating significance, **** ≤ 0.0001 .*

In order to further understand these changes in actin flow key components were inhibited in order to provide insights into whether the force sensing machinery is responsible for detecting this difference in the mobility of the ligand, as defined by the membrane viscosity. Initially, cells were incubated with blebbistatin; this well-known inhibitor of myosin II binds to the myosin-ADP-Pi intermediate complex (254), blocking myosin activity when in the actin detached state. This is shown schematically in Figure 5.5A. High concentrations of blebbistatin (50 μM) have previously been shown to lead to almost non-existent traction forces on elastic substrates (47), and by completely removing the cell's ability to exert force, by pulling via F-actin on the surface, it was believed that actin flow would be significantly affected. Indeed, as shown in Figure 5.5B, this is what was seen; upon incubation of the cells with blebbistatin the actin flow on both DPPC and RGD-Glass was seen to increase. In contrast, actin flow on DOPC showed no significant change. Furthermore, all surfaces were noted to have an actin flow that was comparable to that of DOPC in native cells.

Moving beyond the direct inhibition of actin flow with blebbistatin, vinculin binding was also inhibited. As discussed in the previous chapter, vinculin's activity is auto-inhibited by the head-tail interaction (249), which is proposed to be overcome by the binding of vinculin to a number of ligands simultaneously; for example, actin and talin (107). Furthermore, talin has been shown to have a number of cryptic vinculin binding sites that are exposed upon the unfolding due to mechanical force (104). It is possible that this is the initial step in the activation of vinculin, with it being required for the stabilisation of FAs under force (255). However, a plasmid encoding for VD1, a head-group only form of vinculin, was transfected into the cells to inhibit native vinculin binding to talin. This form of the protein has previously been shown to lead the assembly of VD1-talin complexes within FAs (106). However, without the tail domain this mutated protein is unable to stabilise the talin-mediated link between integrins and

actin (256), thus inhibiting any change in actin flow (Figure 5.6A). The results, shown in Figure 5.6B, quantified from Figure 5.6C, confirm this by demonstrating that cells transfected VD1 plasmid do not show any difference in actin flow regardless of the viscosity of the surface.

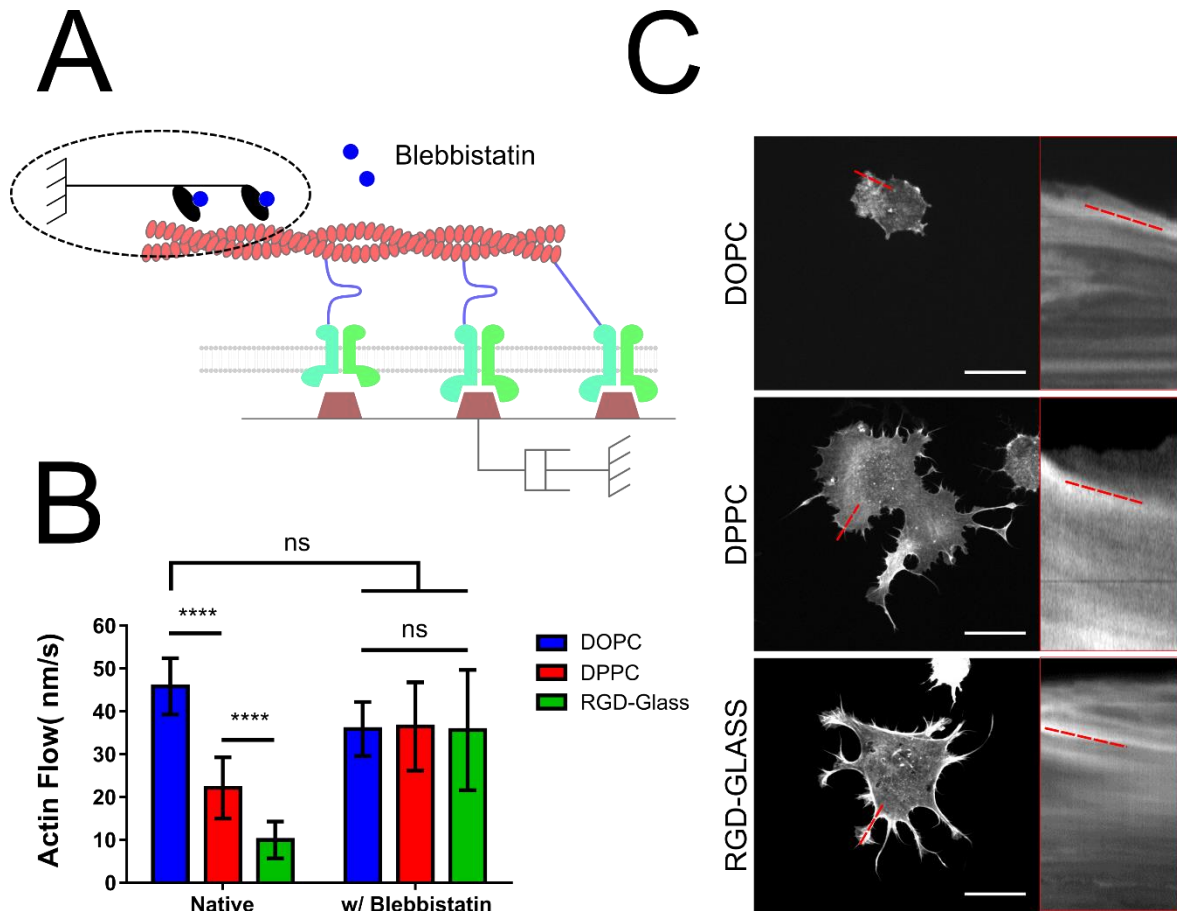


Figure 5.5. Actin Flow upon Myosin II Inhibition (A) Shows the mode of action of the myosin II inhibitor, blebbistatin, which blocks the activity of myosin II rather than its binding to F-actin. (B) Shows the consequent effect of the blocking of myosin II on surfaces of differing viscosity, where the actin flow rate was not statistically significant between any surface. (C) Shows the representative images of cells and their corresponding kymographs used to determine the actin flow. (Scale Bar = 25 μm). P values indicating significance, **** ≤ 0.0001 .

In order to specifically confirm that the VD1 specifically led to a change in actin flow by preventing this force enhancement step the presence and properties of the FAs was determined. As shown in Figure 5.2, the adhesion size increases with viscosity, concomitantly with a reduction in actin flow. Figure 5.7 confirms that this similarity in actin flow between surfaces, regardless of viscosity-defined ligand mobility, is due the forces detected on the surfaced not

being transmitted to the actin cytoskeleton. This is shown by the lack of difference in size of the FAs, which, as discussed in the previous chapter, is indicative of the force exerted on the surface (14, 239).

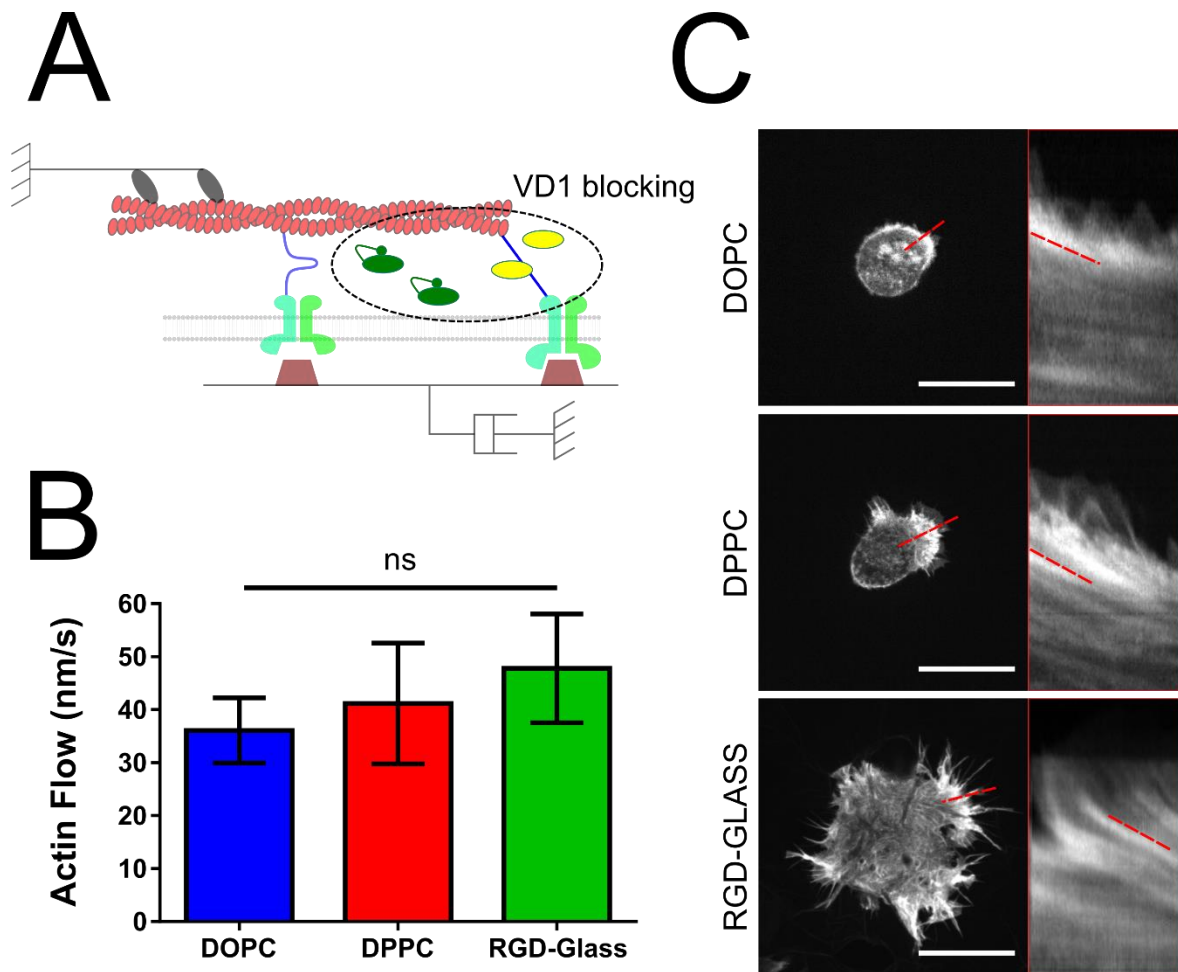


Figure 5.6. Actin Flow upon Vinculin Inhibition. (A) Shows, schematically, the mode of action of VD1, which blocks force enhancement upon substrate binding by preventing the binding of native vinculin. Subsequently, it does not have tail domain through which to bind to F-actin and thus stabilise the talin-mediated link between integrins the cytoskeleton. (B) Shows the consequential effect of transfection of C2C12 cells with VD1, whereby there are no observed differences between the actin flow on any of the surfaces. (C) Shows representative images of cells and kymographs used to determine the difference in actin flow rate in cells on the each of the surfaces. (Scale Bar = 25 μ m). *P* values indicating significance, *ns* > 0.05.

Together these changes in the actin flow, determined by the viscosity-defined ligand mobility are mechanosensitive in nature, with these trends being predicted, qualitatively, by the molecular clutch model. Initially, when addressing actin flow, it is noted that there is a change

when the viscosity is increased i.e. reducing the ligand mobility. Actin flow has been closely linked to force on the surfaces, with previous work noting that the actin flow rate is an important parameter in cell rigidity sensing. This is in conjunction with the associated forces and elasticity of related components (104). Specifically, upon the exertion of force actin flow slows in response to increased force (118, 257). This slowing can be attributed to the linking of the actin cytoskeleton to the ECM (258); relating this to the molecular clutch, the ‘engagement’ of the clutch converts the forces that are generated by the rearward actin flow into force on the surface. According to the model, this coupling of the cytoskeleton to the surface, in turn, leads to force loading on the surface. When considering the mobility of ligands, as dictated by the viscosity, this coupling of the cytoskeleton to the surface would therefore lead to similar effects as those seen in stiffness. The proposed molecular behaviour of cells and the response of the surface are shown schematically in Figure 5.8. First, considering the actin flow on DOPC (left panel, Figure 5.8), where the actin flow is higher the low viscosity of the surface provides a greater mobility to the RGD ligands. Upon binding this leads to a lower force loading rate as the SLB will allow for greater lateral movement of the ligand (denoted as D_H), akin to compliance in a soft elastic substrate. This would prevent the unfolding of force sensitive proteins (Figure 5.1, k_{fold}/k_{unfold}) within the lifetime of the integrin-RGD bond (Figure 5.1, k_{on}/k_{off}). Therefore, force sensitive molecules, such as FAK or talin (the latter indicated in Figure 5.8), would be unable to bind to further stabilising molecules such as vinculin, thus preventing force enhancement, the maturation of FAs (258) and the exertion of forces (47). The opposite is true in the case of DPPC (right panel, Figure 5.8); here the viscosity is high enough to impede the movement of the RGD ligand, reducing the magnitude of ligand displacement, as indicated by D_L . This increases the force loading rate to a timeframe that allows for force-dependent protein unfolding, within the lifetime of the integrin-RGD bond. In turn, as seen in both Figure 4.4 and 5.7, this leads to formation of mature FAs, thus implying the greater exertion of forces (i.e. traction forces) on the surface (240).

By inhibiting any step in the process of transferring the force generated by actin flow into force on the surface it is possible to gain a deeper insight into the system as a whole. In the case of blebbistatin the blocking of myosin-II action, provides an explanation as to why the actin flow increases on DPPC and RGD-Glass and why this is similar to that of DOPC. In contrast to these findings, certain work has noted that this decreases the actin flow rate (259). However,

here the increase in the actin flow rate can be inferred by noting that forces are significantly reduced upon incubation of the cells with blebbistatin (47). This implies a decoupling of the actin flow forces from the ECM, which, as detailed above, would lead to an increase in actin flow rate. Further to this, and indeed more directly providing evidence of the applicability of the clutch model to this system, is the effect of VD1. Upon its inclusion the viscosity-dependent differences in the actin flow were again seen to be removed. However, in contrast to the action of blebbistatin, which directly affects actin flow, the VD1 protein inhibits the coupling of cytoskeletal forces to the ECM. In this way it may be argued that this is more direct evidence of the clutch model. Indeed, despite the localisation of the vinculin to the focal adhesions (Figure 5.7) this does not translate into slower actin flow (Figure 5.6). Previously, it has been determined that vinculin is vital for the coupling of the FAs to the actin flow (258), thus ‘engaging’ the clutch and linking the physical properties of the surface to the cytoskeleton. The observed FA properties are similar with and without VD1 on the surface, indicating that the availability of binding sites for vinculin is the same. As the tail domain is specific for F-actin (248), it is therefore apparent that the stabilisation of FAs that the vinculin provides (255, 256) is thus key in coupling the cytoskeleton to the surface. Thus the higher force loading rates induced by higher viscosity cannot be effectively linked without this stabilising force.

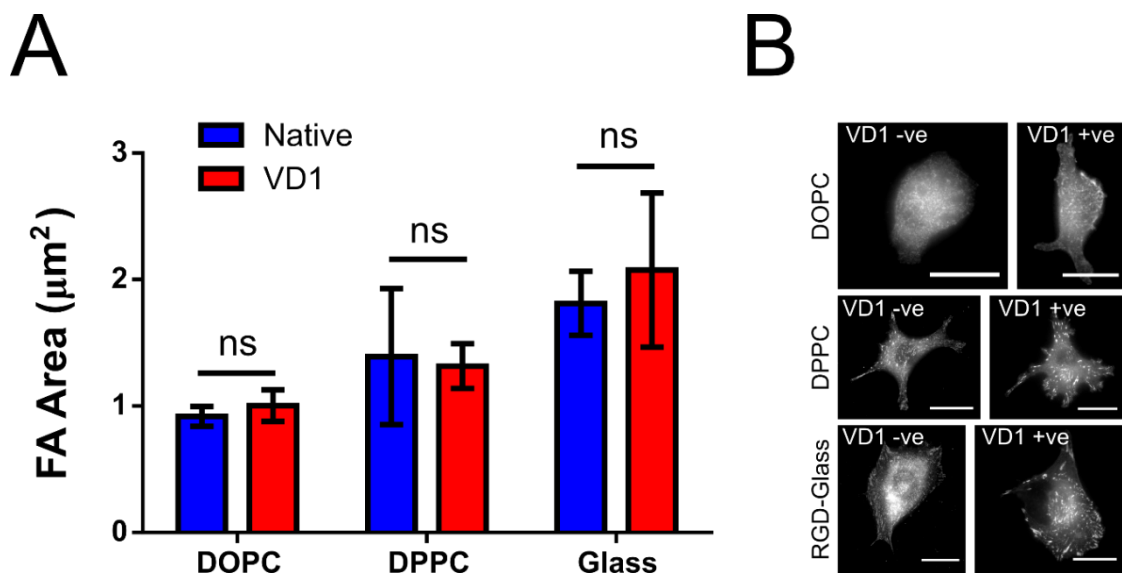


Figure 5.7. Focal Adhesion Properties upon VD1 Transfection. (A) Shows the quantified average FA area in cells (after 3 hrs, as in Chapter 4) on each of the surfaces in native, wild-type cells and those transfected with the VD1 plasmid; statistical analysis through two-way ANOVA showed that there was no difference in FA properties between native and VD1 cells on each surface. (B) Shows the representative images

used to determine the FA properties, with native cells (VD1 -ve) being stained with anti-vinculin monoclonal antibodies. The vinculin head domain encoded by the VD1 plasmid (VD1 +ve) is fluorescent and was not stained for vinculin. (Scale Bar = 25 μm). *P* values indicating significance, *ns* > 0.05.

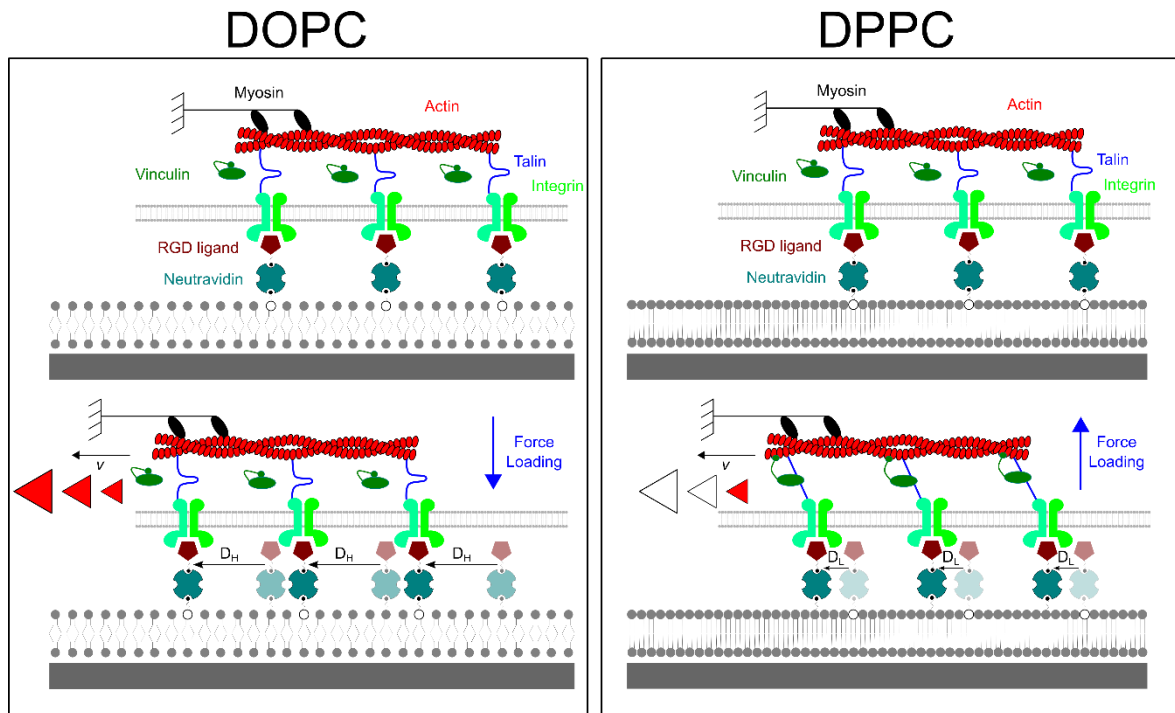


Figure 5.8. Schematic of Cell Behaviour in Response to Surface Viscosity. In DOPC, on the left, the pulling of actin on the RGD ligand through a talin-integrin linkage, displaces the ligand to a large extent, D_H , meaning that the force loading rate is low on molecules such as talin. Therefore, in the case of talin, this prevents, unfolding and so the binding of vinculin and formation of FAs. In DPPC, on the right, the higher viscosity means that ligand displacement is smaller, D_L , when actin pulls on the surface. This, in turn, means that the force loading rate on the talin is higher, allowing unfolding within the integrin-RGD bond lifetime. Vinculin can then bind to exposed sites, thus leading to greater forces exerted on the surface and FA formation.

5.2.3. CONFIRMING MODEL PREDICTIONS IN RESPONSE TO LIGAND DENSITY

As shown in Figure 5.2 the molecular clutch not only makes predictions about the response of the actin flow to viscosity, but also that of the nature of adhesion. Section 5.2.2 has shown that the actin flow behaviour fits with what is expected, through observation of the changes in actin flow upon by inhibition of key molecular components. Predictions regarding adhesion size can also be related to viscosity in a high and low viscosity regime i.e. DPPC (clutch is engaged) and DOPC (clutch is not engaged) respectively. Figure 5.9 shows the predicted behaviour of the adhesion size as the number of ligands are increased at a viscosity where effective coupling of the cytoskeleton to the ECM takes place, e.g. DPPC, (red) and where it is absent, e.g. DOPC (blue).

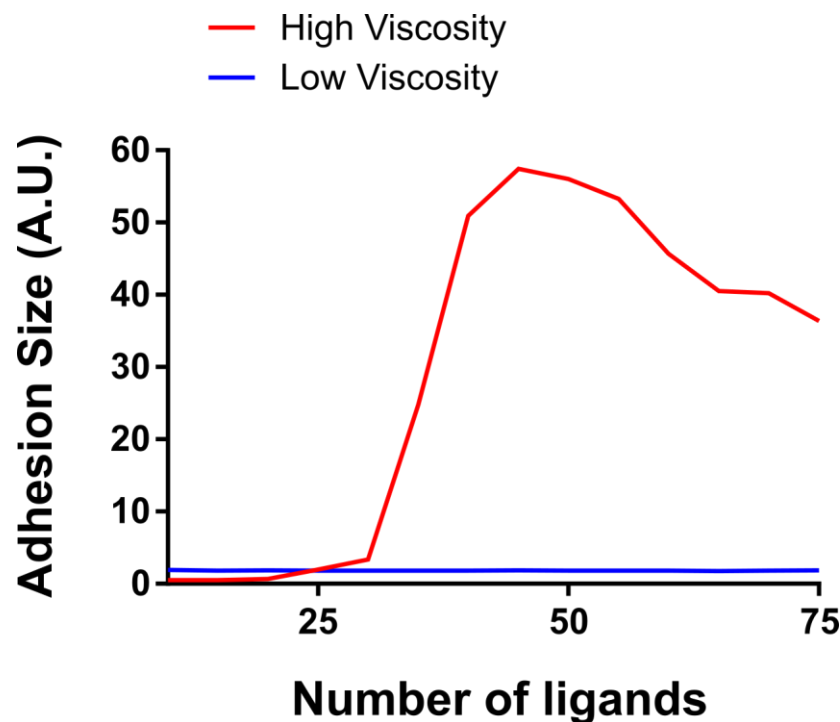


Figure 5.9. Model Prediction of Adhesion Size as Ligand Number Increases. By taking the model at viscosity values where the clutch is and is not ‘engaged’ the change in adhesion size can be predicted. At high viscosity (after engagement, 10^{-2} N.s/m) the number of ligands was seen to increase up to a specific ligand density (~50) and then decreases above this. At low viscosity (before engagement, 10^{-5} N.s/m) the adhesion size shows no change regardless of the number of ligands. Model data provided by Prof. Pere Roca-Cusachs of IBEC, Barcelona.

When considering the number of ligands in the framework of the model, this equates to the number of clutches considered in the system. In the case of the higher viscosity, where cells are capable of exerting force on the surface, increasing the number of ligands increases adhesion size initially. This is due to further recruitment of integrins, induced by force loading (260). However, upon reaching a maximum adhesion size, this then reduces as the number of ligands increases further. This latter trend can be explained by the excessive loading of the integrin-ECM bonds, which, above this point cannot be compensated for by further adhesion growth (260). In the case of low viscosity, the number of ligands has no effect on the adhesion size. This is because the regardless of the degree of force loading the clutch cannot ‘engage’, thus preventing any sort of adhesion formation.

The predictions of these specific regimes are borne out by the results, as shown in Figure 5.10. By changing the ligand density on the SLBs by over 3 orders of magnitude there is a consequent effect on the cells, predominantly in terms of their FA area, but also in terms of their cell size, was analysed. Figures 5.10A and B show the representative image of actin and vinculin in cells on DOPC and DPPC respectively, as well as the distribution of FA area on their respective surfaces. Qualitatively, no actin fibres were seen in all but the cells seeded on the highest ligand density on DOPC. Despite some indications of actin fibre formation there appeared to be no significant differences in the distribution of FA area on DOPC. These characteristics were in contrast to DPPC, where all surfaces showed some degree of actin fibre formation. Furthermore, the FA distribution was significantly affected by the change in ligand density, with a greater proportion of FA having a larger area upon increasing the ligand density. Figure 5.10C shows a positive trend in cell area as ligand density increases on DPPC, but in DOPC significant differences were only seen on the highest ligand density. In terms of FA area (Figure 5.10D), the FA size does not change on DOPC as the ligand density increases; however, on DPPC the FA area was seen to increase as ligand density increased. The statistical differences shown for Figures 5.10C and D are shown in Table 5.1 and 5.2 respectively. These confirm the significance of the trends seen, with cell area seen to have increased significantly with increased viscosity at all ligand densities on DPPC vs. DOPC. However, only at 2 and 10 mol% was FA area larger on DPPC vs. DOPC. Comparing different ligand densities, on DOPC differences were seen between 10 mol% in cell area, but no differences in FA area. However,

on DPPC significant differences were seen in all cases in both cell area and FA area, except between 0.02 and 0.2 mol% in the latter.

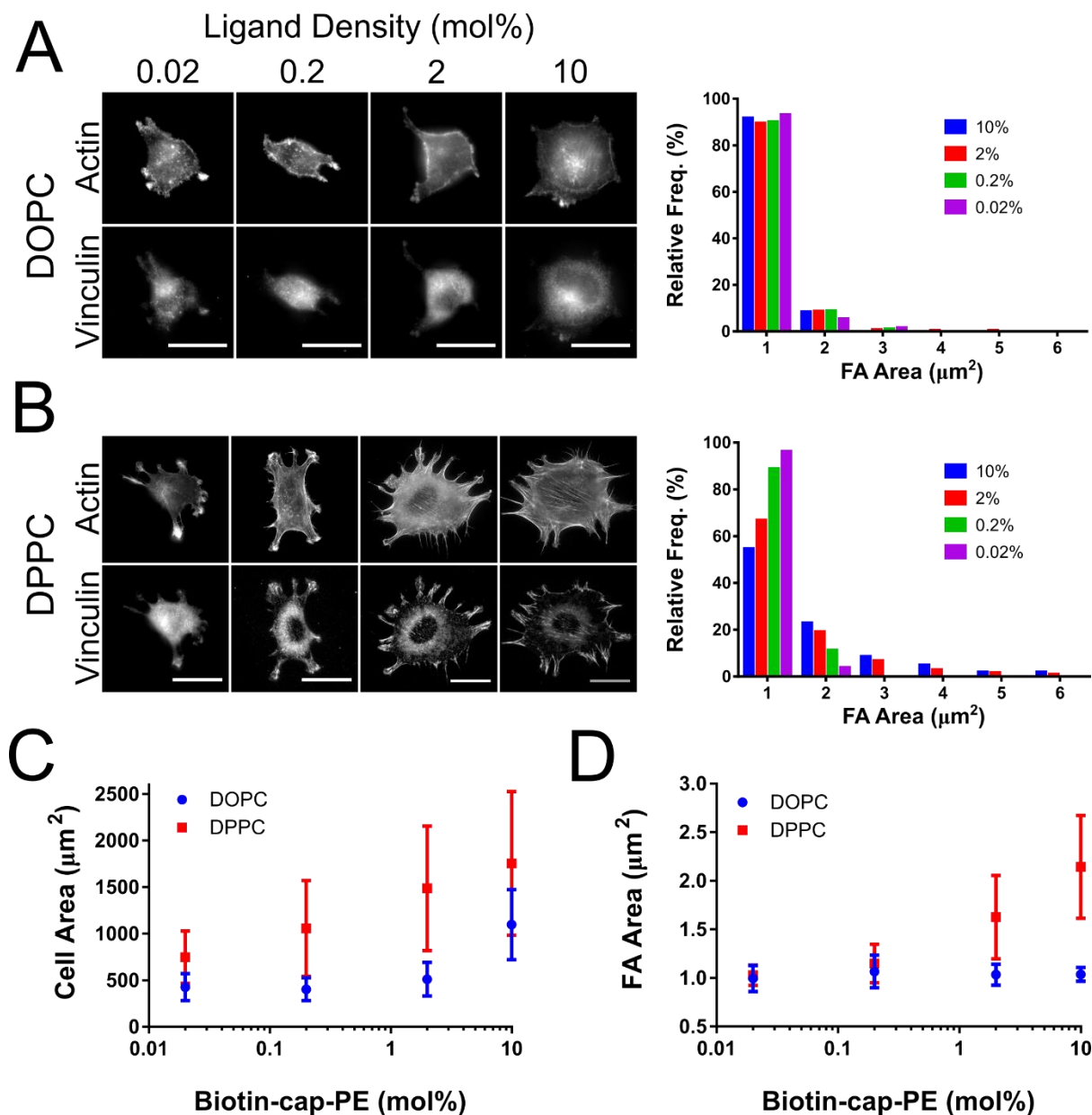


Figure 5.10. The Change in Cell and Focal Adhesion Size with Ligand Density. (A) Shows the representative images of the actin and vinculin stains on DOPC at 0.02, 0.2, 2 and 10 mol% of functionalised lipid. The distribution of FA area on these surfaces is shown to the right of these images, demonstrating that this is similar on all surfaces. (B) Shows this on the DPPC, with the consequent change in the FA distribution as the ligand density changes. (C) Shows the change in average cell area on each SLB as the ligand density changes, and (D) shows the change in FA area under the same conditions. (Scale Bar = $25\mu\text{m}$).

DOPC vs. DPPC

<i>Ligand Density (mol%)</i>	<i>Cell Area</i>	<i>FA Area</i>
0.02	**	ns
0.2	****	ns
2	****	****
10	****	****

Table 5.1. Statistical values comparing the cell and FA area on each ligand density when comparing DOPC to DPPC. P values indicating significance, ns > 0.05, ** ≤ 0.01, **** ≤ 0.0001.

<i>Ligand Density (mol%)</i>	CELL AREA		FA AREA	
	<i>DOPC</i>	<i>DPPC</i>	<i>DOPC</i>	<i>DPPC</i>
0.02 vs. 0.2	ns	****	ns	ns
0.02 vs. 2	ns	****	ns	****
0.02 vs. 10	****	****	ns	****
0.2 vs. 2	ns	****	ns	****
0.2 vs. 10	****	****	ns	****
2 vs. 10	****	**	ns	****

Table 5.2. Statistical comparison between of the cell and FA area ligand density changes on each of the SLBs. P values indicating significance, ns > 0.05, ** ≤ 0.01, **** ≤ 0.0001.

The key message from the results shown in Figure 5.10 is that they support the model predictions shown in Figure 5.8. In the case of DOPC no increase in adhesion size is predicted; based upon the model the force loading rate is simply not high enough regardless of the number of clutches engaged (118, 260). Confirming this demonstrates the further applicability of the molecular clutch model to various aspects of the viscosity response. In contrast to DOPC, the response of FA area in cells on DPPC shows agreement with initial stages of the high viscosity

regime (i.e. 10 – 50 clutches). With no difference between 0.02 and 0.2 mol%, it is therefore likely that these may be associated the minimal change induced by lower amount of clutches. A ligand density of 0.02 mol% may also prevent significant FA formation due to the large inter-ligand spacing, which is estimated to be 129.1 nm, as extrapolated from the 12.9 nm inter-ligand distance observed for 2 mol% in Figure 3.10. Previous work has noted that formation of FAs cannot occur above a ligand spacing of greater than ~60 nm (42, 261). When increasing the ligand density from 0.2 to 2, and then 10 mol%, these densities allow for a greater magnitude of integrin recruitment in response to force, thus explaining the significant differences observed between these three densities. This is also seen to an extent in previous work on the clutch in response to ligand density (48); at specific density the adhesion size increases with increasing density. However, upon reaching a specific stiffness (as with viscosity, shown in Figure 5.9) the adhesions can no longer be reinforced, leading to reduction in adhesion size. While this reduction was not seen here, it may be that the viscosity is not of the right magnitude to see this behaviour. Further, it may also be that the possible clustering of ligands, allowed for in a 2D-fluid environment, may also have an effect.

It is also interesting to note that in the case of DOPC the cell spreading appears, at least partially, to be independent of FA area. This shows some agreement with previous work on ligand mobility (55). Here it was proposed that cell spreading occurs through both FA-dependent and FA-independent mechanisms; while showing that FAs consistently decrease in area with increasing ligand mobility, the cell area showed a biphasic response, first increasing then reducing. While a biphasic response was not seen in this work, the lack of difference in FA area would imply a means for FA-independent cell spreading in DOPC. This may be attributed to a greater number of ligands clustered within the cell area.

5.3. DOWNSTREAM EFFECTS OF LIGAND MOBILITY/SURFACE VISCOSITY

While it is clear from these results the molecular clutch explains the nature of the cell response, the applicability of this system in understanding and manipulating further cell behaviours must also be considered. Previously, it has been shown that the physical properties of the surface can affect various cell behaviours downstream of the initial cell adhesion processes. For

example, pathways associated with proteins, such as the Rac (119), extracellular related kinase (ERK1/2) (12) and rho kinase (ROCK) (32) are upregulated in response to greater stiffness. Further to this, the YAP/TAZ pathway has also been shown to be necessary to induce human mesenchymal stem cell (hMSC) differentiation in response to increasing substrate stiffness (21). Taking this a step further, differentiation is conclusively been shown to be highly dependent on the microenvironment. Of further specific interest to this work is also the observation that mobility of polymers can control differentiation (52). Therefore, this work requires an assessment as to how these mechanisms contribute to and define the nature of the downstream pathways.

5.3.1. VISCOSITY DEPENDENT YAP LOCALISATION

As mentioned previously, YAP is a mechanosensitive transcription factor that localises to the nucleus beyond a specific threshold stiffness (21, 47). As the nature of the cell's viscosity response has been determined above to be similar in mechanisms that of the stiffness response, it therefore would be expected that the localisation of YAP to the nucleus would also change based on the viscosity. Indeed, Figure 5.11 supports this hypothesis, with increased localisation of YAP seen upon increasing the viscosity of surface. YAP was seen to show almost no difference in the amount of the protein in the nucleus when compared to the cytoplasm, with that ratio increasing with cells on DPPC and then again on cells seeded on the RGD-glass control.

YAP is a key component of the Hippo signalling pathway, which regulates the processes of cellular proliferation, differentiation and homeostasis of tissues (262). Beyond this biochemical regulation of YAP, its localisation to nucleus, as well as that of other transcription factors, such as NKX-2.5 and RAR γ (263), has been observed in response to mechanical cues. This pathway is regulated by cell morphology and F-actin mediated phosphorylation (264). Separate from this, previous work has shown that YAP can also be regulated by the cell morphology and cytoskeleton through other pathways, but also by ECM stiffness and Rho activity (21). Specifically, YAP localisation to the nucleus is triggered by mechanical force, which stretches the nuclear pores, increasing molecular transport (265). Through either biochemical or mechanical cues, the consequent nuclear localisation upregulates genes targets relating to cell

proliferation, through co-activation of genes with TEAD proteins being the most widely studied mode of action (262).

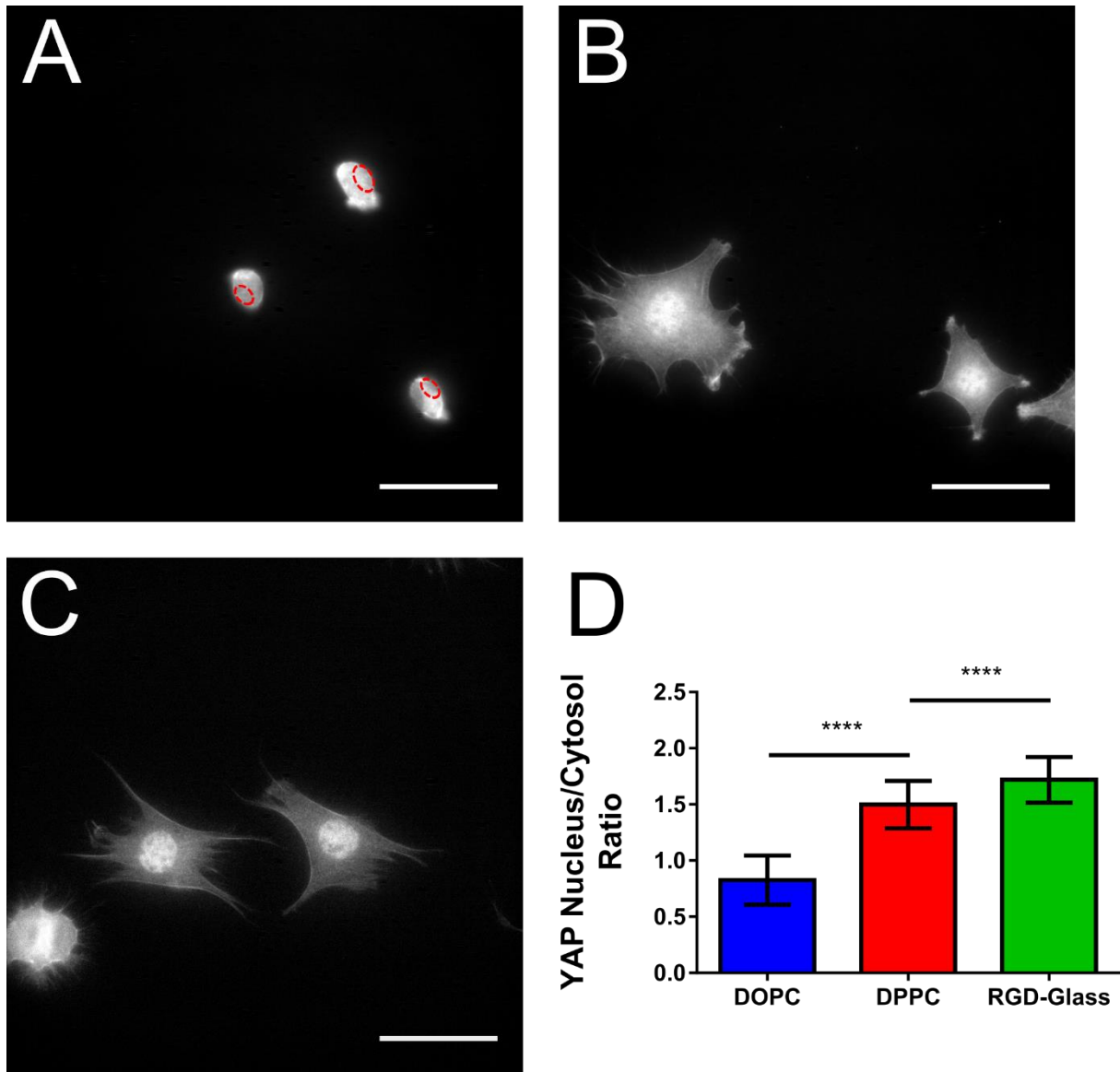


Figure 5.11. YAP Localisation in Response to Viscosity. (A) – (C) Show the representative images of the YAP staining, demonstrating the extent of its localisation to the nucleus on DOPC, DPPC and RGD-Glass respectively. For clarity, on DOPC (A) the location of the nuclei in each cell is indicated by the red-dashed circles. (D) Shows the attained fluorescent intensity in nucleus compared to the cytoplasm immediately surrounding it in all surfaces. (Scale Bar = 50 μ m). *P* values indicating significance, **** ≤ 0.0001 .

These properties, in conjunction with the findings shown in Figure 5.11, serve two key purposes: firstly, this further demonstrates that the sensing of the viscosity is mechanical in nature. This is through analogous responses in YAP localisation to the nucleus with increasing substrate stiffness, in previous work (47, 265), and on these viscous surfaces. What does remain unclear is whether it is the viscosity directly, or the difference in cell morphology and cytoskeletal tension induced by it that controls the YAP localisation. Unlike in previous work (21), the system as it stands is unable to separate the contributions of these two factors. Secondly, the localisation of YAP to the nucleus provides a link between the initial impact of the viscosity on adhesion and spreading, to the further downstream, biochemical changes in cell behaviour, such as upregulation of specific genes and differentiation. This is due to the identified, fundamental role of YAP in the lineage commitment of stem cells. For example, MSCs seeded on higher elastic stiffness will differentiate into osteoblasts, progenitors of bone cells. However, upon softer substrates they will differentiate down the neurogenic lineage (34). YAP was shown to be a key regulator of this process, as inhibition of YAP was capable of inducing commitment of MSCs to an adipogenic lineage, even upon a stiff surface (21). Furthermore, by inducing YAP localisation to the nucleus on soft surfaces it is also possible to inhibit the differentiation of human pluripotent stem cells (hPSCs) into motor neuron cells (266); a cell type known to be more strongly associated with softer surfaces (34). Consequently, these findings on YAP show that the ligand mobility changes, induced by viscosity changes, can not only control adhesion behaviours, but also changes downstream signalling pathways, leading to potential changes in cell behaviours.

5.3.2. CONTROLLING DIFFERENTIATION THROUGH VISCOSITY

In cells that are capable of differentiation, the changing of the local environment has effects, not only on the early stage behaviour of cells, but also of their lineage commitment. This chapter has equated the viscosity-defined ligand mobility to that of stiffness; due to changes in stiffness affecting differentiation, it also stands to reason that changes the viscosity will also elicit a change in the terminal differentiation of capable cell lines. To further test the potential applicability of the SLBs in manipulating cell behaviour, the differentiation of cells on these surfaces was therefore tested. As such the indicators of cellular differentiation of C2C12 myoblasts, the cell line used throughout this study, were used to determine the effect that viscosity has on the differentiation potential of these cells.

Figure 5.12 determines the effect of the viscosity-defined ligand mobility on differentiation by quantifying the change in markers of C2C12 differentiation. Initially, the percentage of cells staining positively for the transcription factor, myogenin, was observed (Figure 5.12A, C – left column). It was shown that upon decreasing viscosity the percentage of cells positive for myogenin was significantly reduced; indeed, DPPC compared with DOPC shows ~30% positive cells, compared with only ~10% positive cells, after 2 days. This trend is continued in terminal differentiation of C2C12s, with more cells staining positively for sarcomeric myosin upon reduced increased viscosity (Figure 5.12B, C – right column).

C2C12s are a mouse myoblast cell line, capable of differentiation, forming myotubes, precursors of skeletal muscle, during the process of myogenesis (267). Previously it has been found that C2C12s differentiate optimally on surfaces of tissue-like stiffness, with ~12 kPa reported as both the *in vivo* tissue stiffness and the optimal stiffness for myotube differentiation (268). While it has been widely accepted that many cell lines differentiate in response to stiffness (10, 34), this work shows specifically that C2C12s are sensitive to mechanical cues. Further, this chapter has thus far shown that the viscosity of the SLBs is detected as a mechanical cue.

The process of differentiation is associated with several transcription factors, such as MyoD, myogenin, Myf5, MRF4 (269) and, interestingly YAP (after 24 hrs) (270), with terminal differentiation being associated with a higher presence of sarcomeric myosin (268). The upregulation of myogenin after 2 days is in line with previous findings, which indicate an increase in myogenin related gene expression (269, 271). Further, sarcomeric myosin was seen to be more prevalent after 4 days on DPPC than DOPC, in line with timeframes used in previous work (56). Overall, these markers of differentiation indicate that the mechanical cues provided by the changes in viscosity-defined ligand mobility significantly affect cellular behaviour at numerous key stages. This presents the potential to use these systems in a more medically applicable system, such as modulating the fate of stem cell lines.

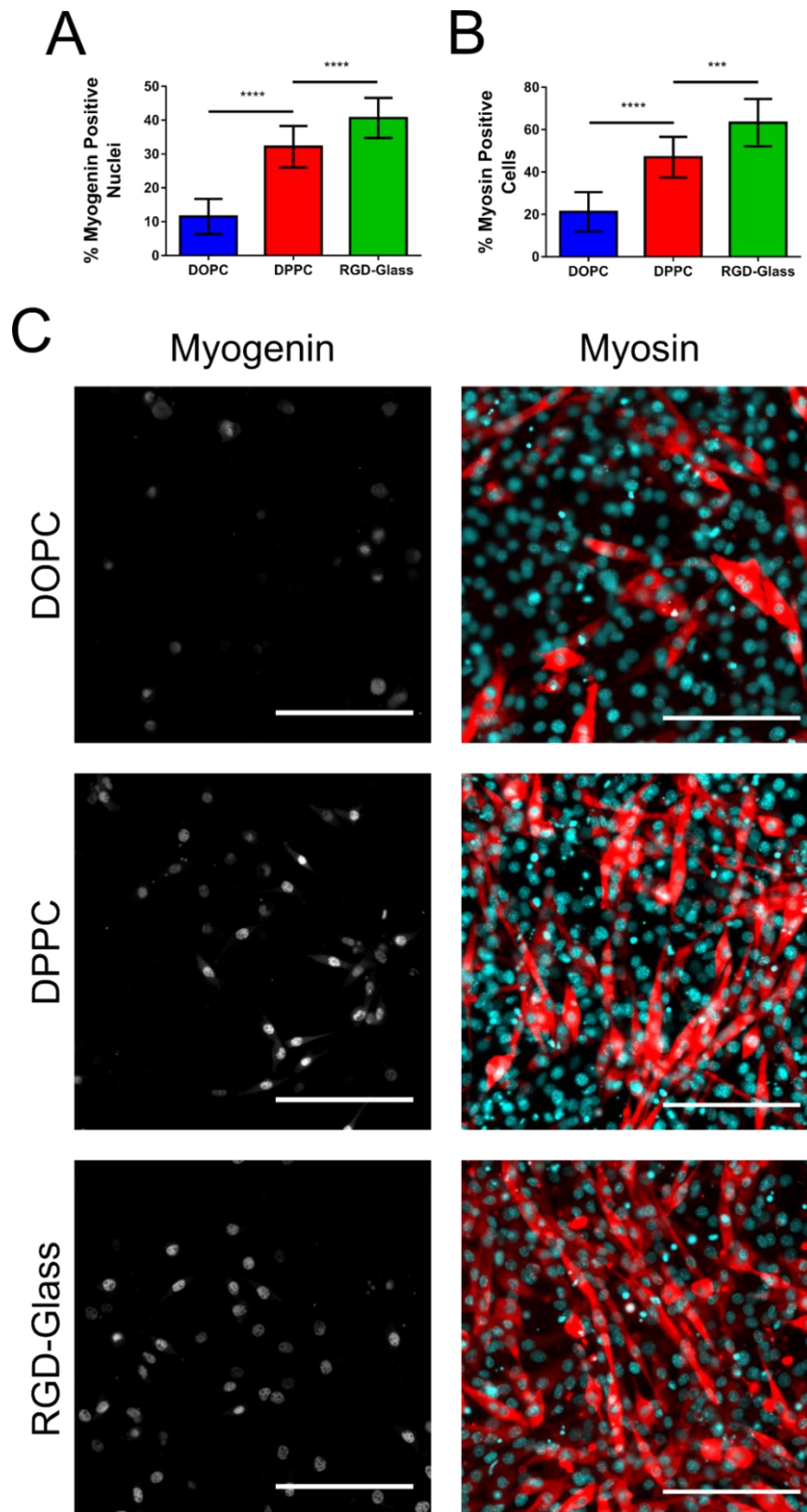


Figure 5.12. Viscosity Dependent Differentiation. (A) Shows the early stages of differentiation of C2C12s, after 2 days, on each of the surfaces through determining the percentage of nuclei

*staining positive for the transcription factor, myogenin. (B) Shows the terminal differentiation of C2C12s, after 4 days, by the percentage of nuclei within the sarcomeric positive cells. (C) Shows the representative images of stained cells at both of these time points. (Scale Bar = 150 μm). P values indicating significance, *** ≤ 0.001 , **** ≤ 0.0001 .*

5.4. CONCLUSIONS

This chapter has focused on the molecular basis for the trends seen in Chapter 4, with the main focus on if and how the response to the ligand mobility can be defined by an overarching molecular concept. By drawing parallels to stiffness, the molecular clutch that had so successfully been used to define the cell response to this physical property, has been used here to understand the concept of ligand mobility, by considering the viscosity of the surface. It was seen that the trend of the model predictions matched with the observed cell behaviour, with a change in actin flow behaviours and adhesion sizes successfully predicted. Furthermore, inhibition of these processes showed behaviour in line with effects predicted by the model. Despite the initial application of the SD equation estimating the viscosity as being significantly lower than required to engage the clutch, a more recent equation relating the diffusion and the viscosity provided more applicable values. In this instance it was considered likely that SD equation is no longer valid; this was due to the huge perturbation of the membrane, due to the binding of the cells. At this much larger length scales the SD equation has been widely noted to become invalid. An alternative equation compensated for this; by adjusting the variable of the characteristic length to the order of a cell radius the viscosity values reach good agreement with that of the model. From this it may be hypothesised that the viscosity of the membrane is significantly higher under the cell, which may be due to the binding of RGD ligands, rendering much the under-cell area significantly more viscous compared with the area outwith the cell.

Moving beyond understanding the nature of the initial cell response to viscosity, the consequential effect of these changes on further biochemical signalling and cell processes was also assessed. It has been shown here that increasing the viscosity, increases the localisation of YAP to the nucleus. As a protein previously associated with the stiffness response, the localisation of YAP further demonstrates the mechanosensitive nature of the response to viscosity and its associated ligand mobility; it also illuminates early downstream translation of

these physical cues into biochemical signals. Further consequential effects, in a medically relevant context, were observed with upregulation of C2C12 differentiation markers upon an increase in viscosity. This therefore implies a possible further avenue of driving the differentiation of cells through viscosity, which will be explored in greater depth in the next chapter.

6. SUPPORTED LIPID BILAYERS FOR MESENCHYMAL STEM CELL CULTURE

6.1. INTRODUCTION

The previous chapters have demonstrated that SLBs are a viable tool through which to understand the cell behaviour in response to viscosity. This can be explained through the molecular clutch model, which equates the viscosity of the surface to the force that cells can exert upon it. Furthermore, through manipulations of this viscosity, and thus the ligand mobility, the cell response can be modulated. This has also shown potential in medically applicable scenarios with higher ligand mobility preventing the differentiation, likely due to a reduced force on the surface.

Stem cells, specifically human mesenchymal stem cells (hMSCs), are of particular interest for investigating the future applicability of the SLB system. While in the cell niche, located in the bone marrow (272) hMSCs are capable of maintaining stemness. However, hMSCs are also capable of differentiating into a number of potential lineages; these include the osteogenic, adipogenic, neurogenic and chondrogenic lineages (273). Driving factors behind the maintenance of stemness or differentiation have been shown *in vitro* to include biochemical (274, 275) and physical factors (16, 34, 49). In the latter, physical properties, such as topography, stiffness and chemistry (10), have been shown to change hMSC phenotype (276). The nature of the cell interaction with the surface is of vital importance to this process (10); in the case of stiffness, surfaces with an elastic modulus characteristic of a specific tissue induced the production of the relevant markers e.g. neural tissue-like stiffness upregulated neural markers (34). It is proposed that the interaction of the cell with the surface, controlled through the adhesive machinery, upregulates vital signalling pathways, which, in turn, induce the processes relevant to external signals (10). SLBs, and the nature of cell's interaction with them, may therefore present a system that may provide a further means of controlling long-term cellular behaviour.

There has been a precedent set in previous work as to the influence of the ligand mobility on stem cell behaviour. Previously, ligand mobility has been shown to have an effect on various cell lines, promoting or preventing adhesion, and changing cellular properties (54, 57). Further, this has been shown to control the behaviour (53, 56) and lineage commitment of differentiation capable of cells (52, 59, 277). Indeed, lipid based systems have been used previously as a platform for these cells (278, 279) and to direct their differentiation (59, 280). In the case of Kocer et al., (2016) (59), however, their initial findings are not in agreement with the work presented in previous chapters; they show that there more spreading on DOPC compared to DPPC and that there is a greater degree of differentiation. This also does not align with other work in the field, which notes cells cannot exert forces on DOPC SLBs, thus remaining rounded (58, 77). This force is vital in regulating the differentiation of cells, with changes in it key to regulating the final lineage of the cell (32). It is therefore reasonable to assume that there is still much investigation needed in order to determine the effect of the viscosity-defined ligand mobility on the behaviour of hMSCs.

Therefore, hMSCs were used here as a proof-of-concept, ascertaining if the previous findings could be directly applied to manipulate the behaviour of differentiation capable cell lines, with a mind to produce a surface that has the potential to manipulate their lineage commitment. Initially, the behaviour of hMSCs on the RGD-presenting lipid bilayers were determined, in terms of adhesion, growth and viability. Further to this, the lack of growth of hMSCs and changes in their behaviour over time on these surfaces required further approaches to promote cell replication. This lead to the investigation of the effect of protein cross-linking and functionalisation of the surface, with a full fibronectin protein as well as a cell-binding fragment. A final strategy, the production of positively charged lipid bilayers, was also tested to determine if electrostatic attraction would allow for more effective cell adhesion and spreading, compared with the peptide/protein functionalised system.

6.2. ADHESION AND GROWTH OF MESENCHYMAL STEM CELLS ON RGD FUNCTIONALISED SUPPORTED LIPID BILAYERS

The previous chapters have demonstrated that SLBs are a suitable platform for cell culture, with a model cell line, both to assess the nature of the adhesions and their potential for use in directing differentiation. Developing this further, this system was applied to the more medically applicable hMSC cell line. It is widely accepted that these cells are capable of differentiating into various cell types, promoting the production of tissues such as cartilage and bone (281). Therefore, the applicability of SLBs to this new cell line was assessed, evaluating its potential for future work.

6.2.1. ADHESION OF MESENCHYMAL STEM CELLS

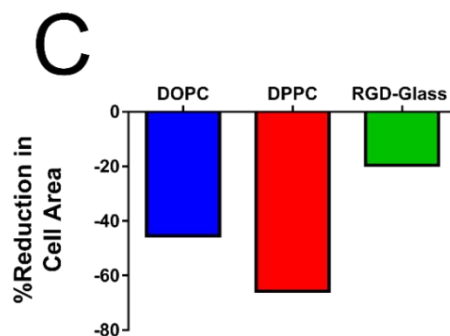
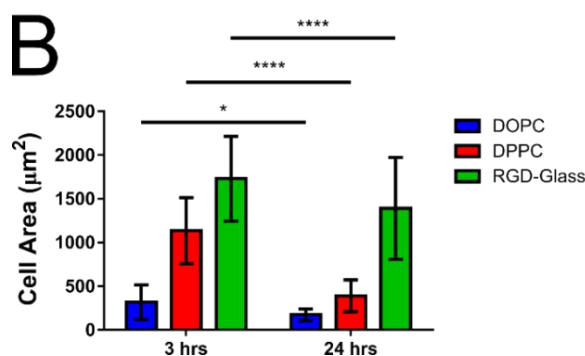
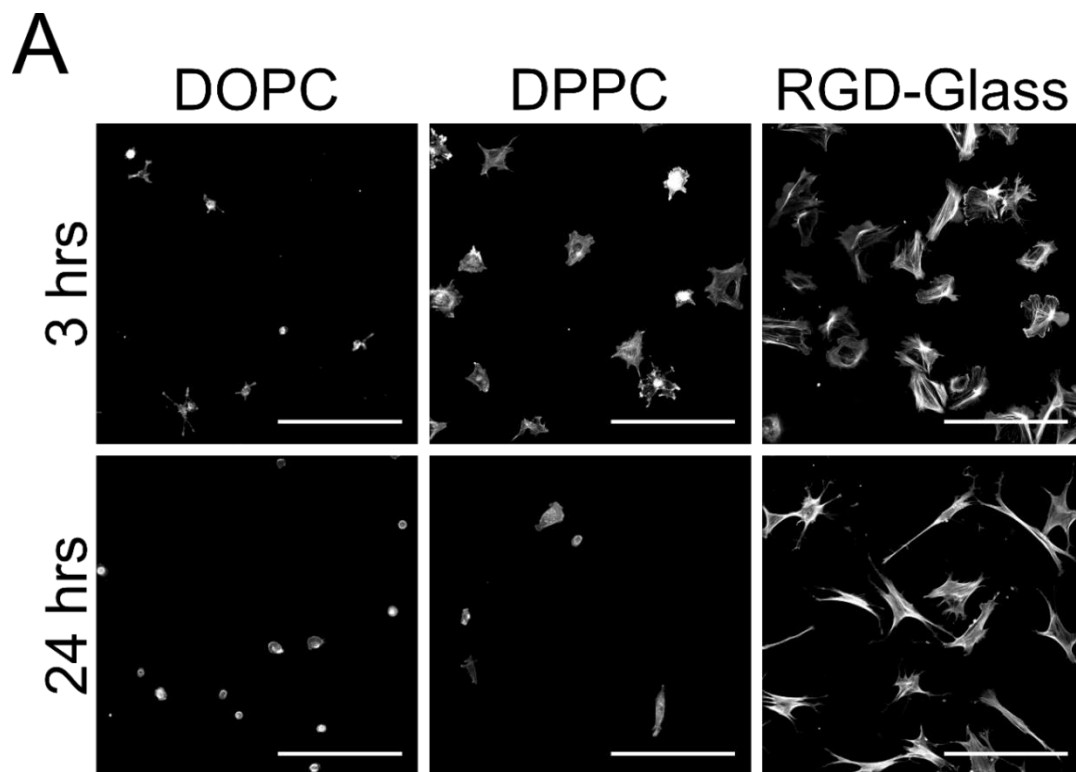


Figure 6.1. hMSC Adhesion of 3 and 24 Hours. (A) Shows the representative images the area of hMSCs on all surfaces, after 3 hrs and 24 hrs of cell culture (Scale Bar = 150 μm). (B) Shows the quantification, demonstrating that there is a reduction in cell area at 24 hrs compared to 3 hrs on all surfaces to differing degrees. (C) Shows the percentage reduction in cell area between 3 and 24 hrs, demonstrating that cells lose a large percentage of area on both DOPC and DPPC, with a smaller reduction on the RGD-Glass control. *P* values indicating significance, * ≤ 0.05 , **** ≤ 0.0001 .

For an initial study hMSCs were first seeded on SLBs used in the previous chapter and the glass control for 3 and 24 hrs. Initial analysis of the cell behaviour on surfaces is shown in Figure 6.1. This shows that in earlier adhesion time points the cells are less spread as the viscosity decreases (Figure 6.1A showing representative images and quantified in Figure 6.1B). However, after 24 hours the cells were shown to have a smaller average cell area in all cases. When determining the extent of the reduction in cell area the percentage of loss in cell area was quantified, showing that the reduction of the cell area on both DOPC and DPPC higher than that of the control. Further, cells on DPPC were seen to be particularly sensitive; initially noted to be well spread, with visible actin filaments, between 3 and 24 hrs over 60% of their total area lost. In addition to this reduction, the focal adhesion (FAs) were quantified at each time point, as shown in Figure 6.2. The representative images of the vinculin stains are shown in Figure 6.2A and show that the FAs on both DPPC and RGD-Glass are well defined at both 3 and 24 hr time points; this is in contrast to DOPC. The images shown in Figure 6.2A are representative of that seen in hMSCs present on the DOPC SLB, demonstrating a diffuse distribution of vinculin present throughout the cell at both time points.

Quantification of the FA area showed that the area of FAs on hMSCs increased at 3 hrs in line with increasing viscosity. However, this does not remain consistent at the 24 hr time point; in the case of DOPC and RGD-Glass the measured FAs were no different between 3 and 24 hrs. However, FAs on DPPC showed a significant decrease in the average FA area after 24 hrs, when compared with 3 hrs. However, quantification maybe limited here in the case of DOPC, due to the diffuse nature of the vinculin stain. While it would suggest that there is only a small difference in FAs between DOPC and DPPC, it is clear from the representative images that

FAs are not present in this system at either time point. While showing that there is a significant difference in FA characteristics of cells between DOPC and DPPC, it also demonstrates that there are some limitations to quantitative analysis in these two extreme cases of surface viscosity.

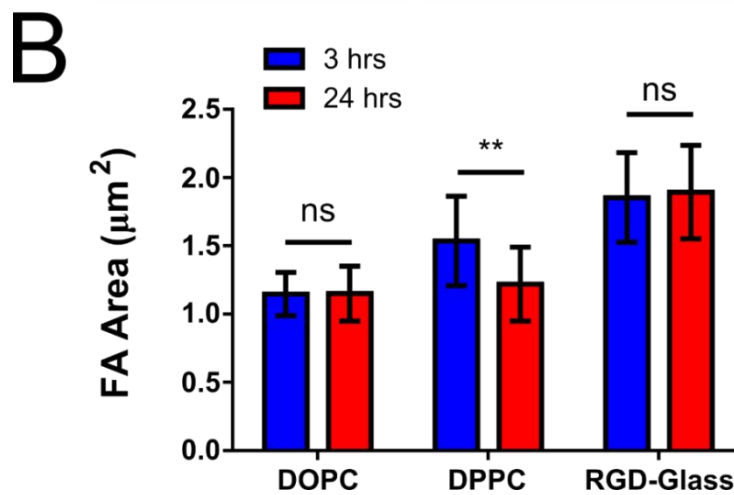
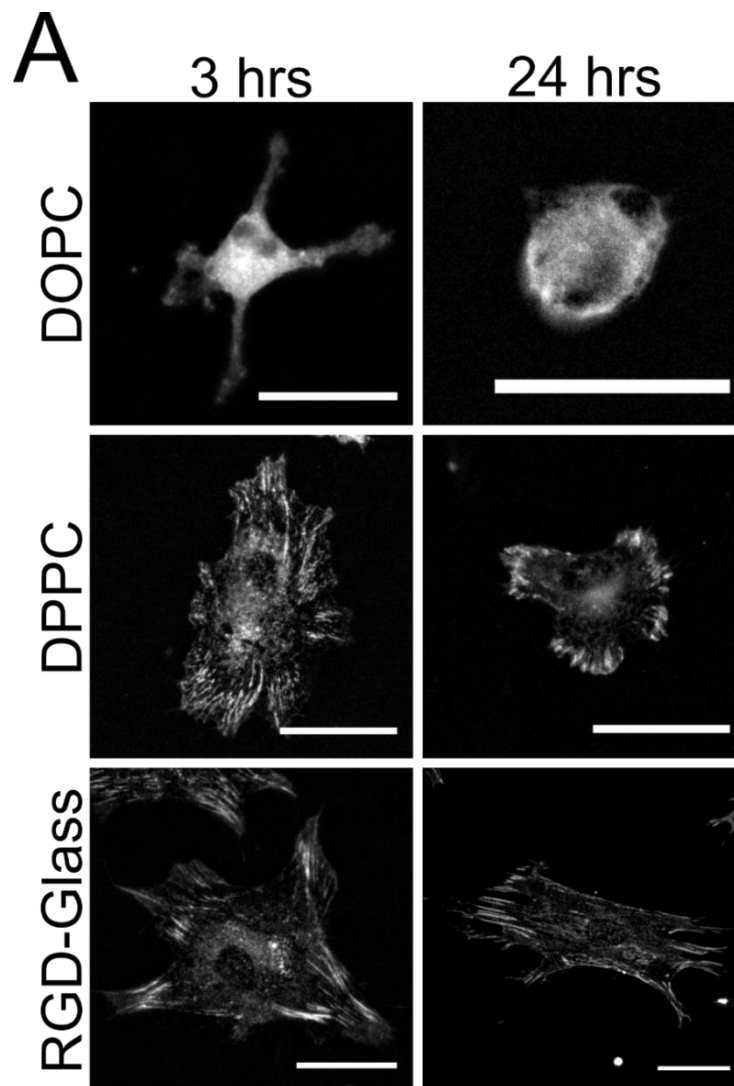


Figure 6.2. Focal Adhesion Area at 3 & 24 hrs on hMSCs. (A) Shows the representative images of FAs, as stained for by vinculin on hMSCs seeded on DOPC, DPPC and RGD-Glass surfaces after 3 and 24 hrs of adhesion, demonstrating both the lack of change in the FAs on DOPC and RGD-Glass, and the significant difference on DPPC (Scale Bar = 25 μ m). (B) Quantifies the area of the FAs over all surfaces and time points, showing that only DPPC has a significant difference in FA area between 3 and 24 hrs. *P* values indicating significance, *ns* > 0.05, ** \leq 0.01.

Considering the changes in overall cell and FA area between 3 and 24 hrs, a principle reason may be that a reduction in ligand density over time leads to the cells becoming rounded. This would likely be caused by the endocytic processes of the cells leading to bilayer breakdown. Indeed, it has been previously shown that the removal of traction forces on the surface leads to an upregulation of endocytic pathways (77). This previous work showed that over a 3 hr culture there was a co-localisation of clathrin machinery (associated with

endocytosis) and the RGD-neutravidin used to adhere the cells to the surface. As there is a reduction of FA size with decreased viscosity, it can also be surmised that there are less forces exerted on the surface (14), thus implying an activation of endocytic pathways. While this previous study used only DOPC, showing only two extreme cases (where there are and are not forces), it may also be possible that there is an interplay between these two pathways, rather than an all or nothing system. Further, it may be the case that with higher forces permitted in DPPC, at least in the short-term, it may be that the degree of endocytosis is reduced, therefore only causing a reduced cell area over a longer time frame (3-24 hrs). This work has shown in the previous chapter, in Figure 5.10, that cells are sensitive to ligand density on lipid bilayers, with lower densities leading to smaller cells, with smaller FAs. However, the question remains as to why this is not the case on C2C12s. While not directly assessed using an actin stain, Figure 5.12 shows, through the myosin stain that C2C12 cells remain spread. This may be due to an inherent difference in the cells ability to respond to the surface. Indeed, Figure 5.10 shows that the FA properties on DPPC and DOPC are similar at lower ligand densities, implying a similar response to the surface.

6.2.2. GROWTH OF MESENCHYMAL STEM CELLS

Observing this unexpected behaviour of MSCs on both the DOPC and DPPC bilayers, it was therefore necessary to determine what the implications of this would be. To this end the degree of growth of the cells on the lipid surfaces, as compared to the control was determined. Furthermore, this was extended to observing the behaviour of MSCs after 5 days, beyond the time point previously used with C2C12 differentiation. As the behaviour of the MSCs was so vastly different to that of C2C12s it was hypothesised that their behaviour on the SLBs would also be different after a number of days in culture.

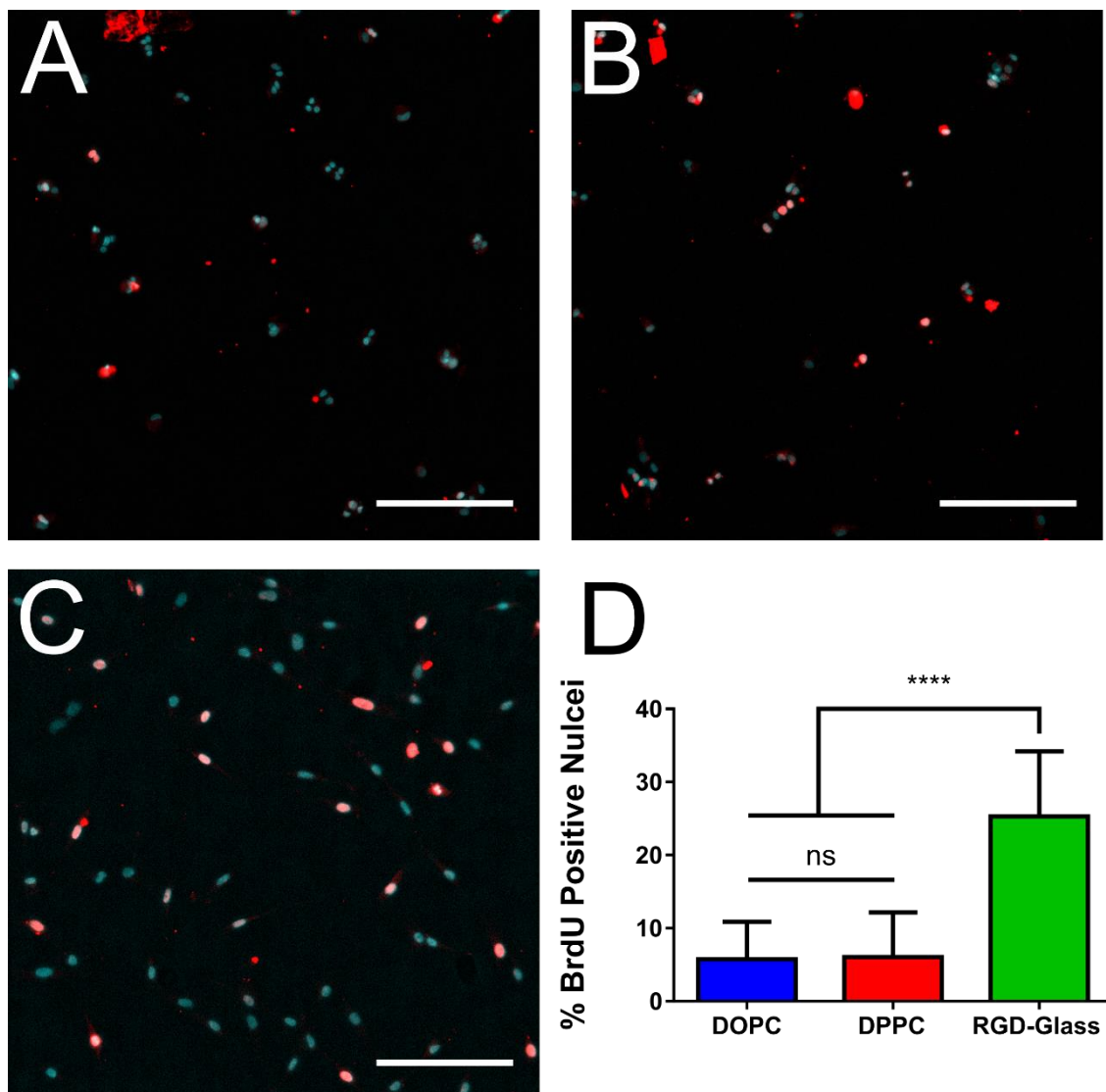


Figure 6.3. Proliferation of hMSCs on SLBs. (A) – (C) Show representative images of cells grown for 1 day on DOPC, DPPC and RGD-Glass respectively, with the nuclei shown in cyan and the BrdU shown in red. The nuclei where there was BrdU present were considered new cells (Scale Bar = 100 μ m). (D) Shows the resulting quantification of % of nuclei staining positively for BrdU, indicating that they are cells that have grown after seeding on the surface rather than in culture. *P* values indicating significance, *ns* > 0.05, **** \leq 0.0001.

In the first instance, analysis was performed as to what affect seeding the cells on the SLBs would have on cell growth. To this end, cells were cultured with BrdU (bromodeoxyuridine); this gives an indication as to extent of cell growth, by being incorporated into the DNA of dividing cells. After a specific time point, in this case 24 hours, the BrdU can then be stained for with anti-BrdU antibodies, fluorescently indicating which cells are new, compared to the originally cultured cells. To analyse this, the nuclei were also stained with DAPI and the number of nuclei staining positive for both DAPI and BrdU were considered to be new. The cell growth was considered to be percentage of new cells and is shown in Figure 6.3. In the case of both DOPC (Figure 6.3A) and DPPC (Figure 6.3B) there appeared to be minimal growth after 24 hrs, while cells on RGD-Glass showed a much higher degree of cell growth. This is confirmed upon quantification (Figure 6.3D); while cells on the RGD-Glass control are capable of growth, with 25% of new cells present after 24 hrs, there was almost no new cells present (~6%) on the both of the lipid bilayers, regardless of the viscosity.

Developing from the initial studies that showed hMSCs lost cell area and did not proliferate on the SLBs, the longer term implications for the cell viability and applicability of the current system was determined. Figure 6.4 shows the cells after 5 days of culture. Interestingly, cells on DOPC (Figure 6.4A) were well spread with defined actin filaments, similar to as previously seen with cells seeded on an RGD-Glass surface. In contrast, cells on DPPC (Figure 6.4B) maintained a similar morphology to that seen after 24 hrs, with minimal spreading and no defined actin stress fibres. Cells on the RGD-Glass were all noted to be highly confluent (Figure 6.4C), with well-defined actin fibres; however, due to their confluency it can only be assumed that they are well spread, in line with the previously observed cell area after 24 hrs. Figure 6.4D quantified the number of cells on each of the surfaces, giving a further indicator of cell growth. Confirming the results of Figure 6.3, the growth rate of cells was severely

diminished on SLBs in comparison to the RGD-Glass. With the dashed line indicating the seeding density of 2,000 cells per cm^2 there is an approximately 2-fold increase in the number of cells present after 5 days in growth media on the SLBs. However, on the RGD-Glass control there is an approximately 7.5-fold increase in the cell density.

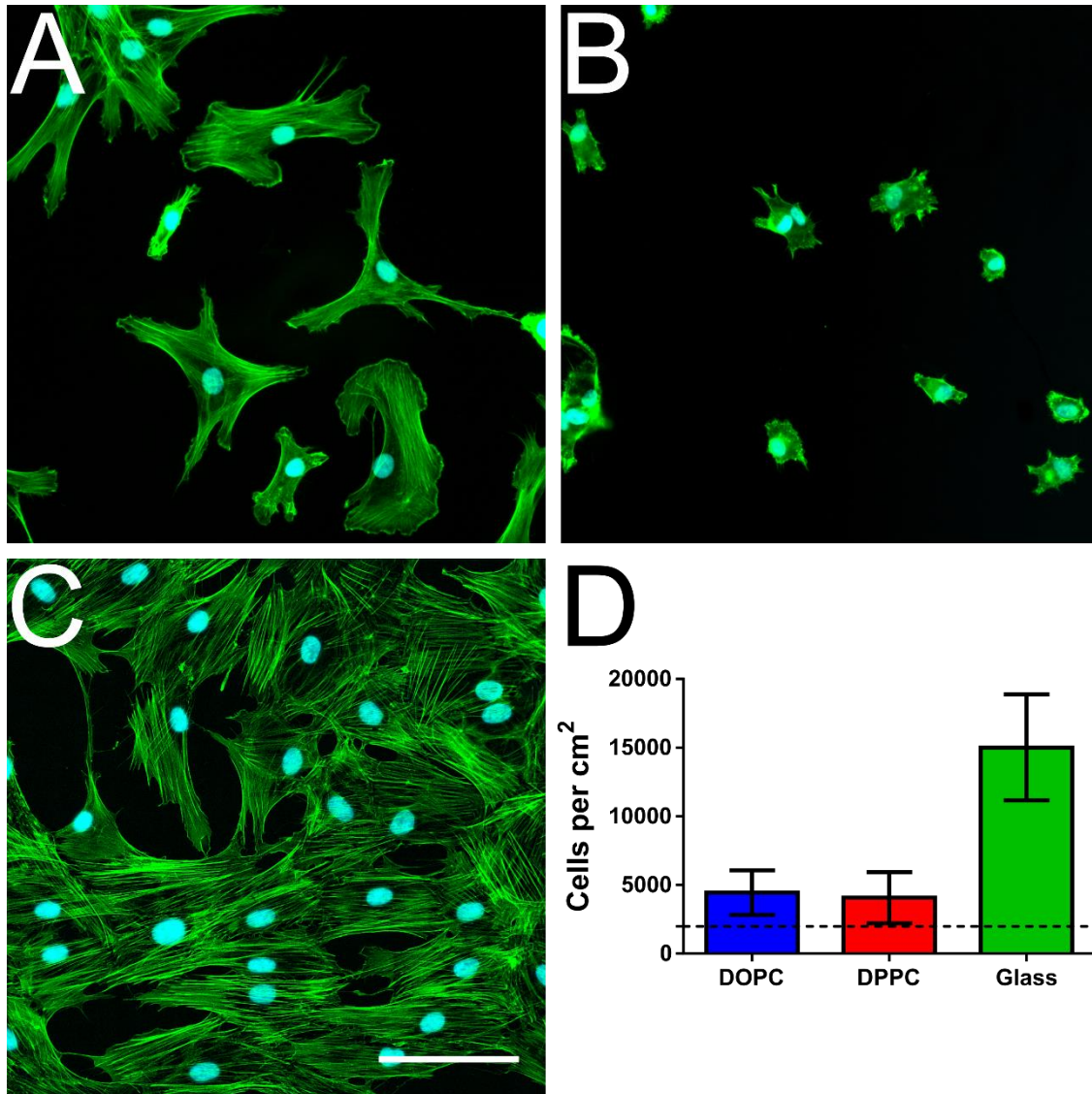


Figure 6.4. Cell Morphology after 5 Days. (A)–(C) Show hMSCs on DOPC, DPPC and RGD-Glass respectively after 5 days of culture in growth media. The dashed line represents the estimated seeding density. It is noted that the cells on DOPC exhibited a more spread morphology than previously seen, whereas cells on DPPC appeared rounded as noted after 24 hrs of culture. (Green = actin, cyan = nuclei, scale bar = 50 μm). (D) Shows the cell number

after 5 days, confirming results shown in Figure 6.3 that shows minimal cell growth on bilayers.

The lack of observed growth on the surface may stem from the previously hypothesised reduction in the number of available ligands. While the consequences of this assumed loss in the short term are a reduction in the overall area of both the cell and the FAs, it would be reasonable to assume that the replication of cells is also affected by this. In a simple sense, it may be that the reduction in the number of available ligands prevents the attachment of further cells on the surface. Therefore, the cells may indeed be undergoing the replication process, but the new cells are not viable due to an inability to bind. This uptake of the SLB components would also explain the behaviour of cells on the DOPC SLB after 5 days. It would appear in this case that the SLB has been broken down and the cells are able to spread on the glass surface. While previous work showed that the cells do not endocytose that to which they cannot bind (77), it may be that some of the bilayer is endocytosed with the ligands; eventually this would lead to defects in the bilayer, presenting the cells with a less mobile surface upon which to spread. As to why this is not seen on DPPC, it may be due to two possible reasons a) the DPPC SLB is somewhat more stable as it is in the gel-phase; indeed, Figure 3.11 showed that a DPPC SLB persists longer than and DOPC SLB; b) the rate of endocytosis is slower in DPPC, due to higher force as discussed in section 6.2.1.

The cell spreading behaviour on DOPC and DPPC after 5 days aligns with work by Kocer et., al (2015), where they noted that cells spread better on DOPC compared to DPPC. However, they noted this from the initial adhesion, which has not been seen here. While their conclusion that a more mobile surface allows for more adhesions, through ligand clustering, and thus a greater spreading is a sensible one, this does not align with the observations made both in this work and in similar work carried out previously; mechanical force is increased on the reduction or limitation of ligand mobility on the SLBs (58, 77, 282). The contrast in hMSC behaviour in the Kocer system, when compared to the current system, may be attributed to defects in the DOPC SLBs allowing the MSCs to spread compared to DPPC. Indeed, they observe cells after 2 weeks of culture on these surfaces, which, it may be assumed, would no longer present a SLB surface upon which to bind. As the current results align well with both various works and the

overarching theory it is likely that, both initial response of hMSCs here and their subsequent behaviour after 5 days is the more likely representation of the cell behaviour.

6.3. SYSTEM DEVELOPMENT

From the above results it is apparent that, while C2C12s are capable of maintaining their viability long enough to promote differentiation, this is not the case with MSCs. It is clear that the viability of the MSCs on both SLBs is not appropriate for more in-depth analysis of the long term potential of SLBs in these systems. Furthermore, there some kind of a change in the DPPC system, occurring between 3 and 24 hours that leads to a decrease in the cell area. Several properties of the SLBs are proposed as causes for this. Firstly, the viscosity; different cells respond differently to physical cues (34, 85), therefore it may be that MSCs are responding differently here. Secondly, the non-fouling nature of the SLBs may also play a role. It is widely accepted that, on surfaces, cells lay down their own matrix (228); however, SLBs would not allow non-specific protein binding, thus preventing this from occurring. Taking into account the dynamic nature of the cell-surface interaction, the presentation of only RGD on the surface would prevent the interaction of any further proteins with the surface. To this end, these SLBs and the presented ligands have been manipulated in an effort to determine what kind of effect on cells these properties have.

6.3.1. PRESENTING PROTEINS AND PROTEIN FRAGMENTS

The initial approach here was to maintain the SLBs composition and manipulate the ligands presented on the surface. To this end the FNIII₇₋₁₀ fragment of FN and the full FN protein were biotinylated to observe the effect that this would have. It was hypothesised that the presence of larger peptide constructs would enhance cell-binding through the presence of further binding domains (e.g. PHRSN synergy site), as well as FN-FN interactions (in the full protein only) allowing for the deposition of further matrix proteins. The initial steps in this process is shown in Figure 6.6; initially, the possible number of binding sites for the biotin molecule, which was conjugated to an NHS-ester group for binding to primary amines, was determined. Figure 6.6A shows the number of primary amine-presenting lysine amino acids present in both the full FN and the fragment, as indicated by the stars. Despite 78 lysine molecules present in the FN and 7 present in the fragment, only 6 biotins were determined to bind to FN and 1 to the fragment.

*molecule was calculated to be approximately 1 for the FNIII₇₋₁₀ fragment and ~6 for full fibronectin. (B) & (C) Show the effect of biotinylation of protein on C2C12 cells by determining the cell area and focal adhesion area respectively. In all cases cells were more spread and had larger focal adhesions on the proteins (coated on glass surfaces) compared to plain glass. In the case of FAs there was no difference between the areas on all proteins. (D) Shows the representative images of cells on each surface. P values indicating significance, ns > 0.05, ** ≤ 0.01, **** ≤ 0.0001.*

After biotinylation, activity of both the protein and the fragment were determined using the model C2C12 cell line. By depositing equal concentrations of the molecules on glass in depleted media (no FBS), the cell response indicated that all the proteins exhibited similar properties. The cell area on all protein-adsorbed surfaces was increased, relative to glass, with biotinylated FNIII₇₋₁₀ showing the largest area. When considering FAs, the similarities between all the protein-adsorbed surfaces was more pronounced, with no differences noted between the FAs on the native and biotinylated proteins. Further, the presence of proteins on the surface increased the FA area, compared to that seen on glass. Biotinylated proteins were then adsorbed on to neutravidin presenting DOPC and DPPC to determine the relative abundance of the protein on the surface (Figure 6.7). As expected this was seen to be similar on both surfaces, regardless of viscosity. Interestingly, despite the increase number of biotin molecules present on fibronectin, compared to the fragment, there was also no difference noted between the relative abundance of either of these proteins. Therefore, the ligand density on the SLBs is likely to be the key factor in determining the amount of protein bound.

After confirming both that the protein is active and present in similar concentrations, hMSCs were bound to the surfaces to determine the cell area after 24 hrs (Figure 6.8). It is clear from these results that the inclusion of these protein moieties has had no effect on the response of the cells to the surfaces after 24 hrs. In all cases cells on DPPC were once again noted to have a small and rounded area, with the average cell area being statistically comparable between all the surfaces, regardless of functionalisation. Interestingly, the FN fragment presented on DOPC was not capable of binding any cells.

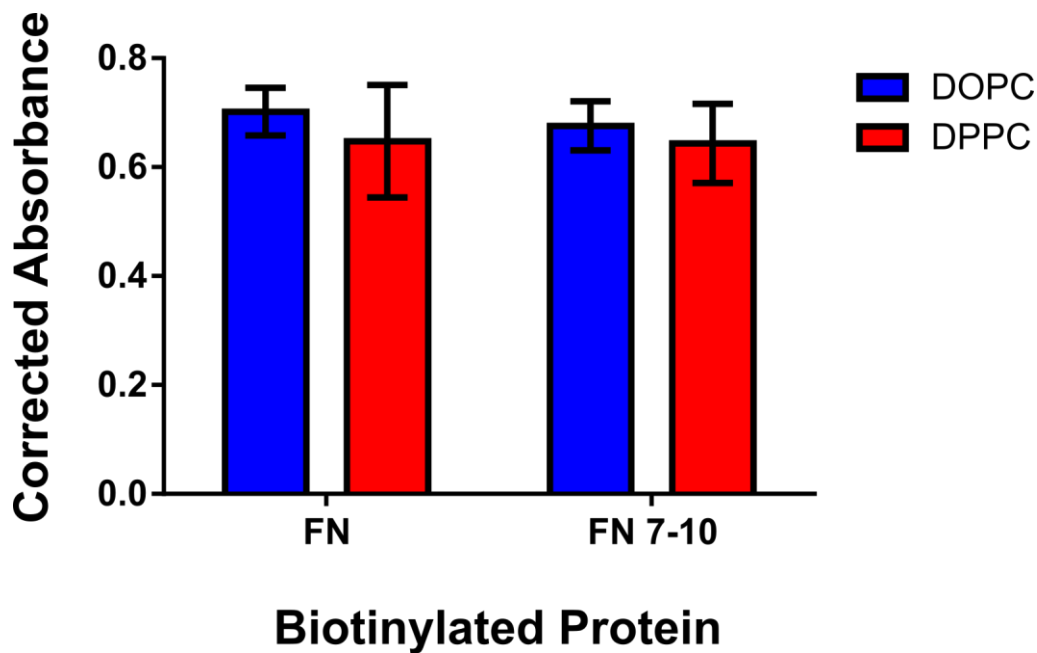


Figure 6.7. Protein on SLBs. An ELISA showing the relative amount of biotinylated protein adsorbed onto the DOPC (blue) and DPPC (red) surfaces. In all cases there was no significant differences in adsorption regardless of the SLB or the protein used.

What is clear from these results is that while the changing the functionality of the SLBs is methodologically simple the use of SLBs as a longer term platform for cell culture requires a different approach than the presentation of various ligands. Previously, it has been shown that the manipulating the viscosity of a SLB can induce the conversion of adsorbed G-actin to filamentous F-actin (283). However, whether or not this also occurs with FN here does not appear to not affect the longer term cell response. Previous work has noted that the endocytosis of proteins on the surface is performed via clathrin-mediated mechanisms (77). This is specific to cell-binding areas of the SLB, with non-functionalised moieties not being endocytosed. Furthermore, clathrin-mediated endocytosis has been observed to occur with particles of up to 200 nm (284), much larger than the 10s of nm size for the full FN protein. Due to this, it is likely that the inclusion of protein does not compensate for this. Originally, it was hoped that the viscosity of the SLBs may also encourage the formation of FN fibrils, which could allow for the deposition of further proteins. However, if the binding points of these networks, i.e. the neutravidin-biotin protein, was endocytosed there would be no further nucleation points for the

matrix proteins to bind, preventing this from occurring also. It is therefore clear from this that the initial model cell membrane requires further development to be applicable in longer term cultures.

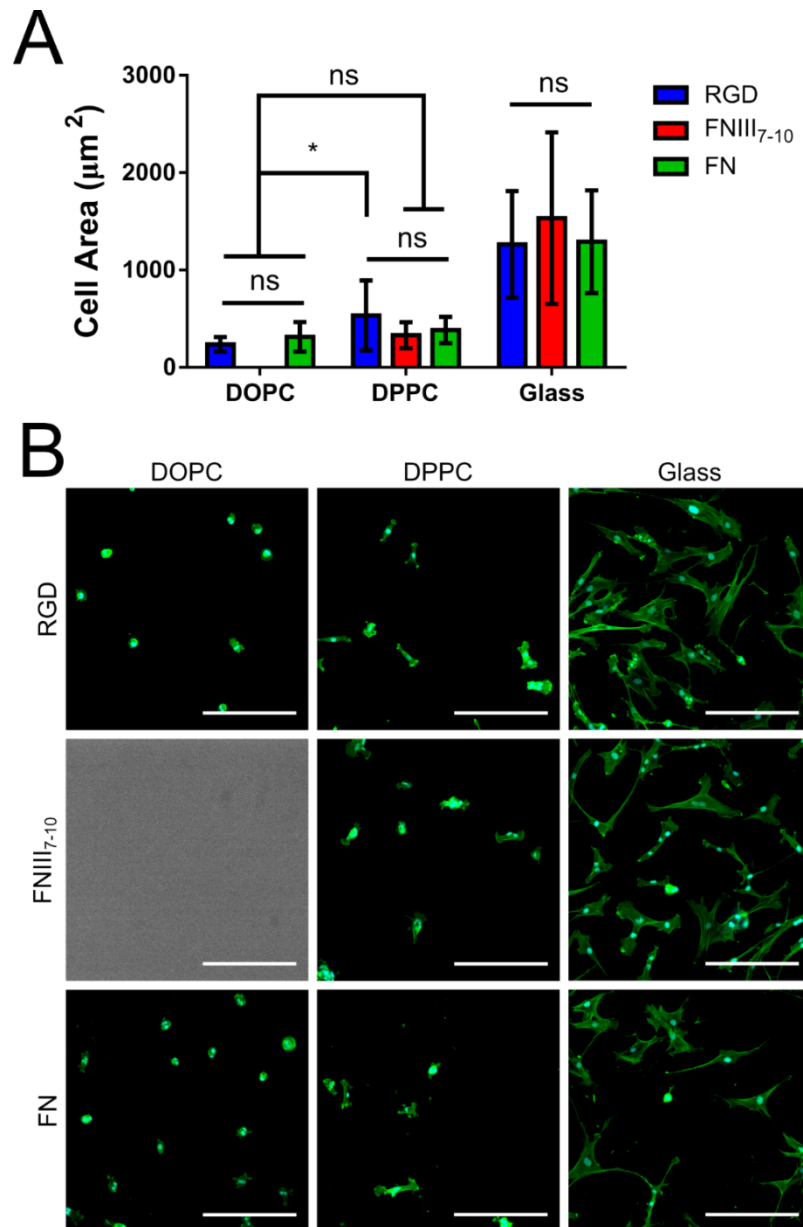


Figure 6.8. Protein Functionalised SLBs. (A) Shows the quantification of the cell area on DOPC, DPPC and glass, with the presentation of RGD peptide, FNIII₇₋₁₀ protein fragment, and FN full protein after 24 hrs. (B) Shows the representative images of cells on each of the surfaces (green = actin, nuclei = blue, Scale Bar = 150 µm). On DOPC functionalised with FNIII₇₋₁₀ no cells were noted to bind on any sample. P values indicating significance, ns > 0.05, * ≤ 0.05.

6.3.2. POSITIVELY CHARGED SUPPORTED LIPID BILAYERS

Electrostatic interactions are a key component of non-specific cell binding and so charged SLBs were used here to ascertain if they may compensate for the cell behaviours seen previously in this chapter. For example, proteins with a high isoelectric point (pI) will be positively charged at neutral pH, which can lead to unwanted interactions in protocols, such as immunostaining of cell proteins. This is due to the nature of the cell membrane, which, due to glycosylation of surface molecules, is considered to have an overall negative charge (285). A specific example is that of avidin, the full protein form of the neutravidin used throughout this thesis. Neutravidin (60 kDa) is a de-glycosylated form of avidin (67 kDa) and thus has a pI of 6.3, rather than the 10 found in avidin. This means that at physiological pH neutravidin is neutral, compared to the positive charge present on the avidin (164). Literature has determined that this positive charge can lead to increased non-specific binding, which was supported by findings here (Figure 6.9). This served as an initial test of the hypothesis that introducing positive charge into the bilayer could, firstly, allow for cell binding and, secondly, prevent the reduction in cell area that may be associated with the irreplaceable loss of ligand from the bilayer. Literature has previously asserted that this approach is applicable to neural cell culture (158), as the charge of a cell membrane is negative; however, this has not been applied to hMSC cultures.

After demonstrating that the model cells (C2C12s) could bind to a positive charge presented on the SLBs (Figure 6.9) a positively charged lipid (DOTAP, Figure 6.10A) was included in the liposome formulations at concentrations from 0 – 30 mol% of charged lipid. Figure 6.10B shows the difference in the hMSC cell adhesion as the amount of positively charged lipid increases between DOPC and DPPC, compared to a glass control. In contrast to the previous chapters, the control in this instance was plain glass, prepared in the same as the glass for SLBs. This was deemed to be more representative of this system, rather than glass presenting RGD ligands. On DOPC, the inclusion of positive charge did not appear to have a significant effect on cell adhesion, with minimal binding of cells on any of the DOPC surfaces after 3 hrs of cell culture. In contrast, upon inclusion of positively charged lipid with DPPC there was a significant increase in cell adhesion, comparable to that of the glass control. DPPC surfaces, without any DOTAP included showed the same extent of cell adhesion as that seen on all DOPC SLBs. Furthermore, fibronectin (FN) was also seeded on the lipid surfaces at 20 µg/ml

prior to cell culture, in order to ascertain if this would have an effect on the cellular properties. This concentration was taken from previous work with polymers, which determined this as an ideal concentration for cellular studies (286, 287). However, Figure 6.10 shows that the inclusion of FN protein has no effect on the cell adsorption, either in the case of DOPC or DPPC, with the cell density seen to be statistically similar to that of the surfaces without fibronectin.

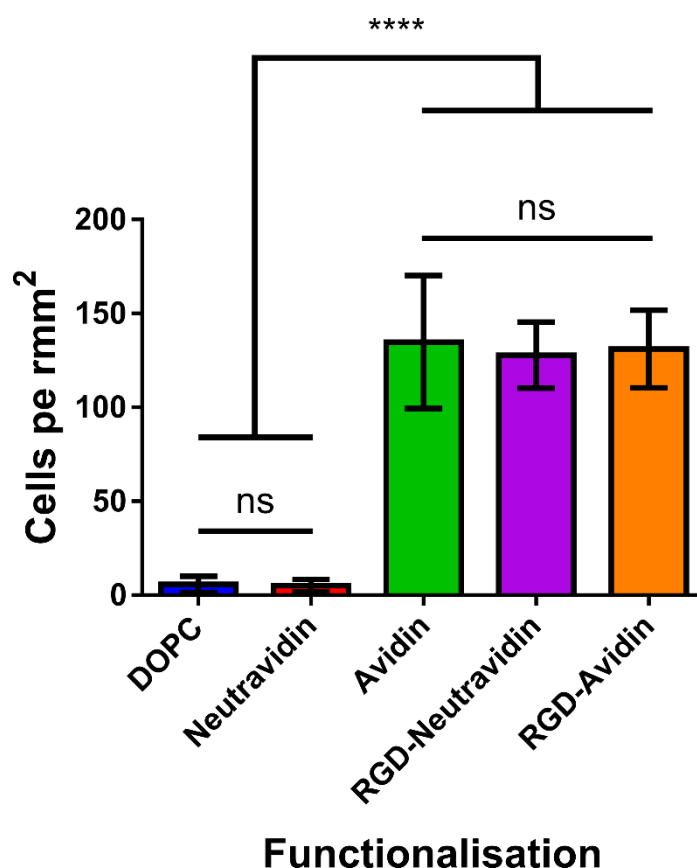


Figure 6.9. Non-specific Binding of C2C12s to SLBs. Using DOPC, this graph shows that the cells bind to avidin regardless of functionality. However, removing the deglycosylated form, neutraavidin, used throughout this thesis shows no binding without RGD present. P values indicating significance, ns > 0.05, **** ≤ 0.0001.

The primary reason for the inclusion of positive charge into the SLBs was so to prevent the loss of area that was seen in cell cultures presenting RGD ligands on non-fouling SLBs. While the lack of binding of cells to DOPC:DOTAP SLBs prevented an accurate assessment of this here, the effectiveness of DOTAP inclusion in DPPC was still able to be assessed. To this end

Figure 6.11 shows the area of hMSCs on DPPC:DOTAP (10 – 30 mol%) after 3 and 24 hrs, with and without the adsorption of FN prior to cell seeding. After being allowed to adhere and spread for 3 hrs the response to cells to FN on each of the surfaces is variable. In both the case of 10 and 30 mol% DOTAP there is a noted difference in cell area. In the latter the effect is as would be expected with FN ((+) FN) inducing an increase in average cell area. However, unusually, in 10 mol% this leads to a decrease in average cell area. Addressing the cells after 24 hrs, any differences initially noted in the cell area, between (-) FN and (+) FN surfaces, were removed; all DPPC:DOTAP surfaces in this case were seen to have no significant differences between cell areas.

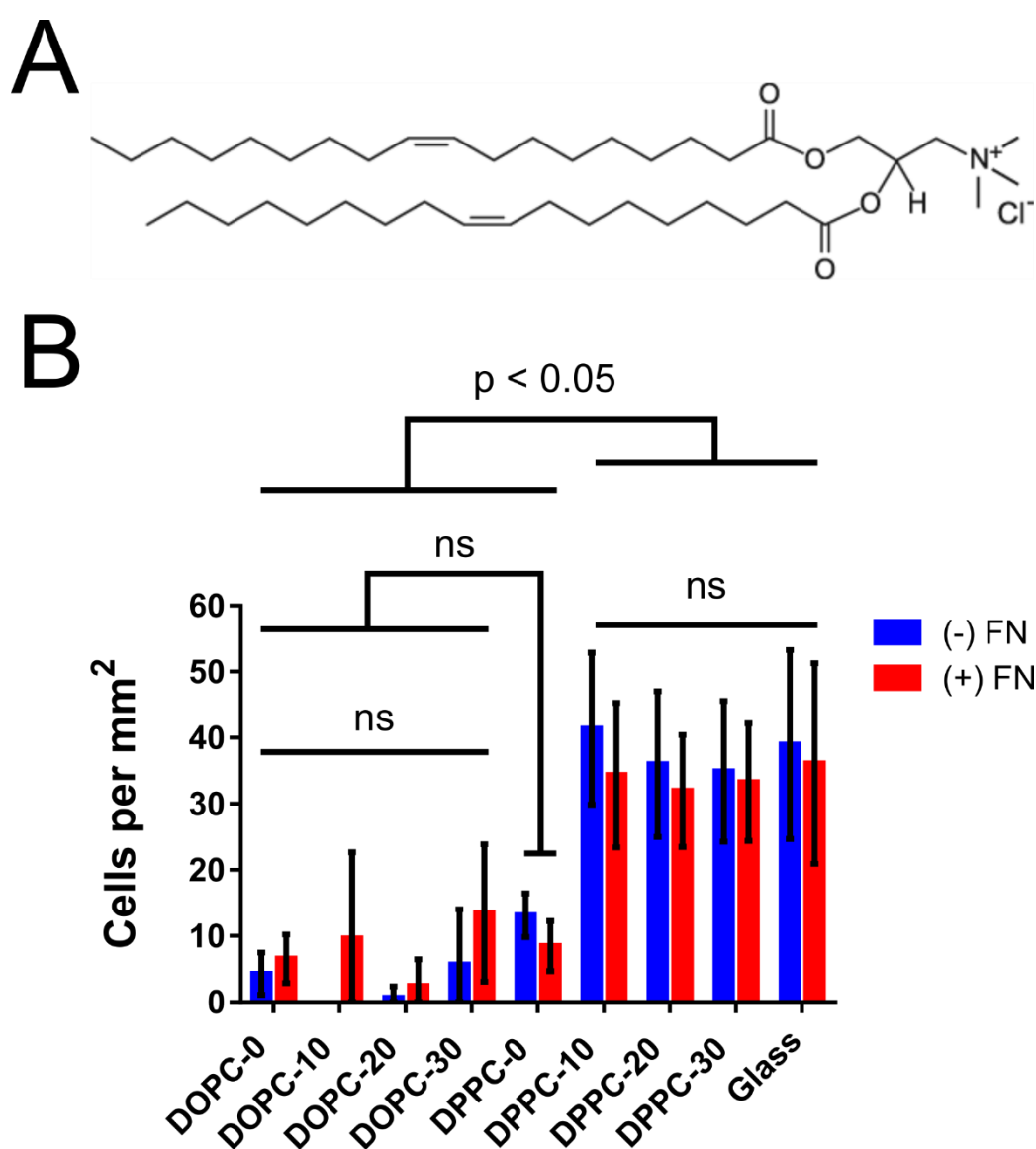


Figure 6.10. Adhesion to SLBs Containing Positively Charged Lipid. (A) Shows the structure of the DOTAP (1,2-dioleoyl-3-trimethylammonium-propane) molecule. (B) Shows the number

of hMSCs adhered per mm² as the mol% of the positively charged DOTAP is changed in both DOPC and DPPC (mol% of DOTAP is indicated by the number after the surface identifier). It also shows the cells adhered when fibronectin (FN) is allowed to adsorb on the surface prior to cell seeding (at 20 µg/ml). P values indicating significance, ns > 0.05.

Comparing the cell areas after 3 and 24 hrs directly allowed for the assessment of any changes in cell area, as shown in Figure 6.12. While there is not a consistent trend in the data shown, it does appear that the inclusion of DOTAP in the DPPC SLB prevents the loss of cell area, seen previously on RGD-containing SLBs. Further to this vinculin was used to determine the presence of any FAs present at both and 3 and 24 hours. Figure 6.13 shows the resulting quantification, demonstrating that there was minimal difference in the FA properties of the cells. This was shown to be true after both 3 and 24 hours as well as when comparing surfaces with and without FN. This is contrast to the glass controls, which show well-defined FAs present on all cells.

While it has previously been shown that positively charged bilayers can allow for the successful culture of neuronal cells (158) the results of culturing hMSCs on these SLBs is mixed. The results here demonstrate a series of cell responses that have both potential and require further study to confirm and optimise the system. Initially, cells were seen to not attach to the fluid phase DOPC no matter the charge, but did attach to all gel phase DPPC SLBs that contained DOTAP. This may be associated with the non-fouling nature of lipid bilayers, which has been variously attributed to both their fluid nature (162), and their overall lack of charge (288). As with much of science the answer is often a combinatorial one, rather than an either/or, which may explain the nature of the cell attachment seen here. While the inclusion of an overall positive charge in the DOPC SLB may attract the negatively charged cell membrane, this may be countered by the low viscosity of the DOPC SLB. However, this is not the case in DPPC; compared to the DOPC the diffusion of the lipid molecules within the SLB is significantly lower, which would not counter the electrostatic attraction between this and the cell membrane, thus allowing more cells to bind.

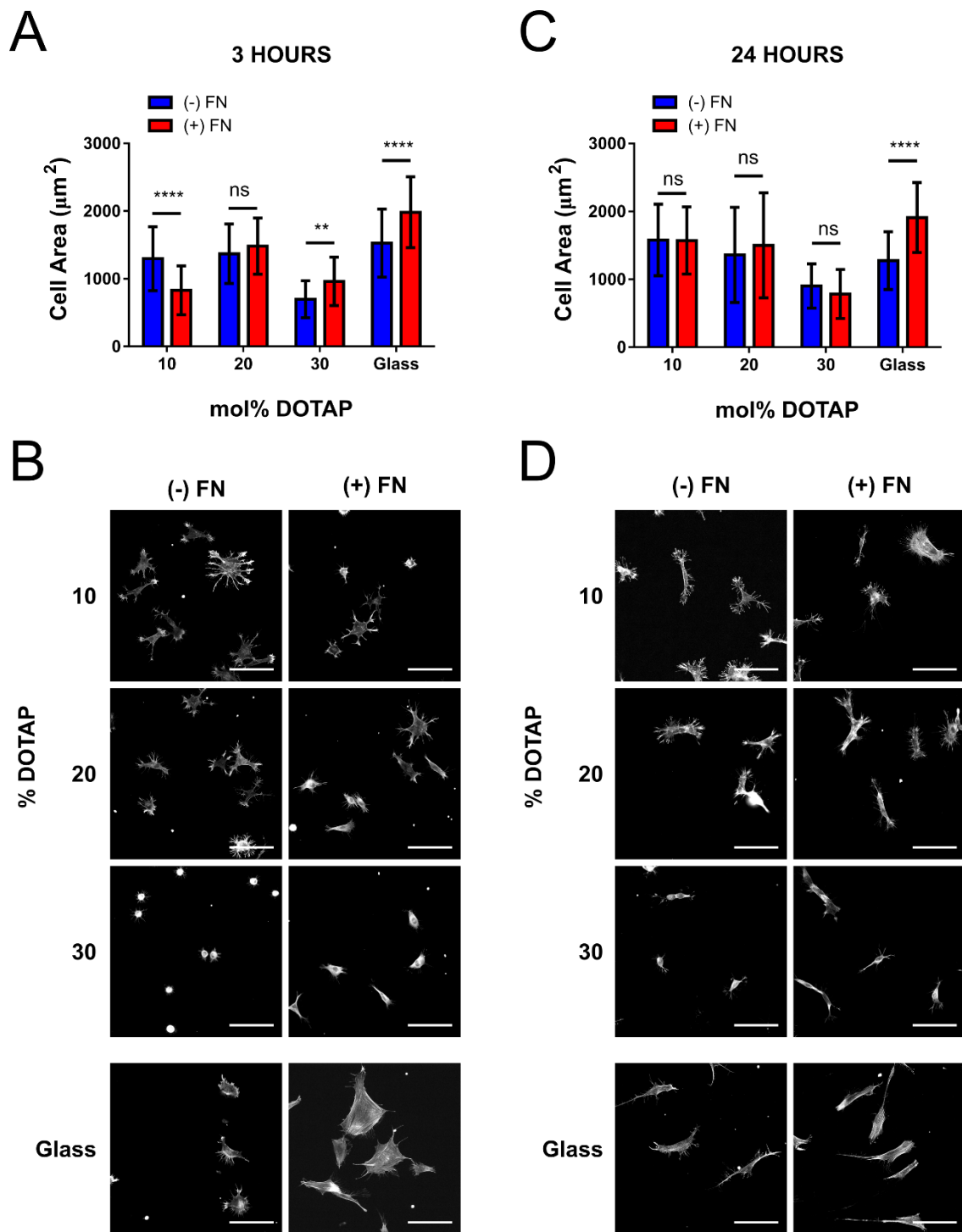


Figure 6.11. Cell Area on DPPC:DOTAP SLBs. (A) Shows the cell area of hMSCs after 3 hours on DPPC, with increasing mol% of DOTAP, with (B) showing the representative images of the surfaces. The effect of FN is also determined with incubation of 20 $\mu\text{g}/\text{ml}$ of FN protein prior to cell seeding. (C) Shows the cell area after cells were allowed to adhere and spread for 24 hrs, again with and without prior adsorption of FN. (D) Shows the representative cell images after 24 hours. In both cases

*FBS free media was used, to allow for direct comparison of cell behaviour over time, with and without matrix protein. P values indicating significance, ns > 0.05, ** ≤ 0.01, **** ≤ 0.0001.*

As only the DPPC SLBs were capable of binding cells to a great enough extent for further analysis, it was only on these surfaces upon which the spreading and FAs were analysed. The results from Figure 6.11 show that the inclusion of positive charge in the DPPC SLBs allows for a greater degree of cell spreading on 10 and 20 mol%, but that the cell area is reduced at 30 mol%. This provides support for the hypothesis of the interplay between the SLB viscosity and the charge of the surface; with DOTAP containing 2 unsaturated bonds, which would increase the fluidity, as with DOPC; therefore, the fluid nature of the DOTAP would disrupt the packing of DPPC, decreasing the viscosity. Thus, as with DOPC, the decreased viscosity counteracts the increased electrostatic interaction; in this case, however, the cell area is reduced, rather than no cell adhesion occurring. Despite these changes in cellular adhesion, Figures 6.11 and 6.12 demonstrate that the introduction of positive charge successfully prevents the reduction of cell area between 3 and 24 hours, as seen with the RGD-functionalised SLBs. This therefore demonstrates the potential of the inclusion of charge in the bilayers as a means through which to promote longer term cultures of hMSCs.

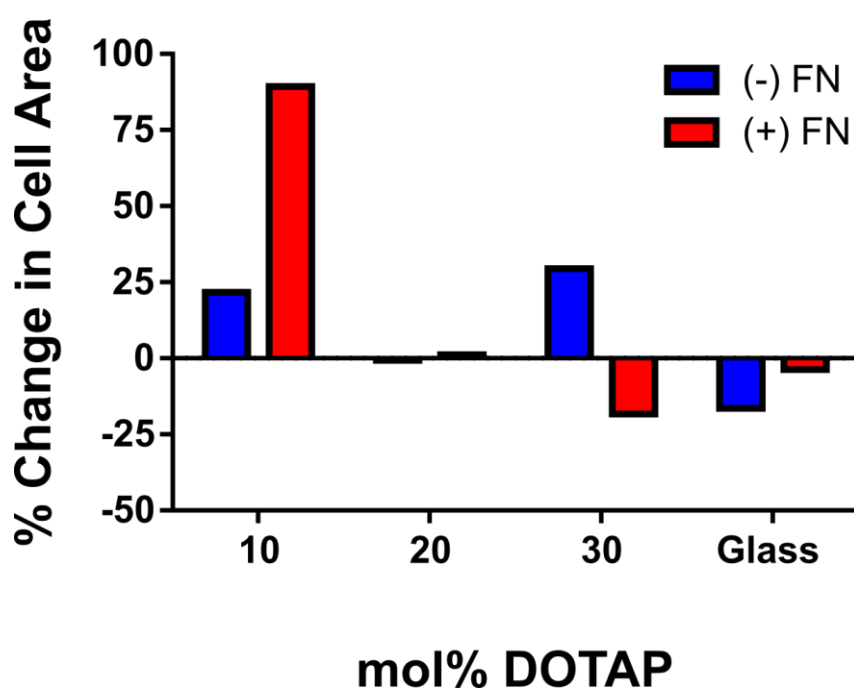


Figure 6.12. Area Change Between 3 and 24 Hours. This shows the percentage of change in the cell area on the DPPC:DOTAP surfaces

between 3 and 24 hrs, when the hMSCs were seeded the SLBs with and without FN.

While the role of FN in cellular adhesion to positively charged SLBs is not clear based on the cell area, an analysis of the FAs in Figure 6.13 proves to show that the effect is negligible. While the spreading of cells may not be consistent it is clear that no clear FAs are present on any of the SLBs at either 3 or 24 hours. This demonstrates that the cell interactions with these SLBs are not integrin mediated. As the interaction of cells with FN is mediated by integrins, and thus FAs, it is also therefore possible that FN does not bind to the SLBs. Therefore, the main means of the cellular interaction with these SLBs is possibly a combination of the mobile and electrostatic components of the bilayer. This is despite the presence of small amounts of positive charge previously shown to permit the binding of actin on SLBs (283). However, this also implies an integrin-independent means of cell spreading on these surfaces, in response to the inclusion of surface charge. This may be explained by DLVO (Derjaguin-Landau-Verwey-Overbeek) theory, which has been used in the past to describe bacterial adhesion to surfaces (289). This theory takes into account the attractive and repulsive forces dictating the interactions of surfaces, with these forces having a role in the initial adhesion of cells on to surfaces (290), before the activation of further, molecular recognition pathways. However, many questions yet remain; it is widely accepted that cells respond to their surface via these very same molecular recognition pathways, but it remains unclear what pathways would be activated here. This surface may be detected through other receptors, with further environment-sensing pathways including growth factor receptors (291), cadherins (170) and syndecans (292). Indeed, it may be that there is very little activation of downstream pathways. Because of this it is also unclear as to whether the inclusion of charge is a threshold-based phenomenon (i.e. all or nothing binding of cells) or would have an incremental effect on the cell behaviour. In any of these cases, further work would be required to elucidate what effect there is on cell behaviour

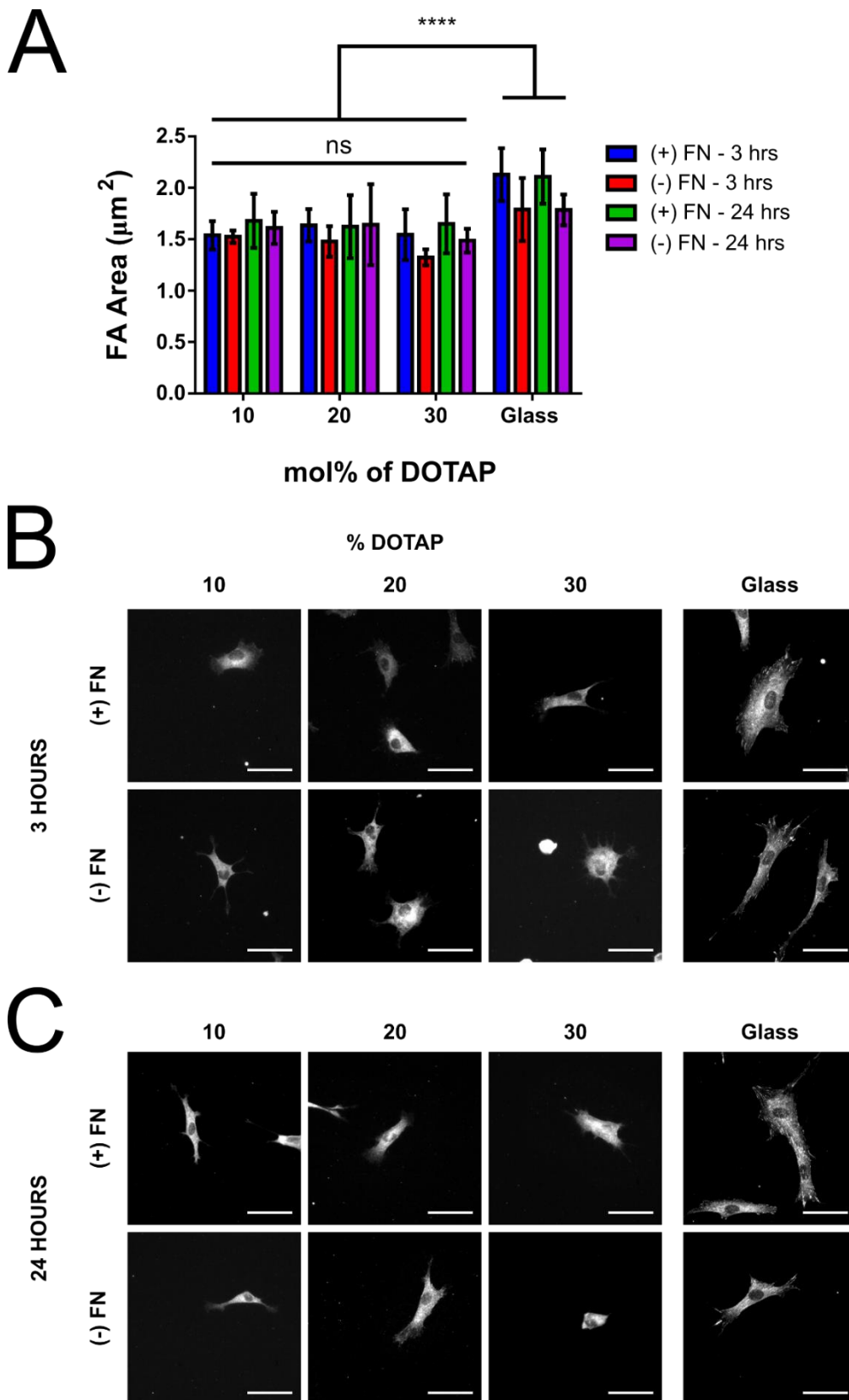


Figure 6.13. Focal Adhesions on DPPC:DOTAP SLBs. (A) Shows the average area of detected focal adhesions present on the DPPC SLBs, when differing mol% of DOTAP is used. This shows that the concentration of DOTAP has no significant effect on the

*FA behaviour and any detected FAs are smaller than those seen on glass surfaces, incubated with and without FN. (B) and (C) show representative images of these cells at 3 and 24 hrs respectively. This demonstrates that the presence of a larger, diffuse vinculin background present in the cells on the DPPC:DOTAP SLBs may induce a false positive of FA area. This is contrasted with glass, which shows well-defined FAs. (Scale Bar = 50 μ m). P values indicating significance, ns > 0.05, **** \leq 0.0001.*

6.4. CONCLUSIONS

This chapter has shown that while there is great potential for SLBs as a cell culture platform, there is further work required to understand the nature of hMSC behaviour. Initially, it was shown that adhesion of hMSCs was similar to that of C2C12s, with cells small and rounded on DOPC and spread, with FAs on DPPC. However, after 24 hours of adhesion cells on the latter, cells area reduced and less FAs were seen. This unusual behaviour has been hypothesised, though not conclusively proven, to be due to the potential loss of ligand on the surface. With lower ligand density showing reduced cell size in Chapter 5, and previous work showing a dependency of endocytosis on forces exerted on the surface (77), it is possible that this may be a root cause. Furthermore, it was seen that the system used for C2C12 culture, prevented growth of hMSCs on the surface over longer time scales, precluding the possible utility of the initial system as a platform for culturing and manipulating hMSCs. While this may also be linked to loss of ligand preventing attachment of new cells, a possible future analysis of the supernatant for the presence of cells may prove this to be the case.

To this end, the system was adjusted firstly by including larger molecules on the surface, including FNIII₇₋₁₀ fragment and full fibronectin. It was thought that the former would introduce the synergy site, capable of enhancing cell binding (182), and the latter would present a more interactive surface, promoting further protein binding and manipulation by the cells. However, this strategy proved to have no effect on the nature of the cells, implying that the dominant factor determining the cell behaviour was an irreplaceable loss of ligand on the surface. Furthermore, cross-linking proved ineffective and the strategy due to cytotoxicity that could not be removed (data not shown). The inclusion of positively charged DOTAP lipid in

the SLBs showed more potential. As previous work has demonstrated that positive charge can promote cell binding (158), due to electrostatic interactions, this was used here. This strategy was successful at different mol% of DOTAP on the DPPC SLBs. Furthermore, the inclusion of positive lipid prevented the loss of cell area after 24 hours. However, the incubation of FN on the surface appears to have no effect. Due to the lack of FAs present this is likely due to the FN not adsorbing on the surface. It may be that further strategies or other ECM proteins may adsorb and promoted stronger interactions. This shows that there is potential for this system for future use in manipulating hMSC behaviour; however, there is further work required in optimising this system.

7. CONCLUSIONS AND FUTURE PERSPECTIVES

7.1. CONCLUSIONS

7.1.1. PRODUCTION AND CHARACTERISATION OF SUPPORTED LIPID BILAYERS WITH DEFINED DIFFUSIVE PROPERTIES

Supported lipid bilayers of distinct characteristics were produced; at 37°C one existed in the fluid-phase, with the contrasting system existing in the gel-phase. The former, DOPC, is associated with a high relative diffusion coefficient, while the latter, DPPC, is associated with a low relative diffusion coefficient. In this chapter (Chapter 3) the principle aim was to determine the characteristics of these systems, most importantly the diffusion coefficient, through fluorescence correlation spectroscopy (FCS). In pursuit of this, the properties affecting the system were determined to be sufficient to induce the formation of a contiguous and defect free SLB, which was assessed via both atomic force and fluorescence microscopy. AFM confirmed the bilayer properties on the sub-micron level, confirming, at a resolution unachievable through normal fluorescence methods, that a defect-free SLB had been formed in the case of both DOPC and DPPC. Further to this, force spectroscopy was performed to ascertain the physical properties of the bilayer. Measuring of the force curves characteristic of SLBs provided information on the thickness of the SLBs. In contrast to the literature, both the DOPC and DPPC SLBs were determined to be of comparable thickness. This was ascribed to electrostatic interactions between the tip and the SLB surface, which have been previously noted to cause measurement issues in the bilayer (177).

FCS, was used to determine the diffusion coefficient, D , in both DOPC and DPPC. The system was first calibrated using FITC beads of defined size, in conjunction with the Stokes-Einstein equation, to determine the width of the illuminating beam. Subsequently, D was determined for both DOPC and DPPC, with the former giving values in good agreement with previously reported results. However, FCS measurements proved more difficult in DPPC, with a greater degree of noise present. This was attributed to the low D of DPPC, with bleaching of the fluorophore within the confocal volume requiring a large concentration of fluorophore to compensate. Using the Saffman-Delbruck equation the diffusion of both DOPC and DPPC was

used to estimate the viscosity values of both, which agreed well with those previously measured in the literature.

Moving beyond the determination of the SLB characteristics, biotin-PE was incorporated at concentrations spanning two orders of magnitude, in order to produce a system capable of supporting cellular adhesion. The biotin-PE was bound to neutravidin, with similar molecules such as avidin being associated with high non-specific binding (164) and streptavidin shown to crystallise on the bilayer in higher concentrations (293). In conjunction with this, a glass control, also presenting neutravidin via silane-crosslinker functionalisation, was also produced. The amount of neutravidin present on the surface was determined via quantitative fluorescence microscopy, first described by Galush et al. (180), and expanded in by Nair et al (184). Using bulk and bilayer standards as calibrations, the amount of neutravidin on the surface was determined to be within the values expected for the surface. The expected values were estimated from the known radius of a single lipid, using this to determine the amount of functionalised, biotin-PE, lipid per μm^2 . The stability of these bilayers was also determined, with both seen to be stable for at least 8 days under cell culture conditions.

While the assessment of the SLBs was determined to be sufficient for the purposes of the rest of the study, further experimentation would add greater understanding of the nature of the SLBs. A direct assessment of bilayer stability in the presence of cells would be of use to determine its applicability in future studies. Further work is also required in understanding the complex nature of the diffusion of molecules within the bilayer.

7.1.2. DETERMINING AND UNDERSTANDING THE NATURE OF THE CELL RESPONSE

The principle aims of chapters 4 and 5 were to determine a) how the cell responded to the varying bilayer properties and b) why the cells behaved in that particular way. To this end, these two chapters were split so as demarcate between the what and the why, with chapter 4 serving as an initial observation as to the behaviour of the cells on the surface and chapter 5 elucidating the molecular mechanisms underlying this behaviour. While it may be that these

are similar in theme, a distinct separation of these into two chapters served to better aid the project narrative.

Initially, it was confirmed that the plain bilayers prevented cellular adhesion, in line with the literature (294). This was true in the case of both DOPC and DPPC, with adhesion promoted upon the functionalisation of the bilayer with neutravidin and biotin-RGD. This also served the purpose of demonstrating that both SLBs were continuous and thus able to prevent significant cell adhesion before functionalisation. Subsequently, the morphology of the cells on each of the SLBs was determined, showing that cells were more spread on the gel phase bilayer. Furthermore, inhibiting two key integrins responsible for cell-binding to the RGD-tripeptide led to a marked decrease in the cell area, implying that the binding of cells was integrin mediated. It is here that the possible mechanical nature of the sensing of the viscosity-defined ligand mobility was first hypothesised. Focal adhesions (FAs) were also assessed for their properties, with larger and more active FAs seen on the gel phase, DPPC SLB, compared with the fluid phase, DOPC SLB. Turning to the literature, it was noted that larger FAs, more spread cells, and a greater extent of actin stress fibres were all markers of mechanotransduction (10). The proteins used to assess the nature of the cellular adhesion, vinculin and pFAK, are also well-known mechanosensitive proteins. This chapter ends with the proposed hypothesis that as the viscosity of the surface decreases (mobility of the ligand thus increases) so too does the force on the surface.

Chapter 5 began by attempting to understand the nature of the cellular response through the molecular clutch model. By substituting the spring (representative of stiffness) for a dashpot (representative of viscosity), the viscosity of the surface was modelled instead of the stiffness. It is this viscosity, related to the diffusion constant, D , that is a key factor determining the mobility of the ligand. The model predictions, calculated by Prof. Pere Roca-Cusachs, show that characteristics such as adhesion size and actin flow increase and reduce respectively, in response to increased viscosity. What was clear immediately is that the viscosity values, calculated via the Saffman-Delbruck (SD) equation, using the FCS-determined diffusion coefficients, did not match the predicted values. It was then noted that other equations related the diffusion and viscosity, previously mentioned in the introduction (Section 1.3.3.) can be used to determine any change in the viscosity. The large discrepancy in attained and predicted

values is therefore associated with the characteristic length of the alternative SD equation (135). It was determined that if this length was determined to be on the order a cell radius then this discrepancy could be alleviated; this then led to agreement, within an order of magnitude, of both the predicted and estimated viscosity values. Further, it was highlighted in larger constructs that the validity of the SD equation breaks down, being unable to predict accurately diffusion of objects at larger length scales.

Testing the model further, the actin flow was determined in both WT cells and cells with myosin II and vinculin inhibited. This showed that interrupting key parts of the apparatus related to the molecular clutch removed any differences in actin flow. Due to the actin flow being a key component of the clutch this provides strong evidence that the molecular clutch model is applicable to the viscosity-defined cell response. Furthermore, inhibition of the vinculin tail showed that while FA size changed in line with the viscosity of the surface, the actin flow showed no difference between conditions, again supporting the clutch model. Developing this further, model predictions were again borne out by showing that when the clutch was active (i.e. in DPPC) there was an increase in adhesion size as ligand density increased. In contrast, cells on DOPC showed no increase in adhesion size regardless of ligand density, as predicted by the low viscosity regime of the model.

Downstream signalling was also tested, showing that the mechanosensitive transcription factor, YAP, localised to the nucleus in response to increased viscosity. In addition to the evidence provided by the molecular clutch, this also implies a mechanical-basing sensing of the viscosity of the surface. Beyond this, it was shown that the mechanical based sensing of the SLBs also led to changes in viscosity, with the differentiation of C2C12 cells inhibited on the low viscosity (high ligand mobility) DOPC SLB. This provided initial evidence that changing the viscosity of the SLB could direct the lineage commitment of differentiation capable cells.

Strong evidence presented in these two chapters shows that: a) the cells respond to the ligand mobility, defined by the viscosity, using mechanosensitive mechanisms, and b) the molecular clutch is applicable to this system, predicting in the right order of magnitude when the cells respond to the surface. However, further work would be required to understand the nature of

the SLBs underneath the cell area. This may further elucidate the nature of the cell response. Furthermore, it would be useful to further adjust the model to take into account the truly fluid nature of the SLB, taking into account, for example, the possible ligand clustering that an unconstrained 2D fluid would allow.

7.1.3. APPLYING SUPPORTED LIPID BILAYERS TO BIOMEDICAL APPLICATIONS

After understanding why cells behaved in a defined way on each of the SLBs the applicability of this model system to test further, medically applicable, scenarios was assessed. Without changing the nature of the DOPC and DPPC SLBs, human mesenchymal stem cells (hMSCs) were adhered on these surfaces for 3 and 24 hours. It was determined that between these two time points cells on both DOPC and DPPC reduced in cell area. The glass control demonstrated that the lack of FBS in the culture media was not responsible for this loss of area. This effect was most pronounced on DPPC, which, in addition to a reduction in cell area, also showed a significant reduction in FA area. This was attributed to the SLBs themselves, specifically to a loss of ligand on both over the time course. This was in light of previous literature that suggested there is a definite loss of functional ligand on the surface, due to cellular endocytosis. Further to this, the growth of hMSCs on the SLBs, tested by incorporation of BrdU into the DNA, was also noted to be minimal and the SLBs unstable after 5 days of culture. This was put into the context of previous, similar work, which determined hMSC differentiation on DOPC and DPPC SLBs. The cell behaviour in the previous work was not in good agreement with the current findings, as well as with the literature. Therefore, as the current results aligned well with the literature, it was surmised that this previous work had not accounted for SLB breakdown over the long time course (~2 weeks) that the cell differentiation was studied. Further, the spreading of cells on DOPC after 5 days of culture indicated that the SLB had been significantly endocytosed on this surface, thus presenting the underlying glass upon which the cells bound. This conclusion was based on the literature that indicated that the removal of cell forces (i.e. in a fluid phase SLB) upregulated endocytosis. Therefore, this would not only account for the DOPC SLB breakdown, but also why a similar cell behaviour was not seen on DPPC; because of the larger cellular forces there was downregulation of endocytosis, thus impeding DPPC SLB breakdown.

In light of these findings two approaches were made to alleviate the loss of cell area. Firstly, the system was altered to present both peptide fragments and full proteins. The hypothesis behind this was that full protein would provide a nucleation point that the cells could manipulate and add to, producing an SLB-supported ECM protein surface. Biotinylation of full fibronectin and the cell binding fragment, type III₇₋₁₀ repeat (a control that contains RGD, but no FN-FN binding sites), showed no reduction in the binding of the cells and the size of FAs. Furthermore, the concentration of biotin-PE lipid was concluded to be key factor determining functionalisation of the SLBs with these molecules; the viscosity and the number of biotins present on the molecule had no significant effect. However, it was found that this had no effect on the cell behaviour between 3 and 24 hours, with cells being of comparable area across all protein functionalisation strategies. Unusually, III₇₋₁₀ on DOPC showed no cellular adhesion, with the cause not known. It was concluded that the non-fouling nature of the surface meant that any loss of functional groups on the surface could not be replaced, preventing any correction of this issue without changing the intrinsic nature of the bilayer.

As an alternative to the presentation of larger constructs the second approach was to include a positively charged lipid in the SLBs. Positive charge has previously been noted to increase cellular binding due to the overall negative charge of the membrane. To that end, the positively charged DOTAP lipid was included in up to 30 mol% in each bilayer. On DOPC, this did not allow for any binding of cells, but all concentrations of DOTAP allowed for cellular adhesion on DPPC. This was attributed to an interplay between the diffusion of the SLBs and their electrostatic charge. While inclusion of DOTAP did prevent a loss in cell area after 24 hours, no FA adhesions were seen to form, raising the question of the impact of electrostatic cellular adhesion on cellular pathways. Further work would be required to elucidate what, if any, pathways of adhesion the cells utilise to bind to and sense the positive charge of these SLBs.

While progress has been made in applying SLBs to a more medically applicable cell line, beyond the model system, further work is required to develop this further. For example, the longer-term stability of SLBs, in the presence of adhering cells, must be addressed; while it was shown chapter 3 that SLBs are stable in cell culture conditions over this time frame, it is unclear how the cells affect the SLB structure Based on the findings in hMSCs it does appear

likely, though unconfirmed, that there is some degree of bilayer breakdown through endocytosis. Therefore, inhibiting endocytosis would also serve to further explain the behaviour of cells on SLBs and their effect on SLB stability and structure. Further, cell behaviour on these positively charged SLBs must be further studied; while successfully shown that positive charge can promote cell adhesion, on gel phase bilayers, it has not been determined how this has an effect cellular behaviour. For example, previous work has established that DOTAP SLBs have a lower diffusion coefficient, and thus higher viscosity, than DOPC (158). This adds extra complexity, and thus a further avenue of research into the interplay of viscosity and charge and how this adapts cellular behaviour.

Moving towards the molecular level, determining the nature, or indeed the presence, of FN on the surface is of great interest. It may be that very little FN binds to the charged lipid surface, or that it is present in globular or fibrillar conformations. Techniques such as a western blot or an ELISA may serve to elucidate this further. In addition, other proteins may also be of interest, with laminin previously demonstrating a fibrillar conformation on DOPC SLBs (82). The means by which cells bind to ECM proteins is also of interest. In this setting it appears that the role of FAs is minimal, but cells may also bind through other pathways; understanding what these pathways are and the relevant downstream signalling molecules and processes may therefore be of interest. Together these additional insights may also serve to develop this positively charged system as a more applicable means of culturing hMSCs and directing their behaviour.

7.2. FUTURE PERSPECTIVES

The nature of SLBs, and the various modalities that they can include, present a wide array of possibilities of further work in this field. They have shown their potential for use in cell culture conditions, as well as a means to direct cell behaviour, through manipulation of their physical properties.

7.2.1. BILAYER MODIFICATIONS

Part of the allure of SLBs is that they can be easily functionalised using simple chemistries, such as the biotin-avidin system. As such, this may be used in future to functionalise bilayers with further molecules of interest. This project has already looked at the potential of both single peptides and larger protein molecules, but these were all related to the fibronectin protein. Previous work has used SLBs to present peptides such as IKVAV (laminin cell-binding sequence) (295), cadherin (161), or collagen (165). However, none of these have investigated how changing the viscosity may affect cell response to these further functionalities. For example, inclusion of the N-cadherin peptide HAVDI has been shown to modulate the cell response to RGD peptides in gels (296). Interestingly, the inclusion of HAVDI with RGD changes how the cell responds to stiffness; as viscosity of the SLBs is detected via similar pathways, it would be reasonable to assume the cell response here would also change. This reveals the possibility of understanding the individual and combined contributions of the components of the ligands and their mobility, and how these interact to induce specific cell responses, through controlling the ligand ratios and the SLB viscosity.

Further to presenting different moieties on the bilayer surface, more intrinsic properties of the bilayer may also be modified. As shown in this work the inclusion of positive charge in the bilayer can promote cellular adhesion. While some previous work has also used DOTAP to alleviate the non-fouling nature of SLBs made up of neutral lipids, other work has also included other molecules associated with the promotion of cellular adhesion. For example, there are also lipids that are associated with a number of cellular processes, such as PIP₂ (297). Several proteins have receptors for this lipid and inclusion of this in an SLB may also serve to control cellular behaviour, through activating cellular pathways.

A key issue in the future of this work was illuminated in chapter 6. After 5 days the stability of the DOPC was compromised in the presence of cells, thus leading to an increase in cell area more akin to cells found on glass. Furthermore, without cells, DOPC was seen to breakdown between 8 – 15 days. However, this presents an opportunity to develop this system further. As mentioned in the introduction, as well as SLBs, tethered SLBs also exist (tSLBs) (154). The SLBs were fit for the initial purpose of this study; however, in the determination of cell's response to the mobility of a ligand on the surface, in longer term applicability studies, tSLBs may be more appropriate. In this context they confer advantages such as longer-term stability

(154). When culturing hMSCs this would be of particular importance, with terminal differentiation occurring over the course of weeks rather than days (16). Additionally, tSLBs also separate the bilayer from the glass support, which would allow for the inclusion of membrane proteins in the system. In SLBs, inclusion of membrane-spanning proteins is impossible, with the close proximity of the SLB and the glass support causing loss of function of included proteins. The use of tSLBs in this context does have some examples (298), but could be expanded further to observe how the viscosity of the membrane affects factors such as cell-cell adhesion and signalling. Furthermore, tSLBs provide a further avenue for the manipulation of the diffusion of the bilayer, thus affecting the viscosity, shown to be vital to understanding the nature of the cell response in chapter 5. Specifically, even small concentrations of immobile lipid introduced into the bilayer have been observed to have a significant effect on the diffusion of surrounding lipid molecules (253). It could be envisaged that a fluid SLB, such as DOPC, could be forced to have an effective viscosity, more similar to the that of DPPC, by rendering a specific percentage of the SLB immobile.

7.2.2. UNDERSTANDING CELL-SURFACE AND CELL-CELL INTERACTIONS

Developing from the presentation of different ligands on an SLB surface, these may also be used to understand the direct role of viscosity-defined ligand mobility in physical interactions between cells and surfaces, or indeed other cells. For example, elegant work by Bharadwaj et al. (299) used a cell, deposited on an AFM cantilever, to determine the nature of interaction with different integrins. A similar modality may be used in cells and SLBs to understand, in greater depth, what is occurring at the cell-SLB interface. With the presentation of different molecules, different systems may be simulated, such as cell-cell contacts and the role of the membrane fluidity in signalling. Furthermore, in the context of the current work, this may allow for the further important contributing factors to be elucidated. For example, the number of binding events and the strength of interaction, could be understood in the context of the viscosity of the SLBs and the mobility of the ligands therein. Together, these would allow the estimation of viscosity-dependent single bond strength. Understanding these forces would allow a greater sense of how the molecular clutch, assessed in chapter 5, responds to the viscosity of the membrane. Furthermore, the tension sensors and molecular tension fluorescence microscopy (MTFM) (174), mentioned previously, in section 1.3.4 may also present an opportunity through which to study the cell-SLB interface in more depth.

7.2.3. APPLICATIONS IN CELL DIFFERENTIATION

Work in chapter 6 has shown that there is some further optimisation that is required for SLBs to be a viable option in the differentiation of medically relevant cell lines, such as hMSCs. Further work, should therefore focus on each of the strategies mentioned in the above sections, using these as a framework through which to produce a system more applicable to this medically relevant context. For example, the introduction of alternate ligands would promote different pathways. Further, the seeding of hMSCs on DOTAP bilayers showed that the interaction is dominated by electrostatic interactions, with minimal FA-mediated response. This may allow for seeding of cells with a reduction in external stimuli. Alternatively, if other pathways are activated by this electrostatic interaction it would be intriguing to ascertain which pathways and why. Beyond this, further strategies should also focus on stabilising this system further. As mentioned in section 8.2.1, tSLBs present the possibility of bilayers with much greater stability, allowing for their use in much longer-term differentiation studies. Successful application of this would allow for a more biomedically relevant applicability of the surface-supported lipid base systems.

Overall, there is a great deal potential of surface-supported lipid systems. This project has served to develop a more complete understanding of how cells respond to the viscosity of a surface. In more specific sense, they have also shown what factors underpin how a cell responds to perturbations in ligand mobility, as a consequence of SLB viscosity. This greater depth of understanding of the factors controlling the cell response allows for more focused guidance on how to develop similar materials in future work.

8. APPENDIX A – DESCRIPTION OF THE MOLECULAR CLUTCH MODEL

To implement the computational clutch model, we took our previously described model as a reference (118), and we carried out a simple modification to consider a viscous rather than elastic substrate. To this end, we modified the equation calculating the total force exerted on the substrate F_{sub} as follows:

$$F_{sub} = \frac{v_u}{\frac{1}{n_{eng}\mu} + \frac{v_u}{n_m F_m}}$$

Where v_u is the contraction speed of myosin motors in the absence of force, μ is the viscosity of each ligand, n_{eng} is the number of engaged (bound) ligands, n_m is the total number of myosin motors, and F_m is the stall force of a single motor. This equation comes from combining our previously used equation to model a linear reduction in myosin contraction speed v with force:

$$v = v_u \left(1 - \frac{F_{sub}}{n_m F_m}\right)$$

With the equation relating force to speed in a viscous system where each engaged ligand contributes with a given viscosity.

$$F_{sub} = n_{eng} v \mu$$

Total force F_{sub} was considered to be distributed evenly among all engaged clutches. For simplicity, we neglected the elasticity of the clutches. This is consistent with our previous works (47, 260, 300), where clutch elasticity was successfully modelled with very high values and played a negligible role as compared to the mechanical properties of the substrate.

All parameter values are of the same order as those employed in previous simulations considering elasticity rather than viscosity (47, 118, 260).

Parameter	Meaning	Value	Origin
n_m	Number of myosin motors	100	Adjusted
n_l	Number of ligands	75	Adjusted
F_m	Myosin motor stall force	2 pN	(301)
v_u	Unloaded myosin motor velocity	110 nm/s	(47, 118)
d_{int}	Initial integrin density on the membrane	$300/\mu\text{m}^2$	(302)
d_{intmax}	Maximum integrin density on the membrane	$1000/\mu\text{m}^2$	Adjusted
K_{ont}	True binding rate	$1 \times 10^{-4} \text{um}^2/\text{s}$	Adjusted, of the order of values reported for $\alpha\text{IIB}\beta 3$ (303)
K_{off}	Unbinding rate, scaling factor applied to force curve reported in (304)	0.5	Adjusted, catch bond dependency from (304)
$F_{threshold}$	Threshold reinforcement force	90 pN	Adjusted, of the order of reported values (305)
d_{add}	Integrins added after each reinforcement event	$6/\mu\text{m}^2$	Does not affect model output
a	Radius of adhesion	550 nm	Adjusted

Table A1. Model parameters.

9. REFERENCES

1. Stevens MM, George JH. Exploring and Engineering the Cell Surface Interface. *Science*. 2005;310(5751):1135-8.
2. Engel J, Chiquet M. An Overview of Extracellular Matrix Structure and Function. In: Mecham RP, editor. *The Extracellular Matrix: an Overview*. Berlin, Heidelberg: Springer Berlin Heidelberg; 2011. p. 1-39.
3. Muiznieks LD, Keeley FW. Molecular assembly and mechanical properties of the extracellular matrix: a fibrous protein perspective. *Biochimica et Biophysica Acta (BBA)-Molecular Basis of Disease*. 2013;1832(7):866-75.
4. Badylak SF, Freytes DO, Gilbert TW. Extracellular matrix as a biological scaffold material: structure and function. *Acta biomaterialia*. 2009;5(1):1-13.
5. Reilly GC, Engler AJ. Intrinsic extracellular matrix properties regulate stem cell differentiation. *Journal of biomechanics*. 2010;43(1):55-62.
6. Taipale J, Keski-Oja J. Growth factors in the extracellular matrix. *The FASEB Journal*. 1997;11(1):51-9.
7. Murphy SV, Atala A. 3D bioprinting of tissues and organs. *Nat Biotechnol*. 2014;32(8):773-85.
8. Galletti PM, Boretos JW. Report on the Consensus Development Conference on "Clinical Applications of Biomaterials," 1–3 November 1983. *J Biomed Mater Res Part A*. 1983;17(3):539-55.
9. Alakpa EV, Burgess KEV, Chung P, Riehle MO, Gadegaard N, Dalby MJ, et al. Nacre Topography Produces Higher Crystallinity in Bone than Chemically Induced Osteogenesis. *ACS nano*. 2017;11(7):6717-27.
10. Murphy WL, McDevitt TC, Engler AJ. Materials as stem cell regulators. *Nat Mater*. 2014;13(6):547-57.
11. Sunyer R, Conte V, Escribano J, Elosegui-Artola A, Labernadie A, Valon L, et al. Collective cell durotaxis emerges from long-range intercellular force transmission. *Science*. 2016;353(6304):1157-61.

12. Kilian KA, Bugarija B, Lahn BT, Mrksich M. Geometric cues for directing the differentiation of mesenchymal stem cells. *Proceedings of the National Academy of Sciences*. 2010;107(11):4872-7.
13. Chen CS, Mrksich M, Huang S, Whitesides GM, Ingber DE. Geometric Control of Cell Life and Death. *Science*. 1997;276(5317):1425-8.
14. Balaban NQ, Schwarz US, Riveline D, Goichberg P, Tzur G, Sabanay I, et al. Force and focal adhesion assembly: a close relationship studied using elastic micropatterned substrates. *Nat Cell Biol*. 2001;3(5):466-72.
15. Hunter A, Archer CW, Walker PS, Blunn GW. Attachment and proliferation of osteoblasts and fibroblasts on biomaterials for orthopaedic use. *Biomaterials*. 1995;16(4):287-95.
16. Dalby MJ, Gadegaard N, Tare R, Andar A, Riehle MO, Herzyk P, et al. The control of human mesenchymal cell differentiation using nanoscale symmetry and disorder. *Nature Materials*. 2007;6(12):997-1003.
17. Barczyk M, Carracedo S, Gullberg D. Integrins. *Cell Tissue Res*. 2010;339(1):269-80.
18. Geiger B, Spatz JP, Bershadsky AD. Environmental sensing through focal adhesions. *Nat Rev Mol Cell Biol*. 2009;10(1):21-33.
19. Winograd-Katz SE, Fässler R, Geiger B, Legate KR. The integrin adhesome: from genes and proteins to human disease. *Nat Rev Mol Cell Biol*. 2014;15:273.
20. Seo CH, Furukawa K, Montagne K, Jeong H, Ushida T. The effect of substrate microtopography on focal adhesion maturation and actin organization via the RhoA/ROCK pathway. *Biomaterials*. 2011;32(36):9568-75.
21. Dupont S, Morsut L, Aragona M, Enzo E, Giulitti S, Cordenonsi M, et al. Role of YAP/TAZ in mechanotransduction. *Nature*. 2011;474(7350):179-83.
22. Alberts B JA, Lewis J, Raff M, Roberts K, Walter P. *Cells and Genomes*. Mol Biol Cell. 6th ed: Garland Science; 2014.
23. Chan YH, Boxer SG. Model membrane systems and their applications. *Curr Opin Chem Biol*. 2007;11(6):581-7.

24. Chang H-I, Yeh M-K. Clinical development of liposome-based drugs: formulation, characterization, and therapeutic efficacy. *International Journal of Nanomedicine*. 2012;7:49-60.
25. Sezgin E, Schwille P. Model membrane platforms to study protein-membrane interactions. *Molecular membrane biology*. 2012;29(5):144-54.
26. Giess F, Friedrich MG, Heberle J, Naumann RL, Knoll W. The Protein-Tethered Lipid Bilayer: A Novel Mimic of the Biological Membrane. *Biophysical Journal*. 2004;87(5):3213-20.
27. Saha K, Keung AJ, Irwin EF, Li Y, Little L, Schaffer DV, et al. Substrate Modulus Directs Neural Stem Cell Behavior. *Biophys J*. 2008;95(9):4426-38.
28. Rho JY, Ashman RB, Turner CH. Young's modulus of trabecular and cortical bone material: ultrasonic and microtensile measurements. *Journal of biomechanics*. 1993;26(2):111-9.
29. Rowley JA, Madlambayan G, Mooney DJ. Alginate hydrogels as synthetic extracellular matrix materials. *Biomaterials*. 1999;20(1):45-53.
30. Gutowski SM, Shoemaker JT, Templeman KL, Wei Y, Latour RA, Jr., Bellamkonda RV, et al. Protease-degradable PEG-maleimide coating with on-demand release of IL-1Ra to improve tissue response to neural electrodes. *Biomaterials*. 2015;44:55-70.
31. Cruz-Acuña R, Quirós M, Farkas AE, Dedhia PH, Huang S, Siuda D, et al. Synthetic hydrogels for human intestinal organoid generation and colonic wound repair. *Nat Cell Biol*. 2017;19:1326.
32. McBeath R, Pirone DM, Nelson CM, Bhadriraju K, Chen CS. Cell shape, cytoskeletal tension, and RhoA regulate stem cell lineage commitment. *Developmental cell*. 2004;6(4):483-95.
33. Zhou J, Aponte-Santamaría C, Sturm S, Bullerjahn JT, Bronowska A, Gräter F. Mechanism of Focal Adhesion Kinase Mechanosensing. *PLOS Computational Biology*. 2015;11(11):e1004593.
34. Engler AJ, Sen S, Sweeney HL, Discher DE. Matrix elasticity directs stem cell lineage specification. *Cell*. 2006;126(4):677-89.

35. Engler AJ, Griffin MA, Sen S, Bonnetnann CG, Sweeney HL, Discher DE. Myotubes differentiate optimally on substrates with tissue-like stiffness: pathological implications for soft or stiff microenvironments. *Journal of Cell Biology*. 2004;166(6):877-87.
36. Wen JH, Vincent LG, Fuhrmann A, Choi YS, Hribar KC, Taylor-Weiner H, et al. Interplay of matrix stiffness and protein tethering in stem cell differentiation. *Nat Mater*. 2014;13(10):979-87.
37. Castellani R, de Ruijter A, Renggli H, Jansen J. Response of rat bone marrow cells to differently roughened titanium discs. *Clin Oral Implants Res*. 1999;10(5):369-78.
38. ter Brugge PJ, Wolke JG, Jansen JA. Effect of calcium phosphate coating crystallinity and implant surface roughness on differentiation of rat bone marrow cells. *J Biomed Mater Res*. 2002;60(1):70-8.
39. Rasmussen CH, Reynolds PM, Petersen DR, Hansson M, McMeeking RM, Dufva M, et al. Enhanced Differentiation of Human Embryonic Stem Cells Toward Definitive Endoderm on Ultrahigh Aspect Ratio Nanopillars. *Advanced Functional Materials*. 2016;26(6):815-23.
40. Zhu B, Lu Q, Yin J, Hu J, Wang Z. Alignment of osteoblast-like cells and cell-produced collagen matrix induced by nanogrooves. *Tissue Eng*. 2005;11(5-6):825-34.
41. Jang J-H, Castano O, Kim H-W. Electrospun materials as potential platforms for bone tissue engineering. *Advanced Drug Delivery Reviews*. 2009;61(12):1065-83.
42. Cavalcanti-Adam EA, Volberg T, Micoulet A, Kessler H, Geiger B, Spatz JP. Cell Spreading and Focal Adhesion Dynamics Are Regulated by Spacing of Integrin Ligands. *Biophys J*. 2007;92(8):2964-74.
43. They M, Pepin A, Dressaire E, Chen Y, Bornens M. Cell distribution of stress fibres in response to the geometry of the adhesive environment. *Cell Motil Cytoskeleton*. 2006;63(6):341-55.
44. They M, Racine V, Piel M, Pepin A, Dimitrov A, Chen Y, et al. Anisotropy of cell adhesive microenvironment governs cell internal organization and orientation of polarity. *Proc Natl Acad Sci U S A*. 2006;103(52):19771-6.
45. Huang J, Gräter SV, Corbellini F, Rinck S, Bock E, Kemkemer R, et al. Impact of Order and Disorder in RGD Nanopatterns on Cell Adhesion. *Nano Lett*. 2009;9(3):1111-6.

46. Watari S, Hayashi K, Wood JA, Russell P, Nealey PF, Murphy CJ, et al. Modulation of osteogenic differentiation in hMSCs cells by submicron topographically-patterned ridges and grooves. *Biomaterials*. 2012;33(1):128-36.
47. Elosegui-Artola A, Oria R, Chen Y, Kosmalska A, Perez-Gonzalez C, Castro N, et al. Mechanical regulation of a molecular clutch defines force transmission and transduction in response to matrix rigidity. *Nat Cell Biol*. 2016;18(5):540-8.
48. Oria R, Wiegand T, Escribano J, Elosegui-Artola A, Uriarte JJ, Moreno-Pulido C, et al. Force loading explains spatial sensing of ligands by cells. *Nature*. 2017;552:219.
49. Benoit DS, Schwartz MP, Durney AR, Anseth KS. Small functional groups for controlled differentiation of hydrogel-encapsulated human mesenchymal stem cells. *Nat Mater*. 2008;7(10):816-23.
50. Zonca MR, Yune PS, Heldt CL, Belfort G, Xie Y. High-Throughput Screening of Substrate Chemistry for Embryonic Stem Cell Attachment, Expansion, and Maintaining Pluripotency. *Macromolecular Bioscience*. 2013;13(2):177-90.
51. Gandavarapu NR, Mariner PD, Schwartz MP, Anseth KS. Extracellular matrix protein adsorption to phosphate-functionalized gels from serum promotes osteogenic differentiation of human mesenchymal stem cells. *Acta Biomater*. 2013;9(1):4525-34.
52. Gonzalez-Garcia C, Moratal D, Oreffo ROC, Dalby MJ, Salmeron-Sanchez M. Surface mobility regulates skeletal stem cell differentiation. *Integr Biol-Uk*. 2012;4(5):531-9.
53. Seo JH, Kakinoki S, Inoue Y, Nam K, Yamaoka T, Ishihara K, et al. The significance of hydrated surface molecular mobility in the control of the morphology of adhering fibroblasts. *Biomaterials*. 2013;34(13):3206-14.
54. Seo JH, Yui N. The effect of molecular mobility of supramolecular polymer surfaces on fibroblast adhesion. *Biomaterials*. 2013;34(1):55-63.
55. Kourouklis AP, Lerum RV, Bermudez H. Cell adhesion mechanisms on laterally mobile polymer films. *Biomaterials*. 2014;35(17):4827-34.
56. Bathawab F, Bennett M, Cantini M, Reboud J, Dalby MJ, Salmerón-Sánchez M. Lateral Chain Length in Polyalkyl Acrylates Determines the Mobility of Fibronectin at the Cell/Material Interface. *Langmuir*. 2016;32(3):800-9.

57. Liu R, Masters KS, Gellman SH. Polymer Chain Length Effects on Fibroblast Attachment on Nylon-3-Modified Surfaces. *Biomacromolecules*. 2012;13(4):1100-5.
58. Yu CH, Rafiq NB, Krishnasamy A, Hartman KL, Jones GE, Bershadsky AD, et al. Integrin-matrix clusters form podosome-like adhesions in the absence of traction forces. *Cell reports*. 2013;5(5):1456-68.
59. Kocer G, Jonkheijm P. Guiding hMSC Adhesion and Differentiation on Supported Lipid Bilayers. *Adv Healthc Mater*. 2017;6(3).
60. Seu KJ, Cambrea LR, Everly RM, Hovis JS. Influence of Lipid Chemistry on Membrane Fluidity: Tail and Headgroup Interactions. *Biophys J*. 2006;91(10):3727-35.
61. Seu KJ, Pandey AP, Haque F, Proctor EA, Ribbe AE, Hovis JS. Effect of surface treatment on diffusion and domain formation in supported lipid bilayers. *Biophys J*. 2007;92(7):2445-50.
62. Chaudhuri O, Gu L, Darnell M, Klumpers D, Bencherif SA, Weaver JC, et al. Substrate stress relaxation regulates cell spreading. *Nat Commun*. 2015;6:6364.
63. Mizutani A, Kikuchi A, Yamato M, Kanazawa H, Okano T. Preparation of thermoresponsive polymer brush surfaces and their interaction with cells. *Biomaterials*. 2008;29(13):2073-81.
64. Richter RP, Bérat R, Brisson AR. Formation of Solid-Supported Lipid Bilayers: An Integrated View. *Langmuir*. 2006;22(8):3497-505.
65. Yu CH, Groves JT. Engineering supported membranes for cell biology. *Medical & biological engineering & computing*. 2010;48(10):955-63.
66. Das C, Sheikh KH, Olmsted PD, Connell SD. Nanoscale mechanical probing of supported lipid bilayers with atomic force microscopy. *Phys Rev E*. 2010;82(4).
67. McMillan DGG, Marritt SJ, Firer-Sherwood MA, Shi L, Richardson DJ, Evans SD, et al. Protein-Protein Interaction Regulates the Direction of Catalysis and Electron Transfer in a Redox Enzyme Complex. *Journal of the American Chemical Society*. 2013;135(28):10550-6.
68. Tanaka M, Sackmann E. Polymer-supported membranes as models of the cell surface. *Nature*. 2005;437:656.
69. Rutishauser U, Sachs L. Receptor mobility and the binding of cells to lectin-coated fibers. *The Journal of cell biology*. 1975;66(1):76-85.

70. Rutishauser U, Sachs L. Receptor Mobility and the Mechanism of Cell-Cell Binding Induced by Concanavalin A. *Proceedings of the National Academy of Sciences*. 1974;71(6):2456-60.
71. Nicolson GL. TEMPERATURE-DEPENDENT MOBILITY OF CONCANAVALIN-A SITES ON TUMOR-CELL SURFACES. *Nature-New Biology*. 1973;243(128):218-20.
72. Mirzadeh H, Shokrolahi F, Daliri M. Effect of silicon rubber crosslink density on fibroblast cell behavior in vitro. *Journal of biomedical materials research Part A*. 2003;67(3):727-32.
73. Tugulu S, Silacci P, Stergiopoulos N, Klok HA. RGD-Functionalized polymer brushes as substrates for the integrin specific adhesion of human umbilical vein endothelial cells. *Biomaterials*. 2007;28(16):2536-46.
74. Andersson M, Suska F, Johansson A, Berglin M, Emanuelsson L, Elwing H, et al. Effect of molecular mobility of polymeric implants on soft tissue reactions: an in vivo study in rats. *Journal of biomedical materials research Part A*. 2008;84(3):652-60.
75. Hsu C-J, Hsieh W-T, Waldman A, Clarke F, Huseby ES, Burkhardt JK, et al. Ligand Mobility Modulates Immunological Synapse Formation and T Cell Activation. *PLoS ONE*. 2012;7(2):e32398.
76. Thid D, Bally M, Holm K, Chessari S, Tosatti S, Textor M, et al. Issues of ligand accessibility and mobility in initial cell attachment. *Langmuir*. 2007;23(23):11693-704.
77. Yu C-h, Rafiq NBM, Cao F, Zhou Y, Krishnasamy A, Biswas KH, et al. Integrin-beta3 clusters recruit clathrin-mediated endocytic machinery in the absence of traction force. *Nat Commun*. 2015;6.
78. Glazier R, Salaita K. Supported lipid bilayer platforms to probe cell mechanobiology. *Biochimica et biophysica acta*. 2017;1859(9 Pt A):1465-82.
79. Yu C-h, Law JBK, Suryana M, Low HY, Sheetz MP. Early integrin binding to Arg-Gly-Asp peptide activates actin polymerization and contractile movement that stimulates outward translocation. *Proceedings of the National Academy of Sciences*. 2011;108(51):20585-90.

80. Machesky L, Jurdic P, Hinz B. Grab, stick, pull and digest: the functional diversity of actin-associated matrix-adhesion structures. Workshop on Invadopodia, Podosomes and Focal Adhesions in Tissue Invasion. *EMBO Reports*. 2008;9(2):139-43.
81. Ge Y, Lin YH, Lautscham LA, Goldmann WH, Fabry B, Naumann CA. N-cadherin-functionalized polymer-tethered multi-bilayer: a cell surface-mimicking substrate to probe cellular mechanosensitivity. *Soft Matter*. 2016;12(40):8274-84.
82. Lautscham LA, Lin CY, Auernheimer V, Naumann CA, Goldmann WH, Fabry B. Biomembrane-mimicking lipid bilayer system as a mechanically tunable cell substrate. *Biomaterials*. 2014;35(10):3198-207.
83. Trappmann B, Gautrot JE, Connelly JT, Strange DGT, Li Y, Oyen ML, et al. Extracellular-matrix tethering regulates stem-cell fate. *Nat Mater*. 2012;11(7):642-9.
84. Wang N, Ingber DE. Control of cytoskeletal mechanics by extracellular matrix, cell shape, and mechanical tension. *Biophysical journal*. 1994;66(6):2181-9.
85. Engler AJ, Griffin MA, Sen S, Bönnemann CG, Sweeney HL, Discher DE. Myotubes differentiate optimally on substrates with tissue-like stiffness. *J Cell Biol*. 2004;166(6):877-87.
86. Pankov R, Yamada KM. Fibronectin at a glance. *J Cell Sci*. 2002;115(20):3861-3.
87. Yamada Y, Kleinman HK. Functional domains of cell adhesion molecules. *Curr Opin Cell Biol*. 1992;4(5):819-23.
88. Birk DE, Brückner P. Collagens, Suprastructures, and Collagen Fibril Assembly. In: Mecham RP, editor. *The Extracellular Matrix: an Overview*. Berlin, Heidelberg: Springer Berlin Heidelberg; 2011. p. 77-115.
89. Wojtowicz AM, Shekaran A, Oest ME, Dupont KM, Templeman KL, Hutmacher DW, et al. Coating of Biomaterial Scaffolds with the Collagen-Mimetic Peptide GFOGER for Bone Defect Repair. *Biomaterials*. 2010;31(9):2574.
90. Rowlands AS, George PA, Cooper-White JJ. Directing osteogenic and myogenic differentiation of MSCs: interplay of stiffness and adhesive ligand presentation. *American journal of physiology Cell physiology*. 2008;295(4):C1037-44.
91. Roca-Cusachs P, Gauthier NC, del Rio A, Sheetz MP. Clustering of $\alpha 5\beta 1$ integrins determines adhesion strength whereas $\alpha v\beta 3$ and talin enable mechanotransduction. *Proceedings of the National Academy of Sciences*. 2009;106(38):16245-50.

92. Breuss JM, Gallo J, DeLisser HM, Klimanskaya IV, Folkesson HG, Pittet JF, et al. Expression of the beta 6 integrin subunit in development, neoplasia and tissue repair suggests a role in epithelial remodeling. *J Cell Sci.* 1995;108 (Pt 6):2241-51.
93. Leiss M, Beckmann K, Giros A, Costell M, Fassler R. The role of integrin binding sites in fibronectin matrix assembly in vivo. *Curr Opin Cell Biol.* 2008;20(5):502-7.
94. Schultz GS, Wysocki A. Interactions between extracellular matrix and growth factors in wound healing. *Wound repair and regeneration : official publication of the Wound Healing Society [and] the European Tissue Repair Society.* 2009;17(2):153-62.
95. Martino MM, Tortelli F, Mochizuki M, Traub S, Ben-David D, Kuhn GA, et al. Engineering the Growth Factor Microenvironment with Fibronectin Domains to Promote Wound and Bone Tissue Healing. *Science Translational Medicine.* 2011;3(100):100ra89-ra89.
96. Martino MM, Hubbell JA. The 12th-14th type III repeats of fibronectin function as a highly promiscuous growth factor-binding domain. *Faseb J.* 2010;24(12):4711-21.
97. Carmeliet P, Jain RK. Molecular mechanisms and clinical applications of angiogenesis. *Nature.* 2011;473:298.
98. Brooks PC, Clark RA, Chersesh DA. Requirement of vascular integrin alpha v beta 3 for angiogenesis. *Science.* 1994;264(5158):569-71.
99. Allen MD, Thomas GJ, Clark S, Dawoud MM, Vallath S, Payne SJ, et al. Altered microenvironment promotes progression of preinvasive breast cancer: myoepithelial expression of alphavbeta6 integrin in DCIS identifies high-risk patients and predicts recurrence. *Clinical cancer research : an official journal of the American Association for Cancer Research.* 2014;20(2):344-57.
100. Zhang X, Jiang G, Cai Y, Monkley SJ, Critchley DR, Sheetz MP. Talin depletion reveals independence of initial cell spreading from integrin activation and traction. *Nat Cell Biol.* 2008;10:1062.
101. Hirata H, Tatsumi H, Sokabe M. Mechanical forces facilitate actin polymerization at focal adhesions in a zyxin-dependent manner. *J Cell Sci.* 2008;121(17):2795-804.
102. Moulisová V, Gonzalez-García C, Cantini M, Rodrigo-Navarro A, Weaver J, Costell M, et al. Engineered microenvironments for synergistic VEGF – Integrin signalling during vascularization. *Biomaterials.* 2017;126(Supplement C):61-74.

103. Margadant F, Chew LL, Hu X, Yu H, Bate N, Zhang X, et al. Mechanotransduction In Vivo by Repeated Talin Stretch-Relaxation Events Depends upon Vinculin. *PLOS Biology*. 2011;9(12):e1001223.
104. del Rio A, Perez-Jimenez R, Liu R, Roca-Cusachs P, Fernandez JM, Sheetz MP. Stretching Single Talin Rod Molecules Activates Vinculin Binding. *Science*. 2009;323(5914):638-41.
105. Geiger B. A 130K protein from chicken gizzard: Its localization at the termini of microfilament bundles in cultured chicken cells. *Cell*. 1979;18(1):193-205.
106. Cohen DM, Kutscher B, Chen H, Murphy DB, Craig SW. A conformational switch in vinculin drives formation and dynamics of a talin-vinculin complex at focal adhesions. *The Journal of biological chemistry*. 2006;281(23):16006-15.
107. Chen H, Choudhury DM, Craig SW. Coincidence of Actin Filaments and Talin Is Required to Activate Vinculin. *J Biol Chem*. 2006;281(52):40389-98.
108. Goldmann WH, Galneder R, Ludwig M, Xu W, Adamson ED, Wang N, et al. Differences in Elasticity of Vinculin-Deficient F9 Cells Measured by Magnetometry and Atomic Force Microscopy. *Experimental Cell Research*. 1998;239(2):235-42.
109. Gallant ND, Michael KE, García AJ. Cell Adhesion Strengthening: Contributions of Adhesive Area, Integrin Binding, and Focal Adhesion Assembly. *Mol Biol Cell*. 2005;16(9):4329-40.
110. Pasapera AM, Schneider IC, Rericha E, Schlaepfer DD, Waterman CM. Myosin II activity regulates vinculin recruitment to focal adhesions through FAK-mediated paxillin phosphorylation. *The Journal of Cell Biology*. 2010;188(6):877-90.
111. Holmes KC. Actin in a twist. *Nature*. 2009;457:389.
112. Pollard TD, Cooper JA. Actin, a Central Player in Cell Shape and Movement. *Science*. 2009;326(5957):1208-12.
113. Yoshigi M, Hoffman LM, Jensen CC, Yost HJ, Beckerle MC. Mechanical force mobilizes zyxin from focal adhesions to actin filaments and regulates cytoskeletal reinforcement. *J Cell Biol*. 2005;171(2):209-15.
114. Case LB, Waterman CM. Integration of actin dynamics and cell adhesion by a three-dimensional, mechanosensitive molecular clutch. *Nat Cell Biol*. 2015;17:955.

115. Chan CE, Odde DJ. Traction Dynamics of Filopodia on Compliant Substrates. *Science*. 2008;322(5908):1687-91.
116. Mitchison T, Kirschner M. Cytoskeletal dynamics and nerve growth. *Neuron*. 1988;1(9):761-72.
117. Chan CE, Odde DJ. Traction dynamics of filopodia on compliant substrates. *Science*. 2008;322(5908):1687-91.
118. Elosegui-Artola A, Bazellières E, Allen MD, Andreu I, Oria R, Sunyer R, et al. Rigidity sensing and adaptation through regulation of integrin types. *Nat Mater*. 2014;13(6):631-7.
119. Bae YH, Mui KL, Hsu BY, Liu SL, Cretu A, Razinia Z, et al. A FAK-Cas-Rac-lamellipodin signaling module transduces extracellular matrix stiffness into mechanosensitive cell cycling. *Science signaling*. 2014;7(330):ra57.
120. Westhoff MA, Serrels B, Fincham VJ, Frame MC, Carragher NO. Src-Mediated Phosphorylation of Focal Adhesion Kinase Couples Actin and Adhesion Dynamics to Survival Signaling. *Molecular and Cellular Biology*. 2004;24(18):8113-33.
121. Burridge K, Wennerberg K. Rho and Rac take center stage. *Cell*. 2004;116(2):167-79.
122. Dubash AD, Wennerberg K, García-Mata R, Menold MM, Arthur WT, Burridge K. A novel role for Lsc/p115 RhoGEF and LARG in regulating RhoA activity downstream of adhesion to fibronectin. *J Cell Sci*. 2007;120(22):3989-98.
123. Kimura K, Ito M, Amano M, Chihara K, Fukata Y, Nakafuku M, et al. Regulation of myosin phosphatase by Rho and Rho-associated kinase (Rho-kinase). *Science*. 1996;273(5272):245-8.
124. Meng Z, Moroishi T, Guan K-L. Mechanisms of Hippo pathway regulation. *Genes & Development*. 2016;30(1):1-17.
125. Benham-Pyle BW, Pruitt BL, Nelson WJ. Mechanical strain induces E-cadherin-dependent Yap1 and β -catenin activation to drive cell cycle entry. *Science*. 2015;348(6238):1024-7.
126. Aragona M, Panciera T, Manfrin A, Giulitti S, Michielin F, Elvassore N, et al. A Mechanical Checkpoint Controls Multicellular Growth through YAP/TAZ Regulation by Actin-Processing Factors. *Cell*. 2013;154(5):1047-59.

127. Varelas X. The Hippo pathway effectors TAZ and YAP in development, homeostasis and disease. *Development*. 2014;141(8):1614-26.
128. Moroishi T, Hansen CG, Guan K-L. The emerging roles of YAP and TAZ in cancer. *Nature Reviews Cancer*. 2015;15:73.
129. Zhao B, Li L, Lei Q, Guan K-L. The Hippo–YAP pathway in organ size control and tumorigenesis: an updated version. *Genes & Development*. 2010;24(9):862-74.
130. Oreffo ROC, Cooper C, Mason C, Clements M. Mesenchymal stem cells. *Stem Cell Reviews*. 2005;1(2):169-78.
131. Israelachvili JN, Mitchell DJ, Ninham BW. Theory of self-assembly of lipid bilayers and vesicles. *Biochimica et Biophysica Acta (BBA) - Biomembranes*. 1977;470(2):185-201.
132. Singer SJ, Nicolson GL. The fluid mosaic model of the structure of cell membranes. *Science*. 1972;175(4023):720-31.
133. Pike LJ. Lipid rafts: bringing order to chaos. *Journal of lipid research*. 2003;44(4):655-67.
134. Martinez MC, Freyssinet JM. Deciphering the plasma membrane hallmarks of apoptotic cells: phosphatidylserine transverse redistribution and calcium entry. *BMC cell biology*. 2001;2:20.
135. Gambin Y, Lopez-Esparza R, Reffay M, Sierrecki E, Gov NS, Genest M, et al. Lateral mobility of proteins in liquid membranes revisited. *Proc Natl Acad Sci U S A*. 2006;103(7):2098-102.
136. Nagle JF. Theory of lipid monolayer and bilayer phase transitions: effect of headgroup interactions. *The Journal of membrane biology*. 1976;27(3):233-50.
137. Marsh D. Analysis of the chainlength dependence of lipid phase transition temperatures: Main and pretransitions of phosphatidylcholines; main and non-lamellar transitions of phosphatidylethanolamines. *Biochimica et Biophysica Acta (BBA) - Biomembranes*. 1991;1062(1):1-6.
138. Cevc G. How membrane chain-melting phase-transition temperature is affected by the lipid chain asymmetry and degree of unsaturation: an effective chain-length model. *Biochemistry*. 1991;30(29):7186-93.

139. Charrier A, Thibaudau F. Main phase transitions in supported lipid single-bilayer. *Biophys J*. 2005;89(2):1094-101.
140. Castellana ET, Cremer PS. Solid supported lipid bilayers: From biophysical studies to sensor design. *Surface Science Reports*. 2006;61(10):429-44.
141. Marin V, Kieffer R, Padmos R, Aubin-Tam M-E. Stable Free-Standing Lipid Bilayer Membranes in Norland Optical Adhesive 81 Microchannels. *Analytical Chemistry*. 2016;88(15):7466-70.
142. Han X, Studer A, Sehr H, Geissbühler I, Di Berardino M, Winkler FK, et al. Nanopore arrays for stable and functional free-standing lipid bilayers. *Advanced Materials*. 2007;19(24):4466-70.
143. Block S, Zhdanov VP, Höök F. Quantification of multivalent interactions by tracking single biological nanoparticle mobility on a lipid membrane. *Nano letters*. 2016;16(7):4382-90.
144. Block S, Fast BJ, Lundgren A, Zhdanov VP, Höök F. Two-dimensional flow nanometry of biological nanoparticles for accurate determination of their size and emission intensity. *Nature Communications*. 2016;7:12956.
145. Reimhult E, Hook F, Kasemo B. Intact vesicle adsorption and supported biomembrane formation from vesicles in solution: Influence of surface chemistry, vesicle size, temperature, and osmotic pressure. *Langmuir*. 2003;19(5):1681-91.
146. Reviakine I, Brisson A. Formation of Supported Phospholipid Bilayers from Unilamellar Vesicles Investigated by Atomic Force Microscopy. *Langmuir*. 2000;16(4):1806-15.
147. Reimhult E, Hook F, Kasemo B. Vesicle adsorption on SiO₂ and TiO₂: Dependence on vesicle size. *J Chem Phys*. 2002;117(16):7401-4.
148. Richter R, Mukhopadhyay A, Brisson A. Pathways of Lipid Vesicle Deposition on Solid Surfaces: A Combined QCM-D and AFM Study. *Biophys J*. 2003;85(5):3035-47.
149. Cha T, Guo A, Zhu XY. Formation of Supported Phospholipid Bilayers on Molecular Surfaces: Role of Surface Charge Density and Electrostatic Interaction. *Biophysical Journal*. 2006;90(4):1270-4.

150. Cho N-J, Frank CW, Kasemo B, Hook F. Quartz crystal microbalance with dissipation monitoring of supported lipid bilayers on various substrates. *Nat Protocols*. 2010;5(6):1096-106.
151. Przybylo M, Sýkora J, Humpolíčková J, Benda A, Zan A, Hof M. Lipid Diffusion in Giant Unilamellar Vesicles Is More than 2 Times Faster than in Supported Phospholipid Bilayers under Identical Conditions. *Langmuir*. 2006;22(22):9096-9.
152. Seeger H, Marino G, Alessandrini A, Facci P. Effect of physical parameters on the main phase transition of supported lipid bilayers. *Biophys J*. 2009;97(4):1067-76.
153. Zhang L, Granick S. Lipid diffusion compared in outer and inner leaflets of planar supported bilayers. *The Journal of chemical physics*. 2005;123(21):211104.
154. Jackman J, Knoll W, Cho N-J. Biotechnology Applications of Tethered Lipid Bilayer Membranes. *Materials*. 2012;5(12):2637.
155. Saffman PG, Delbrück M. Brownian motion in biological membranes. *Proceedings of the National Academy of Sciences*. 1975;72(8):3111-3.
156. Hughes BD, Pailthorpe BA, White LR. The translational and rotational drag on a cylinder moving in a membrane. *Journal of Fluid Mechanics*. 2006;110:349-72.
157. Petrov EP, Schwille P. Translational Diffusion in Lipid Membranes beyond the Saffman-Delbrück Approximation. *Biophys J*. 2008;94(5):L41-L3.
158. Afanasenkau D, Offenhausser A. Positively Charged Supported Lipid Bilayers as a Biomimetic Platform for Neuronal Cell Culture. *Langmuir*. 2012;28(37):13387-94.
159. Ananthanarayanan B, Little L, Schaffer DV, Healy KE, Tirrell M. Neural stem cell adhesion and proliferation on phospholipid bilayers functionalized with RGD peptides. *Biomaterials*. 2010;31(33):8706-15.
160. Andersson AS, Glasmaster K, Sutherland D, Lidberg U, Kasemo B. Cell adhesion on supported lipid bilayers. *J Biomed Mater Res Part A*. 2003;64A(4):622-9.
161. Andreasson-Ochsner M, Romano G, Hakanson M, Smith ML, Leckband DE, Textor M, et al. Single cell 3-D platform to study ligand mobility in cell-cell contact. *Lab Chip*. 2011;11(17):2876-83.

162. Oliver AE, Ngassam V, Dang P, Sanii B, Wu H, Yee CK, et al. Cell Attachment Behavior on Solid and Fluid Substrates Exhibiting Spatial Patterns of Physical Properties. *Langmuir*. 2009;25(12):6992-6.
163. Ivanova OY, Margolis LB. The Use of Phospholipid Film for Shaping Cell Cultures. *Nature*. 1973;242(5394):200-1.
164. Nguyen TT, Sly KL, Conboy JC. Comparison of the Energetics of Avidin, Streptavidin, NeutrAvidin, and Anti-Biotin Antibody Binding to Biotinylated Lipid Bilayer Examined by Second-Harmonic Generation. *Analytical Chemistry*. 2012;84(1):201-8.
165. Huang C-J, Cho N-J, Hsu C-J, Tseng P-Y, Frank CW, Chang Y-C. Type I Collagen-Functionalized Supported Lipid Bilayer as a Cell Culture Platform. *Biomacromolecules*. 2010;11(5):1231-40.
166. Stabley D, Retterer S, Marshall S, Salaita K. Manipulating the Lateral Diffusion of Surface-Anchored EGF Demonstrates that Receptor Clustering Modulates Phosphorylation Levels. *Integrative biology : quantitative biosciences from nano to macro*. 2013;5(4):659-68.
167. Yoshina-Ishii C, Boxer SG. Arrays of Mobile Tethered Vesicles on Supported Lipid Bilayers. *Journal of the American Chemical Society*. 2003;125(13):3696-7.
168. Shen K, Tsai J, Shi P, Kam LC. Self-Aligned Supported Lipid Bilayers for Patterning the Cell-Substrate Interface. *Journal of the American Chemical Society*. 2009;131(37):13204-5.
169. Perez TD, Nelson WJ, Boxer SG, Kam L. E-cadherin tethered to micropatterned supported lipid bilayers as a model for cell adhesion. *Langmuir : the ACS journal of surfaces and colloids*. 2005;21(25):11963-8.
170. Gumbiner BM. Regulation of cadherin-mediated adhesion in morphogenesis. *Nat Rev Mol Cell Biol*. 2005;6:622.
171. Berat R, Remy-Zolghadry M, Gounou C, Manigand C, Tan S, Salto C, et al. Peptide-presenting two-dimensional protein matrix on supported lipid bilayers: An efficient platform for cell adhesion. *Biointerphases*. 2007;2(4):165-72.
172. Zhu X, Wang Z, Zhao A, Huang N, Chen H, Zhou S, et al. Cell adhesion on supported lipid bilayers functionalized with RGD peptides monitored by using a quartz crystal microbalance with dissipation. *Colloids and Surfaces B: Biointerfaces*. 2014;116:459-64.

173. Tseng PY, Chang YC. Tethered Fibronectin Liposomes on Supported Lipid Bilayers as a Prepackaged Controlled-Release Platform for Cell-Based Assays. *Biomacromolecules*. 2012;13(8):2254-62.
174. Ma VP-Y, Liu Y, Blanchfield L, Su H, Evavold BD, Salaita K. Ratiometric Tension Probes for Mapping Receptor Forces and Clustering at Intermembrane Junctions. *Nano Letters*. 2016;16(7):4552-9.
175. Changede R, Xu X, Margadant F, Sheetz Michael P. Nascent Integrin Adhesions Form on All Matrix Rigidities after Integrin Activation. *Developmental Cell*. 35(5):614-21.
176. Seifert U, Berndl K, Lipowsky R. Shape transformations of vesicles: Phase diagram for spontaneous- curvature and bilayer-coupling models. *Physical Review A*. 1991;44(2):1182-202.
177. Attwood S, Choi Y, Leonenko Z. Preparation of DOPC and DPPC Supported Planar Lipid Bilayers for Atomic Force Microscopy and Atomic Force Spectroscopy. *International Journal of Molecular Sciences*. 2013;14(2):3514-39.
178. Lipids AP. Mini-Extruder Assembly Instructions [Available from: <https://avantilipids.com/divisions/equipment/mini-extruder-assembly-instructions/>].
179. Seantier B, Kasemo B. Influence of mono- and divalent ions on the formation of supported phospholipid bilayers via vesicle adsorption. *Langmuir*. 2009;25(10):5767-72.
180. Galush WJ, Nye JA, Groves JT. Quantitative Fluorescence Microscopy Using Supported Lipid Bilayer Standards. *Biophys J*. 2008;95(5):2512-9.
181. Vacklin HP, Tiberg F, Thomas RK. Formation of supported phospholipid bilayers via co-adsorption with beta-D-dodecyl maltoside. *Biochimica et biophysica acta*. 2005;1668(1):17-24.
182. Redick SD, Settles DL, Briscoe G, Erickson HP. Defining Fibronectin's Cell Adhesion Synergy Site by Site-Directed Mutagenesis. *The Journal of Cell Biology*. 2000;149(2):521-7.
183. Fisher T. EZ-Link™ Micro Sulfo-NHS-LC-Biotinylation Kit 2017 [Available from: <https://www.thermofisher.com/order/catalog/product/21935>].
184. Nair PM, Salaita K, Petit RS, Groves JT. Using patterned supported lipid membranes to investigate the role of receptor organization in intercellular signaling. *Nat Protocols*. 2011;6(4):523-39.

185. Edelstein A, Amodaj N, Hoover K, Vale R, Stuurman N. Computer Control of Microscopes Using μ Manager. *Current Protocols in Molecular Biology*: John Wiley & Sons, Inc.; 2001.
186. Schindelin J, Arganda-Carreras I, Frise E, Kaynig V, Longair M, Pietzsch T, et al. Fiji: an open-source platform for biological-image analysis. *Nat Methods*. 2012;9(7):676-82.
187. Selinummi J, Seppala J, Yli-Harja O, Puhakka JA. Software for quantification of labeled bacteria from digital microscope images by automated image analysis. *BioTechniques*. 2005;39(6):859-63.
188. Horzum U, Ozdil B, Pesen-Okvur D. Step-by-step quantitative analysis of focal adhesions. *MethodsX*. 2014;1(Supplement C):56-9.
189. Binnig G, Quate CF, Gerber C. Atomic Force Microscope. *Phys Rev Lett*. 1986;56(9):930-3.
190. Piner RD, Zhu J, Xu F, Hong S, Mirkin CA. "Dip-Pen" Nanolithography. *Science*. 1999;283(5402):661-3.
191. Gross L. Recent advances in submolecular resolution with scanning probe microscopy. *Nat Chem*. 2011;3(4):273-8.
192. Schönherr H, Johnson JM, Lenz P, Frank CW, Boxer SG. Vesicle Adsorption and Lipid Bilayer Formation on Glass Studied by Atomic Force Microscopy. *Langmuir*. 2004;20(26):11600-6.
193. Alessandrini A, Facci P. Phase transitions in supported lipid bilayers studied by AFM. *Soft Matter*. 2014;10(37):7145-64.
194. Garcia-Manyes S, Sanz F. Nanomechanics of lipid bilayers by force spectroscopy with AFM: A perspective. *Biochimica et Biophysica Acta (BBA) - Biomembranes*. 2010;1798(4):741-9.
195. Picas L, Rico F, Scheuring S. Direct Measurement of the Mechanical Properties of Lipid Phases in Supported Bilayers. *Biophys J*. 2012;102(1):L01-L3.
196. Magde D, Elson EL, Webb WW. Fluorescence Correlation Spectroscopy .2. Experimental Realization. *Biopolymers*. 1974;13(1):29-61.

197. Rigler R, Mets U, Widengren J, Kask P. Fluorescence Correlation Spectroscopy with High Count Rate and Low-Background - Analysis of Translational Diffusion. *Eur Biophys J Biophys*. 1993;22(3):169-75.
198. Eigen M, Rigler R. Sorting single molecules: application to diagnostics and evolutionary biotechnology. *Proceedings of the National Academy of Sciences*. 1994;91(13):5740-7.
199. Kim SA, Heinze KG, Schwille P. Fluorescence correlation spectroscopy in living cells. *Nature methods*. 2007;4(11):963-73.
200. Yu SR, Burkhardt M, Nowak M, Ries J, Petrasek Z, Scholpp S, et al. Fgf8 morphogen gradient forms by a source-sink mechanism with freely diffusing molecules. *Nature*. 2009;461(7263):533-6.
201. Ries J, Yu SR, Burkhardt M, Brand M, Schwille P. Modular scanning FCS quantifies receptor-ligand interactions in living multicellular organisms. *Nature methods*. 2009;6(9):643-5.
202. Salaita K, Nair PM, Petit RS, Neve RM, Das D, Gray JW, et al. Restriction of Receptor Movement Alters Cellular Response: Physical Force Sensing by EphA2. *Science*. 2010;327(5971):1380-5.
203. Endres Nicholas F, Das R, Smith Adam W, Arkhipov A, Kovacs E, Huang Y, et al. Conformational Coupling across the Plasma Membrane in Activation of the EGF Receptor. *Cell*. 2013;152(3):543-56.
204. Zhang Y, Ge C, Zhu C, Salaita K. DNA-based digital tension probes reveal integrin forces during early cell adhesion. *Nature communications*. 2014;5.
205. Ladha S, Mackie AR, Harvey LJ, Clark DC, Lea EJ, Brullemans M, et al. Lateral diffusion in planar lipid bilayers: a fluorescence recovery after photobleaching investigation of its modulation by lipid composition, cholesterol, or alamethicin content and divalent cations. *Biophys J*. 1996;71(3):1364-73.
206. Patching SG. Surface plasmon resonance spectroscopy for characterisation of membrane protein–ligand interactions and its potential for drug discovery. *Biochimica et Biophysica Acta (BBA) - Biomembranes*. 2014;1838(1, Part A):43-55.

207. Stroumpoulis D, Parra A, Tirrell M. A kinetic study of vesicle fusion on silicon dioxide surfaces by ellipsometry. *AIChE Journal*. 2006;52(8):2931-7.
208. Mayer LD, Hope MJ, Cullis PR. Vesicles of variable sizes produced by a rapid extrusion procedure. *Biochimica et biophysica acta*. 1986;858(1):161-8.
209. Hunter DG, Frisken BJ. Effect of Extrusion Pressure and Lipid Properties on the Size and Polydispersity of Lipid Vesicles. *Biophys J*. 1998;74(6):2996-3002.
210. Richter RP, Brisson A. Characterization of Lipid Bilayers and Protein Assemblies Supported on Rough Surfaces by Atomic Force Microscopy. *Langmuir*. 2003;19(5):1632-40.
211. Lewis BA, Engelman DM. Lipid bilayer thickness varies linearly with acyl chain length in fluid phosphatidylcholine vesicles. *J Mol Biol*. 1983;166(2):211-7.
212. Ries J, Schwille P. Fluorescence correlation spectroscopy. *Bioessays*. 2012;34(5):361-8.
213. Przybylo M, Sykora J, Humpolickova J, Benda A, Zan A, Hof M. Lipid diffusion in giant unilamellar vesicles is more than 2 times faster than in supported phospholipid bilayers under identical conditions. *Langmuir*. 2006;22(22):9096-9.
214. Stanich CA, Honerkamp-Smith AR, Putzel GG, Warth CS, Lamprecht AK, Mandal P, et al. Coarsening dynamics of domains in lipid membranes. *Biophys J*. 2013;105(2):444-54.
215. Herold C, Schwille P, Petrov EP. DNA condensation at freestanding cationic lipid bilayers. *Phys Rev Lett*. 2010;104(14):148102.
216. Mills TT, Huang J, Feigenson GW, Nagle JF. Effects of cholesterol and unsaturated DOPC lipid on chain packing of saturated gel-phase DPPC bilayers. *General physiology and biophysics*. 2009;28(2):126-39.
217. Zeng X, Xu G, Gao Y, An Y. Surface Wettability of (3-Aminopropyl)triethoxysilane Self-Assembled Monolayers. *The Journal of Physical Chemistry B*. 2011;115(3):450-4.
218. Nagle JF, Tristram-Nagle S. Structure of lipid bilayers. *Biochimica et biophysica acta*. 2000;1469(3):159-95.
219. Livnah O, Bayer EA, Wilchek M, Sussman JL. Three-dimensional structures of avidin and the avidin-biotin complex. *Proc Natl Acad Sci U S A*. 1993;90(11):5076-80.
220. Xiong J-P, Stehle T, Diefenbach B, Zhang R, Dunker R, Scott DL, et al. Crystal Structure of the Extracellular Segment of Integrin $\alpha V\beta 3$. *Science*. 2001;294(5541):339-45.

221. Möller I, Seeger S. Solid supported lipid bilayers from artificial and natural lipid mixtures—long-term stable, homogeneous and reproducible. *Journal of Materials Chemistry B*. 2015;3(29):6046-56.
222. Frantz C, Stewart KM, Weaver VM. The extracellular matrix at a glance. *J Cell Sci*. 2010;123(24):4195-200.
223. Plow EF, Haas TA, Zhang L, Loftus J, Smith JW. Ligand Binding to Integrins. *J Biol Chem*. 2000;275(29):21785-8.
224. Taipale J, Keski-Oja J. Growth factors in the extracellular matrix. *The FASEB Journal*. 1997;11(1):51-9.
225. Lo CM, Wang HB, Dembo M, Wang YL. Cell movement is guided by the rigidity of the substrate. *Biophys J*. 2000;79(1):144-52.
226. Yeung T, Georges PC, Flanagan LA, Marg B, Ortiz M, Funaki M, et al. Effects of substrate stiffness on cell morphology, cytoskeletal structure, and adhesion. *Cell Motil Cytoskel*. 2005;60(1):24-34.
227. Chaudhuri O, Gu L, Klumpers D, Darnell M, Bencherif SA, Weaver JC, et al. Hydrogels with tunable stress relaxation regulate stem cell fate and activity. *Nat Mater*. 2016;15(3):326-34.
228. Cantini M, Gonzalez-Garcia C, Llopis-Hernandez V, Salmeron-Sanchez M. Material-Driven Fibronectin Fibrillogenesis. In: Horbett T, Brash JL, Norde W, editors. *Proteins at Interfaces Iii: State of the Art*. ACS Symposium Series. 1120. Washington: Amer Chemical Soc; 2012. p. 471-96.
229. Salmeron-Sanchez M, Rico P, Moratal D, Lee TT, Schwarzbauer JE, Garcia AJ. Role of material-driven fibronectin fibrillogenesis in cell differentiation. *Biomaterials*. 2011;32(8):2099-105.
230. Llopis-Hernandez V, Cantini M, Gonzalez-Garcia C, Cheng ZA, Yang J, Tsimbouri PM, et al. Material-driven fibronectin assembly for high-efficiency presentation of growth factors. *Science advances*. 2016;2(8):e1600188.
231. Thakar D, Dalonneau F, Migliorini E, Lortat-Jacob H, Boturyn D, Albiges-Rizo C, et al. Binding of the chemokine CXCL12alpha to its natural extracellular matrix ligand heparan sulfate enables myoblast adhesion and facilitates cell motility. *Biomaterials*. 2017;123:24-38.

232. Margolis LB, Vasilieva EJ, Vasiliev JM, Gelfand IM. Upper surfaces of epithelial sheets and of fluid lipid films are nonadhesive for platelets. *Proc Natl Acad Sci U S A*. 1979;76(5):2303-5.
233. Andersson A-S, Glasmästar K, Sutherland D, Lidberg U, Kasemo B. Cell adhesion on supported lipid bilayers. *J Biomed Mater Res Part A*. 2003;64A(4):622-9.
234. Pierschbacher MD, Ruoslahti E. Influence of stereochemistry of the sequence Arg-Gly-Asp-Xaa on binding specificity in cell adhesion. *The Journal of biological chemistry*. 1987;262(36):17294-8.
235. Kuhlman W, Taniguchi I, Griffith LG, Mayes AM. Interplay between PEO tether length and ligand spacing governs cell spreading on RGD-modified PMMA-g-PEO comb copolymers. *Biomacromolecules*. 2007;8(10):3206-13.
236. Endlich N, Otey CA, Kriz W, Endlich K. Movement of stress fibers away from focal adhesions identifies focal adhesions as sites of stress fiber assembly in stationary cells. *Cell Motil Cytoskel*. 2007;64(12):966-76.
237. Hynes RO. Integrins: Bidirectional, Allosteric Signaling Machines. *Cell*. 2002;110(6):673-87.
238. Burridge K, Guilluy C. Focal adhesions, stress fibers and mechanical tension. *Experimental Cell Research*. 2016;343(1):14-20.
239. Goffin JM, Pittet P, Csucs G, Lussi JW, Meister J-J, Hinz B. Focal adhesion size controls tension-dependent recruitment of α -smooth muscle actin to stress fibers. *J Cell Biol*. 2006;172(2):259-68.
240. Han Sangyoon J, Bielawski Kevin S, Ting Lucas H, Rodriguez Marita L, Sniadecki Nathan J. Decoupling Substrate Stiffness, Spread Area, and Micropost Density: A Close Spatial Relationship between Traction Forces and Focal Adhesions. *Biophys J*. 2012;103(4):640-8.
241. Weng S, Fu J. Synergistic regulation of cell function by matrix rigidity and adhesive pattern. *Biomaterials*. 2011;32(36):9584-93.
242. Geiger B, Bershadsky A, Pankov R, Yamada KM. Transmembrane crosstalk between the extracellular matrix and the cytoskeleton. *Nat Rev Mol Cell Biol*. 2001;2(11):793-805.

243. Kioka N, Sakata S, Kawauchi T, Amachi T, Akiyama SK, Okazaki K, et al. Vinexin: a novel vinculin-binding protein with multiple SH3 domains enhances actin cytoskeletal organization. *J Cell Biol.* 1999;144(1):59-69.
244. DeMali KA, Barlow CA, Burridge K. Recruitment of the Arp2/3 complex to vinculin: coupling membrane protrusion to matrix adhesion. *J Cell Biol.* 2002;159(5):881-91.
245. Yao M, Goult BT, Chen H, Cong P, Sheetz MP, Yan J. Mechanical activation of vinculin binding to talin locks talin in an unfolded conformation. *Scientific Reports.* 2014;4:4610.
246. Dumbauld DW, Garcia AJ. A helping hand: How vinculin contributes to cell-matrix and cell-cell force transfer. *Cell adhesion & migration.* 2014;8(6):550-7.
247. Grashoff C, Hoffman BD, Brenner MD, Zhou R, Parsons M, Yang MT, et al. Measuring mechanical tension across vinculin reveals regulation of focal adhesion dynamics. *Nature.* 2010;466(7303):263-6.
248. Ezzell RM, Goldmann WH, Wang N, Parasharama N, Ingber DE. Vinculin Promotes Cell Spreading by Mechanically Coupling Integrins to the Cytoskeleton. *Experimental Cell Research.* 1997;231(1):14-26.
249. Case LB, Baird MA, Shtengel G, Campbell SL, Hess HF, Davidson MW, et al. Molecular mechanism of vinculin activation and nanoscale spatial organization in focal adhesions. *Nat Cell Biol.* 2015;17(7):880-92.
250. Brindle NP, Holt MR, Davies JE, Price CJ, Critchley DR. The focal-adhesion vasodilator-stimulated phosphoprotein (VASP) binds to the proline-rich domain in vinculin. *The Biochemical journal.* 1996;318 (Pt 3):753-7.
251. Goldmann WH, Ingber DE. Intact Vinculin Protein Is Required for Control of Cell Shape, Cell Mechanics, and rac-Dependent Lamellipodia Formation. *Biochem Biophys Res Commun.* 2002;290(2):749-55.
252. Mitra SK, Hanson DA, Schlaepfer DD. Focal adhesion kinase: in command and control of cell motility. *Nat Rev Mol Cell Biol.* 2005;6(1):56-68.
253. Deverall MA, Gindl E, Sinner EK, Besir H, Ruehe J, Saxton MJ, et al. Membrane Lateral Mobility Obstructed by Polymer-Tethered Lipids Studied at the Single Molecule Level. *Biophys J.* 2005;88(3):1875-86.

254. Kovács M, Tóth J, Hetényi C, Málnási-Csizmadia A, Sellers JR. Mechanism of Blebbistatin Inhibition of Myosin II. *J Biol Chem*. 2004;279(34):35557-63.
255. Grashoff C, Hoffman BD, Brenner MD, Zhou R, Parsons M, Yang MT, et al. Measuring mechanical tension across vinculin reveals regulation of focal adhesion dynamics. *Nature*. 2010;466(7303):263-6.
256. Humphries JD, Wang P, Streuli C, Geiger B, Humphries MJ, Ballestrem C. Vinculin controls focal adhesion formation by direct interactions with talin and actin. *The Journal of Cell Biology*. 2007;179(5):1043-57.
257. Kress H, Stelzer EHK, Holzer D, Buss F, Griffiths G, Rohrbach A. Filopodia act as phagocytic tentacles and pull with discrete steps and a load-dependent velocity. *Proc Natl Acad Sci U S A*. 2007;104(28):11633-8.
258. Thievensen I, Thompson PM, Berlemont S, Plevock KM, Plotnikov SV, Zemljic-Harpf A, et al. Vinculin–actin interaction couples actin retrograde flow to focal adhesions, but is dispensable for focal adhesion growth. *The Journal of Cell Biology*. 2013;202(1):163-77.
259. Van Goor D, Hyland C, Schaefer AW, Forscher P. The Role of Actin Turnover in Retrograde Actin Network Flow in Neuronal Growth Cones. *PLOS ONE*. 2012;7(2):e30959.
260. Oria R WT, Escribano J, Elosegui-Artola A, Uriarte JJ, Moreno-Pulido C, Platzman I, Delcanale P, Albertazzi L, Navajas D, Trepas X, García-Aznar JM, Cavalcanti-Adam EA, Roca-Cusachs P Force loading explains cell spatial sensing of ligands. *Nature*. 2017;In press.
261. Schwartzman M, Palma M, Sable J, Abramson J, Hu X, Sheetz MP, et al. Nanolithographic Control of the Spatial Organization of Cellular Adhesion Receptors at the Single-Molecule Level. *Nano Lett*. 2011;11(3):1306-12.
262. Hansen CG, Moroishi T, Guan K-L. YAP and TAZ: a nexus for Hippo signaling and beyond. *Trends in cell biology*. 2015;25(9):499-513.
263. Cho S, Irianto J, Discher DE. Mechanosensing by the nucleus: From pathways to scaling relationships. *The Journal of Cell Biology*. 2017;216(2):305-15.
264. Wada K-I, Itoga K, Okano T, Yonemura S, Sasaki H. Hippo pathway regulation by cell morphology and stress fibers. *Development*. 2011;138(18):3907-14.

265. Elosegui-Artola A, Andreu I, Beedle AEM, Lezamiz A, Uroz M, Kosmalka AJ, et al. Force Triggers YAP Nuclear Entry by Regulating Transport across Nuclear Pores. *Cell*. 2017;171(6):1397-410.e14.
266. Sun Y, Yong KMA, Villa-Diaz LG, Zhang X, Chen W, Philson R, et al. Hippo/YAP-mediated rigidity-dependent motor neuron differentiation of human pluripotent stem cells. *Nat Mater*. 2014;13(6):599-604.
267. Rajan S, Dang HCP, Djambazian H, Zuzan H, Fedyshyn Y, Ketela T, et al. Analysis of early C2C12 myogenesis identifies stably and differentially expressed transcriptional regulators whose knock-down inhibits myoblast differentiation. *Physiological Genomics*. 2012;44(2):183-97.
268. Engler AJ, Griffin MA, Sen S, Bönnemann CG, Sweeney HL, Discher DE. Myotubes differentiate optimally on substrates with tissue-like stiffness: pathological implications for soft or stiff microenvironments. *The Journal of Cell Biology*. 2004;166(6):877-87.
269. Ferri P, Barbieri E, Burattini S, Guescini M, D'Emilio A, Biagiotti L, et al. Expression and subcellular localization of myogenic regulatory factors during the differentiation of skeletal muscle C2C12 myoblasts. *Journal of cellular biochemistry*. 2009;108(6):1302-17.
270. Watt KI, Judson R, Medlow P, Reid K, Kurth TB, Burniston JG, et al. Yap is a novel regulator of C2C12 myogenesis. *Biochem Biophys Res Commun*. 2010;393(4):619-24.
271. Tomczak KK, Marinescu VD, Ramoni MF, Sanoudou D, Montanaro F, Han M, et al. Expression profiling and identification of novel genes involved in myogenic differentiation. *Faseb J*. 2004;18(2):403-5.
272. Bianco P, Robey PG, Simmons PJ. Mesenchymal Stem Cells: Revisiting History, Concepts, and Assays. *Cell stem cell*. 2008;2(4):313-9.
273. Pittenger MF, Mackay AM, Beck SC, Jaiswal RK, Douglas R, Mosca JD, et al. Multilineage potential of adult human mesenchymal stem cells. *Science*. 1999;284(5411):143-7.
274. Jaiswal N, Haynesworth SE, Caplan AI, Bruder SP. Osteogenic differentiation of purified, culture-expanded human mesenchymal stem cells in vitro. *Journal of cellular biochemistry*. 1997;64(2):295-312.

275. Castelo-Branco G, Rawal N, Arenas E. GSK-3 β inhibition/ β -catenin stabilization in ventral midbrain precursors increases differentiation into dopamine neurons. *J Cell Sci.* 2004;117(Pt 24):5731-7.
276. Dalby MJ, García AJ, Salmeron-Sanchez M. Receptor control in mesenchymal stem cell engineering. *Nature Reviews Materials.* 2018;3:17091.
277. Evans SF, Docheva D, Bernecker A, Colnot C, Richter RP, Tate MLK. Solid-supported lipid bilayers to drive stem cell fate and tissue architecture using periosteum derived progenitor cells. *Biomaterials.* 2013;34(8):1878-87.
278. Thid D, Holm K, Eriksson PS, Ekeröth J, Kasemo B, Gold J. Supported phospholipid bilayers as a platform for neural progenitor cell culture. *J Biomed Mater Res Part A.* 2008;84A(4):940-53.
279. Huth M, Hertrich S, Mezo G, Madarasz E, Nickel B. Neural Stem Cell Spreading on Lipid Based Artificial Cell Surfaces, Characterized by Combined X-ray and Neutron Reflectometry. *Materials.* 2010;3(11):4994-5006.
280. Garcia AS, Dellatore SM, Messersmith PB, Miller WM. Effects of supported lipid monolayer fluidity on the adhesion of hematopoietic progenitor cell lines to fibronectin-derived peptide ligands for $\alpha 5\beta 1$ and $\alpha 4\beta 1$ integrins. *Langmuir.* 2009;25(5):2994-3002.
281. Uccelli A, Moretta L, Pistoia V. Mesenchymal stem cells in health and disease. *Nat Rev Immunol.* 2008;8(9):726-36.
282. Biswas KH, Hartman KL, Yu C-h, Harrison OJ, Song H, Smith AW, et al. E-cadherin junction formation involves an active kinetic nucleation process. *Proceedings of the National Academy of Sciences.* 2015;112(35):10932-7.
283. Heath George R, Johnson Benjamin RG, Olmsted Peter D, Connell Simon D, Evans Stephen D. Actin Assembly at Model-Supported Lipid Bilayers. *Biophys J.* 2013;105(10):2355-65.
284. REJMAN J, OBERLE V, ZUHORN IS, HOEKSTRA D. Size-dependent internalization of particles via the pathways of clathrin- and caveolae-mediated endocytosis. *Biochemical Journal.* 2004;377(1):159-69.
285. Forest V, Cottier M, Pourchez J. Electrostatic interactions favor the binding of positive nanoparticles on cells: A reductive theory. *Nano Today.* 2015;10(6):677-80.

286. Guerra NB, Gonzalez-Garcia C, Llopis V, Rodriguez-Hernandez JC, Moratal D, Rico P, et al. Subtle variations in polymer chemistry modulate substrate stiffness and fibronectin activity. *Soft Matter*. 2010;6(19):4748-55.
287. Rico P, Rodriguez Hernandez JC, Moratal D, Altankov G, Monleon Pradas M, Salmeron-Sanchez M. Substrate-Induced Assembly of Fibronectin into Networks: Influence of Surface Chemistry and Effect on Osteoblast Adhesion. *Tissue Eng Part A*. 2009;15(11):3271-81.
288. Ivanova OY, Margolis LB. The Use of Phospholipid Film for Shaping Cell Cultures. *Nature*. 1973;242:200.
289. Hermansson M. The DLVO theory in microbial adhesion. *Colloids and Surfaces B: Biointerfaces*. 1999;14(1):105-19.
290. Dan N. The effect of charge regulation on cell adhesion to substrates: salt-induced repulsion. *Colloids and Surfaces B: Biointerfaces*. 2003;27(1):41-7.
291. Hu Y, Guimond SE, Travers P, Cadman S, Hohenester E, Turnbull JE, et al. Novel Mechanisms of Fibroblast Growth Factor Receptor 1 Regulation by Extracellular Matrix Protein Anosmin-1. *J Biol Chem*. 2009;284(43):29905-20.
292. Salmivirta M, Jalkanen M. Syndecan family of cell surface proteoglycans: developmentally regulated receptors for extracellular effector molecules. *Experientia*. 1995;51(9-10):863-72.
293. Horton MR, Reich C, Gast AP, Rädler JO, Nickel B. Structure and Dynamics of Crystalline Protein Layers Bound to Supported Lipid Bilayers. *Langmuir*. 2007;23(11):6263-9.
294. Andersson AS, Glasmastar K, Sutherland D, Lidberg U, Kasemo B. Cell adhesion on supported lipid bilayers. *Journal of biomedical materials research Part A*. 2003;64(4):622-9.
295. Svedhem S, Dahlborg D, Ekeröth J, Kelly J, Hook F, Gold J. In situ peptide-modified supported lipid bilayers for controlled cell attachment. *Langmuir*. 2003;19(17):6730-6.
296. Cosgrove BD, Mui KL, Driscoll TP, Caliari SR, Mehta KD, Assoian RK, et al. N-cadherin adhesive interactions modulate matrix mechanosensing and fate commitment of mesenchymal stem cells. *Nature Materials*. 2016;15:1297.

297. McLaughlin S, Wang J, Gambhir A, Murray D. PIP(2) and proteins: interactions, organization, and information flow. *Annual review of biophysics and biomolecular structure*. 2002;31:151-75.
298. Tanaka M, Sackmann E. Polymer-supported membranes as models of the cell surface. *Nature*. 2005;437(7059):656-63.
299. Bharadwaj M, Strohmeyer N, Colo GP, Helenius J, Beerenwinkel N, Schiller HB, et al. α V-class integrins exert dual roles on α 5 β 1 integrins to strengthen adhesion to fibronectin. *Nature Communications*. 2017;8:14348.
300. Bazellieres E, Conte V, Elosegui-Artola A, Serra-Picamal X, Bintanel-Morcillo M, Roca-Cusachs P, et al. Control of cell–cell forces and collective cell dynamics by the intercellular adhesome. *Nat Cell Biol*. 2015;17(4):409-20.
301. Molloy JE, Burns JE, Kendrick-Jones J, Tregear RT, White DC. Movement and force produced by a single myosin head. *Nature*. 1995;378(6553):209-12.
302. Elosegui-Artola A, Bazellieres E, Allen MD, Andreu I, Oria R, Sunyer R, et al. Rigidity sensing and adaptation through regulation of integrin types. *Nature materials*. 2014;13(6):631-7.
303. Litvinov RI, Mekler A, Shuman H, Bennett JS, Barsegov V, Weisel JW. Resolving two-dimensional kinetics of the integrin α IIb β 3-fibrinogen interactions using binding-unbinding correlation spectroscopy. *J Biol Chem*. 2012;287(42):35275-85.
304. Kong F, Garcia AJ, Mould AP, Humphries MJ, Zhu C. Demonstration of catch bonds between an integrin and its ligand. *J Cell Biol*. 2009;185(7):1275-84.
305. Roca-Cusachs P, Iskratsch T, Sheetz MP. Finding the weakest link - exploring integrin-mediated mechanical molecular pathways. *JCell Sci*. 2012;125(Pt 13):3025-38.